Ashish Kumar Gadicherla
Promotor: Prof. Dr. Luc Leybaert

Role and contribution of mitochondrial complex I, connexin 43 and calcium sensitive potassium channels in cardiac ischemia-reperfusion injury

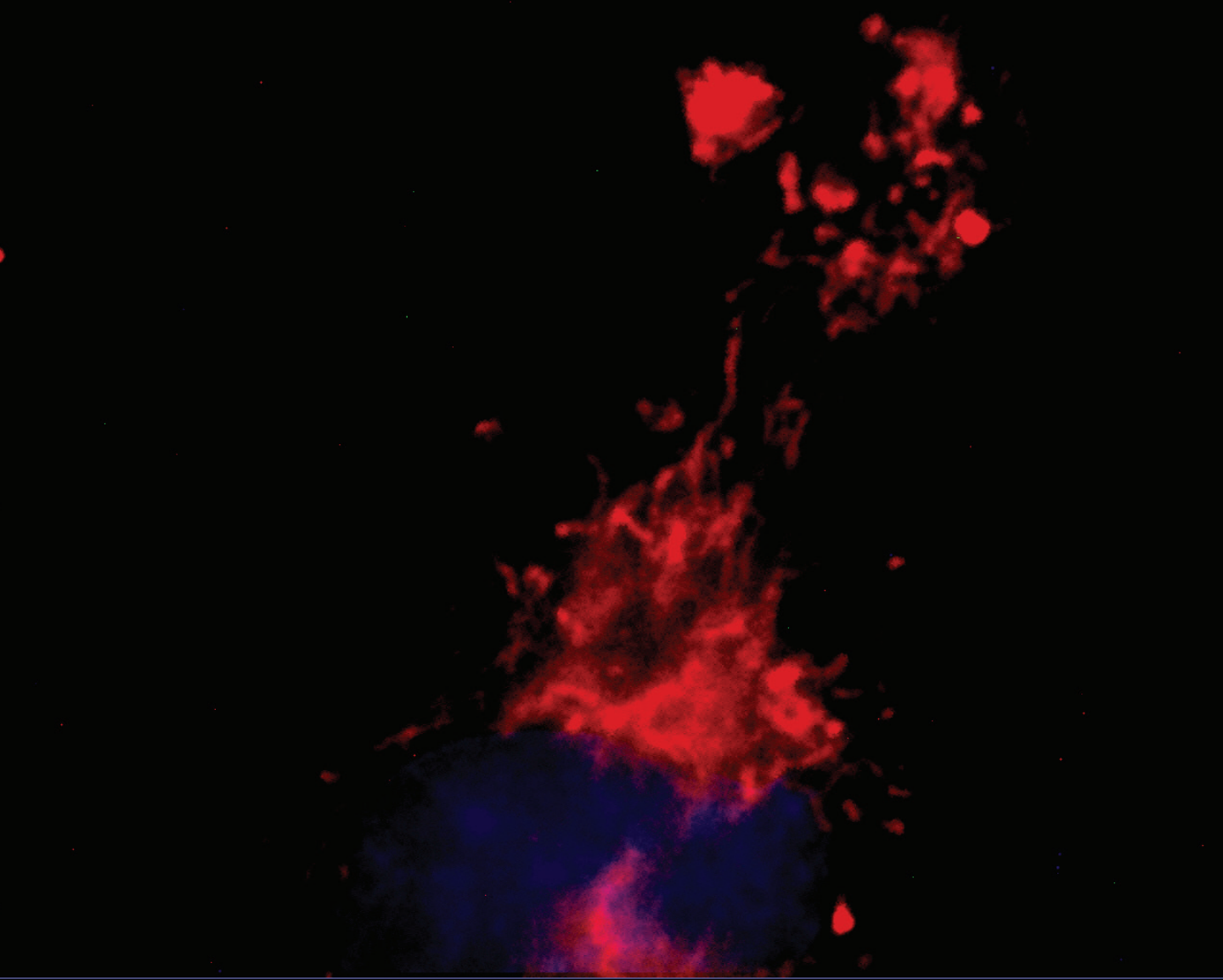

UNIVERSITEIT GENT

fwo

Thesis submitted in fulfillment of the requirements for the degree of "Doctor in Science: Biotechnology"

Faculty of Sciences



FACULTEIT WETENSCHAPPEN

Role and contribution of mitochondrial connexin43, complex I and calcium sensitive potassium channels in cardiac ischemia-reperfusion injury

Ashish Kumar Gadicherla

Thesis submitted in partial fulfillment of the requirements for the degree of "Doctor in Sciences: Biotechnology"

Academic year: 2015-16

Faculty of Sciences

Promoters

Prof. Dr. Luc Leybaert

Prof. Dr. Alexander Panfilov

Dr. Dmitri Krysko

Role and contribution of mitochondrial connexin43, complex I and calcium sensitive potassium channels in cardiac ischemia-reperfusion injury

Ashish Kumar Gadicherla[1]

Promoters:

Prof. Dr. Luc Leybaert[1]
Prof. Dr. Alexander Panfilov[2]
Dr. Dmitri Krysko[3,4]

Examination Committee:

Chair: Prof. Dr. Johan Grooten[3,4]
Secretary: Prof. Dr. Peter Brouckaert[3,4]
Reading Committee:
Prof. Dr. Rainer Schulz[5]
Prof. Dr. Rudy Van Coster[6]
Prof. Dr. Llewelyn Roderick[7]
Prof. Dr. Jolanda van Hengel[1]
Dr. Ronald Driesen[7]

1. Department of Basic Medical Sciences, Faculty of Medicine and Health Sciences, Ghent University. De Pintelaan 185, Blok B, 9000-Gent, Belgium.
2. Department of Physics and Astronomy, Faculty of Sciences, Ghent University. Krijgslaan 281, S9, 9000-Gent, Belgium.
3. Department of Biomedical Molecular Biology, Faculty of Sciences, Ghent University.
4. Inflammation Research Center, VIB - Ghent University, Technologiepark 927, 9052-Gent (Zwijnaarde), Belgium.
5. Physiologisches Institut, Fachbereich Medizin der Justus-Liebig-Universität, Aulweg 129, 35392 Giessen, Germany.

6. Department of Pediatrics and Genetics, Faculty of Medicine, Ghent University. De Pintelaan 185, K6, 9000-Gent, Belgium.
7. Morphology Department, Biomedical Research Institute, Hasselt University, Agoralaan Building C, 3590 Diepenbeek, Belgium.

A few words of acknowledgment...

Written acknowledgements cannot fully convey my gratitude for all the people who have contributed to my accomplishments. Having said that, my first sincere thanks go to Dr. Leybaert for giving me the opportunity to start my PhD, and having the confidence in me to do the job. Without his guidance and constant support over the years, none of this would have been possible. The freedom he gave me to explore other avenues have contributed immensely to my becoming a better scientist than I ever thought was possible. I sincerely thank him for encouraging and allowing me to do part of my studies in the US. I thank Dr. Wai-Meng Kwok for allowing me to spend extended periods of time working under his guidance. He was a great mentor and encouraged me to expand my horizons at every possible opportunity. I thank Dr. Rainer Schulz for his constant guidance in my work over the last four years. His guidance and critiques have made me a better scientist and have contributed immensely to my project. Sincere gratitude to University of Gent. I am proud to call UGent my *alma mater*. Special thanks to FWO for awarding me travel grants to be able to pursue part of my project at the Medical College of Wisconsin. Sincere gratitude to Dr. Stowe and Dr. Camara for believing in me, and encouraging me to push my boundaries and helping me land where I am right now.

My sincere thanks go out to my "colleagues" in my lab. The word *colleagues* cannot fully express the relationship, the camaraderie and friendship we developed over the years, but since that is where it started, I must acknowledge it. Thank you everyone for putting up with an extremely loud person who laughed and perhaps annoyed you a little too much. But since you never complained, I can't really be held responsible for the inconvenience caused. Thank you everyone for being guinea pigs in trying out my various baking and cooking expeditions. Hope you enjoyed at least some of it. Well, not the pumpkin pie I suppose! I will keep that in mind, just FYI.

Elke, Marijke and Nan- I was sure I would be killed by one of you guys in the first weeks of my life in the lab, when every ten minutes I would bug one of you three to help me with something or the other. However, I did try and rotate between the three of you. That perhaps didn't really help very much, but... You are one of the best colleagues/mentors/co-conspirators one can ever possibly have! I have learnt so much from you guys and that learning is something that will be a part of my life forever. Thank you! Melissa- you were a great help in navigating the complicated academic and bureaucratic system at UGent. Ellen and Thu- what would I do without your help in the lab! Ellen- you are one of the best people and resource managers! Thanks for all your help over the years with my incessant questions about how to do things ranging from paper work in the lab to having to call the electricity company to correct the incorrect meter readings I gave which would have given me bills equivalent to my annual pay check! Thu- I hope you find your orange Le Creuset pots. If not, you know who to contact.

Maarten, Alessio, Delphine, Valerie and Kasia- the new kids on the block! Some of the most talented people one has the privilege to work with. I wish you all the best in your PhD projects and your future endeavors! You deserve all the best and some more. Special thanks to Diego who probably had to put up with questions on my technical necessities more at home than at work! Thanks for your help in getting my couch back in shape! Tom and Sam- you were the coolest two people I have ever known. Always up for a laugh. I miss that.

Now that acknowledgements to my “work family” are done (phew!)- Marijke, Nan and Maarten- are you up for pizza or burger this Friday? Or La Mestizza?

Mummy & Nana, Akka & Bava, Annayya & Vadina- thanks for all your support through the years. Thanks for putting up with my absence for a majority of the time when important things in your lives were happening including lovely Shlok, Dushyanth, Shukla and Aadya! Although you were not physically present with me, I have always felt your good wishes, without which none of this would have been possible at all.

To the Dillons: Mary, Mary K & Peter, Peggy & Peter, Patty, Ann & Jay—thanks for welcoming me with open arms and giving me an American family. Thanks for your encouragement and support at every turn, and for putting up with my periodic absences at family gatherings. In any case, I will start serving cocktails at 4PM sharp. So if anyone wants something, you better tell me soon.

Michael- the one person I reserve most of my gratitude for. Words alone cannot express how much your love and support has meant during these past four years, and continue to be every day. Enduring separation for years on end is not something anyone would willingly put up with. I thank you from the bottom of my heart for putting up with it, and helping me cope with it at the same time. Your encouragement to pursue my dreams and aspirations has opened up the world for me. Your presence in my life has made me a different person, one I myself did not know existed. Thank you!

Last but not least, to all the people who have not been mentioned in the preceding words and yet have contributed to my pleasant stay and work at UGent and in Belgium- thank you very much!

Table of contents

Commonly used abbreviations

- $[Ca^{2+}]$ Calcium concentration
- $[Ca^{2+}]_i$ Intracellular calcium concentration
- $[Ca^{2+}]_m$ Intramitochondrial calcium concentration
- ANT Adenine nucleotide translocase
- APD Action potential duration
- ATP Adenine Triphosphate
- BGA b-glycerrhetinic acid
- BK_{Ca} Calcium sensitive potassium channel, large conductance
- CaM Calmodulin
- CaM-KII Calmodulin kinase-II
- CaMBD Calmodulin binding domain
- CF Coronary flow
- CHE_m Mitochondrial calcium-hydrogen exchanger
- CPC Calcium induced pre-conditioning
- Cx43 Connexin 43
- ELISA Enzyme Linked Immuno Sorbent assay
- EPR Electron paramagnetic resonance
- FADH Flavin adenine dinucleotide (reduced)
- GJ Gap junction
- GSK-3β Glycogen synthase-kinase 3β
- HC Hemichannel
- HCMD High calcium microdomains
- HK-II Hexokinase-II
- HPLC High performance liquid chromatography
- HR Heart rate
- HSP90 Heat shock protein 90
- HUVEC Human umbilical vessel endothelial cell
- I_{Ca} Calcium current
- IEF Iso-electric focusing
- IEM Immuno-electron microscopy

- IFM — Interfibrillar mitochondria
- I_K — Potassium current
- IK_{Ca} — Calcium sensitive potassium channel- intermediate conductance
- IMAC — Inner membrane anion channel
- IMM — Mitochondrial inner membrane
- I_{Na} — Sodium current
- IP3 — Inositol tri-phosphate
- IPC — Ischemic pre-conditioning
- IR — Ischemia-reperfusion
- KATP, K_{ATP} — ATP sensitive potassium channel
- KHE — Potassium hydrogen exchanger
- KR — Krebs-Ringer's buffer
- LETM1 — Leucine Zipper EF hand containing
- LVP — Left ventricular pressure
- $m[Ca^{2+}]$ — Mitochondrial calcium
- MCU — Mitochondrial calcium uniporter
- MICU — Mitochondrial calcium uniporter regulatory subunit
- mitoCx43 — Mitochondrial connexin 43
- mKHE — Mitochondrial potassium hydrogen exchanger
- MPTP — Mitochondrial permeability transition pore
- mRyR — Mitochondrial ryanodine receptor
- MS — Mass spectrometry
- NADH — Nicotinamide adenine dinucleotide (reduced)
- NCE — Sodium-Calcium exchange
- NICE — Sodium independent calcium exchanger
- NMDA — N-methyl D-aspartate receptor
- OMM — Mitochondrial outer membrane
- OXPHOS — Oxidative phosphorylation
- pH_m — Mitochondrial pH
- PKC — Protein kinase-C

- P_o Open probability
- POC Ischemic post-conditioning
- PPC Pharmacological pre-conditioning
- PTM Post translational modification
- RaM Rapid uptake mode
- Ran Ranolazine
- CI Respiratory control index
- ROS Reactive oxygen species
- RyR Ryanodine receptor
- SK_{Ca} Calcium sensitive potassium channel, small conductance
- SNCE Stepped normalized collision energy
- SR Sarcoplasmic reticulum
- SSM Sub-sarcolemmal mitochondria
- TIM Translocase of inner membrane
- TLC Thin layer chromatography
- TOM Translocase of outer membrane
- UCP Uncoupling protein
- VDAC Voltage dependent anion channel
- $\Delta\psi_m$ Mitochondrial membrane potential
- ψ_H Mitochondrial proton gradient

Samenvatting

Mitochondriën worden beschouwd als de 'energiecentrales' van de cel. Naast hun belangrijke functie in het produceren van energie, zijn ze ook cruciaal voor de ion homeostase en de cellulaire integriteit. Een groot aantal mitochondriale aandoeningen zijn reeds geïdentificeerd waaronder diabetes type II, cardiovasculaire ziektes, kanker en neurodegeneratieve aandoeningen. De celfysiologie steunt in belangrijke mate op de zuurstofafhankelijke energieproductie die plaatsvindt in de mitochondriën. Hierin spelen de elektronentransportketen en verschillende ionkanalen, aanwezig in de buitenste en binnenste mitochondriale membraan, een cruciale rol. Verscheidene studies hebben echter het belang van de respiratoire keten, niet enkel in ATP productie, maar ook in de generatie van schadelijke hoeveelheden reactieve zuurstofradicalen in diverse pathologische condities aangetoond, waaronder cardiale ischemie reperfusie (IR) schade. Niet enkel het mitochondriaal DNA, maar ook de elektronentransportketen en mitochondriale proteïnen zijn belangrijke doelwitten van de reactieve zuurstofradicalen. In het kader van deze observaties zijn mitochondriën voorgesteld als nieuwe, prominente therapeutische doelwitten. De componenten die kunnen bijdragen tot een mitochondriale dysfunctie zijn echter nog niet volledig geïdentificeerd.

De focus van deze thesis was voornamelijk gericht op de respiratoire keten en de ionkanalen, twee mitochondriale componenten die betrokken zijn in de energieproductie en de ion homeostase. Daarenboven werd de toepassing van mitochondriaal gerichte medicijnen en peptiden in het moduleren van celdood geïnduceerd door mitochondriale dysfunctie verder onderzocht.

In her eerste hoofdstuk, beschrijf ik de karakterisatie van een nieuw geïdentificeerd Cx43 eiwit in subsarcolemmale mitochondriën in cardiomyocyten. Voorgaande studies hebben aangetoond dat Cx43 een belangrijke speler is in de mitochondriale opname van calcium en kalium. De exacte functie van Cx43 ter hoogte van de mitochondriale membraan was echter nog niet volledig opgehelderd. Aan de hand van elektrofysiologische studies, heb ik aangetoond dat Cx43 functionele kanalen vormt in de mitochondriale membraan waarvan de activiteit kan geblokkeerd worden met behulp van Cx43 gerichte peptiden. Het effect van deze peptiden werd verder

bestudeerd op de mitochondriale calcium opname, een kritische factor in het celdoodproces. In een volgende stap werd dan ook het effect van deze peptiden op celdood geïnduceerd door verschillende apoptotische stimuli zoals ceramide, staurosporine en het cardiotoxische doxorubine nagegaan. Deze agentia induceren apoptose via de intrinsieke, mitochondriaal gemedieerde pathway. Samengevat resulteerden de bovenstaande experimenten in de belangrijke bevinding dat mitochondriaal Cx43 een efficiënter en belangrijker doelwit is om celdood te voorkomen dan enkel Cx43 ter hoogte van de plasma membraan. Verder werd het cardioprotectief effect van Cx43 gerichte peptiden nagegaan in harten blootgesteld aan IR. Deze peptiden reduceerden significant de grootte van het infarct wanneer ze toegediend werden voor de inductie van ischemie en aanwezig waren tijdens de eerste 10 min van reperfusie. Dit wijst op een cruciale rol van Cx43, zowel aanwezig in de mitochondriën als in de plasma membraan, in cardiale schade veroorzaakt door ischemie.

In het tweede hoofdstuk, werden de protectieve effecten van ranolazine, een inhibitor van het respiratoir complex I, op IR bestudeerd. Hiernaast werden ook de effecten van IR schade op complex I in kaart gebracht. Samengevat onderlijnen de bevindingen van dit onderzoek niet alleen de belangrijke rol van het respiratoir complex in het onderhouden van de cellulaire energiebalans maar ze benadrukken ook de cruciale rol voor het behouden van de complex I geassocieerde structuren in de mitochondriën. Daarenboven tonen de resultaten ook de voordelige effecten van ranolazine aan in het beperken van de ontwikkeling van een ischemisch infarct, in het bijzonder wanneer ranolazine toegediend wordt tijdens de kritische beginfase van reperfusie.

In het derde hoofdstuk, identificeerde en karakteriseerde ik een nieuw calcium gevoelig kalium kanaal in de binnenste mitochondriale membraan. De rol van mitochondriale ionkanalen in het behouden van de cellulaire ion homeostase is een belangrijke focus van veel recente onderzoeken. Mitochondriën spelen een prominente rol in de intracellulaire calcium en kalium buffering. Aangezien een calcium en kalium dyshomeostase een belangrijk kenmerk is van celdood, is een accurate kennis van de mitochondriale ionkanalen noodzakelijk voor de ontwikkeling van meer gerichte therapieën. In deze studie, identificeerde ik een nieuw kalium kanaal met een lage conductantie, waarvan de activiteit gevoelig is voor calcium en geblokkeerd wordt door apamine,

een gekende blokker van het SKCa kanaal in de plasmamembraan. De kanaalactiviteit werd verder ook geïnhibeerd door NS1619, welke een protectief effect heeft tegen cardiale IR schade.

Samengevat wijzen de resultaten behaald in deze thesis op de belangrijke maar ook complexe rol die mitochondriale energieproductie en ion homeostase kunnen spelen in het behoud van de cellulaire integriteit en hoe deze kennis verder kan toegepast worden voor de ontwikkeling van efficiënte therapeutische doelwitten gericht op de behandeling van mitochondriale aandoeningen.

Summary

Mitochondria have recently been acknowledged to be not only responsible for the fulfillment of energy requirements of the cell, but also for the maintenance of ion homeostasis and ultimately in the determination of cell fate. Indeed, a host of mitochondrial-associated diseases have been identified in the last few years including diabetes type II, cardiovascular diseases, cancer and neurodegenerative disease in addition to others. Cells depend on energy generated by mitochondrial consumption of oxygen. A critical feature of mitochondria in cellular energy and homeostasis is the electron transport chain and the various ion channels located in the mitochondrial membranes (inner and outer). Various studies have proven the importance of respiratory complexes in not just ATP production but also in the generation of reactive oxygen species, in deleterious amounts in pathological conditions such as cardiac ischemia-reperfusion injury. As such, the electron transport chain and the mitochondrial proteins, in addition to mitochondrial DNA are targets of the deleterious effects exerted by the reactive oxygen species. In light of these observations over the course of the last few years, mitochondria have emerged to be a leading therapeutic target, yet the important mitochondrial proteins involved have not been fully explored.

In the present thesis, I focus on two important aspects of mitochondria in energy and ion homeostasis- the respiratory complexes involved in generation of ATP and the ion channels of mitochondria responsible for the ion homeostasis of mitochondria and in turn the cell. In addition, I explore the use of mitochondria targeted drugs and peptides to mitigate cell death induced by mitochondrial dysfunction.

In the first chapter, I characterize the role of connexin43 protein in the cardiac subsarcolemmal mitochondria. Previous studies have shown that mitochondrial connexin43 is a player in mitochondrial uptake of calcium and potassium, but a specific identification of the channel was still lacking. In my studies, I performed electrophysiological studies on connexin43 purified from cardiac subsarcolemmal mitochondria and found that not only does mitochondrial connexin43 form a functional channel, but also that the channel activity can be blocked by the use of connexin43 targeting peptides. Since modulation of mitochondrial calcium dynamics is a critical

player in cell death, I further studied the effect of the peptides on cell death induced by various mitochondrial targeting apoptotic stimuli such as the ones induced by ceramide, staurosporine and cardio-toxic doxorubicin. These studies showed that targeting mitochondrial connexin43 is much more beneficial in preventing cell death than targeting just the plasmalemmal connexin43. To further investigate the beneficial effect of connexin43 targeting peptides in cardioprotection, I tested their effect on hearts exposed to ischemia-reperfusion injury and found that they significantly reduced infarct size, when administered before the onset of ischemia and being present during the initial 10 minutes of reperfusion, pointing towards a critical role for connexin43- both mitochondrial and plasmalemmal, in ischemic injury.

In the second chapter, I determine the role of a mitochondrial complex I targeting drug- ranolazine in ameliorating the deleterious effects of 30 minutes of ischemia and 10 minutes of reperfusion (IR), in addition to characterizing the effects of IR injury on respiratory complex I. The findings from this chapter not only underscore the importance of respiratory complex I in maintenance of cellular energy balance but also the critical role for maintenance of complex I associated structures within the mitochondria. In addition, I also show that targeted therapy such as ranolazine, especially when used within the critical time period of initial reperfusion, is beneficial in restricting the development of infarct size- a major deleterious outcome of ischemic injury.

In the third chapter, I identify and characterize a novel potassium channel located in the inner mitochondrial membrane- the small conductance calcium sensitive potassium channel. The role of mitochondrial ion channels in maintenance of cellular ion homeostasis has been the focus of many recent studies, with the common observation that mitochondria act as strong buffers of calcium and potassium, whose imbalance is an important feature of cell death. Given this information, knowledge of mitochondrial ion channels is necessary for development of targeted therapies. In my studies, I identified a putative small conductance calcium sensitive potassium channel, the activity of which was sensitive to calcium and was blocked by apamin- a known blocker of the SK_{Ca} channel in the plasma membrane. In addition, the channel activity was also sensitive to NS1619, which when administered to the heart prior to IR injury, showed a protective effect.

In summary, my thesis elucidates the complex part mitochondrial energy and ion homeostasis

have in the maintenance of cellular integrity and how this knowledge can be explored for the development of effective therapeutic targets aimed at ameliorating various mitochondrial associated disorders

Chapter 1

Introduction

1.1 General introduction

Ischemic heart disease is one of the leading causes of death in industrialized nations. Cardiac ischemic disease can lead to a myriad of clinical outcomes including acute myocardial infarction, sudden cardiac death, arrhythmias and heart failure. The cause of ischemic injury is a blockage of oxygen supply to the tissue, associated with the blockage of an artery. In case of cardiac ischemia, it is usually a result of occlusion of the coronary artery. In such cases, upon removal of the occlusion, reperfusion of the ischemic tissue restores oxygen supply thereby preventing tissue damage. A major indicator of damage to the myocardium following ischemic injury is infarct size. Even though the metabolic changes associated with ischemic injury can be restored eventually via therapeutics and/or natural healing of the tissue, the structural changes brought upon the myocardium by the infarct are permanent and lead to remodeling of the ventricular tissue which can lead to heart failure[1].

Infarct size is a major determinant of mortality, and limitation of its size has been an important objective of strategies to improve clinical outcomes. Different approaches employing physiological pathways and drugs have since been used towards this goal. Murry et al. firstly demonstrated that brief episodes of ischemia-reperfusion (IR) in dogs are beneficial for myocardial preservation after 40 minutes of ischemia[2]. This phenomenon of inducing protection by short pulses of ischemia before a longer ischemic insult is termed ischemic pre-conditioning (IPC). Many studies have been performed to elucidate the mechanisms involved in IPC. IPC induced protection is conferred over two periods of time: the acute protection, which disappears within 2 hours of IPC, and another one appearing after 24-48 hours, which lasts much longer up to 96 hours[3]. Given the different molecular players involved in acute and delayed protection, the efficiency of protection also differs, with acute phase protection being stronger than late phase protection[3]. The acute phase relies on recruitment of readily available cellular factors such as anti-oxidant enzymes[2] whereas the delayed phase protection depends on proteins, such as catalase, HSP72 and SOD[4], whose increased expression is triggered by the acute phase. These enzymes are thought to be produced in response to a slightly increased ROS generation observed during the brief ischemic pulses followed by reperfusion[4]. ROS generation is thought to be sufficient to trigger downstream protective pathways but not enough to be lethal by themselves[4].

One of the major molecules associated with IPC is adenosine which triggers downstream protective pathways[5]. Adenosine activates protein kinase C (PKC), which in turn activates the downstream reperfusion injury salvage kinase (RISK) pathway and the endothelial nitric oxide synthase (eNOS)/protein kinase G (PKG) pathways. The major action of adenosine activated RISK pathway is at reperfusion, as studies have shown that use of adenosine receptor antagonist and thus blockage of RISK pathway abrogates IPC induced protection[6]. Javodov et al. showed that IPC inhibits the mitochondrial permeability transition pore (MPTP) opening during index ischemia, possibly through mild uncoupling of oxidative phosphorylation (OXPHOS) without blockage of the electron transport chain[7].

However IPC is not clinically useful, given the unpredictability of ischemic injury. Another strategy for protection of the myocardium following IR injury involves short pulses of ischemia following the longer index ischemia, called post conditioning (POC). This phenomenon has been shown to be cardioprotective in dogs, and it affords protection similar in extent to pre-conditioning[8]. Argaud et al. showed that POC also prevents MPTP opening[9]. As with IPC, the exact mechanism by which POC affords protection is not yet clearly known. However, nitric oxide (NO), generated from eNOS is also causally involved in POC[10]. Hydrogen sulfide, synthesized by cystathione-β-synthase and carbon monoxide synthesized by heme oxygenase are also thought to be involved in protection afforded by POC[11,12]. Peptide hormones such as natriuretic peptide and adrenomedullin also afford protection against IR injury, via a POC mode and involve NO, mitochondrial K_{ATP} channels and RISK or surface activating factor enhancement (SAFE) pathway[13]. Given the difficulty of angioplasty (by which patients receive IPC or POC), pharmacological agents mimicking them have been developed with a continued focus on development of novel and better therapeutic agents. The use of therapeutic agents to induce cardioprotection via IPC or POC is termed “pharmacological.” as opposed to “ischemic”.

Pharmacological preconditioning (PPC) has been achieved via the use of volatile anesthetics such as isoflurane, halothane and desflurane. PPC using volatile anesthetics was first demonstrated by Freedman et al. in isolated rat heart exposed to global ischemia[14]. Warltier et al. further reported the protective effects of halothane and isoflurane on stunned myocardium of dogs during reperfusion[15]. Novalija and Stowe reported that PPC via anesthetics mimicked IPC[16]. Acute PPC

involves phosphorylation and translocation of pre-existing proteins while delayed PPC involves *de novo* protein synthesis[17–21].

In addition to IPC, POC and PPC, temperature has also been used to protect the myocardium. Riess et al. showed that hypothermia protects heart against ischemic insult after a variety of surgical procedures. Beneficial effects seen after hypothermia include better tissue perfusion, improved metabolic and mechanical function, reduced arrhythmias as well as reduced infarct size as shown by Riess et al.[22]. Furthermore, hypothermia has also been shown to reduce ROS generation in the mitochondria[22].

A key cellular event during IR injury and the protective mechanisms described above is the change in cellular redox state[23]. Change in redox state is a key signaling mechanism in modulation of transcription, translation and cell death. Mitochondria play an important role in maintenance of the cellular redox state which is achieved by mitochondrial regulation of cellular ion homeostasis, given the fact that mitochondria have high Ca^{2+} and K^+ buffering[24]. For example potassium (K^+) selective or anion selective pores are known to be important in regulating mitochondrial volume- a key factor in maintenance of ionic balance in the cytosol[25]. Under physiological conditions, the opening of mitochondrial ion channels leads to a change in membrane potential (from the normal value of -180 mV) which is compensated by increased substrate production, net oxidation of the matrix and a change in ROS generation[25]. Key mitochondrial channels whose role in cellular life and death have been well characterized include the mitochondrial ATP sensitive K^+ channels (mitoK_{ATP}), the mitochondrial calcium (Ca^{2+}) sensitive K^+ channels (mitoK_{Ca}), mitochondrial Ca^{2+} uniporter (MCU), MPTP and the inner membrane anion channel (IMAC).

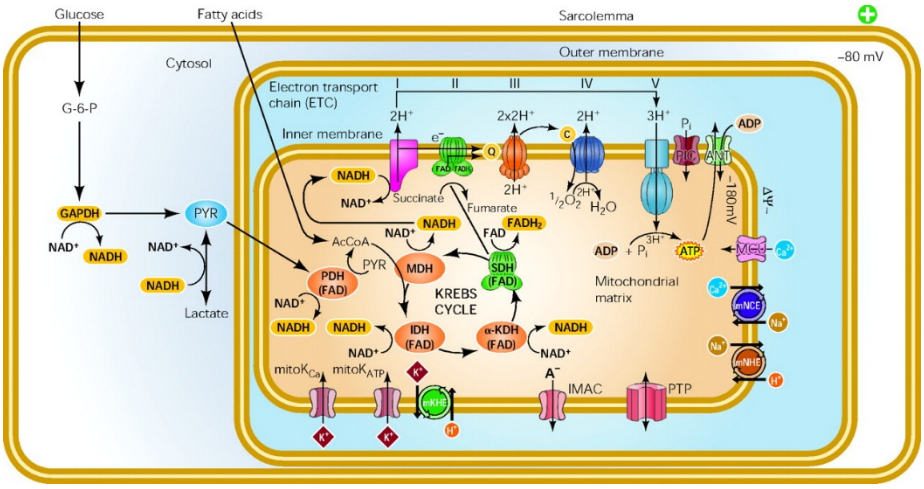

Figure 1: Overview of mitochondrial role on cellular ion and energy homeostasis

The mitochondrial outer membrane (OMM), which is permeable to large solutes and proteins has been shown to contain the voltage dependent anion channel (VDAC), and porins. In addition, translocases, which act as chaperones for transportation of proteins to the inner and outer mitochondrial membranes have also been shown to act as pores, although their role as ion channels is as yet unclear. The MPTP is also thought to be a channel in the OMM albeit in conjunction with inner mitochondrial membrane (IMM) proteins[26,27]. One interesting aspect with regard to permeability transition is that an increase in permeability of the OMM does not always correlate with an increase in permeability of the IMM thereby indicating that the MPTP is not solely composed of OMM proteins.

Mitochondrial ATP generation and local energy demand are crucial for cell functioning. Cellular Ca^{2+} is an important player in this coupling and Ca^{2+} activation of mitochondrial oxidative phosphorylation has been known for a longtime[28]. Mitochondrial Ca^{2+} handling is controlled by tightly regulated influx and efflux pathways. The influx pathways include the MCU, rapid uptake mode (RaM), and the putative mitochondrial ryanodine receptors (mRyR). Influx of Ca^{2+} into the mitochondria is controlled by membrane potential. Efflux of Ca^{2+} involves sodium (Na^{+})/ Ca^{2+} exchanger (NCE) and H^{+}/ Ca^{2+} exchanger with the NCE being electrogenic and therefore membrane potential–dependent[29]. Recent studies have suggested that connexin 43 (Cx43) also influences mitochondrial Ca^{2+} [(30)]. The other mechanism by which Ca^{2+} can exit from the mitochondria is the previously described MPTP.

There are two well-known IMM K^+ channels playing an important role in ischemic injury: the mitochondrial K_{ATP} (mito K_{ATP}) channel, whose activation has been shown to be one of the key mechanisms that counteract ischemic injury[31] and mitoK_{Ca} channels, whose opening has also been shown to be cytoprotective[32]. Recent studies have shown that Cx43 plays a major role in K^+ uptake by the mitochondria[33]. Other studies, have shown that mitochondrial Cx43 is involved in IPC[34]. Even though a clear link between Cx43's protective role in IPC and K^+ uptake influenced by Cx43 is yet to be established, it is clear that Cx43 does influence IPC via a K^+ dependent mechanism.

Several studies have shown that mitochondria are both targets and sources of cell damage during IR injury[26]. Indeed, IR injury results in damage to the respiratory chain with impairment of OXPHOS, which as described above is critical in maintenance of cellular energetics. Mitochondrial damage favors oxidative stress via the production of ROS by complexes I[35] and III[36]. These ROS act as signaling molecules for apoptosis through a decrease in mitochondrial membrane potential and through MPTP opening. MPTP opening is a key event in IR injury because it leads to an influx of solutes into the mitochondrial matrix, which in turn leads to matrix swelling and ultimately in the release of cytochrome c, a key activator of apoptotic pathways. Even though MPTP is recognized as a multiprotein complex, the individual units comprising the complex are as yet not fully known. It is speculated that it is composed of VDAC, ANT, cyclophilin D and HK-II[37] and dimers of the F_0F_1 ATP synthase[38].

The focus of the current thesis is directed to a better understanding of the contribution of mitochondrial Cx43 channels, mitochondrial K_{Ca} (mitoK_{Ca}) channels and the respiratory complex I in ischemic injury. I will further discuss the role of Cx43 in mitochondria (mitoCx43) as an ion channel contributing to mitochondrial Ca^{2+} entry thereby leading to cell death. This will be complimented by investigations towards potential blockers of mitoCx43 related Ca^{2+} entry and cell death. Additionally, I will discuss the identification and characterization of the mitoK_{Ca} channel, specifically the small conductance subtype, in cardiac mitochondria and the effect of IR injury on mitochondrial respiratory complex I.

1.2 Calcium and mitochondria

Cardiac excitation is based on plasma membrane ion fluxes (called sarcolemmal ion fluxes in the context of cardiomyocytes) that are coupled to cytosolic Ca^{2+} and contraction. Excitation is initiated by the opening of voltage gated Na^+ channels and Na^+ current influx (I_{Na}) leading to the generation of action potential upstroke (phase 0). This phase is limited by fast inactivation of I_{Na} and the activation of transient outward K^+ channels, resulting in early and partial repolarization which is the action potential (AP) notch (phase 1), followed by the plateau phase (phase 2). During the phase 2, membrane conductance falls significantly as the inward and outward currents are inactivated[39]. Due to the time- and voltage- dependent gating properties of K^+ channels, K^+ currents (I_K) are small and only capable of balancing relatively small remaining inward Ca^{2+} current (I_{Ca}), via the L-type Ca^{2+} channels. This causes the repolarization rate at plateau voltages to be slow. Also, due to high membrane resistance, small currents such as the Na^+/Ca^+ exchange current, the Na^+/K^+-ATPase current or I_{Ca} can destabilize the plateau membrane potential resulting in arrhythmias[40].

The cardiomyocyte plasma membrane has transverse invaginations called T-tubules that reach deep into the myocytes. T-tubules make close contact with junctional sarcoplasmic reticulum cisternae. L-type Ca^{2+} channels are present in high densities at these clefts in close proximity to the ryanodine receptor (RyR2)- the SR Ca^{2+} release channel. I_{Ca} causes a local increase in Ca^{2+} concentration [Ca^{2+}] to trigger RyR2 opening, thereby releasing Ca^{2+} from the SR during excitation-contraction coupling. This Ca^{2+}-induced Ca^{2+} release amplifies the SR Ca^{2+} influx. The rise in [Ca^{2+}] is transient because of the rapid inactivation of I_{Ca}, RyR2 closure and simultaneous activation of Ca^{2+} removal pathways. Sarcolemmal Na^+/Ca^{2+} exchanger, sarcolemmal Ca^{2+}-ATPase and the MCU are responsible for Ca^{2+} removal. The intracellular and extracellular free [Ca^{2+}] are normally approximately 0.1 and 1000-2000 μmol/L respectively. However, since the total cell Ca^{2+} content is approximately 1000 μmol/L, it can be said that almost 99% of the total cell Ca^{2+} content is bound to proteins, phospholipids or sequestered into the ER and mitochondria[41].

Mitochondria have a high capacity of buffering cytosolic Ca^{2+}. In the mammalian heart,

mitochondria are more abundant than in any other tissue and account for about a third of the cell volume[42]. Mitochondria experience regular repetitive elevations in intracellular Ca^{2+}. The abundant interfibrillar mitochondria are in close proximity to the sarcoplasmic reticulum and are influenced by Ca^{2+} release from RyR2 opening[43,44]. Although the global [Ca^{2+}] increases from 100 nM to ~500 nM with each heartbeat, the microdomains of the SR-mitochondrial contacts (approximately 5-100 nm apart) experience an effective [Ca^{2+}] of about 10-20 μM[45].

The uptake of Ca^{2+} and the activation of the mitochondria not only depends on the global [Ca^{2+}] in the cytosol but also the distance between the microdomains experiencing the increase in [Ca^{2+}]. The morphological feature of the cell where the SR and mitochondria come into close proximity forms the basis for the confinement of this cytoplasmic microdomain which can influence the mitochondria[46,47]. These high-Ca^{2+} microdomains (HCMDs) are short lived but form rapidly in the perimitochondrial cytoplasm where inositol 1,4,5-trisphosphate (IP_3) sensitive Ca^{2+} stores are present. The induction of mitochondrial Ca^{2+} signal induced by insulin producing cells or in adrenal chromaffin cells is attributed to this HCMD Ca^{2+} hotspots[46,47]. The importance of a HCMD is that the existence of such a microdomain facilitates an efficient Ca^{2+} transfer between the ER/SR and mitochondria to match the energy produced by the mitochondria to demand by Ca^{2+} dependent processes such as the excitation contraction coupling machinery[48]. A study estimated that areas within 500 nm from a HCMD take up much more Ca^{2+} than mitochondria more than 500 nm away from HCMD[49]. In addition, the kinetics of Ca^{2+} uptake were also significantly different between the two populations indicating that the uptake mechanisms between the two populations are different or at the very least, the same players have different affinities for Ca^{2+}. However, it is highly unlikely that the same channel in two mitochondrial populations within the same cell would act differently, pointing to the existence of a different uptake mechanism among the two mitochondrial subpopulations.

Even though there exists a range of [Ca^{2+}] through which mitochondria take up Ca^{2+} from the cytosol, it has been shown that mitochondrial Ca^{2+} uptake occurs readily above cytoplasmic [Ca^{2+}] of about half a micromolar[50,51]. Other studies have reported the generation of mitochondrial [Ca^{2+}] transients in spite of the lack of HCMDs[52]. Still other studies[53] have shown a range of cytoplasmic [Ca^{2+}] ranging from 200-1000 nM for mitochondrial Ca^{2+} uptake.

In addition to the modulation of cytoplasmic [Ca^{2+}], mitochondrial Ca^{2+} also has other roles, especially in the regulation of mitochondrial OXPHOS. Intramitochondrial Ca^{2+} has been observed to activate pyruvate dehydrogenase, isocitrate dehydrogenase and α- ketoglutarate dehydrogenase- all key enzymes of the Kreb's cycle[54]. Other loci within the electron transport chain such as F_0F_1ATPase, the adenine nucleotide translocase (ANT) have also been shown to be Ca^{2+} activated[55] indicating that mitochondrial Ca^{2+} may act as one of the controls of cellular metabolism. The amount of Ca^{2+} taken up by the mitochondria is sufficient to activate the Ca^{2+} sensitive dehydrogenases increasing the amount of NADH[54].

In addition to the role of mitochondrial Ca^{2+} in maintenance of cellular Ca^{2+} transients and indirect control of cellular metabolism, evidence also points to the role of Ca^{2+} in control of apoptosis and necrosis of the cell, a key event of which is the release of cytochrome *c* or of the apoptosis inducing factor. Evidence points to the overload of mitochondrial Ca^{2+} leading to the opening of MPTP, leading to the release of these apoptotic factors[56].

Mitochondrial entry and exit of Ca^{2+} is very tightly controlled given the importance of maintenance of the integrity of IMM for proper functioning of the mitochondria. Entry of Ca^{2+} is mostly through the ruthenium red sensitive MCU complex, and a second mode of uptake- the rapid uptake mode (RaM). The MCU complex is composed of the uniporter pore and regulatory subunits, mitochondrial Ca^{2+} uptake 1 and 2 (MICU1 and MICU2). MCU is an integral membrane protein that is essential for the electrophysiologically defined uniporter current[57]. MICU1 contains EF-hand Ca^{2+} binding domains and is found in the inter membrane space and essentially functions as a Ca^{2+} sensing gate keeper, allowing the channel to be closed when the external [Ca^{2+}] is low and to open when Ca^{2+} transient rises[58]. The role and functions of MICU2 have not yet been fully characterized. The uniporter complex as a whole is sensitive to the hexavalent cation ruthenium red- a glycoprotein stain. On the other hand, it is activated at low Ca^{2+} concentrations by polyamines such as spermine[59] and also by adenine nucleotides[60].

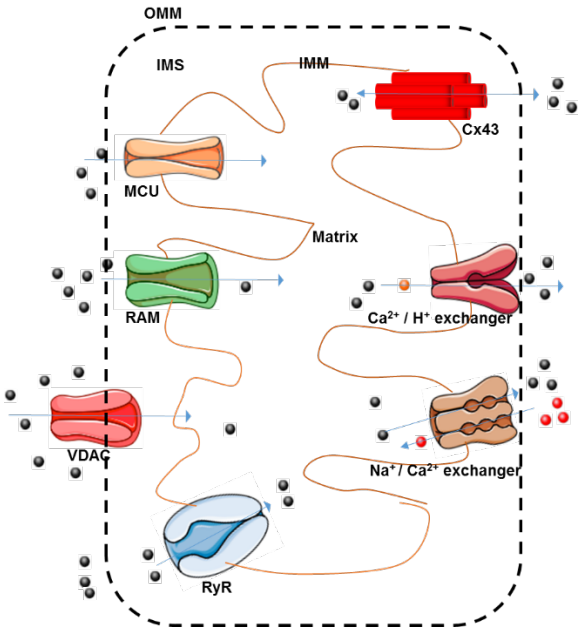

Figure 2: Mitochondrial Ca^{2+} channels. OMM: Outer mitochondrial membrane; IMM: Inner mitochondrial membrane; IMS: Inter membrane space; Cx43: Connexin 43; MCU: Mitochondrial Ca^{2+} uniporter; RAM: Rapid uptake mode; VDAC: Voltage dependent anion channel; RyR: Ryanodine receptor; Black spheres: Ca^{2+}; Red spheres: Na^{+}; Arrows indicate direction of ion movement.

Evidence for very rapid Ca^{2+} uptake into the mitochondria was first seen in liver mitochondria[61]. Similar observations of a very rapid uptake in the initial transient followed by an uptake similar to that of the MCU was seen in heart mitochondria as well as the brain mitochondria, suggesting a wide presence of a rapid uptake mode[62]. The main characteristic differentiating the RaM from the MCU is the very high rate of Ca^{2+} uptake via RaM at the beginning of every pulse and its inhibition very soon after that, which is thought via the binding of Ca^{2+} from the pulse itself to an external site that essentially blocks RaM[61]. Pharmacologically, RaM is inhibited by uncouplers which dissipate the mitochondrial membrane potential, suggesting that electrochemical gradient is the driving force behind Ca^{2+} uptake by RaM. Questions about the cellular identity of the RaM being from the mitochondria or the ER were answered by the use of thapsigargin- a potent inhibitor of ATPase responsible for ER Ca^{2+} uptake[63]. These studies showed no effect of thapsigargin on RaM uptake of Ca^{2+} by the mitochondria. RaM is also inhibited by ruthenium red, although a much higher concentration is needed for RaM inhibition (greater than 0.1 nM) than MCU inhibition (0.003 nM)[64].

In addition to the MCU and the RaM, other proposed mitochondrial Ca^{2+} influx mechanisms include the mitochondrial ryanodine receptor (mRyR1), uncoupling proteins (UCP), leucine zipper-EF-hand containing transmembrane protein1 (LETM1) and the canonical transient receptor potential channel 3 (TRPC3)[65].

Mitochondrial RyR1 forms a ryanodine receptor in the IMM that participates in mitochondrial Ca^{2+} uptake in cardiomyocytes and neurons. It is present not only in native cardiomyocytes but also in cultured cardiac myoblasts. mRyR1 is inhibited by high concentrations of ryanodine and ruthenium red. Exhibiting a high Ca^{2+} sensitive current of about 500-800pS in planar lipid bilayer experiments, mRyR1 represents a putative mitochondrial Ca^{2+} intake route[66].

UCP are transporters located on the IMM responsible for proton leaks, thus uncoupling the OXPHOS from ATP synthesis. Trenker et al. reported the importance of the presence of UCP for Ca^{2+} uptake by the MCU[67]. However, it is not clearly known if UCP actually transports Ca^{2+} into the mitochondria. The function of LETM1, a highly conserved eukaryotic IMM protein, is controversial with studies identifying it as a K^+/H^+ exchanger and also as Ca^{2+}/H^+ exchanger, inhibited by ruthenium red. Later studies, however showed that LETM1 is Ca^{2+}/H^+ antiporter insensitive to ruthenium red[68].

Because of the large internally negative membrane potential across the IMM, Ca^{2+} efflux is electrically uphill. The two modes of Ca^{2+} efflux that are non-depolarizing are the Na^+ dependent and the Na^+ independent mechanisms (non-depolarizing means that the mitochondrial membrane potential is not lost). They exhibit very distinct kinetics and differential sensitivities to inhibitors. The Na^+ dependent Ca^{2+} efflux mechanism in heart is known to exchange Ca^{2+} for Sr^{2+} or Na^+. Baysal et al. found that Na^+ dependent Ca^{2+} efflux could pump Ca^{2+} out of the mitochondria against a Ca^{2+} gradient whose energy is at least twice that of the Na^+ gradient, mediated by the exchange of two Na^+ for one Ca^{2+} (non-electrogenic) or three Na^+ for one Ca^{2+} (electrogenic)[69].

The Na^+ independent Ca^{2+} efflux mechanism also transports Ca^{2+}, Sr^{2+} or Mn^{2+} from the matrix to the intermembrane space[70]. This transport is electroneutral[71]. However no specific cations are known to be exchanged for Ca^{2+} leading to the presumption that it was essentially a Ca^{2+}/H^+

exchanger. However, other studies[72] showing a decrease in this efflux with increasing matrix alkalinity suggest that this mechanism is not a passive exchange of Ca^{2+} for H^{+}. This mechanism is sensitive to CN^{-} [(73)], low levels of uncoupler CCCP[74] and high concentrations (2 μM) of ruthenium red[75].

Another Ca^{2+} efflux pathway, albeit a depolarizing mechanism is the opening of the mitochondrial permeability transition pore. As the name suggests, it is essentially a pore in the IMM linked to necrotic and apoptotic cell death. As stated earlier, the exact composition of the MPTP is not yet known. Many chemicals and free radicals promote MPTP opening. Most of these agents modulate opening by decreasing the Ca^{2+} threshold needed for MPTP opening. However an overload of Ca^{2+} in the mitochondrial matrix is, by itself, sufficient to trigger MPTP opening. In cardiac IR, for example, the Ca^{2+} dysregulation in the cytoplasm leads to Ca^{2+} dysregulation in the mitochondria, leading to mitochondrial Ca^{2+} overload and promotes MPTP opening. This is often preceded by excess mitochondrial ROS formation.

In conclusion, a clear balanced Ca^{2+} homeostasis, both in the cytoplasm as well as in the mitochondria is essential for normal cellular functioning and any dysregulation can be fatal to the cell and ultimately the organ affected.

1.3 Connexin 43

Connexins are a family of proteins (named according to their molecular weight) whose well documented role is to form cell communication channels called gap junctions in which two hexameric structures of connexins (called connexons) from apposing cells fuse together to form the gap junction channel. In addition to gap junction channels, which are found at cell-cell contacts and are often organized as arrays of gap junction channels called gap junction plaques, these hexameric structures can also remain as hemichannels (HCs) when unapposed. These channels allow free passage of ions and metabolites less than 1.5 kDa in weight between the cells in case of gap junctions and the cytosol and the extracellular milieu in case of HCs.

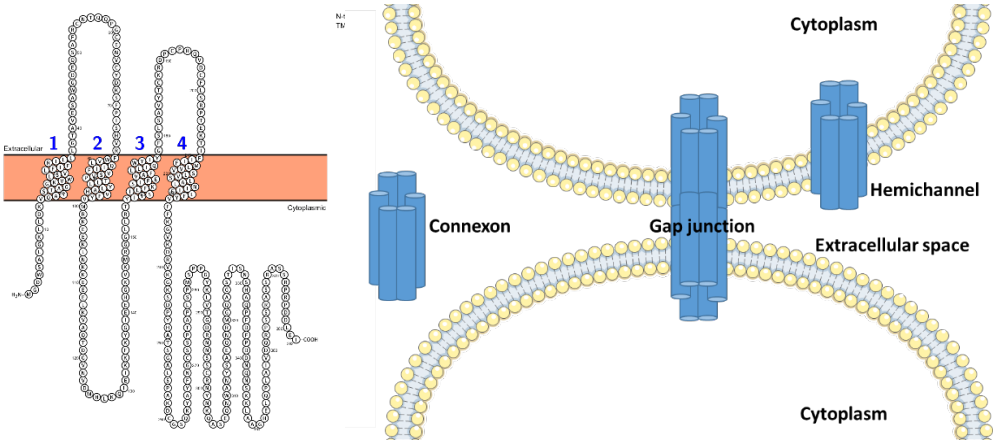

Figure 3: Connexin 43 topology and assemblies. NT: N-terminus; EL-1: extracellular loop 1; CL: cytoplasmic loop; EL2: extracellular loop 2; CT: C-terminus

Connexin distribution is cell and tissue dependent and the most ubiquitous of all connexins is connexin 43 (Cx43)[76,77]. In spite of the ubiquitous distribution of connexins, their half-life is remarkably short. For example the half-life of Cx43 in the heart has been shown to be 1-2 hrs[78,79]. It is possible that connexins have such a short life time in order for the cell to rapidly respond to physiological requirements of either increased or decreased coupling. Just as with other classical integral membrane proteins, connexins are thought to thread into the ER via the translocon and encoded start and stop transfer sequences. Connexin oligomerization occurs in the ER[80], except for Cx43, which was shown to be present in monomeric form in the Golgi apparatus and to oligomerize in the trans-Golgi network[81]. Even though connexins are not glycosylated, it has been

shown that cysteine residues form disulfide bonds between extracellular loops (ELs)[82]. Further evidence suggests that Cx43 is transiently phosphorylated early in the secretory pathway[83,84] and the majority of Cx43 phosphorylation occurs when it reaches the plasma membrane[85].

Upon exiting the trans-Golgi network, connexins enter a variety of intermediate structures of different sizes and shapes including connexons[86–88], and their transport is mediated in part by microtubules[87,89]. Upon insertion into the plasma membrane, connexons (with each connexin monomer being composed of the N-terminus (NT), four trans-membrane domains, two extracellular loops (EL-1, EL-2), cytoplasmic loop (CL) and C-terminus (CT)) freely diffuse within the lipid bilayer[88] and guided by N-and E-cadherin based adhesion events, dock with connexons from adjacent cells to form gap junction channels[90,91]. The connexons may also remain as unapposed HCs.

Connexin channel regulation

Connexin channels (both gap junctions and HCs) are regulated by voltage, intra- and extra-cellular Ca^{2+}, intra- and extra-cellular pH as well as phosphorylation status of the protein itself. The activity of gap junctions and HCs are voltage dependent with gap junctions being regulated to a large extent by trans-junctional voltage (voltage across the cells sharing the gap junction) and HCs by the membrane potential. Under physiological conditions, since the membrane potential of adjacent cells is equal, the trans-junctional voltage is zero leading to open gap junctions consequently establishing a pathway for movement of ions, metabolites and signaling molecules along the concentration gradient between cells. However, when adjacent cells develop different membrane potentials, due to a deviation of junctional voltage, gap junctional communication decreases and can eventually cease, as seen in cardiac arrhythmias. HCs in contrast are typically closed under physiological conditions to prevent loss of metabolites and ions. However, HCs can open when there is membrane depolarization. Upon depolarization of the membrane to positive voltages, HCs open by a slow gating mechanism resembling transitions associated with extracellular loop domain docking[92–94]. Fast gating is also observed in HCs and can be activated via both positive and negative potential transitions. As such, voltage behavior of connexin HCs can be either uni- or bipolar. For bipolar HCs, currents increase with depolarization but decrease to fast states when

inside potentials approach positivity[95,96].

Lowering of intracellular pH inhibits gap junctional communication in a dose dependent manner. Severe acidification, as seen in ischemia, can lead to an intracellular pH approaching 6, and it has been demonstrated that gap junctions are blocked around the same pH-6[(97)]. Connexin HCs are also sensitive to extracellular pH[98], in addition to extracellular pH. However, it is possible that H^+ entry through open channels can close HCs just as gap junctions are closed by cytoplasmic H^+. Indeed, direct protonation of Cx43 has been described[99].

Lowenstein and Rose first demonstrated that Ca^{2+} was a cytoplasmic factor regulating gap junction communication[100], where they demonstrated that microinjection of 50 μM Ca^{2+} uncoupled gap junctions within the vicinity of injection, whereas channels farther away were unaffected. In neonatal rat cardiomyocytes Ca^{2+} induced uncoupling was observed at a [Ca^{2+}] of 400 μM[101]. Whereas gap junctions are only sensitive to intracellular [Ca^{2+}], HC activity is modulated by both intra- and extra-cellular [Ca^{2+}]. Lowering of extracellular [Ca^{2+}] has been shown to trigger HC opening[102–104]. Modulation of HC activity by intracellular [Ca^{2+}] was first shown by Cotrina et al. who showed Cx43 HC mediated ATP release triggered by activation of IP3-linked purinoreceptors[105]. A role for intracellular [Ca^{2+}] was later confirmed by studies showing Cx32 and Cx43 mediated ATP release via photoliberation of caged-IP3 and caged Ca^{2+} or Ca^{2+} ionophores[106–108]. The range of [Ca^{2+}] for HC activation was shown as between 200-1000 nM, with a maximal activity at 500 nM[108,109]. Absence of Cx43 HC activation at high [Ca^{2+}] was confirmed in cardiomyocytes where intracellular [Ca^{2+}] above 500 nM closed HCs[110]. Wang et al. also showed that a mild elevation of [Ca^{2+}] from 200-500 nM shifted membrane potential dependence of Cx43 HC and that HCs were activated at lower positive potentials and also that elevation of intracellular [Ca^{2+}] to micromolar concentrations[111].

Phosphorylation of proteins is a widespread mechanism of functional modulation and its effects on channel function can include stabilization of open or closed states and alteration of kinetic transitions between states[112]. Most connexins contain phosphorylation sites in the CT domain and all connexins have been demonstrated to be phosphoproteins either in vivo or in vitro[113]. Cx43 has been shown to be phosphorylated at multiple sites by multiple kinases and contains three

PKA/PKC binding motifs in the CT domain. It has been demonstrated that injection of PKA can rapidly increase Cx43 mediated junctional communication[114]. Serine phosphorylation of human or rat Cx43 by PKC, but not PKA has been shown to decrease LY permeability as well as decreased channel conductivity[115]. Studies have also shown that alkaline phosphatase treatment of Cx43, increases Cx43 permeability and channel activity in Cx43 incorporated into lipid bilayer vesicles indicating the importance of phosphorylation status on Cx43 activity.

Connexin mimetic peptides as tools for Cx43 channel modulation

Pharmacological agents such as halothane, octane and the glycyrrhizic derivatives such as carbenoxolone are general connexin channel inhibitors that suffer from poor selectivity in that they affect all connexin types, all connexin channel types (gap junctions, HCs), and have major off-target effects. Obviously, cardioprotection may necessitate more specific targeting. For example, in most cases, gap junctional coupling needs to be preserved in order to avoid conduction problems and consequent arrhythmia. By contrast, sarcolemmal HCs may benefit from being inhibited to counteract their deleterious effects as demonstrated by Wang et al[116]. During the 1980's experiments performed in the Warner group indicated that connexin mimetic peptides could be used as inhibitors of gap junctions[117]. These peptides mimic selected amino-acid sequences of the well conserved extracellular loops of Cxs (for example, ^{43}Gap26 and ^{43}Gap27 for Cx43 and ^{32}Gap27 for Cx32) or the highly variable intracellular loop (for example, Gap24 for Cx32, and L2 and Gap19 for Cx43). Various studies[106,108,111,118,119] have shown that short exposure of cells to Gap26 or Gap27 first inhibits HCs (within minutes) whereas longer exposures (several hours) are needed to also inhibit gap junctions. Wang et al showed that Gap26 and Gap27 also counteract the lowering of the activation voltage for HC opening exerted by a slight increase of cytoplasmic Ca^{2+} [(111)]. It needs to be added that despite the fact that Gap26/Gap27 peptides have been used since the 80's to block gap junctions, the actual interaction site with the connexin protein is still unknown. The only evidence available up to date is that these peptides interact with the extracellular loops of the protein, based on atomic force microscopy[120]. Despite a significant shortage of mechanistic insights, Gap26/Gap27 peptides have been extensively applied to probe their cell protective potential, with beneficial effects of Gap26 and on cardiac IR injury[121], Peptide5, derived from EL2 of Cx43, was shown to reduce damage following ex-vivo as well as

in-vivo spinal cord injury model[122] .

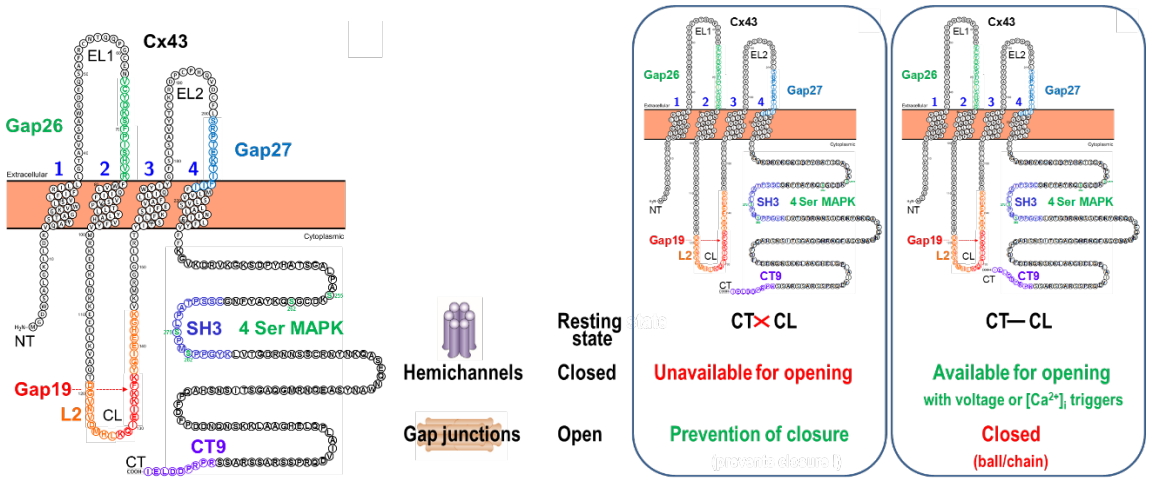

Figure 4: Connexin 43 topology showing the peptidomimetics derived from protein sequence. (Left panel). Differential regulation of hemichannels and gao junctions based on CT-CL interactions (Right panel)

In contrast to extracellular loop mimetic peptides (Gap26/Gap27), intracellular loop mimetics like L2 and Gap19 peptides identical to Cx43 amino acid sequences, act as specific HC blockers while at the same time they prevent the closure of gap junctions[123,124]. Wang et al. used Gap19 to protect against cardiac IR based on the hypothesis that opening of hemichannels, triggered by various signaling events during ischemia and reperfusion, may trigger the loss of essential metabolites and induce ion shifts that lead to cell swelling and cell death[123].

In order to understand how L2 and Gap19 peptides inhibit HCs, one needs to consider the effect of loop-tail interactions of the Cx43 protein. Ponsaerts et al. [124] and Wang et al.[123] found that interaction of the Cx43 CT with the cytoplasmic loop (CL) is necessary to bring HCs in a state that is available for opening in response to triggers like voltage steps to positive membrane potentials or increases in cytoplasmic Ca^{2+} concentration[111]. L2 and Gap19 bind to the CT and therefore hinder CT-CL loop-tail interaction[124,125]. In the absence of loop-tail interaction, HCs remain in a closed state that is refractive to voltage or Ca^{2+} stimulation.

Most remarkably, Cx43 loop-tail interactions have opposite effects on gap junctions: CT-CL interaction indeed closes gap junctions according to a ball-and-chain paradigm[126,127]. The exact reason why loop-tail interaction have distinct effects on gap junctions and HCs is currently not known. However, it is plausible that the conformational change that occurs when two HCs dock to form a gap junction, bring the channel in a distinct conformational state such that loop-tail

interaction has a different outcome. In line with this distinct conformational state, one should also consider the fact that in the resting state, gap junctions are open while HCs are closed.

It is thought that gap junction closure associated with acidosis and IR is mediated by loop-tail interaction[128,129]. Based on the observation that CT-CL interaction closes gap junctions, Verma et al. developed a series of peptides called RXP, which can bind to Cx43 CT domain and therefore prevent acidosis induced or chemically triggered cardiac gap junction closure[130]. The common feature among the series of peptides is that they share the consensus sequence of RXP (Arginine (R)- Proline (P) and any amino acid(X)). Of the series, a 34 amino acid sequence called RXP-E was found to preserve intercellular communication and action potential propagation between cardiac cells. These studies were later followed up to determine the core active sequence, which eventually led to the development of linear octapeptide RRNYRRNY[131]. The common idea behind developing RRNYRRNY and related peptides[131] was that these could be used as drugs to prevent gap junction closure and arrhythmia, in particular ventricular fibrillation, following IR injury.

Cx43 in cell death

The role and functions of gap junctions and HCs has been well documented not only in cell-cell communication but also in cell growth[132], cell differentiation and cell death[133,134], bystander cell death[119], cell adhesion[135] and cell migration[136,137].

Cx based communication has been shown to be altered during cell death. In the early phases of apoptosis, gap junctional communication is necessary[138–140]. Conversely, use of gap junction inhibitors such as carbenoxolone (Cbx) and 18β-glycerrhetinic acid (18β-GA) has been shown to prevent apoptosis[140–142]. On the other hand, tumor promoters and phenobarbital which are known to counteract apoptosis have been shown to inhibit gap junctional communication[143,144]. GJs have also been implicated in the spread of cell death signals in a phenomenon called bystander death[119,145,146], in which cell death signaling molecules spread from dying cells to neighboring healthy cells. Connexins, not just in the form of GJs but also HCs are implicated in cell death. Many signals that trigger HC opening are also involved in signaling cascades leading to cell death[147] including intracellular Ca^{2+} changes, protein oxidation and nitrosylation reactions. HCs, being essentially pores, can set off cell death by depolarizing the membrane, collapse of ion homeostasis, loss of metabolites and elevation of cytoplasmic Ca^{2+} [148,149].

The involvement of HCs in cell death, especially ischemic cell death has been demonstrated in many studies. Astrocytes and neonatal rat cardiomyocytes, when exposed to ischemia like conditions showed increased Cx43 HC opening and consequent increase in cell death[150–153]. The molecular mechanisms of HC activation by ischemia is not well known. However, studies have indicated that dephosphorylation (and consequent increased activation of HCs) and/or oxidation of protein may be responsible[150,154]. Retamal et al. have also shown that s-nitrosylation of intracellular Cx43 cysteine residues by NO leads to HC opening[154]. Activation of HCs can lead to uptake of toxic cell death signaling molecules or loss of crucial metabolites needed for cell survival[104,134,155–157].

Cx43 in the heart

In the normal heart, sarcolemmal connexins are located almost exclusively at the intercalated discs of the myocardium, where they are present as gap junction plaques surrounded by HCs[158,159]. Cx40 is present in the conduction system and atrium, and Cx45 plays a role during development and is also found in adult hearts in the conduction system and at the border between myocytes and fibroblasts[160]. Cx32, present at the atrioventricular nodal region can form functional HCs[161]. Furthermore, Cx43, Cx40 and Cx37 are also present in endothelial cells[162]. The primary role of cardiac connexins under physiological conditions is to form gap junctions which act as conduits for the conduction of electrical impulses from one cell to the other in a coordinated fashion. Of all the connexins present in the heart Cx40 and Cx43 are the major proteins involved in conduction system with Cx40 and 43 mediating the spread of excitation in the atria whereas Cx43 gap junctions are responsible for the electrical propagation in the ventricular myocytes[125,163]. The degree of electrical connectivity between the cells is in large part regulated by the open probability of gap junctions with any decrease in gap junction opening leading to shunting of the electrical pathway, which ultimately leads to arrhythmias due to lack of electrical coordination.

The phenomenon of closure of gap junctions during ischemia was first proposed by McCallister et al.[164], supported by later observations that during ischemia there are drastic changes in electrical coupling[165,166] and cytosolic dearrangements of gap junctions during ischemia[167]. These dearrangements were later shown as lateralization of Cx43 from the intercalated disc to the lateral

margins of cardiomyocytes following ischemia[168]. This lateralization is thought to be one of the causes of arrhythmias in ischemic heart disease in addition to changes in Cx expression and alterations in phosphorylation states of Cx leading to dysregulation of channel opening. During ischemia, there is a progressive increase in $[Ca^{2+}]_i$, decrease in intracellular pH, increase in protein phosphatase 1 activity, and reduced protein kinase activity- all phenomena that increase HC activity as previously described.

Lampe et al. showed that lateralized Cx43 was more dephosphorylated than Cx43 at intercalated discs[169], and this can be attributed to conduction velocity slowing and enhanced susceptibility to ventricular tachycardia in canine ventricles[170]. A mouse model of pressure overload induced hypertrophy also demonstrated heterogeneous distribution of ventricular Cx43[(171)] and also in patients with non-ischemic cardiomyopathy[172,173]. Increased localization of Cx43 HCs at the lateral membranes combined with increased opening can lead to disruption of membrane potential and unabated leakage of metabolites including ATP, leading to increased cell stress and cell death.

Recently, there have been a number of reports showing an important role for Cx43 in mitochondria and how its role is implicated in ischemia-reperfusion injury in particular. The importance of mitochondria in maintenance of cellular ion homeostasis and the newly emerging role for Cx43 which has been shown to affect ion homeostasis, at a cellular level make it all the more important to develop an overview of how Cx43 can alter this cellular homeostasis ultimately affecting cell survival and death.

Mitochondrial connexin 43: the location

Interest in cardiac mitochondrial Cx43 (mitoCx43) has only recently started given the observations made with regard to the role of mitochondria in ion homeostasis and cell death. MitoCx43 was first documented in endothelial cells, in a study that correlated the function of Cx43 with hyperhomocystinemia in which homocysteine exposed HUVECs showed an increased expression of Cx43[(174)]. Cx43 was first shown to be present in the mitochondria of cardiac ventricular myocytes[175] with the help of immunological colocalization of mitochondria and connexin 43. The specificity of the antibody used was demonstrated using a inducible knockout model for Cx43-

$Cx43^{Cre\text{-}ER(T)/fl}$ [175,176], in which Cx43 ablation is obtained by insertion of 4-hydroxytamoxufen inducible Cre recombinase into the endogenous Cx43 locus[177]. Further fractionation of the sub-populations of mitochondria from cardiomyocytes showed that Cx43 is present mostly in the subsarcolemmal mitochondria and in very limited amounts in the interfibrillar population[178].

Given the lack of a mitochondrial targeting sequence on Cx43, it is perplexing as to how Cx43 is targeted to the mitochondria. Previous studies have shown that Tom20, a member of the TOM family of proteins and heat shock protein 90 are involved in the transport and incorporation of Cx43 in the mitochondria[179]. Rodriguez-Sinovas et al.[179] and Srisakuldee et al.[30] have shown electron immunomicrographs locating Cx43 in the inner mitochondrial membrane. The Tom20 pathway transports Cx43 to the OMM, and in line with this Cx43 has been described to be also present in the OMM[176]. It is currently not known how Cx43 is transported from the OMM to IMM.

Mitochondrial Cx43 in physiological conditions

Mitochondrial Cx43 has been implicated in K^+ uptake, by the formation of a putative HC in the IMM[33]. Open HCs indeed allow the passage of common ions like Na^+, K^+, Ca^{2+} and Mg^{2+} [153]. The conclusive evidence for mitochondrial Cx43 HCs was based on the use of $Cx43^{Cre\text{-}ER(T)/fl}$ and the use of interfibrillar mitochondria, which have been shown to contain significantly less Cx43 than subsarcolemmal mitochondria[178]. The specificity of mitoCx43 playing a role in K^+ uptake was also determined by the use of connexin mimetic peptide Gap19, which interacts with the C-terminal tail (CT) of Cx43 and inhibits Cx43 HCs, while slightly promoting gap junction intercellular communication[123]. Recently, Srisakuldee et al. have shown that subsarcolemmal mitochondria (containing Cx43), isolated from hearts that were treated with FGF-2 to simulate the effect of pre-conditioning, have a higher Ca^{2+} retention capacity compared to vehicle treated hearts, implicating a role for mitoCx43 in mitochondrial Ca^{2+} homeostasis[30]. Interestingly, increased mitochondrial Ca^{2+} retention capacity was associated with a concomitant increase in mitoCx43 phosphorylation, indicating a complex interplay between cytosolic factors and mitoCx43. Several lines of evidence point to mitoCx43 as a player in Ca^{2+} and K^+ homeostasis in mitochondria, which may contribute and influence the cellular ion homeostasis. However, studies demonstrating the presence of Cx43 as a HC or HC like structure in mitochondria facilitating small ion fluxes are currently lacking and are warranted.

The other important role ascribed to mitoCx43 relates to the fact that its modulation alters respiratory complex I activity[180]. This is an important observation given the fact that mitochondrial respiratory complex I is one of the major sources of ROS during ischemia-reperfusion and modulation of the function of complex I has been demonstrated to act in a cardioprotective manner[56,181]. Some studies indicate that mitoCx43 may be implicated in the generation of ROS in the context of IPC, which will be discussed in detail in the next section. The same study shows that mitochondrial complex II activity was not affected[180]. This is also significant given the fact that complex II is a matrix protein whereas complex I is a membrane associated structure. If Cx43 is indeed associated with complex I in the IMM, Cx43 might be able to influence complex I activity, ATP production and oxygen consumption as shown by Boengler et al.[180]

Mitochondrial Cx43 – a target in pathophysiological conditions

Most studies showing that mitoCx43 is involved in affording the beneficial effects of IPC have focused on the association of Cx43 with PKC[30,182], Tom20[30,179] and HSP90[179,183].

In studies where animals were treated with IPC inducing protocols, an increased expression of mitoCx43 was observed within 20 min[175]. The authors suggest that this might be due to a change in the trafficking of Cx43 rather than a *de novo* Cx43 expression and incorporation into mitochondria, a process that is as yet still poorly understood as already mentioned. Diazoxide and menadione are known to afford cardioprotection by inducing a low level of ROS generation[31], which triggers downstream cardioprotective pathways. The sites of action of diazoxide- and menadione-stimulated ROS generation are apparently distinct, with menadione having for a larger spectrum of putative ROS generation sites than diazoxide. Heinzel et al. used heterozygous $Cx43^{+/-}$ animals to differentiate between the protective effect attributed to diazoxide vs. menadione and the implications of Cx43 in the same. Their study showed a loss of diazoxide induced cardioprotection in Cx43 deficient animals, but not in menadione treated animals, implicating a role of Cx43 in ROS induced cardioprotection, especially in IPC[184]. In a similar study, using POC, no difference between Cx43 deficient and wild-type controls was seen in infarct sizes[185] suggesting that the presence of Cx43 is required for IPC but not for POC.

In studies simulating IPC by the use of IGF-1, there was an increase in mitoCx43 along with increased cytoprotection[186]. In a recent study[30] simulating IPC by the use of FGF-2 in mice, it was observed that there was a significant increase in Ca^{2+} retention capacity of the mitoCx43 containing subsarcolemmal mitochondria and also a significant increase in mitochondrial PKC, compared to interfibrillar mitochondria, which are devoid of Cx43, providing another layer of evidence for the protective role of mitoCx43 in IPC. These observations were also supported by the use of the connexin channel inhibitor peptide Gap27, which affects gap junctions as well as hemichannels composed of Cx43 and Cx37[111,118,187,188]. A further direct evidence of the protective role of mitoCx43 was provided by Lu et al.[189] where mitochondria specific over-expression of Cx43, obtained by the use of Cx43 containing shuttle vector, simulates pre-conditioning like cytoprotection in stem cells, and they show that this cardioprotective effect is afforded by a shift in Bcl-Xl/Bak balance[190].

Further studies to explain the role of mitoCx43 in cardioprotection have shown that mitoCx43 plays a role in preventing cell death by apoptosis. Application of the non-specific connexin channel blocking agents heptanol and β-glycyrrhetinic acid (BGA), promoted Ca^{2+} release through MPTP and the subsequent release of cytochrome *c* from cardiomyocyte mitochondria[176]. Along the same line, Trudeau et al. demonstrated that down-regulation of mitoCx43 by high glucose triggers a change in mitochondrial morphology and the release of cytochrome *c,* leading to increased apoptosis in retinal cells[191]. While these studies support the concept that mitoCx43 acts in a protective manner, one should be cautious in interpreting the reported data. First, work with non-specific connexin channel inhibitors is intrinsically prone to interpretation errors as the reported effects may well relate to off-target drug effects. Second, none of the drugs or experimental manipulations, have specific effects on mitoCx43 only. One should always consider at least three different levels of connexins that can be affected: those incorporated in gap junctions in the plasma membrane, those in plasma membrane HCs and those in the mitochondria. Additionally, it should be added that gap junctions may act as a Janus face with two different sides: a side that can rescue cells under stress by providing crucial and essential metabolic molecules, and another side that promotes cell death by passing cell death messengers[119,192–194].

1.4 Mitochondrial Complex I

Mitochondrial ATP is produced by the oxidative phosphorylation machinery. OXPHOS couples the phosphorylation of ADP and electron transfer through a chain of oxidoreductase reactions. These oxidoreductase reactions are carried out by five enzymes/enzyme complexes in the IMM: NADH:Ubiquinone oxidoreductase (Complex I, CI), Succinate:Ubiquinone oxidoreductase (Complex II, CII), Ubiquinol:Cytochrome *c* oxidoreductase (Complex III, CIII), Cytochrome *C* oxidase (Complex IV, CIV) and the ATP synthase (Complex V, CV). Complex I is the biggest of five respiratory complexes and CII is the smallest. Each of these five complexes is essential and four of the five complexes CI thru CIV pump a total of 5 protons from the matrix to the intermembrane space per pump cycle, which is essential for the maintenance of the mitochondrial membrane potential. The protons flow back via CV, which acts in a reverse mode producing ATP as opposed to the normal mode where ATP hydrolysis feeds transport. In addition to their role in OXPHOS, the complexes also play important roles in generation of ROS which can either be deleterious or beneficial, based on the context and extent of their generation.

Eukaryotic CI is located in the IMM protruding into the matrix to form an "L" shaped structure. Forty five subunits are identified as comprising the bovine CI, which is closely related to human CI[195]. The subunits are named according to their apparent molecular weights (75, 51, 49, 30 and 24 kDa subunits), or for the first four amino acids of the mature protein sequences (PSST and TYKY) or for the NADH dehydrogenase products of the mitochondrial DNA (ND1 to ND6 and ND4L) 14 of these subunits are conserved and are sufficient for energy transduction[195]. The other subunits differ from species to species. The core conserved subunits form two domains supported by the supernumerary subunits. Seven of the 14 subunits are hydrophilic and constitute the redox domain and are present in the matrix and the 7 hydrophobic units are present in the IMM[196,197]. In eukaryotes, the hydrophobic subunits are mitochondrial encoded whereas the supernumerary units are nuclear encoded[198,199]. The seven hydrophilic subunits form a Y shaped domain encasing the cofactor cohort of complex I: a flavin nucleotide for NADH oxidation and a chain of 7 Fe-S clusters (one [2Fe-2S] and 6 [4Fe-4S] - labeled N1 thru N7, though not necessarily present in that order)[196]. The 7 clusters are split on either side of the flavin moiety with the 2Fe-2S cluster lying on one side of the flavin and the other 6 on the other side. The last cluster in the chain donates

electrons to the quinone[200]. Subunits ND2, ND4 and ND5 are structurally similar and are related to the subunits of Mrp family of Na^+/H^+ antiporters indicating that they are likely sites of proton transfer across the membrane. These subunits are at a significant distance away from the FeS cluster chain and the quinine binding site. Hence coupling of the redox and transport processes require long range energy transfer through the protein[201]. This long range energy transfer forms a key factor in the generation of ROS especially in IR given a lack of receptor oxygen and availability of free electrons, which in turn react with any available oxygen forming ROS and nitrogen moieties forming reactive nitrogen species (RNS). Excess ROS and RNS generation is a key deleterious event in IR injury.

Complex I in ischemia-reperfusion

Acidification of cytosol following ischemia has been shown to be the key factor behind the blockage of complex I[202]. This blockage of complex I is a precursor of mitochondrial dysfunction following IR. The consequence of blockade of complex I, during reperfusion is an increase in the production of ROS, which ultimately leads to the opening of MPTP, following various pathways such as post-translational modifications induced by ROS and ROS induced dysfunction of ion channels leading to Ca^{2+} overload, and the induction of cell death. Superoxide anion production by antimycin inhibited bovine heart mitochondrial particles with NADH was first reported by Turrens et al[35]. The site of this production was deduced as the respiratory complex I based on the observation that superoxide generation was reduced in the presence of rotenone- a complex I blocker. Takeshige et al. showed for the first time that complex I was indeed the site of formation of NADH and NADPH-dependent superoxide formation[203]. Kang et al. showed differential kinetics of superoxide formation by complex I with NADH dependent reactions being much faster than those induced by NADPH[204]. Hence numerous studies have focused on the beneficial effect of partial or complete blockage of complex I for decrease in ROS during the critical initial phase of reperfusion where there is an increase in oxygen availability.

Although complex I itself is a major source of ROS, complex III is the principal site of superoxide generation during oxidation of complex I substrates and hence the hypothesis that blockage of complex I essentially depletes complex III of the electrons needed for the generation of superoxide,

protecting the mitochondria and consequently the heart. This blockage can be achieved during ischemia or reperfusion. Blockade of electron transport at complex I by rotenone immediately before ischemia preserves respiration through cytochrome oxidase in the distal electron transport chain and significantly reduces cytochrome *c* loss from the mitochondria during ischemia[205].

As previously stated, blockage of complex I using rotenone can be a protective strategy in IR. However, since rotenone is a non-reversible blocker of complex I, this is not a permissible strategy as it would compromise resumption of normal OXPHOS needed for the recovery of cellular function. Hence Chen et al. used amobarbital, a reversible complex I blocker to block complex I activity immediately before IR and observed a significant reduction in infarct size, and decreased H_2O_2 and cytochrome *c* release[206]. In further studies, Aldakkak et al. found that even though administration of amobarbital at ischemia increased superoxide and NADH levels and decreased mitochondrial Ca^{2+}, during ischemia, superoxide levels and mitochondrial Ca^{2+} were lower and ultimately a decrease in infarct size- consistent with a decrease in complex I activity and consequent better preservation of cardiac tissue[207]. Xu et al. also showed that a transient blockage of complex I activity achieved by extracellular acidification at the onset of reperfusion also led to a better preservation of tissue following ischemic injury[202]. The protective effect of the blockage of complex I is also observed in aging induced myocardial injury and mitochondrial dysfunction[208].

1.5 Potassium channels of the IMM

As stated previously, mitochondria play an important role in energy homeostasis of the cell. Apart from this function, they are also involved in cell death and survival. The key player in this phenomenon is the integrity of the mitochondrial membranes. The strict control of IMM permeability and mitochondrial membrane potential is vital for efficient ATP synthesis, whereas a loss of this strict control is an indicator of cell death. As such, K^+ entry into the mitochondria is an important mechanism for control of IMM integrity.

Transportation of K^+ into the mitochondria occurs via ion channels, similar to cellular K^+ entry via plasma membrane channels. K^+ channels in the IMM include the mitoK_{ATP}, the voltage dependent K^+ channels (mitoKv1.3), the TWIK-related Acid Sensitive K^+ channel-3 (TASK-3) channels and the BK_{Ca} with mitochondrial connexin-43 being shown to be a player as well.

Electrophysiological evidence for the presence of mitoK_{ATP} channels was first shown by Inoue et al. on patch clamped mitoplasts (obtained by incubating mitochondria in a hypotonic solution leading to mitochondrial swelling and ultimately rupture of the OMM) where K^+ influx into the mitoplasts was blocked by matrix ATP (ATP added via the patch pipette)[209]. The channel properties were similar to those of the plasma membrane K_{ATP} channels although of much lower unitary conductance. Although no other studies have been able to demonstrate the same channel activity in mitoplasts, Paucek et al. purified and incorporated a 54kDa channel in planar lipid bilayers that was sensitive to ATP[210]. An interesting finding in these studies was that the channel exhibited polarity: ATP added to the *trans* but not the *cis* chamber inhibited the channel. These studies were later replicated by Zhang et al. who furthermore showed that MgATP inhibited the channel in a dose dependent manner and that they were activated by GTP, but only when added to the *trans* side of the bilayer[211].

Mitochondrial voltage gated channels of the Kv1.3 type were reported for the first time by Szabo et al. in mitoplasts as channels with a unitary conductance of ~17pS and inhibited by margatoxin- a Kv1.3 selective toxin[212]. The channel exhibited properties similar to the Kv1.3 channel of the plasma membrane.

TASK- is a two pore K^+ channel, identified in the mitochondria of melanoma and keratinocyte cells by immunochemical and molecular biology methods[213]. Mitochondrial localization of functional TASK-3 was shown by Toczilowska-Maminska using mitoplasts from HaCaT keratinoycte cell lines with a single channel conductance of 83pS at positive voltages and 12pS at negative voltages in symmetric 150mM KCl. Lidocaine and acidic pH, known to inhibit plasma-membrane TASK-3 completely blocked channel activity[214].

The role of Cx43 in mitochondrial K^+ uptake was first demonstrated in permeabilized cardiomyocytes by Miro-Casas et al.[215] They showed that in isolated and permeabilized cardiomyocytes K^+ uptake could be inhibited by 18α-glycerrhetinic acid a non-specific connexin channel blocker. This was taken to a further level by Boengler et al. who determined K^+ uptake in cardiac mitochondria and found reduced uptake in the presence of the specific Cx43 HC blocking peptide Gap19 and in mitochondria isolated from induced Cx43 knock down animals ($Cx43^{ER(T)/fl}$ mice)[33].

Ca^{2+} sensitive K^+ channels were first discovered in red blood cells where their activation results in hyperpolarization and cell shrinkage[216]. K_{Ca} currents were first described in the nervous system in mollusc neurons[217] and cat spinal motor neurons[218]. It was shown in non-innervated skeletal muscle that afterhyperpolarization following action potential burst was mediated by K_{Ca} channels of small conductance. One of the differentiating factors between K_{Ca} channels is their antagonists, for example, BK_{Ca} channels are blocked by iberiotoxin[219] and SK_{Ca} are blocked by apamin[220], with their sensitivity to antagonists being highly selective. The other difference between the BK_{Ca} and SK_{Ca} channels is that BK_{Ca} is voltage and Ca^{2+} dependent whereas SK_{Ca} is voltage independent and is only regulated by Ca^{2+} [(221)].

K_{Ca} channels were first detected in mitochondria from human glioma cells in 1999 by Siemen et al. using mitoplast patch clamp experiments[222]. The channels showed a conductance of 300 pS and were inhibited by the K^+ channel blocker iberiotoxin and charybdotoxin resembling the properties BK_{Ca} channels of the plasma membrane. These channels were first described in cardiac mitochondria by Xu et al. where the K_{Ca} opener NS1619 accelerated K^+ uptake into mitochondria and the toxins- iberiotoxin and charybdotoxin blunted this uptake[223]. They also showed that

antibodies against BK type K_{Ca} channel cross react with purified mitochondrial membrane. Other studies have also shown indirect evidence for the presence of these channels in the mitochondria by the use of channel openers and their effect on cardioprotection[32,224].

SK_{Ca} have been described to-date in neurons in the central nervous system, in skeletal muscle cells, glandular cells and T lymphocytes, and their distribution among various tissues is splice variant dependent[225,226]. Although voltage independent, the current voltage relationship of SK_{Ca} shows an inward rectification that is the consequence of voltage dependent block by intracellular divalent cations. At positive membrane potentials Ca^{2+} not only activates the channel but also blocks it in a concentration dependent manner. Low [Ca^{2+}] (300-700nM) activates SK_{Ca} channels with Hill coefficients of 3-5, suggesting that the binding of more than one Ca^{2+} ion is necessary for channel activation[227]. Ca^{2+} binding to the SK_{Ca} also requires each α subunit to be linked to calmodulin (CaM), at a region called the CaM binding domain[228]. Ca^{2+} binding to CaM induces conformational changes in CaM, which in turn results in a conformational change of the α-subunit leading to opening of the channel.

Mitochondrial potassium channels and IR injury

Electrophoretic influx of K^+ into the mitochondria causes membrane depolarization, matrix alkalinization and matrix swelling. Each of these effects, individually or synergistically are associated with an increase in production of ROS. ROS generation, as previously explained is a critical feature in induction of IPC. Mitochondrial K^+ channels, especially mitoK_{ATP} and BK_{Ca} have been demonstrated to be linked to the induction of IPC.

Garlid et al. first described that most of the K_{ATP} openers affected not only plasma membrane K_{ATP} channels but also those present in mitochondria (mitoK_{ATP} channels)[31], suggesting that mitoK_{ATP} was a major player in IPC and cardioprotection[25]. K_{ATP} channel openers indeed mimic IPC while K_{ATP} channel blockers prevent IPC induced protection. Auchampach et al. showed that glibenclamide and 5-hydroxydecanoate (5-HD), two K_{ATP} channel blockers, abolished the protective effect of IPC[229]. Yao and Gross further showed that a combination of subthreshold IPC and subthreshold dose of bimakalim (another K_{ATP} opener) protected against ischemic injury[230].

Various other studies confirmed the deleterious effect of K_{ATP} blockers on IPC protection in rabbits, rats, pigs and man[230,231]. The role of K_{ATP} channels in Ca^{2+} pre-conditioning (CPC) was shown by Kouchi et al.[232]. It needs to be added that most of these studies presumed that the protective effect afforded by K_{ATP} channel openers was due to their effect on the sarcolemmal K_{ATP} channels. Opening of sarcolemmal K_{ATP} shortens action potential duration (APD) and thereby reduces Ca^{2+} entry and the risk of cellular Ca^{2+} overload, thus acting in a cardioprotective manner. As already mentioned before, Garlid et al. showed that most of the K_{ATP} openers also opened mitoK_{ATP} channels[31], putting mitoK_{ATP} forward as a player in IPC. They followed these observations by studies demonstrating that cardiac sarcolemmal K_{ATP} channels were insensitive to diazoxide and 5-HD whereas mitoK_{ATP} channels were sensitive to both drugs.

A primary mechanism involved in IR injury is an increase in intracellular Ca^{2+} concentration, as has been previously mentioned. Yang et al. reported a decrease in endothelial SK_{Ca} currents following 60 min ischemia and 30 min reperfusion in porcine arteries[233] suggesting the importance of SK_{Ca} channel activity in protection of the endothelium following IR. The protection of myocardium, by the protection of endothelium is linked primarily to the generation of NO by eNOS and the endothelial derived hyperpolarizing factor (EDHF), which maintains vascular tone preventing hypercontracture and maintaining oxygenation of the tissue. By maintenance of SK_{Ca} channel activity, EDHF mediated vasorelaxation can be preserved, which is critical in mitigating cardiac myocardial damage during IR. Endothelial membrane hyperpolarization as a result of SK_{Ca} opening is conducted along the endothelium via homocellular endothelial gap junctions and transmitted to smooth muscle cells through myoendothelial gap junctions to cause vasodilatation, thus affording the protection[234].

The protective effect of SK_{Ca} channel opening is not restricted to the cardiac tissue. In studies involving global cerebral ischemia in mice, Allen et al. showed that SK2 channel opening, achieved via the use of 1-EBIO, reduced CA-1 neuronal cell death and improved cognitive outcome[235].

Tanabe et al. showed apamin sensitive K_{Ca} current in CA3 pyramidal neurons and that its blockage was associated with a cellular Ca^{2+} overload inducing an ischemia like effect[236]. On the other hand

they also showed that opening of these apamin sensitive channels was cytoprotective. In contrast, Cipolla & Godfrey showed that the reduction in basal tone of cerebral parenchymal arterioles following IR injury was reversed by the use of SK_{Ca} blocker apamin[237], indicating that SK_{Ca} channel is activated by IR. Yang et al. also showed that application of apamin on cerebral arterioles increased their basal tone[238] indicating the important role of SK_{Ca} in regulation of muscle tone of the vasculature.

The PPC like effect observed by the use of K_{Ca} channel openers has been known but the mechanism is not fully known. The findings by Siemen et al. and Xu et al. showing the protective effect of BK_{Ca} channel opener NS-1619 against IR injury led to the theory that the channel openers act upon the mitochondrial BK_{Ca} similar to the effect of diazoxide. Stowe et al. showed that cardiac mitochondrial pre-conditioning is afforded by the opening of the BK_{Ca} and also that it is dependent on the production of superoxide radicals produced during ischemic injury[32]. Heinen et al. showed that BK_{Ca} channel opening increases mitochondrial respiration and in turn enhances the production of ROS, while maintaining the mitochondrial membrane potential[224]- a critical feature of protection against IR injury. However, in a follow up study they showed that ROS production induced by reverse electron flow observed during ischemia is attenuated by the activation of mitoK_{Ca} channels[239]. They argue that ROS produced by complex I, a major source of ROS in contrast to complex III are effected by the opening of mitoK_{Ca} channels. The observation that NS-1619, a BK_{Ca} opener has a biphasic effect on mitochondrial respiration, membrane potential and superoxide generation leads to the hypothesis that other mitoK_{Ca} channels can also play a role in PPC.

Chapter 2
Aims

The role of mitochondrial ion channels and respiratory complexes in the development of ischemia-reperfusion induced damage on cardiac tissue is a wide field with novel players being discovered on a regular basis. In order to develop effective therapeutics and treatment modalities for ischemic injury, it is imperative to study and characterize these novel as well as established factors. Based on this premise, and the hypothesis that maintenance of mitochondrial ion and energy homeostasis of the cell is crucial for cell survival in cases of oxidative stress such as ischemia-reperfusion injury, the aims of the study were formulated.

1. Mitochondrial Cx43 forms hemichannels that contribute to calcium entry and cell death

Ashish K. Gadicherla, Nan Wang, Marco Bulic, Esperanza Agullo-Pascual, Alessio Lissoni, Maarten A. De Smet, Mario Delmar, Dmitri V. Krysko, Amadou Camara, Klaus-Dieter Schlüter, Rainer Schulz, Wai-Meng Kwok, Luc Leybaert. *Manuscript in preparation.*

- Mitochondrial ion homeostasis is maintained by a myriad of factors including ion channels/transporters, mitochondrial inner membrane potential and mitochondrial matrix pH. Each of the transporters and ion channels are influenced by, and can influence, the membrane potential and consequently the matrix pH leading to a tightly regulated sequence to maintain ion homeostasis[24,25]. Of crucial importance in maintenance of cellular energy and ion homeostasis is the mitochondrial balance of calcium and potassium involving channels and/or transporters. Mitochondrial Cx43 has been shown to be involved in homeostasis of potassium and calcium[33,215,240,241], albeit without a direct attribution of its mitochondrial presence as a channel. Mitochondrial Cx43 has also been shown to play a major indirect role in IPC[184]. In the present work, I started form the hypothesis that mitochondrial Cx43 may act as a Ca^{2+}-permeable channel, facilitating mitochondrial Ca^{2+} entry and leading to increased mitochondrial Ca^{2+} and thus cell death. I investigated this hypothesis by various approaches, including uptake studies of hemichannel-permeable dyes, biophysical analysis of channels reconstituted from Cx43 protein isolated from cardiomyocytes, mitochondrial Ca^{2+} imaging studies, cell death studies, *in vitro* hypoxia-reoxygenation studies and *ex vivo* ischemia-reperfusion studies. Central to my approach was the use of various inhibitors of connexin channels and/or hemichannels. Most of these

inhibitor tools were peptides identical to sequences of the Cx43 protein (mimetic peptides)[242]. I also investigated the effect of RRNYRRNY peptide (RRNY) on Cx43 hemichannels. RRNY is a non-mimetic peptide, which was designed based on the pharmacophore of the interaction of the loop of Cx43 with the tail of the protein (loop-tail interaction)[131]. This peptide was shown previously to prevent gap junction closure under ischemic conditions by disrupting loop-tail interactions. Here, I hypothesized that RRNY would in fact inhibit Cx43 hemichannels, based on its loop-tail interaction preventive effect. These investigations are the subject of the first manuscript of this thesis, which is also the core of my doctoral research work performed in the Physiology group at Ghent University, Belgium, in collaboration with the Medical College of Wisconsin, USA.

2. Damage to mitochondrial complex I during cardiac ischemia-reperfusion injury is reduced indirectly by anti-anginal drug ranolazine

Ashish K. Gadicherla, David F. Stowe, William E. Antholine, Meiying Yang, and Amadou K.S. Camara.

Biochim Biophys Acta. 2012 March; 1817(3): 419–429

- The role of mitochondrial complex I in cellular energy homeostasis and also in the generation of ROS during IR injury is well known, with pharmacological agents blocking its activity during IR injury being shown to reduce IR injury[205,206]. However, most of the pharmacological agents studied so far bind to complex I irreversibly, causing permanent dysfunction of complex I. Some pharmacological agents, such as ranolazine, a clinically used anti-anginal drug[243–247] have been shown to reduce complex I activity, based on the observation of decreased ROS generation in ranolazine treated mitochondria[56]. However, the mechanism by which ranolazine acts to reduce ROS generation is far from understood. In order to study the protective effect attributed to ranolazine via complex I, I studied the structural/functional aspects of complex I, how electron flow through complex I can be maintained, and how structural integrity of mitochondrial membrane can be maintained by the use of ranolazine during IR injury in guinea pig isolated hearts. These aspects were published in the form of a manuscript. The work published in the manuscript was performed at Mitochondrial Biology Lab, at the Medical College of Wisconsin

3. Protection against cardiac injury by small Ca^{2+}-sensitive K^+ channels identified in guinea pig cardiac inner mitochondrial membrane

David F. Stowe, **Ashish K. Gadicherla**, Yifan Zhou, Mohammed Aldakkak, Qunli Cheng, Wai-Meng Kwok, Ming Tao Jiang, James S. Heisner, MeiYing Yang, Amadou K.S. Camara
Biochim Biophys Acta. 2013 February; 1828(2): 427–442

- IPC as a protective mechanism against IR injury has been shown to involve many players, including mitochondrial inner membrane potassium channels such as the K_{ATP}, and K_{Ca} channels[3]. PPC has also been shown to involve mitochondrial potassium channels, specifically the BK_{Ca}[32,224]. Previous studies have indicated that NS-1619, a BK_{Ca} channel opener, induces PPC[32]. NS-1619 has been shown to induce a bi-phasic effect on mitochondrial ROS generation and bio-energetics, respiration and ATP generation, in isolated cardiac ventricular mitochondria[224]. However, given the absence of BK_{Ca} in the cardiac mitochondrial inner membrane, it is likely that NS-1619 exerts its protective effect through a different K_{Ca} channel. With the aim of determination of this mitochondrial target of NS1619's protective effect, I identified a novel channel- the SK_{Ca} in the cardiac ventricular mitochondria using confocal and electron microscopy techniques followed by the characterization of purified channel in planar lipid bilayers. I also demonstrated that activation of SK_{Ca} by the use of DCEBIO resulted in preserved mitochondrial bioenergetics and improved hemodynamic parameters following IR, which were reversed when DCEBIO was co-administered with SK_{Ca} antagonist NS8593. The work published in the manuscript was performed at Mitochondrial Biology Lab, at the Medical College of Wisconsin.

Chapter 3
Experimental work

3.1 Mitochondrial Cx43 forms hemichannels that contribute to calcium entry and cell death

Ashish Kumar Gadicherla[1], Nan Wang[1], Marco Bulic[2], Esperanza Agullo-Pascual[3], Alessio Lisoni[1], Maarten De Smet[1], Mario Delmar[3], Dmitri V. Krysko[4], Amadou Camara[5], Klaus-Dieter Schlüter[2], Rainer Schulz[2], Wai-Meng Kwok[5], Luc Leybaert[1]

[1]Physiology Group, Department of Basic Medical Sciences, Faculty of Medicine & Health Sciences, Ghent University, 9000 Ghent, Belgium

[2]Physiologisches Institut, Justus-Liebig-Univiersität Giessen, Giessen, Germany.

[3]The Leon H Charney Division of Cardiology, New York University School of Medicine. New York, NY, USA

[4]Inflammation Research Center, VIB, Ghent, Belgium and Department of Biomedical Molecular Biology, Ghent University, Ghent, Belgium

[5]Department of Anesthesiology, Medical College of Wisconsin, Milwaukee, WI 53226, USA

Corresponding author:

Luc Leybaert,

De Pintelaan 185 (Block B, Rm 031), 9000 Ghent, Belgium

Telephone: +32 9 332 3366

Fax: +32 9 332 3059

Luc.Leybaert@UGent.be

Abstract

Mitochondrial connexin 43 (Cx43) plays a key role in cytoprotection caused by repeated exposure to short periods of non-lethal ischemia/reperfusion, a condition known as ischemic preconditioning. However, connexins form channels that are calcium (Ca^{2+}) permeable and may also potentially lead to mitochondrial Ca^{2+} overload and cell death. Here, we studied the role of Cx43 in facilitating mitochondrial Ca^{2+} entry and investigated its downstream consequences. To that purpose, we used various connexin targeting peptides interacting with extracellular (Gap26) and intracellular (Gap19, RRNYRRNY) Cx43 domains and tested their effect on mitochondrial dye- and Ca^{2+}-uptake, electrophysiological properties of plasmalemmal and mitochondrial Cx43 channels, and cell injury/cell death. Our results in isolated mice cardiac subsarcolemmal mitochondria indicate that Cx43 forms hemichannels that contribute to Ca^{2+} entry and may trigger permeability transition and cell injury/death. RRNYRRNY displayed the strongest effects in all assays and inhibited plasma membrane as well as mitochondrial Cx43 hemichannels. RRNYRRNY also strongly reduced the infarct size in *ex vivo* cardiac ischemia-reperfusion studies. These results indicate that Cx43 contributes to mitochondrial Ca^{2+} homeostasis and is involved in triggering cell injury/death pathways.

Keywords:

Mitochondria/Connexin43/Ischemia/Calcium/peptidomimetics

1. Introduction

Cardiac mitochondria play a crucial role in the maintenance of cellular bioenergetics and intracellular ion homeostasis, especially of calcium (Ca^{2+}) and potassium (K^{+}) ions. Cellular Ca^{2+} homeostasis is maintained in a very stringent manner by the cyclical uptake and release by the endoplasmic reticulum and mitochondria respectively[248]. These cyclical events are crucial to maintain the cardiac rhythm and any disturbance may lead to arrhythmia, cell death and tissue damage as observed in cardiac failure and ischemia-reperfusion injury[249]. Recent evidence points to a role of connexin 43 (Cx43), a plasma membrane protein involved in intercellular communication and in mitochondrial homeostasis of Ca^{2+} and K^{+} [33,215,240,241]. Mitochondrial Cx43 (mitoCx43), located in subsarcolemmal mitochondria (SSM) but not in interfibrillar mitochondria (IFM)[178] , is known for its role in ischemic preconditioning, which acts cardioprotectively as a result of brief ischemia/reperfusion episodes preceding a long lasting index ischemia (ischemic period lasting longer than 5 minutes). MitoCx43 is also involved in protection and survival of stem cells transplanted in the infarcted heart[186,189,190]. In contrast, protection by POC, meaning exposure to sublethal doses of ischemia/reperfusion after a long lasting index ischemia, is Cx43-independent[185]. Protection by mitoCx43 has been linked to reactive oxygen species (ROS) generation, mitochondrial K_{ATP} channels[182], PKC signaling and stimulation of translocase of outer membrane-20 (Tom20) that facilitates Cx43 transport[30,179,182,183,250,251]. Diazoxide that promotes mitochondrial ROS generation, induces preconditioning-like cardioprotection in a Cx43-dependent manner[184]**.** PKC phosphorylates mitoCx43[30,252], whereas heat shock protein-90 (HSP90) stimulates the TOM20 pathway mediating rapid Cx43 translocation to the inner mitochondrial membrane[178,179,186]. PKC is also involved in fibroblast growth factor-2 (FGF-2) induced preconditioning and cardioprotection, with protection linked to increased mitochondrial Ca^{2+} retention capacity[30]**.**The latter study indicates that mitoCx43 protects by mitigating Ca^{2+} overload, mitochondrial permeability transition and cell death. In principle, Cx43 hemichannels (HCs) are non-selective large conductance (200-220 pS)[111,116] Ca^{2+}-permeable channels that may facilitate mitochondrial Ca^{2+} entry[253–256]. Inner mitochondrial membrane Cx43 has indeed been proposed to be present as a hexameric HC[179]. Thus HCs might directly contribute to mitochondrial Ca^{2+}entry/overload, permeability transition and cell death. In the present work we explored the role of mitoCx43 HCs as a mitochondrial Ca^{2+} entry pathway leading to cell injury and cell death.

We used isolated cardiac mitochondria and applied various approaches including dye uptake studies, mitochondrial Ca^{2+} imaging, patch-clamp and lipid bilayer studies to investigate HC function. Additionally, we applied various Cx43 modulatory peptides and characterized their effect on mitoCx43 HCs. In particular we used Gap26 as a connexin channel blocker that targets Cx43 but also other connexins and Gap19 as a specific Cx43 HC blocker[111] (Fig. 1A). We included RRNYRRNY (RRNY) peptide that was developed as a tool to prevent gap junction closure and risk of post infarct ventricular arrhythmia[131,257]. RRNY design was based on the pharmacophore for the binding of the Cx43 cytoplasmic loop (CL) to the C-terminal tail (CT) (loop-tail interaction), an interaction that closes gap junction channels possibly by a ball and chain mechanism[131]. RRNY binding to the CT prevents loop-tail interaction and thus prevents gap junction closure, f.e. as induced by acidosis[131]. We recently reported that the gap junction closing loop-tail interaction is actually necessary for Cx43 HC opening in response to trigger conditions[111,116]. As a consequence, we hypothesized that RRNY is a Cx43 HC inhibitor as it will prevent loop-tail interaction and impose upon Cx43 HCs a state that is unavailable for opening. Our data show for the first time that mitoCx43 HCs contribute to mitochondrial Ca^{2+} entry, with subsequent activation of permeability transition and cell death. RRNY potently inhibited opening of Cx43 HCs in the plasma membrane as well as in mitochondria. It also strongly protected against ischemia-reperfusion injury in isolated cardiomyocytes and in Langendorff perfused hearts. Thus, the family of Cx43 channels provide three distinct pathways that may contribute to cell dysfunction/cell death: by gap junction-mediated bystander effects[119,193,194], by a plasma membrane HC leakage pore[116] and by mitochondrial HC Ca^{2+} entry. In heart, RRNY protects by its HC blocking repertoire while its gap junction promotive effect may protect against loss of conduction and induction of arrhythmia.

2. Results

2.1 Mitochondrial labeling of Cx43, native detection and mitochondrial dye uptake

Mitochondria isolated from mice ventricles were loaded with the mitochondrial dye mitotracker red and subsequently immunostained for Cx43. Cx43-positive mitochondria were observed in the

mixed mitochondrial preparation and were significantly more numerous in the SSM fraction compared to the IFM fraction (64 ± 6% in SSM versus 23 ± 4 % in IFM; n = 6; $p<0.05$) (Fig.1B), as reported by others[178].

In order to determine the molecular associations of Cx43 in the mitochondria, SSM were solubilized in digitonin and dodecylmaltoside under native conditions and electrophoresed. Probing with Cx43 antibody showed that Cx43 is present at 1MDa and 250 kDa molecular weights indicating that it is present as a complex. Probing the same membrane with antibody against Complex I subunit NDUFA9 revealed a band at 1 MDa indicating that Cx43 and complex I co-migrated (Fig.1C). Other commonly attributed mechanistic associations of Cx43 such as GSK-3β, CAM-KII and PKC-ε[258] could not be detected at those bands. This suggests the 250 kDa band may represent the hexameric form of Cx43 (6 x 43 kDa) corresponding to the HC (connexon) configuration of the protein.

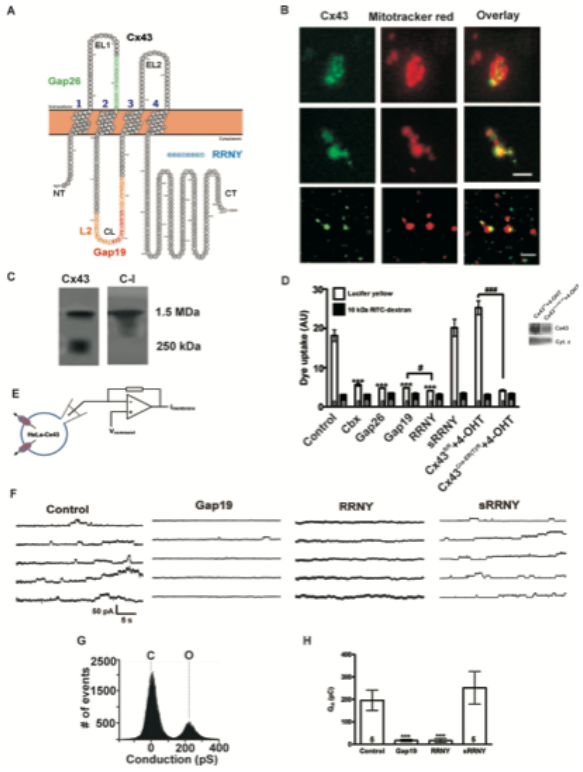

Fig. 1. Connexin-targeting peptides, mitochondrial Cx43 and characterization of RRNY. (A) Peptides used in this study. Gap26 (green) is identical to a 13 amino acid sequence on the extracellular loop 1 (EL1) of Cx43 while Gap19 (red) is a sequence from the cytoplasmic loop (CL). RRNY (blue) was developed based on RXP-E peptide (not shown), which itself derives from L2 peptide[126,257]. The L2 sequence (orange) on Cx43 includes the Gap19 sequence. NMR studies on a cyclic RRNY analogue has indicated interaction with various sites on the C-terminal tail (CT) of

Cx43[130] (B) Cx43 immunostaining of isolated cardiac ventricular mitochondria loaded with mitotracker red. Top panels are images obtained from mixed (SSM/IFM) mitochondria, middle panels are SSM and lower panels show super resolution imaging of SSM. (C) SSM isolated from mouse cardiac ventricles solubilized under native conditions were analyzed for Cx43. Bands at approximately 1 MDa and 250 kDa were observed, suggesting that Cx43 exists in a HC like structure. (D) Uptake of Cx43 HC permeant Lucifer Yellow (LY, 50 μM) and HC impermeant 10 kDa RITC dextran (10 μM) were measured in the presence and absence of Cx43 HC modulators to determine if mitoCx43 forms functional channels. Cbx, Gap26, Gap19 and RRNY all blocked LY uptake while not affecting 10 kDa RITC dextran uptake. LY dye uptake was absent in mitochondria from Cx43 deficient Cre/Flox animals while normal in Flox/Flox control animals (both receiving tamoxifen, 4-OHT). *** indicates $p<0.005$ vs. Control. Scale bar= 2.5μm. Western blot at the right illustrates Cx43 knock-down in Cre/Flox 4-OHT mitochondria compared to Flox/Flox control. (E) Patch-clamp recording setup used for experiments shown in F-H. (F) Representative current traces of patch-clamp experiments on Cx43 expressing HeLa cells in control and with peptides (voltage steps from -30 to +60 mV; Gap19 and RRNY added to the pipette solution at 100 μM). (G) Conductance histogram showing opening activity characterized by a single channel conductance of ~220 pS (control). (H) Summary data of unitary current charge transfer (Q_m) illustrating strong inhibition by Gap19 and RRNY (n =6). ** indicates $p<0.01$ vs. Control.

To determine whether the mitochondrial HCs were open, we performed dye uptake studies on SSM suspensions with HC permeable Lucifer yellow (LY; MW 457, 50 μM) and HC impermeable 10 kDa RITC-dextran (50 μg/ml). Fig. 1D demonstrates strong LY uptake, without any stimulation, while uptake of the 10 kDa RITC-dextran was very low. Carbenoxolone (Cbx, a non-specific Cx channel blocker; 100 μM), Gap26 (a peptide Cx channel blocker with rapid effects on HCs and slower effects on gap junctions; 100 μM[111], Gap19 (a specific Cx43 HC blocker which does not inhibit gap junctions; 100 μM[123]) and RRNY peptide (100 μM) all strongly (3-4 fold) reduced LY uptake while having no effect on 10 kDa RITC-dextran uptake (Fig.1D). Of all substances tested, RRNY had the strongest effect. Control scrambled RRNY peptide did not inhibit LY or RITC-dextran uptake. LY uptake was also strongly (6 fold) reduced in mitochondria isolated from $Cx43^{Cre\text{-}ER(T)/fl}$ mice treated with tamoxifen (tamoxifen inducible Cx43 KO) compared to uptake in control $Cx43^{fl/fl}$ animals receiving tamoxifen (Fig. 1D). Fig. 1D inset illustrates Western blot analysis demonstrating 73 ± 8% knockdown of mitoCx43 (~4 fold reduction) in tamoxifen treated $Cx43^{Cre\text{-}ER(T)/fl}$ mice compared to tamoxifen treated $Cx43^{fl/fl}$ control animals (n = 6; $p<0.05$).

Because RRNY inhibited mitochondrial dye uptake as all other Cx channel inhibitors, we tested its HC-blocking potential in single channel patch-clamp recordings on HeLa cells stably transfected with Cx43. Fig. 1E-H demonstrate that Gap19 and RRNY strongly inhibit plasma membrane unitary current activity characterized by a single channel conductance of ~220 pS, which is typical for Cx43 plasma membrane HCs in HeLa cells.

2.2 Electrophysiological characterization of mitoCx43 using planar lipid bilayers

We performed further studies on purified mitoCx43, isolated from mice cardiac ventricles and incorporated into planar lipid bilayers (Fig. 2A). The experiments demonstrated a linear voltage dependence characterized by a single channel conductance of 132 ± 13 pS (n = 6 isolations from different animals) (Fig. 2C and D). Gap19 and RRNY (concentrations as used for dye uptake) significantly reduced the open probability of single channel activity; reduction by RRNY was 3 fold, significantly stronger as compared to Gap19 (Fig. 2B and E). We investigated the effect of dephosphorylation of Cx43 by adding alkaline phosphatase (100 units, cis compartment) and found it to increase open probability by a factor of 3 (Fig. 2B and E).

We repeated the lipid bilayer experiments with plasmalemmal instead of mitoCx43 purified from cardiac ventricles. These experiments showed a single channel conductance of 206 ± 26 pS (n = 6) (Fig. 2G), close to the ~200 pS we observed previously in pig ventricular cardiomyocytes[111,123]. Gap19 and RRNY significantly reduced open probability (~3 fold for RRNY which acted most potently), as observed in the experiments with mitoCx43 (Fig. 2F and H). Similar to mitoCx43, and in line with reports from others on plasma membrane Cx43 HCs[259,260], dephosphorylation of Cx43 from plasma membrane also significantly increased the channel open probability (Fig. 2F and H).

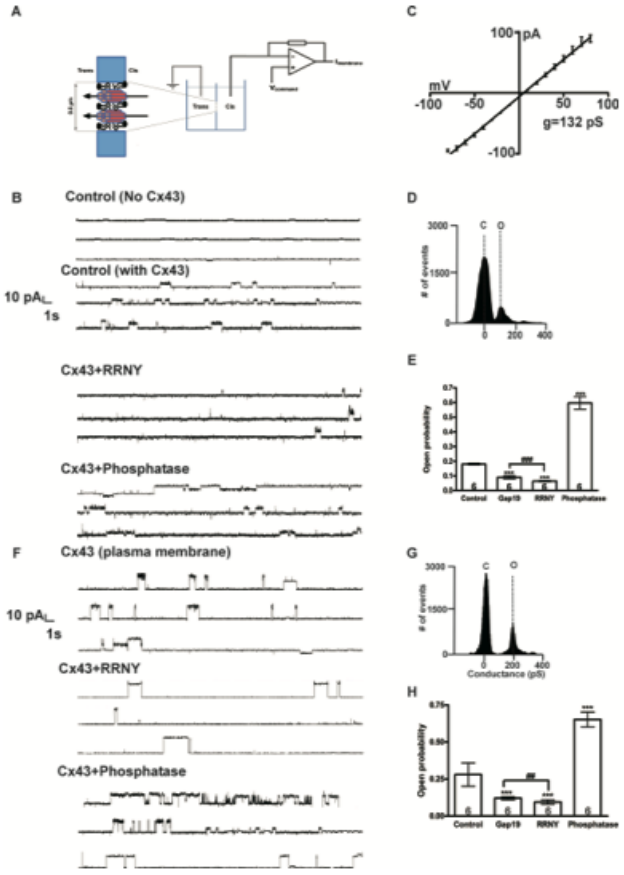

Fig. 2. Electrophysiological characterisation of mitochondrial Cx43 in planar lipid bilayer experiments. (A). Schematic view of the experimental setup with voltage clamp amplifier. Voltage steps to +50 mV and compounds tested were added at the cis side (B) Example traces of SSM-derived Cx43 incorporated into the lipid bilayer under control conditions and in the presence of RRNY or phosphatase. (C) I-V plot demonstrating that unitary event activity in the traces is characterized by a single channel conductance of 132 pS (n=6). (D) All point histogram of control traces demonstrating single channel conductance of 130 pS. (E) Summary data demonstrating Gap19 and RRNY inhibition of channel open probability; alkaline phosphatase strongly increased the open probability. (F) Example traces of plasma membrane-derived Cx43 incorporated into the lipid bilayer under control conditions and in the presence of RRNY or phosphatase. (G) All point histogram of control traces demonstrating single channel conductance of 200 pS. (H) Summary data demonstrating Gap19 and RRNY inhibition and phosphatase promotion of channel open probability. * indicates $p<0.05$ vs. Control.

2.3 Cx43 mediated mitochondrial Ca^{2+} uptake and labeling of mitochondria with FITC-Gap19

Cx43 has been suggested to play a role in mitochondrial Ca^{2+} uptake[30]. Moreover, Cx43 HCs are Ca^{2+} permeable[255] and so we further investigated intramitochondrial changes in Ca^{2+} concentration in response to externally applied Ca^{2+} pulses. To that purpose, we seeded

mitochondria preloaded with the low affinity Ca^{2+} indicator Rhod-FF on poly-L-lysine coated coverslips and recorded their response to perfusion with 50 μM free Ca^{2+} containing buffer on a Ca^{2+} imaging microscope (Fig. 3A). The area under the curve (AUC) of the Ca^{2+} transients recorded in IFM was significantly (3 fold) larger compared to those in SSM (Fig. 3B-E). Moreover, treatment with ruthenium red and verapamil to block Ca^{2+} entry via the mitochondrial Ca^{2+} uniporter (MCU) and Na^{+}/Ca^{2+} exchanger[261] respectively, strongly suppressed the AUC of the Ca^{2+} transients in IFM and had a small yet significant effect in SSM (Fig.3D-E).

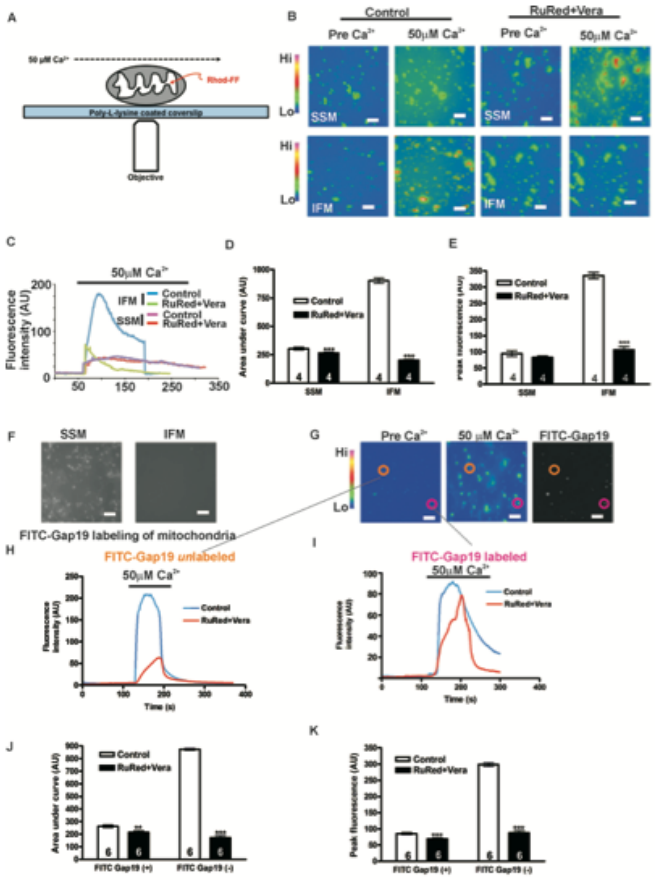

Fig. 3. Mitochondrial Ca^{2+} imaging experiments. (A) Schematic diagram of the setup. Cardiac ventricular mitochondria loaded with Ca^{2+} sensitive dye Rhod-FF, and immobilized on poly-lysine coated coverslips were perfused with experimental buffer and exposed to 50 μM free Ca^{2+} pulses. (B) Differential responses of SSM and IFM to the Ca^{2+} challenge. Mitochondrial Ca^{2+} responses in SSM (top four images) and IFM (bottom four) under control conditions and in the presence of ruthenium red (RuRed) and verapamil (Vera). (C) Representative Ca^{2+} traces recorded from imaging experiments as shown in B. (D) Summary data of mitochondrial Ca^{2+} accumulation (measured as AUC in the Ca^{2+} traces). Treatment with RuRed and Vera added 2 min before Ca^{2+} perfusion significantly reduced the mitochondrial Ca^{2+} accumulation (AUC bar chart on left) and peak fluorescence (bar chart on right) associated with Rhod-FF. The decrease in AUC and peak fluorescence was much more in IFM compared to SSM. (B) In order to separate the two populations from a mixed population, following Ca^{2+} challenge, mitochondria were perfused with FITC-Gap19. Only SSM, which contain Cx43 are labeled with FITC-Gap19 whereas IFM, which do not contain Cx43, are not labeled (gray scale images). Representative traces obtained from point analysis of labeled and unlabeled

particles are shown. RuRed and Vera. were used at 20 µM concentration in experimental buffer Peptides and Cbx were used at 100 µM concentration. * indicates $p<0.05$ vs. Control. Scale bar= 20µm

To limit mitochondrial processing steps, we repeated these experiments on mixed populations of mitochondria and stained them, after Ca^{2+} imaging, with 100 µM FITC-labeled Gap19. Gap19 binds to the C-terminal end of Cx43 with an affinity of ~2.5 µM[123]. Validation experiments on separated mitochondrial fractions demonstrated that FITC-Gap19 fluorescence was only observed in the SSM fraction while not in IFM (n=4) (Fig.3F). Moreover, Ca^{2+} imaging on mixed mitochondria followed by trace analysis in FITC-Gap19 positive and negative mitochondria demonstrated the same responses to ruthenium red and verapamil as observed when experiments were done in separated SSM/IFM fractions (Fig.3G-K). We applied the FITC-Gap19 staining procedure for the Ca^{2+} imaging experiments described next.

2.4 Mitochondrial Ca^{2+} entry is significantly affected by Cx HC inhibitors

We tested the effect of HC block on mitochondrial Ca^{2+} transients triggered by Ca^{2+} 50 µM pulses. These experiments were done in the presence of ruthenium red and verapamil to reduce background Ca^{2+} changes via the MCU and Na^{+}/Ca^{2+} exchanger. In FITC-Gap19 positive mitochondria, the AUC and peak fluorescence of the Ca^{2+} transients were significantly reduced by Cbx, Gap26, Gap19 and RRNY, while scrambled RRNY peptide had no effect (Fig.4A, C-F). In contrast, analysis of traces from FITC-Gap19 negative mitochondria demonstrated no significant change in AUC (Fig. 4B).

We further analysed the kinetics of mitochondrial Ca^{2+} changes. The rise time (from 10 to 90 %, t_{10-90}) was significantly prolonged by HC block, most strongly by RRNY (Fig. 4E). Some traces showed an abrupt drop of Ca^{2+} indicator fluorescence during exposure to the 50 µM Ca^{2+} pulse (Fig. 4A). All blockers prolonged the time from the onset of the Ca^{2+} change to the sudden drop of fluorescence; the effect was most pronounced for RRNY which prolonged the duration by a factor of 9 (Fig. 4F). By contrast, sRRNY did not alter t_{10-90} and Ca^{2+} transient duration (Fig. 4D-F).

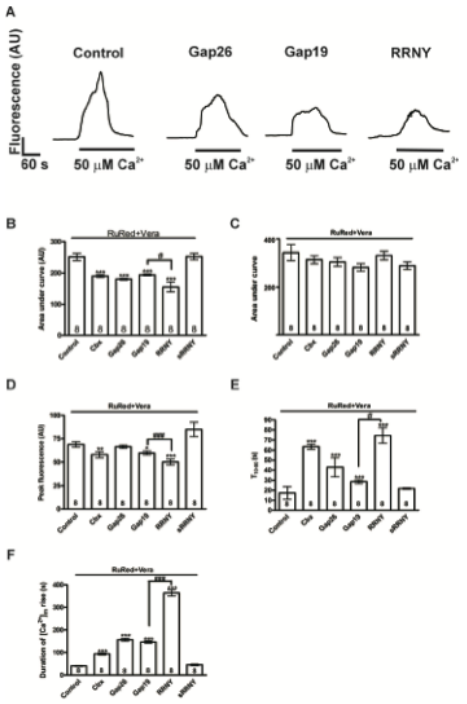

Fig. 4. Effect of HC inhibitors on mitochondrial Ca^{2+} loading. (A) Example mitochondrial Ca^{2+} traces in response to a 50 μM Ca^{2+} challenge and effect of peptides. (B) Average data on area under curve, (C) peak fluorescence, (D) rise time for 10-90%, and (E) total duration of the Ca^{2+} fluorescence signal. All experiments were performed in the presence of RuRed and Vera (20 μM). Peptides and Cbx concentrations were 100 μM. * indicates $p<0.05$ vs. Control; ** $p<0.01$; *** $p<0.005$.

The sudden drop of Ca^{2+} indicator fluorescence during exposure to the 50 μM Ca^{2+} pulse possibly indicates permeability transition as a result of Ca^{2+} overload[56]. We therefore performed additional experiments in which we measured extramitochondrial Ca^{2+} with calcium green as an indicator making use of mitochondrial suspensions and a fluorimeter setup (Fig. 5A). Mitochondria were challenged with serial pulses of 20 μM Ca^{2+} concentration every minute, resulting in Ca^{2+} indicator fluorescence jumps in the solution followed by a slow decline indicative of Ca2+ uptake by the mitochondria (Fig. 5B). After repeated Ca^{2+} challenges, the fluorescence suddenly started to progressively increase indicative of mitochondrial Ca^{2+} release caused by permeability transition[56]. The number of Ca^{2+} pulses needed for this transition were then counted and compared. Fig. 5C demonstrates that all HC blockers, except Gap26, significantly increased the number of Ca^{2+} pulses necessary to obtain permeability transition; RRNY again was most potent with respect to this assay (almost tripling the number of pulses) whereas sRRNY had no effect.

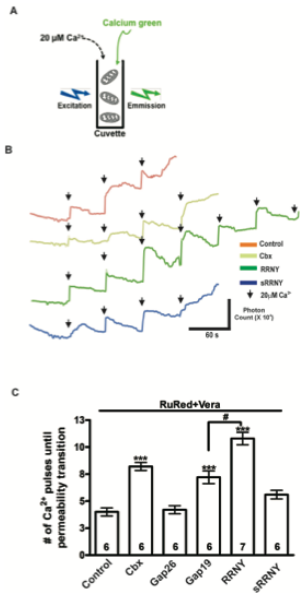

Fig. 5. Extramitochondrial Ca^{2+} measurements and permeability transition in SSM. (A) Cuvette fluorimetry setup. Mitochondria were exposed to repeated 20 μM Ca^{2+} pulses until fluorescence suddenly started to increase independently of the Ca^{2+} pulse, indicating mitochondrial Ca^{2+} release caused by permeability transition. (C) Average data from experiments shown in B. Carbenoxolone, Gap19 and RRNY significantly increased the number of pulses to achieve permeability transition while Gap26 and sRRNY had no effect. *** indicates $p<0.005$ vs. Control.

2.5 RRNY protects against cell death induced by doxorubicin, ceramide and staurosporine

We next verified in H9C2 cardiac cells if the protective effect of HC inhibition on mitochondrial Ca^{2+} loading and permeability transition translates to protection against cell death. Peptides for these studies were linked to the TAT translocation sequence to facilitate cell penetration, since the site of interaction of the peptides is intracellular[123]. We used three different agents for inducing cell death: staurosporine, a PKC inhibitor triggering apoptosis[262], apoptosis-inducing ceramide[263] and the cardiotoxic drug doxorubicin[264]. In the staurosporine experiments, cell death was quantified by a pan-caspase assay while cell viability was assayed for ceramide and doxorubicin. In all assays, TAT-RRNY acted in a protective way; TAT-Gap19 only displayed protection in the doxorubicin model (Fig. 6A-C).

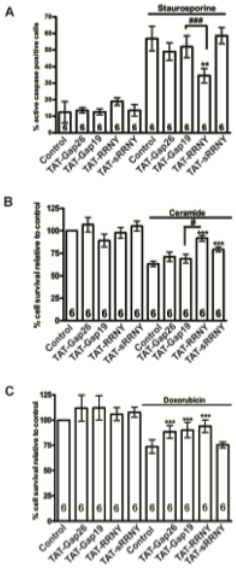

Fig. 6. Effect of HC inhibitors on cell death. (A) Cell death induced by staurosporine (B) by ceramide, and (C) by the cardiotoxic drug doxorubicin (C). In all three studies, TAT-RRNY significantly increased cellular resistance to apoptosis (A) or cell survival (B, C) while Gap26 and Gap19 had variable effects in these assays. Peptides were used at 100μM concentration. *indicates $p<0.05$ against Control; ** $p<0.01$; *** $p<0.005$.

2.6 RRNY protects against cardiomyocyte cell death induced by hypoxia-reoxygenation, and reduces the infarct size in ex vivo experiments

Some reports suggest that cell penetrating TAT peptide alone leads to increased pro-apoptotic Bad and Bax signaling and a decrease in anti-apoptotic Bcl-2, reducing caspase-3 activation[265]- all closely associated with mitochondrial ion homeostasis. Hence, to avoid influence of TAT in cardiomyocyte and ex-vivo studies, we used TAT free versions of the Cx targeting peptides. We previously demonstrated that Gap19 has intrinsic membrane permeability[123] and further evaluated the RRNY ability to permeate the cell membrane. We found that FITC-labeled RRNY significantly accumulated into the cell without TAT sequence (Influx ratio (ratio of internalized fluorescence and external fluorescence) of 20%), probably related to its high content of positively charged arginine residues (as for Gap19 that has 4 lysine residues; Fig. 1A).

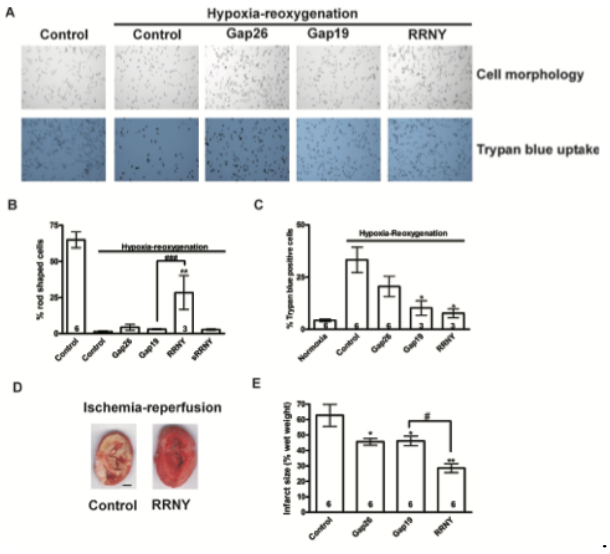

Fig. 7. Effects of HC inhibitors on cardiac ischemia-reperfusion injury. (A) Representative images of experiments on neonatal mice cardiomyocytes exposed to 30 min of hypoxia and 120 min of reoxygenation and probed for cell morphology and trypan blue uptake indicative of cell death. (B) RRNY significantly increased the percentage of rod-shaped cells (C) while RRNY and Gap19 decreased trypan blue uptake. (D) Ex-vivo Langendorff ischemia-reperfusion studies in mouse hearts. Peptides were perfused 1 min before induction of a 30 min ischemia period and were present the first 10 min of a 120min reperfusion period. (E) Gap26, Gap19 and RRNY all reduced the infarct size compared to Control but the effect of RRNY was strongest. *indicates $p<0.05$ against Control.

Mouse ventricular cardiomyocyte morphology and cell death were assessed under conditions of hypoxia-reoxygenation induced by oxygen and substrate depletion for 30 min followed by normoxia and substrate availability for 60 min in the presence or absence of the HC blockers. Cell morphology was assessed as the percentage of rod shaped cells, and cell death as the percentage of trypan blue positive cells (loss of sarcolemmal integrity). Fig. 7A shows representative images of trypan blue uptake and changes in cell morphology associated with hypoxia-reoxygenation and their amelioration in the presence of peptides, especially RRNY. Fig. 7B illustrates that hypoxia-reoxygenation reduced the rod-shaped cardiomyocyte population almost 12 fold; RRNY strongly promoted the fraction of rod-shaped cardiomyocytes while none of the other peptides tested had any effect. Fig. 7C demonstrates a ~6 fold increase of trypan blue positive cardiomyocytes after exposure to hypoxia-reoxygenation and these counts were significantly reduced by Gap19 (~3 fold) and RRNY (~4 fold).

We next performed experiments on mouse hearts subjected to ex vivo Langendorff perfusion to assess the effect of HC blocking peptides on infarct size. Hearts were perfused with 100 μM of the

peptides 1 min before the onset of ischemia and were present during the initial 10 min of reperfusion. The infarct size (surface area), measured by permeation of triphenyl tetrazolium chloride and normalized to wet weight of the heart, was ~60 % under control conditions and was significantly reduced by Gap26, Gap19 and RRNY peptides (Fig. 7E). RRNY had the strongest effect, reducing the infarct area to ~50 % of the area observed in non-treated hearts.

Discussion

MitoCx43 has been suggested to exist in a HC-like configuration[179,215]; our native gel electrophoresis studies demonstrating a clear 250 kDa band support this view. Dye uptake with HC-permeable LY was strongly reduced in mitochondria isolated from Cx43 KD animals and occurred in the absence of any trigger, indicating that some Cx43 HCs are open. The mitochondrial membrane potential is inside negative and in the range of 150-180 mV. If IMM Cx43 is oriented with its CT, CL and NT looking outward (intermembrane space), then this side of the protein will experience an outside positive 150-180 mV, which is far above the voltage threshold for plasma membrane-based Cx43 HC opening (40-50 mV[111]). Alternatively, when the extracellular loops (ELs) are looking outside, HCs are also expected to be open because of the low cytoplasmic Ca^{2+} concentration that is known to open plasma membrane-located HCs[266,267]. Thus, whatever the Cx43 orientation is, HCs in the inner mitochondrial membrane are expected to be open (a not unusual shunt pathway given the presence of uncoupling proteins[250]). Accordingly, perfusing isolated mitochondria with 50 μM Ca^{2+} solution, under conditions of Ca^{2+} uniporter and Na^{+}/Ca^{2+} exchanger blockade, provokes intramitochondrial Ca^{2+} changes as expected from their Ca^{2+} permeability. Channels reconstituted from SSM-enriched Cx43 protein indeed demonstrated a large single channel conductance of ~130 pS, lower but still in the same order of magnitude of their plasmalemmal counterparts. Importantly, the channels were non-selective as indicated by the 0 mV reversal potential (Fig. 2C) and were modulated by phosphatase treatment to a similar extent as channels reconstituted from plasmalemmal Cx43 (Fig. 2E and H). Of note, the effect of Gap19 and RRNY on hemichannels was very comparable in SSM-based Cx43 hemichannels (Fig. 2E) and their plasmalemmal counterparts (Fig. 2H).

The ability of mitochondria to buffer intramitochondrial Ca^{2+} is of crucial importance in a variety of pathophysiological processes such as ischemia-reperfusion. This buffering capacity is limited and once a threshold is surpassed, mitochondrial permeability transition occurs leading to the release of Ca^{2+}, and cytotoxic molecules such as cytochrome *c*[268,269]. The extramitochondrial Ca^{2+} measurements (Fig. 5) demonstrated that HC inhibition, especially with RRNY, leads to increased resistance against Ca^{2+}-triggered permeability transition. The cell death/viability studies on immortalized cardiac cell lines confirmed a protective effect of HC blockade and this was also noted in cardiomyocytes subjected to hypoxia-reoxygenation and in ex-vivo Langendorff perfused hearts exposed to ischemia-reperfusion. In the latter case, peptides were present in the heart during ischemia and the initial 10 minutes of reperfusion. This protective effect may be attributable to inhibition of mitochondrial Ca^{2+} entry but may also relate to ROS generation. Cx43 targeting peptides decrease complex I respiratory activity[180], which contributes as a major ROS source; as a consequence, blocking its activity mitigates ROS production and limits infarct size[181,207,270]. Thus, protection by RRNY and other peptides used in this study may act directly via Ca^{2+} or via Ca^{2+}-dependent or independent ROS production. Of crucial importance is the fact that the peptides were present during the entire duration of ischemia and the initial ten minutes of reperfusion.

In contrast to our findings with Cbx that restricted Ca^{2+} entry and prolonged permeability transition, others have shown that carbenoxolone promotes permeability transition by targeting Cx43[240]. However, the target of Cbx in mitochondria responsible for permeability transition are the various thiol groups on respiratory complex I. Also, the effect of Cbx is shown to be bi-modal with concentrations of less than 10 μM being protective against permeability transition, and higher concentrations having a deleterious effect[271,272]. Indeed, blocking complex I using Cx43 inhibitors has been shown to reduce ROS generation giving further evidence to the protective effect of inhibiting Cx43 HCs.

Not all peptides used in this study had an equivalent effect on unitary currents, Ca^{2+} dynamics, cell death and/or infarct size. This may be caused by distinct interaction/binding properties with Cx43, by different accessibilities of the target motifs or by different spectra of connexin channels targeted. For example, Gap26 blocks HCs by interacting with the ELs[116,123]. If the ELs are inside

the mitochondria, then Gap26 may only be able to access them by permeating through the open HC pore. With the ELs inside, the CT is outside and readily available for interactions with Gap19 and RRNY that have the CT as their target. Another reason for the distinct potencies on cell death and/or tissue damage may be linked to the spectrum of effects of these peptides on channels and HCs. Gap26 first blocks plasma membrane HCs[111] and with some delay also gap junctions[118,119,273]; it also blocks Cx37 junctional channels in vascular endothelial cells[274]. Gap19 is specific for Cx43 and only inhibits HCs, not gap junctions[123]. RRNY was developed as a tool to prevent gap junction closure in cardiac ischemia[131,257]. We here show that RRNY inhibits Cx43 HCs in the plasma membrane as well as in mitochondria. In fact, the mitochondrial effect on dye uptake and unitary currents was stronger than that of Gap19. Thus, compared to the other peptides, RRNY may act at three levels: preventing gap junction closure, inhibiting HCs in the plasma membrane and inhibiting mitochondrial HCs. Such action at three fronts is probably the reason why its protection on ex-vivo Langendorff perfused hearts exposed to ischemia-reperfusion was stronger than that of Gap19 (~25% reduction by Gap19 versus ~50% reduction by RRNY).

It has been shown that mitoCx43 is involved in protection linked to ischemic preconditioning[34,175,275]. Here, we show that mitoCx43 HCs contribute to cell injury/death and that blocking Cx43 HCs acts beneficially. The contrast between these two effects are linked to fundamental differences in the experimental models used. Ischemic preconditioning is generated by short pulses of ischemia/reperfusion, which generate small amounts of ROS from complex I triggering downstream protective pathways that include increased mitochondrial Ca^{2+} retention capacity amongst others[30]. In the case of index ischemia without preconditioning, however, blocking complex I is a major protective strategy[181]. We here demonstrate that in the absence of preconditioning, mitoCx43 play a detrimental role mediated by mitochondrial HC mediated Ca^{2+} entry. Moreover, HC mitochondrial Ca^{2+} entry may well be suppressed under conditions of ischemic preconditioning. PKC phosphorylation of Cx43 observed in ischemic preconditioning[30] invariably leads to decreased channel function, both at the level of GJs[276] and HCs[277] and, as a result, may inhibit HC-linked mitochondrial Ca^{2+} entry acting protectively.

In conclusion, these results demonstrate that Cx43 contributes to mitochondrial Ca^{2+} entry that activates cascades leading to cell injury/cell death. This cascade was most potently inhibited by

RRNY peptide that targets three levels of connexin channels: inhibition of mitochondrial HCs, inhibition of HCs in the plasma membrane and prevention of closure of gap junction connections between cells.

3. Materials and methods

3.1 Isolation of cardiac ventricular mitochondria

All animal experiments were performed with permission from the Committee on ethical usage of animals of the Ghent University. Male C57/Bl6 mice, 12-14 weeks of age, were anesthetized by a mixture of ketamine/xylazine (25 mg/kg body weight). The mice were also injected with heparin (1000 mg/kg) to prevent coagulation. Following induction of anesthesia, animals were sacrificed by cervical dislocation and rapid thoracotomy to excise heart. Hearts were immediately dropped into isolation buffer (in mM: 200 mannitol, 300 sucrose, 5 KH_2PO_4, 5 MOPS, 1 EGTA, 0.1% BSA and 0.5 mg/ml butylated hydroxy toluene as an anti-oxidant; pH adjusted to 7.15 with KOH)[181]. Hearts were then washed twice and atria and extraventricular tissue removed. The cleaned and trimmed ventricles were chopped to approximately 1 mm cubes and homogenized using a Potter Elveheijm homogenizer. Preparation of mixed mitochondria was done by centrifugation of the suspension at 700X *g* (10 min), followed by recentrifugation of the supernatant at 7500 g (10 min) and collection of the resultant pellet that was stored on ice until usage[178]. For separation of the SSM fraction, the suspension was centrifuged at 700X *g* (10 min) and the supernatant was recentrifuged at 7000X *g* for 10 min. The resultant pellet enriched in SSM was stored on ice for further use. The pellet from the first centrifugation was resuspended in isolation buffer and incubated on ice for 10 min, in the presence of protease (Bacterial type II, Sigma). It was then centrifuged at 700X *g* (10 min), followed by centrifugation of the supernatant at 7000X *g*. The resultant pellet containing IFM was stored on ice until further usage.

3.2 Mitochondrial immunochemical localization of Cx43

Mitochondria were loaded with MitosoxRed-CMX ROS mitochondrial dye (500 nM) for 30 min. Following this, mitochondria immobilized on poly-lysine coated cover slips were fixed with 4% paraformaldehyde for 1 h. Following 3 washes with PBS the mitochondria were permeabilized

with 0.1% Triton X-100 for 5 min and then incubated in 2% BSA to block non-specific antibody binding for 1 h. Following this, rabbit anti-Cx43 antibodies (Sigma Aldrich) labeled with Alexa-488 (Invitrogen) was added to the coverslips and incubated overnight. Coverslips were then washed 3 times with PBS and stored under Vectashield fluorescence recovery agent (Vector Labs) until imaging. Unlabeled antiCx43 antibody was used as antibody control and unloaded mitochondria were used as mitochondrial dye control. Imaging was performed on Leica XPS-8 for confocal imaging. Super resolution imaging by direct stochastic optical reconstruction microscopy (dSTORM) was performed as previously described[278]. Briefly, SSM from mice heart ventricles were isolated and treated as described until the addition of primary antibody against Cx43. Following this, mitochondria were incubated with secondary anti-rabbit antibody conjugated to Alexa-647. Imaging conditions were achieved by the addition of 200 mM mercaptoethanolamine and an oxygen scavenging system to the fluorophore containing solution combined with appropriate laser excitation. Movies containing a minimum of 2000 frames were used to generate reconstructed super-resolved images. Image analysis was performed using ImageJ software. Images were processed with a smoothing filter, adjusted for brightness and contrast and filtered to a threshold to obtain a binary image.

3.3 Native detection of mitoCx43

Mitochondria isolated as described above were solubilized in buffer containing 0.1% digitonin and 1% dodecylmaltoside by incubation on ice for 15 min. The suspension was centrifuged at 32000x *g* for 10 min and supernatant collected. Protein concentration in the supernatant was determined via BioRad BCA protein assay. 50 μg of protein was loaded into each well of a 3-8% acrylamide gel and electrophoresis performed at 125 V for 2.5-3 hrs using non denaturing electrophoresis buffer. The proteins were then blotted onto PVDF membranes at a constant current of 100 mA/cm² for 3 h. Following blotting, the membranes were blocked with 5% milk in Tris buffered saline containing 0.1% Tween-20 (TBS_t) for 1h. Membranes were then incubated overnight in 5% milk containing anti-Cx43 antibody and subsequently washed 3 times with TBS_t and incubated in appropriate secondary antibody. Antibody binding was detected using chemiluminescence (Pierce, Belgium). To determine if Cx43 co-electrophoresed with other proteins, the same membrane was used for detection of complex I subunit NDUFA9 (Invitrogen, USA) or PKC-ε (Millipore, USA)

or CamKII (Millipore, USA) or GSK-3β (Millipore, USA) following antibody stripping.

3.4 Mitochondrial dye uptake

Dye uptake studies were done with the Cx43 HC permeant dye Lucifer Yellow (LY) and impermeant 10-kDa Rhodamine B isothiocyanate (RITC)-dextran. SSM were pelleted and resuspended at 0.5 mg/mL in experimental buffer (in mM: 150 KCl, 7 NaCl, 2 KH_2PO_4, 1 $MgCl_2$, 6 MOPS, pH 7.2, 6 succinate, 0.25 ADP, and 0.5 µM of rotenone). After 5 min incubation at 25°C, 50 µM LY (LY CH dilithium salt, L0259, Sigma) and 25 µg/mL RITC-dextran 10S (RITC-dextran, R888, Sigma) were added simultaneously and allowed to permeate for 25 min. Mitochondria were subsequently washed and resuspended in the same experimental buffer. Fluorescence for LY was read at 535 nm and for RITC-dextran at 600 nm using a plate reader[215] (Miro-Casas *et al*, 2009). Peptides were added immediately prior to the addition of LY and were present throughout the experiment.

3.5 Patch clamp studies of HeLaCx43 cells

Hela-Cx43 cells were bathed in a recording chamber filled with a modified Krebs–Ringer solution consisting of (in mM): 150 NaCl, 6 CsCl, 2 $CaCl_2$, 2 $MgCl_2$, 1 $BaCl_2$, 2 pyruvate, 5 glucose, 5 HEPES and pH adjusted to 7.4. The standard whole-cell recording pipette solution was composed of (in mM): 130 CsCl, 10 Na-aspartate, 1.1 $CaCl_2$, 1 $MgCl_2$, 2 EGTA, 10 tetraethylammonium (TEA)-Cl and 5 HEPES; pH was adjusted to 7.2 and [Ca^{2+}] was 200 nM as calculated with Webmax Standard software application (http://www.stanford.edu/~cpatton/webmaxcS.htm). Single channel recordings were performed by making use of an EPC 7 PLUS patch-clamp amplifier (HEKA Elektronik, Lambrecht/Pfalz, Germany). Data were acquired at 5kHz using a NI USB-6221 data acquisition device from National Instruments (Austin, TX, USA) and an acquisition software WinWCP designed by Dr. J. Dempster (University of Strathclyde, U.K.). Resting membrane potential was -30 mV and 30 s lasting voltage steps to +60 mV were applied to activate HC opening. All currents in whole-cell configuration were filtered at 1 kHz (7-pole Besselfilter). For single channel analysis, holding currents were subtracted from the recorded current traces, giving traces that only contained unitary current events. Unitary conductances were

calculated from the elementary current transitions Δi as: $\gamma = \Delta i / V_m$. The charge transfer Q_m was quantified by integrating unitary current activity over the duration of the applied voltage step.

3.6 Isolation and enrichment of Cx43 from mitochondria and plasma membrane

Mitochondria isolated as described above were solubilized using 0.1% dodecylmaltoside and 0.1% digitonin in the presence of phosphatase and protease inhibitors (PPI). Following solubilization, 50 μg protein suspension added to 2.75 ml dH_2O, 15% glycerol and 15% DL-Dithiothreitol. Proteins were then subjected to isoelectric focusing (IEF) using ampholytes (pI: 3.5-10) in BioRad Microrotofor cell for 6 h at a constant voltage of 400V under non-denaturing conditions (4°C). Following separation the ten fractions were collected and analyzed for Cx43 using Western blotting. The fraction with highest concentration of Cx43 (pI 8.6) was collected and subjected to a second IEF under similar conditions in the presence of ampholytes (pI 5-10). The fraction containing enriched Cx43, identified using Western blot, was desalted and concentrated by centrifugation at 16000X *g* for 30 min using a 3 kDa filter[279]. In case of enrichment of Cx43 from plasma membrane, plasma membrane fractions were separated from non-plasma membrane fractions of C57/Bl6 mice heart ventricles using plasma membrane protein extraction kit (Cat. No. AB65400, Abcam, USA) and differential solubilization as the separation principle. In brief, ventricles were homogenized using solubilization buffer containing PPI. The homogenate was centrifuged at 700X *g* for 10 min. The supernatant was centrifuged again at 10000X *g* for 30 min at 4°C. The supernatant containing cytosolic fractions was discarded and the pellet containing total cellular membrane fractions was suspended in upper phase and mixed with lower phase. Following centrifugation at 1000X *g* for 5 min. The upper phase containing plasma membrane fractions was collected and further purified by re-centrifugation following addition of lower phase. Both the plasma membrane and non-plasma membrane protein fractions were collected and stored at -80°C until further use in IEF for enrichment of Cx43. Figure 8 shows a representative blot of the purified Cx43.

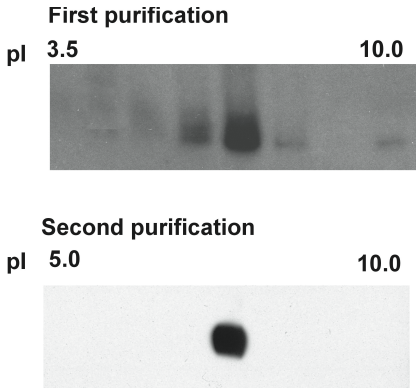

Fig.8: Representative blot of purified Cx43 using isoelectric focusing

3.7 Planar lipid bilayer studies

Channel activity of the purified and enriched Cx43 protein was monitored by incorporation into a planar lipid bilayer, as previously described[280]. Briefly, phospholipids were prepared by mixing phosphatidyl-ethanolamine, phosphatidyl-serine, phosphatidyl-choline, and cardiolipin (Avanti Polar Lipids) in a ratio of 5:4:1:0.3 (v/v). The phospholipids were dried under N_2 and re-suspended in n-decane to a final concentration of 25 mg/mL. The *cis/trans* chambers contained symmetrical solutions of 10 mM HEPES, 200 mM KCl and 100 μM $CaCl_2$ at pH 7.4. The *trans* chamber was held at virtual ground while the *cis* chamber was held at the command voltages. Cx43 protein, peptides and bovine alkaline phosphatase were added into the *cis* chamber. Currents were sampled at 5 kHz and low pass filtered at 1 kHz using a voltage clamp amplifier (Axopatch 200B, Molecular Devices) connected to a digitizer (DigiData 1440, Molecular Devices), and recorded in 1 min segments. The pClamp software (version 10, Molecular Devices) was used for data acquisition and analysis. For analysis, additional low-pass filtering was applied at 200 Hz.

3.8 Mitochondrial Ca^{2+} uptake

Mitochondria isolated as described above, either subpopulations or mixed populations were loaded with 25 μM of low affinity Ca^{2+} sensitive dye Rhod-FF (K_d = 19 μM) by incubation in a buffer containing (in mM) 30 KCl, 120 sucrose, 10 HEPES, 1 EGTA, 10 succinate, 1 Pi, 0.5 MgCl2, 0.04 Ca, pH 7.2 (buffer A) for 30 minutes and excess dye washed by centrifugation at 8000x*g* for 10 min. The mitochondria were resuspended in the same buffer but without Rhod-FF and stored on ice until use. For Ca^{2+} imaging, mitochondria were immobilized on poly-l-lysine coated coverslips

and superfused with the same buffer containing mitochondrial Ca^{2+} uniporter blocking ruthenium red (RuRed: 20 μM) and Na^{+}-Ca^{2+} exchanger blocking verapamil (Vera: 20 μM), with or without peptides (buffer B). Following imaging for 2 minutes (3 minutes in case of treatment with peptides), mitochondria were superfused with 50 μM free Ca^{2+} containing buffer (buffer C) and images acquired for a further 7 minutes and then washed with buffer B. In case of experiments using combined populations, mitochondria were then superfused with a buffer containing 100 μM FITC-labeled Gap19 for one minute and washed for a further one minute and image acquired. For analysis, images acquired during Ca^{2+} challenge were superposed on FITC-Gap19 perfusion. Only the points positive for FITC-Gap19 labeling were analysed as Cx43 positive mitochondria. Point analysis was performed using FluoFrames inhouse software developed by Dr. Luc Leybaert.

In case of Ca^{2+} studies where extra mitochondrial Ca^{2+} was measured, mitochondria were suspended in respiration buffer (buffer containing (in mM): 130 KCl, 5 K_2HPO_4, 20 MOPS, and 2.5 EGTA, with 1 μM $Na_4P_2O_7$, and 0.1% BSA, pH 7.15 adjusted with KOH)) in the presence of 10 mM succinate and 50 nM of the fluorescent dye calcium green (50 nM, Invitrogen) to measure extra mitochondrial Ca^{2+} in a cuvette-based spectrophotometer (model QM-8; Photon Technology International, Birmingham, NJ). [Ca^{2+}] was monitored by fluorescence at 490 nm excitation and 531 nm emission. After stabilization, pulses of $CaCl_2$ (to yield 20 μM increases in Ca^{2+}) were added every 60 s until permeability transition as indicated by a final increase in Ca^{2+} fluorescence without any added Ca^{2+} pulse[56]. Results from four replicates per heart were averaged.

3.9 Cell viability/cell death studies

In order to assess the effect of peptides on Ca^{2+} accumulation and cell death, we assessed cell viability and apoptosis on confluent H9C2 cells induced by doxorubicin, ceramide and staurosporine. Cells were incubated with either doxorubicin or ceramide in the presence or absence of peptides for 24 hours. Following the incubation period, MTT cell viability assay was performed as per manufacturer's instructions (Cat. no. V13154, Invitrogen, USA). Results are shown as values normalized to no cell death trigger control. In case of staurosporine induced cell death model, cells were treated with staurosporine either in the presence or absence of peptides for 4

hours. Following incubation, cells were washed and incubated in a medium containing 30mM propidium iodide and active caspase-3 indicator for 30 minutes, and washed. The cells were then fixed and stained for propidium iodide and caspase-3 indicator positivity following manufacturer's instructions (Cat. no. 10402, Biotium, USA). Results are presented as percentage positivity relative to control condition (100%).

In further studies on effect of HC blockers on cell death, cardiomyocytes isolated from C57/Bl6 mice were subjected to hypoxia re-oxygenation in the presence or absence of HC blockers- Gap26, Gap19 and RRNY. Briefly, isolated mice cardiac myocytes were attached on glass-cover slips and introduced into a perfusion chamber and superfused with a flow rate of 0.5 ml/min. The buffers were transferred into the perfusion chamber through gas-tight steel capillaries. Ischemic conditions were simulated by perfusion of cells with anoxic, glucose-free media (pH 6.4) as described previously. After 10 min of normoxic perfusion, myocytes were exposed to simulated ischemia for 15 min and subsequently reoxygenated by perfusion of a normoxic, glucose-containing standard buffer (pH 7.4) for up to 30 min. PO2 of ischemic buffer was less than 1 mmHg as determined by a polarographic oxygen sensor. At defined time points after reoxygenation, cover slips were transferred to a microscope and five randomly selected pictures were taken for each cover slip. Ischemic tolerant cardiomyocytes were identified by their rod-shape structure. Hypercontracture leading to round-shaped cells was used as criteria to identify irreversible damaged myocytes. Trypan blue exclusion test was used to judge about sarcolemmal integrity[281]

3.10 Ex vivo Langendorff ischemia-reperfusion studies in mouse hearts

Hearts extracted from C57/Bl6 mice were subjected to ex vivo Langendorff perfusion. In groups subjected to ischemia reperfusion, following stabilization of hemodynamic parameters and a baseline perfusion of 10 min, hearts were subjected to global ischemia by clamping oxygenated buffer flow for 30 min and reperfused for 120 min. In the treated groups, peptides were perfused immediately before onset of ischemia and were present during entire ischemic period and initial 10 min of reperfusion. Control hearts which did not receive treatment were perfused for 160 min following 10 min stabilization. Following this, ventricles were cut into 2 mm transverse sections with a heart matrix and incubated in 1% 2,3,5-triphenyltetrazolium chloride (TTC) in 0.1 M

KH_2PO_4 buffer (pH 7.4, 38°C) for 10 min. TTC stains viable tissue red, indicating the presence of a formazan precipitate that results from TTC reduction by dehydrogenase enzymes present in viable tissue. All slices were digitally imaged on green background by a photoscanner, and the infarcted areas of each slice were measured automatically by planimetry using ImageJ-1.44i software (National Institutes of Health, Bethesda, MD), its ColorThreshold plug-in, and in-house macro ensuring fast and operator-independent measurements[282]. Infarcted areas of individual slices were averaged on the basis of their weight to calculate the total infarction of both ventricles.

Statistics

Results are expressed as means ± SEM. Statistical evaluation was performed using Students t-test or one way ANOVA, as appropriate. P-values <0.05 were considered as statistically significant.

Experimental contribution

Ashish Kumar Gadicherla: Designed, performed and analyzed all experiments with isolated mitochondria, planar lipid bilayer studies; confocal and super resolution imaging; cell death studies; ex-vivo Langendorff studies; prepared manuscript

Nan Wang: Performed electrophysiology studies on HelaCx43 cells (Fig. 1F-H); reviewed and edited manuscript

Marco Bulic: Performed and analyzed cell morphology and trypan blue uptake studies on isolated cardiomyocytes (Fig. 7A-C)

Esperanza Agullo- Pascual: Guided and planned super resolution imaging (Fig. 1B, lower three panels).

Alessio Lissoni: Helped with genetically modified animals; reviewed and edited manuscript

Maarten De Smet: Helped with genetically modified animals; reviewed and edited manuscript

Mario Delmar: Guided and planned super resolution imaging (Fig. 1B, lower three panels),

Dmitri V. Krysko: Provided scientific input for the studies, reviewed and edited manuscript

Amadou Camara: Guided proteomics experiments for planar lipid bilayer studies, reviewed and edited manuscript

Klaus-Dieter Schlüter: Guided and planned cell morphology and trypan blue uptake studies on isolated cardiomyocytes

Rainer Schulz: Guided and provided scientific input for the studies, reviewed and edited manuscript

Wai-Meng Kwok: Guided planar lipid bilayer studies, reviewed and edited manuscript

Luc Leybaert: Guided and provided scientific input for the studies, validated data, reviewed and edited manuscript.

3.2 Damage to mitochondrial complex I during cardiac ischemia-reperfusion injury is reduced indirectly by anti-anginal drug ranolazine

Ashish Gadicherla, MS [a], David F. Stowe, MD, PhD [a,b,d-f], William E. Antholine, PhD [c], Meiying Yang, PhD [a], and Amadou K.S. Camara, PhD [b,d,*]

[a]*Department of Anesthesiology, Medical College of Wisconsin, Milwaukee, WI 53226, USA*
[b]*Department of Physiology, Medical College of Wisconsin, Milwaukee, WI 53226, USA*
[c]*Department of Biophysics, Medical College of Wisconsin, Milwaukee, WI 53226, USA*
[d]*Cardiovascular Research Center, Medical College of Wisconsin, Milwaukee, WI 53226, USA*
[e]*Research Service, Veterans Affairs Medical Center, Milwaukee, WI 53295, USA*
[f] *Department of Biomedical Engineering, Marquette University, Milwaukee, WI 53233, USA*

* Corresponding author: Amadou K.S. Camara, PhD, M4240, 8701 Watertown Plank Rd, Medical College of Wisconsin, Milwaukee, WI 53226. Phone: (414) 456-, Fax: (414) 456-6507, email: aksc@mcw.edu

This work was published in part in abstract form: *Biophys J* 98:2068.pos, 2010; *FASEB J* 519.13, 2010; *Anesth Res Soc* 808.pos, 2010; *Biophys J* 100:2500.pos, 2011.

Short title: Protection of complex I during cardiac injury

Abstract

Ranolazine (Ran), an anti-anginal drug, is a late Na^+ channel current blocker that is also believed to attenuate fatty acid oxidation and mitochondrial respiratory complex I activity, especially during ischemia. In this study, we investigated if Ran's protective effect against cardiac ischemia-reperfusion (IR) injury is mediated at the mitochondrial level and specifically if respiratory complex I (NADH oxidoreductase) function is protected. We treated isolated and perfused guinea pig hearts with Ran just before 30 min ischemia and then isolated cardiac mitochondria at the end of 30 min ischemia and/or 30 min ischemia followed by 10 min reperfusion. We utilized spectrophotometric and histochemical techniques to assay complex I activity, western blot analysis for complex I subunit NDUFA9, electron paramagnetic resonance for activity of complex I Fe-S clusters, ELISA for determination of protein acetylation, native gel histochemical staining for respiratory supercomplex assemblies, and high pressure liquid chromatography for cardiolipin integrity; cardiac mechanical function was measured during IR. Ran treated hearts showed higher complex I activity and greater detectable complex I protein levels compared to untreated IR hearts. Ran treatment also led to more normalized electron transfer via Fe-S centers, supercomplex assembly and cardiolipin integrity. These improvements in complex I structure and function with Ran were associated with improved cardiac function after IR. These protective effects of Ran are not likely mediated directly on mitochondria, but via indirect cytosolic mechanisms which lead to decreased reactive oxygen species generation, which in turn leads to less oxidation and structural preservation of complex I.

Key words

Complex I, mitochondria, IR injury, ranolazine, EPR, heart

1. Introduction

It is now evident that mitochondria play an important role in mediating both protection and damage during cardiac ischemia-reperfusion (IR) injury. An important target for protection is mitochondrial complex I (NADH-Ubiquinone oxidoreductase)[207,283]. Complex I is a large, multi-subunit, integral membrane protein highly susceptible to functional and structural damage during IR injury[284,285]. Complex I is bound by cardiolipin, a highly unsaturated fatty acid in the inner mitochondrial membrane (IMM). Cardiolipin is essential for maintaining functional and structural integrity of the respiratory complexes and to assure efficient transfer of electrons within subunits of the complexes and between the complexes[286]. The transfer of electrons via sequential oxidation-reduction of Fe in the seven Fe-S clusters of complex I exemplifies this critical role of cardiolipin[287,288]. Because cardiolipin is susceptible to oxidative attack by reactive O_2 species (ROS)[289,290] leading to peroxidation and carbon chain breakdown[291] the assemblies of respiratory complexes are also dependent on integrity of cardiolipin.

Ranolazine (Ran) is a clinically used drug known to reduce cardiac dysrhythmias[244–247] and tissue damage after ischemia-reperfusion injury (IR)[292]. During IR injury, Na^+ can slowly enter myocytes during phase 3 of the action potential to initiate dysrhythmias[247]. As a late Na^+ channel current blocker[243] Ran is thought to protect hearts by reducing the incidence of dysrhythmias during IR injury. However, since Ran prevents intracellular Na^+ loading, particularly during ischemia, it could also decrease cytosolic Ca^{2+} overload via Na^+/Ca^{2+} exchange (NCE) and consequently decrease mitochondrial Ca^{2+} (m[Ca^{2+}]) overload[293]; Ca^{2+} overload is thought to cause increased production of ROS and to trigger cell apoptosis by release of cytochrome *c*. These events may underlie, at least in part, the protection afforded by Ran against cardiac tissue damage during IR.

In a recent isolated heart study of IR injury[56], we found that Ran treatment just before ischemia reduced ROS emission and cytosolic and m[Ca^{2+}] loading and, in isolated mitochondria, reduced cytochrome *c* release and delayed opening of the mitochondrial permeability transition pore (mPTP) during cardiac IR injury. Other reports suggest that Ran exerts a cardioprotective effect by switching substrate utilization from fatty acids to glucose metabolism[292,294,295], which reduces mitochondrial O_2 demand and that Ran partially blocks respiratory complex I activity[296]. Although prior studies give insight into Ran's mode of cardioprotection, there is no direct evidence that Ran

attenuates mitochondrial dysfunction during IR injury.

Given the role of complex I in generating ROS during IR[297,298] and the crucial role of cardiolipin[291,297,298] in promoting efficient electron transfer, we sought to determine changes in complex I following IR injury and any beneficial biophysical and biochemical effects of Ran on complex I during IR. Because it is unclear if Ran directly targets mitochondria to protect against IR injury, we hypothesized that Ran, when present during ischemia, preserves cardiolipin and supercomplex assembly integrity, and especially complex I activity, by its effect to reduce ROS emission and oxidation of mitochondrial components as a primary mechanism to protect against cardiac IR injury.

2. Results

2.1. Spectrophotometric determination of complex I activity

Representative traces of complex I activity, monitored in an absorbance spectrophotometer as the rate of oxidation of NADH to NAD^+ in the presence of UQ_{10}, illustrate differences dependent on the treatment (Fig. 1A). In summarized data from 4 individual hearts from each of the 5 experimental groups (Fig. 1B) TC exhibited a NADH oxidation rate of 122±5 nM/min/mg protein with a large decrease in oxidation rate after I30 to 49±8 nM/min/mg, but partial restoration to 106±1 nM/min/mg in RanI30. Similarly, there was a large decrease in complex I activity after IR to 70±4 nM/min/mg, which was completely restored to 123±7 nM/min/mg in RanIR. In RanTC, no changes were seen in complex I activity (Data not shown). In preliminary experiments to determine if Ran directly alters mitochondrial complex I activity in fractured mitochondria, Ran was added to freeze-thaw fractured mitochondria from the TC, I30 and IR groups, followed by measurement of complex I activity; the result was a slight but insignificant decrease in activity (Data not shown).

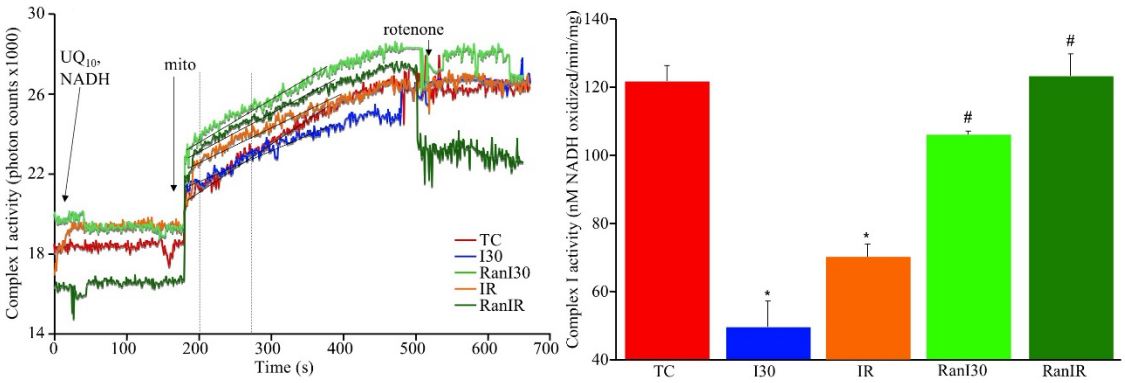

Fig. 1 A: Representative spectrophotometric assay of complex I activity, in solubilized mitochondria during cardiac IR depicting the time points of addition of substrate, enzyme and the inhibitor. **B**: Summary data shows I30 alone reduced the activity of the enzyme, which was restored by treatment with ranolazine (Ran). Reperfusion itself corrected the decrease in activity, but this was not as pronounced as with Ran on reperfusion. Note that the activities depicted in **B** have been corrected for rotenone sensitivity and normalized to citrate synthase levels. N= 4/group; # indicates $p<0.05$ vs. TC

2.2. Histochemical staining for complex I function in gel

A representative gel (Fig. 2A) for NBT-oxidoreductase activity, reflecting complex I function with or without ischemia, reperfusion and Ran, illustrates decreased band density after I30 and IR but higher band density in RanI30 group. Summary data (Fig. 2B) showed that band density decreased after I30 (87±3%) and IR (87±5%) compared to the normalized TC (100%). Ran treatment before ischemia resulted in a significantly higher band density (RanI30 =95±4%) *vs.* I30 alone, whereas band density RanIR (91±4%) was not greater than that for IR alone.

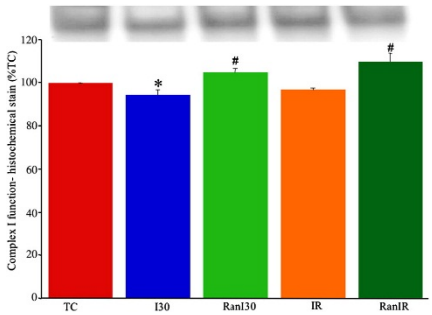

Fig. 2A: Representative histochemical gel staining of complex I activity, in solubilized mitochondria, measured as NBT-oxidoreductase, during cardiac IR. **B:** Summary data shows I30 alone resulted in lower staining than in TC and IR. Ran treatment increased staining, indicating improved complex I function. N= 4/group; # indicates $p<0.05$ vs. TC

2.3. Supercomplex assemblies detected by native gels

A representative image of a native gel (Fig. 3A) stained by Coomassie Brilliant Blue illustrates a

supercomplex comprised of complexes I, III and IV as identified by histochemical staining. Summary data (Fig. 3B) showed that band intensity for the supercomplex I+III+IV (TC 100%) was lower in I30 (96±1%) but restored to control levels in RanI30 (100±2%). Band intensity for the IR (100±3%) and RanIR (104±4%) groups were not different from the TC. Complex I was not found to associate further with complexes II and V to form other supercomplexes.

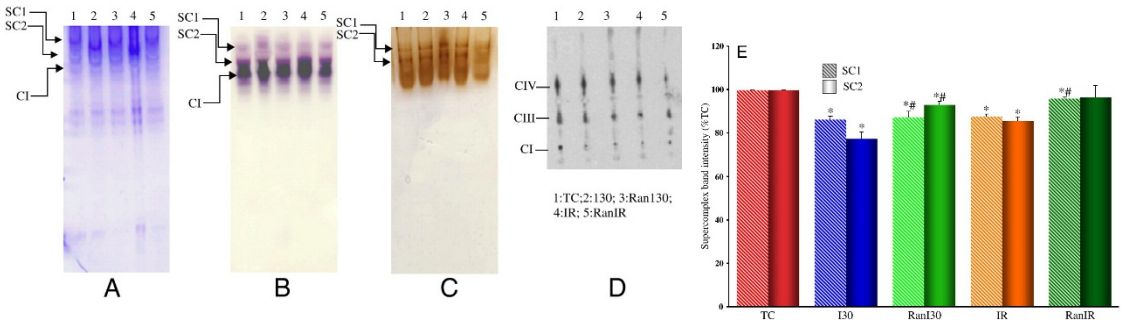

Fig. 3 Representative detection of supercomplex I, III, and IV assemblies, in solubilized mitochondria, by native gel electrophoresis during IR (A-D). Summary data shows that ischemia reduced the integrity of the supercomplex assembly. Both reperfusion and Ran treatment during ischemia restored assembly integrity to TC levels (E). Complex I did not associate with complexes II or V. N= 4/group; # indicates $p<0.05$ vs. TC

2.4. Determination of integrity of complex I subunit NDUFA9 by western blots

A representative blot for the complex I subunit NDUFA9 (Fig. 4A) from hearts subjected to IR ± Ran illustrates decreased intensity in I30 and restoration in RanI30 and RanIR. Complex IV subunit I was used as the loading control. Summary data (Fig. 4B) showed that compared to TC (100%) the anti-NDUFA9 immune reactive band intensity was significantly lower in I30 (84±9%) but was restored in RanI30 (109±7%). Band densities for IR (101±4%) and RanIR (112±7%) groups were not different from the TC group.

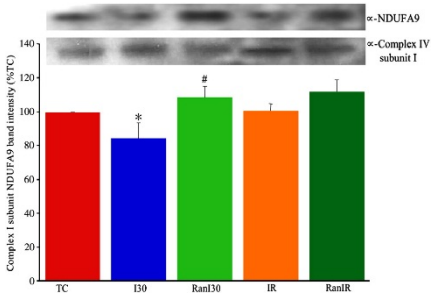

Fig. 4 Representative Western blot detection of complex I subunit NDUFA9 during IR. Summary data shows that ischemia reduced the amount of detectable subunit, indicating a loss of protein or protein damage. Both reperfusion and Ran treatment during ischemia restored protein levels to TC levels. N= 4/group; # indicates $p<0.05$ vs. TC

2.5. Analysis of acetylation of mitochondrial proteins using ELISA

The optical density for acetylated mitochondrial proteins, as detected by ELISA, showed an overall decrease in all groups compared to TC (76±4.9 arb. units) (data not represented graphically). I30 showed the least acetylation (41.7±3.1 arb. units), whereas IR partially restored the acetylation (57.8±4.6 arb. units). Treatment with Ran partially restored acetylation in both groups (Ran I30 = 56.5±2.7 arb. units; RanIR = 59.8±2.3 arb. units). Values for each treatment group were significantly lower than the TC group, and there was statistically significant difference ($p<0.05$) between I30 and RanI30, but not between IR and RanIR.

2.6. Electron transfer in Fe-S clusters by electron paramagnetic resonance

Averaged peak intensities (4 hearts per group) of Fe-S resonance signals (in arb. units) showed differences in peak signals dependent on the treatments (Fig 5A). The g=2.023 signal was assigned to S3, the 3Fe-4S cluster of complex II, or to mitochondrial aconitase, g=2.006 to the semi-ubiquinone radical, g=1.94 to cluster N1b of complex I or to cluster SI of complex II, and g=1.89 to cluster N4 of complex I or to the Rieske center of complex III, respectively. Summary data (Fig. 5B) showed that compared to TC (3.1±1.4 arb. units), neither I30 (2.7±0.8) nor IR (4.2±0.6) significantly altered the g=2.023 signal. However, Ran treatment reduced the g=2.023 signal further in RanI30 (1.6±0.4), but not in RanIR (4.2±1.0). There was a significant increase in the g=2.006 radical in I30 (1.49±0.07), which was reduced back to TC (0.87±0.09) in IR (1.06±0.03). Ran treatment also reduced the g=2.006 signal (RanI30=1.29±0.09; RanIR=1.02±0.04). There was also a significant increase in signals pertaining to g=1.94 and 1.89 during ischemia, which returned to TC levels after reperfusion. The contribution at g=1.94 for N4 can be verified by the changes noted at g=1.89; thus the contribution of N1b and S1 can be estimated after evaluating the contribution of N4. The signal at g=1.94, contributed by N3, is small as estimated by the weak signal at g=1.86, the low field g-value for the signal from N3. Similarly the contribution to the signal at g=1.92 from N2 is weak as determined by the absence of signal from the low field g-value for N2 at 2.05.

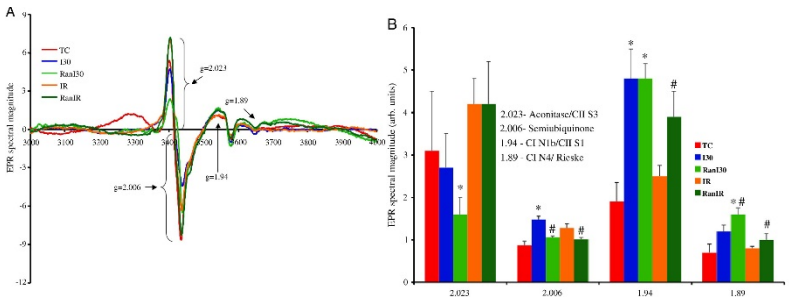

Fig. 5 A: Representative traces of EPR signals during IR denoting changes in three mitochondrial Fe-S clusters and semiubiquinone ($Q^{\bullet}$). **B:** Summary data shows the changes in spectral magnitudes of the Fe-S clusters and $Q^{\bullet}$. Ischemia increased electron transfer within complex I and $Q^{\bullet}$; this was reversed on reperfusion. Ran had a small effect to decrease electron transfer during reperfusion. I, II, II = respiratory complexes; N and Rieske = FeS clusters.

2.7. Determination of cardiolipin integrity by HPLC

Representative HPLC traces of cardiolipin integrity were different depending on treatment (Fig. 6A). Compared to the cardiolipin standard TC (93±2 arb. units), there were significant decreases in the areas under the curves in I30 (56±21 arb. units) and more so in IR (32±12 arb. units) groups reflective of damaged cardiolipin. In summary data (Fig.6B) the RanI30 group (49±15 arb. units) showed no improvement over I30 alone, but the RanIR (69±8 arb. units) group showed a larger area under the peak reflective of less fragmented cardiolipin. The number of peaks as detected by HPLC was also higher (reflecting more fragmented species) in I30 and IR groups compared to RanI30 and RanIR groups, respectively (Fig. 6A).

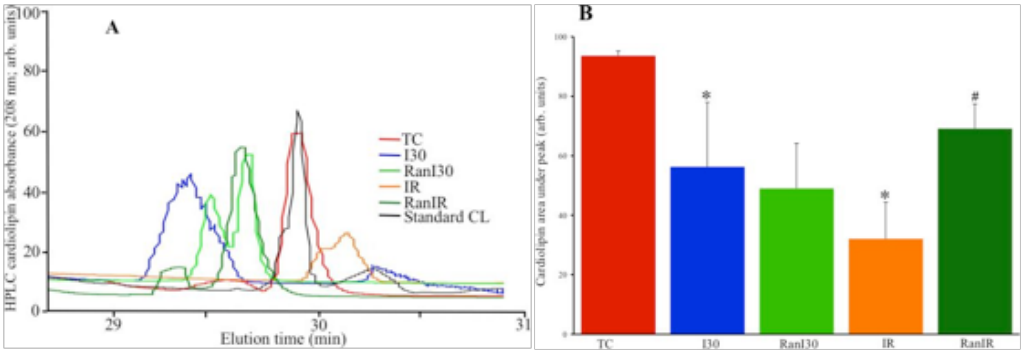

Fig. 6. A: Representative traces of cardiolipin integrity by HPLC analysis during IR. **B:** Summary data shows that ischemia alone reduced the area under the major peak of cardiolipin, and reperfusion decreased it further. Treatment with ranolazine restored peak heights and also decreased the number of peaks, indicating that ranolazine treatment preserves cardiolipin. N= 4/group; # indicates $p<0.05$ vs. TC

2.8. Improved cardiac function after IR injury with ranolazine

Heart rate, coronary flow, diastolic LVP, and developed (systolic-diastolic) LVP remained unchanged during continuous perfusion of hearts for 60 min (TC, data not displayed) after which time hearts were harvested for examination of complex I function using the methods described above. At the end of 30 min no flow global ischemia there was no heart beat and diastolic LVP was elevated (Table); after 10 min reperfusion heart rate and coronary flow were similar to those of the time control in all IR groups. Diastolic LVP was more elevated in the IR group than in the RanIR group and developed LVP was more depressed in the IR group than in the RanIR group. These data indicate that Ran had a protective effect on reducing contracture during ischemia and on increasing contractile function on reperfusion. These protective effects were associated with improvements in several assays of complex I function and the integrity of its support structure cardiolipin.

3. Discussion

3.1. Summary of findings

Complex I is a major source of ROS during IR[297,299] and this increase in ROS is a major cause for the poor return of cardiac function after IR injury[207,239]. For that reason we used several experimental tools to search for deleterious biochemical and biophysical changes in respiratory complex I integrity and function in hearts subjected to 30 ischemia alone, or to ischemia plus 10 min reperfusion. Ran, which is reported to have cardio-protective effects on cardiac tissue[244–247] by switching substrate preference[294,295] among other proposed effects[292] was examined for its potential to attenuate damage to complex I and to improve cardiac function when present during ischemia.

We found that ischemia alone a) reduced the rate of NADH oxidation, b) reduced protein acetylation, c) decreased complex I function, d) reduced supercomplex assembly, e) decreased the detection of a complex I subunit, f) increased the reduced state several fold in three distinct Fe-S clusters in complex I and/or complex II [2Fe-2S in N1b and/or S1 and the 4Fe-4S cluster N4, and in complex I N4 and/or Rieske center in complex III], increased the signal at 2.006 (semi-

ubiquinone radical) but did not alter the signal at 2.023 [S3 in complex II and/or aconitase] and, g) reduced the structural integrity of cardiolipin, a supporting structure for mitochondrial complexes. Compared to ischemia alone, treatment with Ran during ischemia resulted in full or partial restoration of: a) the rate of NADH oxidation, b) the acetylation of mitochondrial proteins, c) the detection of complex I subunit, and d) the supercomplex assembly.

During the short 10 min reperfusion period, complex I dysfunction persisted, acetylation levels remained lower, and cardiolipin showed greater disintegration. Because the expression levels of respiratory complex I subunits are not likely to change given the short time period of our protocols, any reduction in complex I subunit band intensity probably reflects compromised integrity of the subunit's structure. The reduction in NADH oxidation rate with reperfusion alone was reversed and cardiolipin integrity was improved by Ran treatment. Electron transfer through N1b of complex I and/or SI of complex II was improved by Ran on reperfusion and through N4 of complex I or the Rieske center of complex III. Each of these changes observed after Ran treatment was associated with improved cardiac relaxation during ischemia and improved contractile function during reperfusion. However, Ran did not alter complex I activity when applied directly to fragmented mitochondria from the TC, I30, or IR groups.

Our study lends support to our hypothesis that Ran treatment leads to partial protection of mitochondria, as shown in part, by improved complex I activity, restored e^- transfer through some Fe-S clusters, and retained supercomplex assembly and cardiolipin integrity. Moreover, this range of protection implies that Ran is not likely to have a direct molecular interaction with complex I, which is substantiated by our finding that Ran had no effect on activity when added directly to fractured mitochondria. Hence we conclude that Ran acts indirectly at another site to reduce damage to mitochondrial structures. We suggest that by lowering ROS emission with reduced cytosolic and m[Ca^{2+}] loading, as shown recently by us[56], Ran indiscriminately reduces oxidative damage to complex I and to its supporting structures (among other mitochondrial and cytosolic molecules). Our study demonstrates the extent of structural and functional damage to complex I with IR injury and the important role of a non-mitochondrial targeted drug to indirectly protect mitochondrial function.

3.2. ROS and damage to respiratory complexes during cardiac injury

Superoxide radicals ($O_2^{\bullet-}$) are produced in small amounts in mitochondria under O_2 and substrate replete conditions, but the balance between $O_2^{\bullet-}$ generation and free radical scavenging, (ROS emission), is altered in high oxidative conditions such as IR injury[26,283,298,300]. These $O_2^{\bullet-}$ radicals and their downstream products attack all types of cellular molecules, i.e. proteins, lipids, carbohydrates, and D(R)NA, thereby altering their structure and function[301,302]. Although all major biomolecules are susceptible to oxidative damage, the extent of this damage is dependent on the molecular structure, the length of exposure to ROS, the concentration and kind of ROS, and the capacity of ROS scavengers available.

Respiratory complexes differ in their susceptibility to IR injury. Complexes I and III are believed to be more susceptible to injury than complexes II, IV, and V[298]. A useful kinetic test for an effect of Ran to protect respiratory complex I against IR injury is the measure of catalytic conversion rate of NADH to NAD^+ in complex I during IR. Although complex III is reported to be a major source of $O_2^{\bullet-}$ generation[283,285,303,304], many studies have implicated complex I to be the most susceptible of respiratory complexes to ischemic damage[297,305]. Complex I is also a major site of e^- leak during IR; this is likely to drive e^- transfer backward through complex I toward the NADH binding site[207,306,307]. Indeed, in our collateral histochemical and kinetic experiments we found that complex I function was attenuated; this is consistent with the increased (backward) e^- transfer in complex I and the decreased (forward) e^- transfer in complex II[298,308].

Interventions to limit backward e^- transfer from complex II into complex I may be helpful in attenuating ROS release[207,306,308]. Indeed, Chen et al.[308] showed previously that amobarbital, a complex I blocker at the rotenone site, itself slightly enhanced generation of $O_2^{\bullet-}$ before ischemia but attenuated $O_2^{\bullet-}$ emission during IR; we suggest that this may be attributable to inhibited backward e^- transfer, thus preserving mitochondrial redox state[207]. Other modulators of complex I are also known to have protective effects against IR injury[305]. The decreased rate of NADH oxidation in ischemic hearts, compared to reperfused hearts, might also be due to a lack of the e^- acceptor O_2. When reperfusion begins there is an abrupt availability of O_2, and hence a higher rate of activity. In support of this, we found faster respiratory complex I activity in Ran -treated hearts than in the untreated ischemia and IR groups

3.3. Mechanism of mitochondrial protection by ranolazine during cardiac IR injury

Ranolazine is a clinically useful anti-anginal drug[245,309] that was found originally to block the late Na^+ current that occurs with ischemia[247,310,311]. But others have reported that Ran induces a switch from the usual substrate preference from fatty acids to glucose, and that it partially blocks complex I at an unconfirmed site, particularly in uncoupled mitochondria[296]. If Ran were indeed a partial complex I blocker *in vivo* as Wyatt et al. reported in *in vitro* isolated mitochondria[296], this might contribute to preserving its structure and function during IR injury as we found. It is unknown if Ran penetrates membranes effectively due to its hydrophilic structure. It is conceivable that a fat soluble metabolite of Ran is a direct mitochondrial protective drug, but this will require direct evidence of a metabolite with actions on complexes and other mitochondrial targets. Because we found that Ran had no direct effects on mitochondrial function when applied directly to isolated, energized mitochondria[56] or to fractured mitochondria, we believe it is unlikely to directly target complex I or any other mitochondrial protein.

During ischemia there is an increase in cytosolic [Na^+] due to failure of the Na^+/K^+ ATPase pump and an increase in toxic intermediates[312]. This triggers NCE, which results in increased cell Ca^{2+} loading, and consequently, m[Ca^{2+}] loading which may lead to mitochondrial oxidative damage by "Ca^{2+}-induced ROS release"[300,313]. Increased m[Ca^{2+}] contributes to an increase in ROS emission under certain circumstances, either by increasing the rate of $O_2^{\bullet-}$ generation or by reducing the rate of ROS scavenging[293,313,314]. Mitigating NCE was shown to reduce m[Ca^{2+}] loading and thus to induce a cardioprotective effect[314]. Therefore we postulated that Ran induces its protective effect by reducing NCE in the cytosolic compartment to reduce Ca^{2+} loading, and by extension, to mitigate m[Ca^{2+}] loading. Our conclusion derives from the principal earlier finding that Ran is a late Na^+ channel current blocker[247,310,311,315], and our report that Ran reduces m[Ca^{2+}] overload and ROS emission during late ischemia and 60 min reperfusion[56]. This decrease in ROS may or may not be a direct consequence of an improved electron transport chain activity or excess Ca^{2+}. However, Song et al. reported that Ran attenuated H_2O_2 -induced cytosolic Ca^{2+} overload and cardiac contractile dysfunction[314] suggesting that "ROS induced Ca^{2+} loading" can be attenuated by Ran.

The oxidative stress that occurs in ischemia is known to activate deacetylases[316,317], which cause a decrease in lysine acetylation. Deacetylation can disturb the secondary and tertiary associations among proteins and/or their subunits. Hence it is possible that by preserving acetylation, a reversible PTM, this might help preserve the integrity of mitochondrial proteins. Ran treatment attenuated the lysine deacetylation of mitochondrial proteins during ischemia. If Ran could access the mitochondrial matrix, it might interfere with the action of deacetylases to protect the proteins but there is no direct evidence for this.

3.3. Electron transfer in complex I and protective effect of ranolazine during cardiac IR injury

Changes in EPR spectra can occur due to many factors, including but not limited to: a loss of one or more Fe-S clusters, a saturated oxidation or reduction potential, and proximity of neighboring clusters. Complex I subunits with their Fe-S clusters mediate single e^- transfer so any damage to these subunits or Fe-S clusters will cause disrupted e^- transfer. Once an e^- enters the Fe-S cluster chain, its further movement is affected by the redox states of the following Fe-S clusters[288,318] From FMN one e^- enters a transport chain consisting of one binuclear and the six tetranuclear Fe-S clusters leading (during forward e^- transfer) to the ubiquinone (Q) binding site (FMN → N3→N1b–N4–N5–N6a–N6b→N2 → $Q^{\bullet}$→Q)[319] and ultimately to complex II. In our study, we observed no significant change in the g=2.023 signal representing the 3Fe-4S cluster, S3, of complex II IR. In contrast, results of Myers et al. reported a decrease in the aconitase signal (with the same g value) following oxidative stress with chromium radicals[320]. There was a significant increase in the amount of the EPR detectable semi-ubiquinone ($Q^{\bullet}$) radical during ischemia, and this was reduced by reperfusion as well as by Ran treatment. It should be noted however, that $Q^{\bullet}$ is one of the several free radicals generated during ischemia, and hence this is not representative of the total oxidative stress in the tissue.

In contrast to S3 of complex II, there were significant increases in the signal intensities for g = 1.94 and 1.89 during ischemia that decreased again on reperfusion; this could represent reverse e^- transfer during ischemia within complex I. It is difficult to ascertain the exact source of this signal because it can emanate from cluster N1b of complex I or SI of complex II. Although other clusters like the 4Fe-4S and N3 have a g-value close to 1.94 (1.93 for N3) the complementary peak (2.04

for N3) is too weak to detect, implying there is little contribution of signal from N3 at 1.93. Thus the 1.94 signal is attributed to N1b and/or S1.

Reverse e^- transfer is believed to occur in the respiratory chain during ischemia, particularly within complex I[306]. Our results support this assumption. It is plausible from the EPR spectra of N1b (g=1.94) and N4 (g=1.89) clusters that ischemia can cause a severe back up of e^- to cause reverse e^- transfer back in complex I. Reperfusion appeared to largely correct this e^- back up, whereas ranolazine did not affect signal intensity during ischemia, but increased it on reperfusion. The reason for this is unclear. Similarly, we observed an increase in signal intensity for g = 1.89 during ischemia. Again, this signal can be attributed to either cluster N4 of complex I or the Rieske center of complex III; however, since most of this signal was generated by the N4 cluster (as noticed after spectral splitting at higher resolution), we conclude that the changes we observed were due to cluster N4 and not to the Rieske center.

The signal at g=2.023, assigned to the oxidized state of the 3Fe-4S, S3 cluster in complex II decreased with ischemia and fell even more during ischemia with ranolazine, but recovered during reperfusion with or without ranolazine. We can attribute the decrease in the 2.023 signal to greater e^- flow through complex II, thus reducing the S3 center. This complements the suggestion that there is a reverse e^- transfer during ischemia.

3.4. Cardiolipin integrity and protective effect of ranolazine during cardiac injury

Cardiolipin, as a highly unsaturated, fatty acid molecule, is prone to ROS attack with the most commonly encountered changes being lipid peroxidation and carbon chain breakdown[304]. The qualitative mobility of cardiolipin was assessed using HPLC by a change in area under the peak, compared to the cardiolipin standard, and by the appearance of secondary peaks with different retention times; these changes represent distortion of cardiolipin. Moreover, cardiolipin has a high content of oxidatively sensitive linoleic acid, a phospholipid unique to mitochondria. Its location in the IMM makes it extremely susceptible to oxidative damage by ROS, whether acutely as in IR injury or chronically as in aging[289,290]. Cardiolipin is necessary not only for the assembly of each respiratory complex and the supercomplexes, but also for the proper functioning of respiratory

complexes; thus any fragmentation or damage to cardiolipin reflects on the performance of the respiratory complexes[286,291,297].

Ran is also reported to partially inhibit fatty acid oxidation[294,295] and to stimulate glucose oxidation in hearts during normoxia, ischemia, and IR[295,321]. Thus Ran may also act as a metabolic modulator[294,295] that promotes more efficient use of O_2 and substrates. A reduction in ROS emission would likely reduce oxidative damage to cardiolipin, as suggested by our HPLC experiments, in which Ran -treated hearts exhibited a partial restoration toward the control cardiolipin HPLC spectra. Our data showing restoration of cardiolipin integrity, along with improvements in complex I structure and activity in the Ran treated hearts, are consistent with another study showing that restoration of cardiolipin content in mitochondria can improve complex I activity[297].

3.5. Conclusions

Protection of hearts against IR injury by ranolazine is associated with mitochondrial protection. Although Ran exerts a protective effect on complex I and its supporting structures, it is doubtful from our study that Ran mediates its protection by directly interacting at complex I, given our finding that Ran had no direct effect on complex I activity, or on any other mitochondrial function we measured in intact or fragmented mitochondria. The reversal or attenuation of complex I dysfunction, albeit indirect, by Ran points out the importance of complex I integrity and function as important factors in restoring cardiac function. Moreover, given the effects we observed and other studies from the literature, Ran appears to protect hearts in various ways, including but not limited to blocking the late Na^+ current. Concomitant decreases in m[Ca^{2+}] overload and ROS emission, induced by Ran, are the probable factors that lead to preservation of cardiolipin and less backward e^- transfer through the Fe-S clusters of complex I, thereby improving its efficiency in function and NADH oxidizing capability. Nevertheless, our study emphasizes the extent of injury to complex I and other mitochondrial structures, and expresses the importance of understanding the mechanisms of compounds to protect mitochondria during cardiac IR injury.

4. Materials and Methods

4.1. Isolated heart preparation and functional assessment

The Institutional Animal Care and Usage Committee of the Medical College of Wisconsin approved all animal studies. Guinea pig hearts (n=43) were isolated and prepared for constant pressure perfusion studies as previously published[207,224,322,323]. Briefly, animals were injected i.p. with 10 mg/kg ketamine to induce anesthesia and with 5000 units heparin to prevent coagulation. Following decapitation and thoracotomy, hearts were removed and perfused with Krebs-Ringer's buffer (KR) (in mM 138 Na^+, 4.5 K^+, 1.2 Mg^{2+}, 2.5 Ca^{2+}, 134 Cl^-, 15 HCO_3^-, 1.2 $H_2PO_4^-$, 11.5 glucose, 2 pyruvate, 16 mannitol, 0.05 EDTA and 5 U/L insulin) gassed with 3% CO_2, 97% O_2 at pH 7.4 and 37°C. A saline filled balloon catheter attached to a transducer was used to measure left ventricular pressure (LVP). Diastolic LVP was set initially to zero in order to monitor any increase and an indicator of diastolic contracture, a marker of ischemic injury. Coronary flow was measured using an ultrasonic flowmeter (model T106X, Transonic Systems) placed directly into the aortic inflow line. Spontaneous heart rate was monitored using bipolar electrodes placed on the right atrial and ventricular walls.

4.2. Protocols for isolated, perfused heart

Given that IR injury is time dependent[299,324,325], we used an experimental protocol of 30 min of ischemia followed by 10 min reperfusion to assess changes in complex I. Once heart rate and LVP had stabilized each heart was subjected to one of the following six protocols: 60 min of control perfusion (TC) (n=8); 30 min global ischemia (I30) (n=8); 30 min global ischemia followed by 10 min of reperfusion (IR) (n=8); 10 μM Ran given 1 min prior to 30 min global ischemia (RanI30) (n=8); 10 μM Ran given 1 min before 30 min global ischemia followed by 10 min reperfusion (RanIR) (n=8) and 10 μM Ran given for 1 min followed by 40 min of KR perfusion (RanTC) (n=3). At the end of each experiment, some hearts were immediately immersed into liquid N_2 for later assessment of changes in electron paramagnetic resonance (EPR) signals, or for later determination of cardiolipin integrity by high pressure liquid chromatography (HPLC); alternatively mitochondria were isolated, as described below, for western blotting, analysis of supercomplex assemblies and assessment of complex I activity (NADH oxidation).

4.3. Isolation of mitochondria

At the conclusion of each protocol, hearts were immediately removed from the perfusion apparatus and mitochondria were isolated as previously described[224,326]. In brief, ventricles were excised, placed in isolation buffer (in mM: 200 mannitol, 5 KH_2PO_4, 5 MOPS, 1 EGTA, 0.1% BSA and 0.5 mg/ml butylated hydroxy toluene as an anti-oxidant (pH adjusted to 7.15 with KOH), and minced into fine pieces. The suspension was homogenized for 30 s in 2.5 ml isolation buffer containing 5 U/ml protease and for another 1 min after adding 17 ml isolation buffer. The suspension was centrifuged at 8,000 *g* for 10 min. The pellet was re-suspended in 25 ml isolation buffer and centrifuged at 750 *g* for 10 min, the supernatant was centrifuged again at 8,000 *g* for 10 min, and the final pellet, enriched in mitochondria, was re-suspended in 0.5 ml isolation buffer and stored at -80°C until further use.

4.4. Assessment of mitochondrial complex I activity

Mitochondria isolated as described above were centrifuged at 10,000 *g* and the pellet was re-suspended and washed in hypotonic buffer containing 25 mM potassium phosphate buffer with 5 mM $MgCl_2$ at pH 7.2 by centrifugation at 10,000 *g*. After dilution to the appropriate concentration, mitochondria were subjected to three rounds of freeze-thaw cycles in the same hypotonic buffer. The fractured mitochondria were used for assay of dynamic respiratory complex I activity using a cuvette based spectrophotometer (PTI- model QM-8, Photon Technology International).

Complex I activity was measured by monitoring the dynamic change in absorbance from oxidation of NADH to NAD^+ at 340 nm in a pH 7.2 buffer containing 25 mM potassium phosphate buffer with 5 mM $MgCl_2$, 2 mM KCN, 2.5 mg/ml BSA, 13 mM NADH, and 65 mM ubiquinone (UQ_{10})[327]. Briefly, after a 3 min baseline measurement, 5 µg of the mitochondrial lysate was added and absorbance was recorded continuously for another 5 min; this was followed by absorbance recorded for 3 min after 2 µg rotenone to completely block complex I activity. The rate of absorbance after adding rotenone was subtracted from the initial rate of change in absorbance, due to addition of mitochondria, to obtain rotenone sensitive activity. The rates of enzyme activity of all groups were normalized to citrate synthase activity levels to account for difference in active enzyme at the time of isolation. Rate of activity was calculated using the extinction coefficient of NADH as 6.81 mM^{-1} cm^{-1} [(327)].

4.5. Detection of supercomplex assemblies and histochemical staining of complex I

Mitochondrial respiratory complexes are integrated into multi-complex assemblies that can be detected using native gel electrophoresis[328,329] with the use of mild detergents to solubilize the mitochondrial membranes while preserving both the functional and structural integrity of the complexes. First, freshly isolated mitochondria were disrupted using the method of Schägger et al[330]. Briefly, 400 μg of pelleted mitochondria was re-suspended in pH 7.0 buffer containing 50 mM NaCl, 50 mM imidazole/HCl, 2 mM 6-aminohexanoic acid, and 1 mM EDTA. Next mitochondria were solubilized by adding dodecylmaltoside (2.5 g/g) and digitonin (6.0 g/g), followed by incubation on ice for 10 min and centrifugation at 16,000 *g* for 30 min. Then the supernatant was retained and 5 μl of 50% glycerol was added. Non-gradient, clear native gels (8% acrylamide) were used for resolving supercomplexes and individual complexes (Wittig et al. 2007). Gels were used either for Coomassie staining or histochemical staining to assess mitochondrial complex I function.

For Coomassie staining, gels were stained for 20 min in 0.2% Brilliant Blue G in methanol:acetic acid:water (MAW) (40:7:53 v/v), and later destained with MAW. After destaining, the gels were scanned using a desktop scanner (CanoScan 8400F) and densitometry was performed using the ImageJ program (National Institutes of Health, Bethesda, MD). Respiratory complex I function was detected by incubating the gel in 5 mM Tris-HCl, pH 7.4, containing 0.5 mg/ml Nitro Blue Tetrazolium chloride (NBT) and 2.5 mg/ml NADH. Bands were visible after 5 min incubation. The gels were transferred into Tris-HCl at pH 7.4 and scanned for densitometry. Complex III was detected by incubating the gels in 50 mM sodium phosphate buffer at pH 7.2 containing 0.5 mg/ml diaminobenzidine. Bands were visible after 45 min of staining. Gels were scanned for densitometry and reused for detecting complex IV function by transferring the gels into 50 mM sodium phosphate buffer at pH 7.2 containing 0.5 mg/ml diaminobenzidine and 5 mM cytochrome *c*[331]. Histochemical staining of complexes III and IV was performed to determine supercomplex components.

4.6. Western blot detection of complex I

Complex I subunit NDUFA9 is an integral membrane subunit, and is also known to be more prone to post translational modifications (PTM) than other subunits[332]. Hence any changes in levels of

this subunit indicate compromised membrane integrity and possible alterations in the PTMs of the subunit. Mitochondrial protein (50 µg) was solubilized in Laemmli buffer and resolved using sodium dodecyl sulphate- polyacrylamide gel electrophoresis (SDS-PAGE) as described by Laemmli[333] and transferred onto poly vinilidine difluoride membranes using Transblot System (Bio-Rad, Carlsbad, CA) in 50 mM tricine and 7.5 mM imidazole transfer buffer. Membranes were blocked with 10% non-fat dry milk in Tris Buffered Saline- TBS_t (25 mM Tris-HCl at pH 7.5, 50 mM NaCl and 0.1% Tween 20) by incubating for 1 h followed by incubation in anti- NDUFA9 antibody (Invitrogen, CA) solution overnight at 4 °C. After three washes with TBS_t the membrane was incubated with an appropriate secondary antibody conjugated to horse-radish peroxidase for 3 h. After five washes with TBS_t the membrane was incubated in enhanced chemiluminescence detection solution (ECL-Plus, GE-Amersham) and exposed to X-ray film for autoradiography. Equivalent protein loading was confirmed using an antibody against cytochrome *c* oxidase (complex IV) subunit 1 (Invitrogen, CA) since complex IV is relatively resistant to IR injury than complex I at 10 min of reperfusion[299,324,325].

4.7. Acetylation of mitochondrial protein

A common PTM is acetylation. Total mitochondrial protein acetylation was analyzed using Enzyme Linked Immuno Sorbent Assay (ELISA). Mitochondria, isolated as described above, were solubilized by suspension in phosphate buffered saline, pH 7.4, by the addition of 0.5 % Tween-20. 20 µg of the lysed protein was suspended in 50 µl of sodium carbonate-bicarbonate buffer, pH 7.4 and coated overnight in a 96 well plate. The wells were washed with PBS and blocked with 1% BSA. After three washes, anti-acetyl lysine antibody was added to each well. Following a three-hour incubation, the wells were washed again in PBS, and incubated with appropriate secondary antibody. Color development was achieved by the use of a solution containing o-phenyline diamine, citric acid, and hydrogen peroxide. The plate was scanned for optical density measurements at 490 nm[334].

4.8. Electron paramagnetic resonance

An EPR system (Elexsys 580 Pulse EPR spectrometer, Bruker, Billerica, MA) was used to detect the transfer of electrons (e^-) through respiratory complexes I and II (succinate dehydrogenase) resulting from the successive oxidation/reduction of Fe in Fe-S clusters. Treated or untreated

isolated hearts (n=4 per group) were immediately transferred to liquid N_2 at the end of the protocol and ground to a fine powder. The powder was transferred into quartz glass tubes which were stored at -80°C until analysis. EPR signals were obtained by scanning the samples in a high intensity magnetic field (3000-4000 G) at 10 Kelvin, 9.6 GHz, 5 mW microwave power and 5 G amplitude modulation. Each sample was scanned 9 times and spectra were averaged[320,335]. Signal intensities were measured for *g'*s of 2.023 (3Fe-4S attributed to cluster S3 of complex II or mitochondrial aconitase), 2.006 (attributed to semi-ubiquinone radical, $Q^{\bullet}$), 1.94 (2Fe-2S attributed to N1b of complex I or S1 of complex II), and 1.89 (4Fe-4S attributed to N4 of complex I and to the Rieske center of complex III[336].

4.9. Isolation and analysis of cardiolipin by HPLC

The integrity of cardiolipin isolated from minced heart tissue was assessed using HPLC (System Gold, Beckman Coulter, Fullerton, CA). HPLC detects difference in molecular weight, and thus different species, by the change in mobility of individual molecules through the HPLC column. Lipids were extracted from hearts using a modified method of Hara et al[337]. Briefly, hearts were removed from the perfusion system after treatments and quickly frozen in liquid N_2 and ground to a fine powder. Approximately 1 g of powdered tissue was added to 18 ml hexane:isopropanol (3:2) and mixed for 1 min. The suspension was filtered through Whatman no. 5 filter paper. The powdered tissue was washed twice with 2 ml hexane:isopropanol. Isolated lipids were then analyzed and estimated for cardiolipin content using thin layer chromatography (TLC). Briefly, 200 µl of each sample was loaded onto a Whatman silica gel-60 TLC plate and allowed to dry; 50 µg of purified bovine heart cardiolipin was used as the standard. Lipids were separated using chloroform:methanol:acetic acid:water (55:37.5:3:2) (Barcelo-Coblijn & Murphy, 2008). Bands were visualized by exposure to iodine vapors for 5 min. The ratio of band intensity for each group's cardiolipin was estimated and total lipids in each fraction were calculated. Appropriate amount of lipids equivalent to 200 µg of cardiolipin was dried under N_2 gas and resuspended in 20 µl hexane:isopropanol (3:2) and then injected into the HPLC. HPLC analysis was performed using the method of Barcelo-Coblijn et al. at 208 nm[338].

4.10. Statistical evaluation of data

For the intact heart studies, measurements for each group were compared at baseline, during the

brief treatment with or without ranolazine before ischemia, at 30 min ischemia, and at 10 min reperfusion. For all other studies, measurements for each group were measured at the end of the protocol. All data are expressed as mean ± SEM. Between groups and within group individual values were subject to two-way analysis of variance to determine overall significance. If F values were significant ($P < 0.05$), post hoc comparisons of means tests (Student-Newman-Keuls) were used to compare the groups within each subset. In mitochondrial studies, statistical analysis was performed similarly. Differences between means were considered significant when $P < 0.05$ (two-tailed).

Disclosures

The authors have no disclosures to make.

Acknowledgments

This work was supported in part by grants from the American Heart Association (0855940G, D.F. Stowe), the National Institutes of Health (R01 HL095122, A.K.S. Camara, and R01 HL089514, D.F. Stowe), and the Veterans Administration (VA Merit 8204-05P, D.F. Stowe).

Experimental contribution:

Ashish K. Gadicherla: Performed and analyzed spectroscopy and gel based complex-I assays, performed and analyzed native and denatured blots, performed and analyzed electron paramagnetic resonance studies, performed and analyzed TLC and HPLC studies wrote and edited manuscript

David F. Stowe: Designed and guided experiments, validated data, reviewed and edited manuscript

William E. Antholine: Planned, guided and validated electron paramagnetic resonance studies

MeiYing Yang: Performed and analyzed ELISA, reviewed and edited manuscript

Amadou K.S. Camara: Designed and guided experiments, validated data, reviewed and edited manuscript

3.3 Protection against cardiac injury by small Ca^{2+}-sensitive K^+ channels identified in guinea pig cardiac inner mitochondrial membrane

David F. Stowe[a,b,,d,e,f], Ashish K. Gadicherla[a], Yifan Zhou[c], Mohammed Aldakkak[a], Qunli Cheng[a], Wai-Meng Kwok[a,c], Ming Tao Jiang[a], James S. Heisner[a], MeiYing Yang[a], Amadou K.S. Camara[a,e]

[a] *Department of Anesthesiology, Medical College of Wisconsin, Milwaukee, WI, USA*

[b] *Department of Physiology, Medical College of Wisconsin, Milwaukee, WI, USA*

[c] *Department of Pharmacology and Toxicology, Medical College of Wisconsin, Milwaukee, WI, USA*

[d] *Department of Biomedical Engineering, Marquette University, Milwaukee, WI, USA*

[e] *Cardiovascular Research Center, The Medical College of Wisconsin, Milwaukee, WI, USA*

[f] *Research Service, Zablocki VA Medical Center, Milwaukee, WI, USA*

Please address all correspondence to: David F. Stowe, M.D., Ph.D., M4280, 8701 Watertown Plank Road, Medical College of Wisconsin, Milwaukee, Wisconsin 53226 USA,
email: dfstowe@mcw.edu

Abbreviated title: cardiac mitochondrial small Ca^{2+} sensitive K^+ channels

Highlights: We have identified small conductance Ca^{2+} -sensitive K^+ channels in the inner mitochondrial membrane of guinea pig cardiac ventricular mitochondria where they appear to have a key role in pre-conditioning hearts against ischemia-reperfusion injury via a mechanism that is dependent on generation of oxygen free radicals.

Key words: cardiac mitochondria; inner mitochondrial membrane; cell signaling; ischemia-reperfusion injury; oxidant stress; small conductance Ca^{2+} -sensitive K^+ channel

Abbreviations: IR, ischemia-reperfusion; SK_{Ca}, small conductance Ca^{2+} -sensitive K^+ channel; BK_{Ca}, big conductance Ca^{2+} -sensitive K^+ channel; K_{ATP}, ATP -sensitive K^+ channel; DCEB, 5,6-dichloro-1-ethyl-1,3-dihydro-2H-benzimidazol-2-one; IMM, inner mitochondrial membrane;

TBAP, Mn(III) tetrakis (4-benzoic acid) porphyrin; PPC, pharmacological pre-conditioning; TRAM, TRAM-34: 1-[(2-chlorophenyl) (diphenyl)methyl]-1*H*-pyrazole; GLIB, glibenclamide; PAX, paxilline; BSA, bovine serum albumin; IEM, immune-electron microscopy; MS, mass spectroscopy; NS8593, N-[(1R)-1,2,3,4-tetrahydro-1-naphthalenyl]-1H-benzimidazol-2-amine hydrochloride; UCL 1684, 6,10-diaza-3(1,3)8,(1,4)-dibenzena-1,5(1,4)-diquinolinacy clodecaphane

Abstract

We tested if small conductance, Ca^{2+}-sensitive K^+ channels (SK_{Ca}) pre-condition hearts against ischemia-reperfusion (IR) injury by improving mitochondrial (m) bioenergetics, if O_2–derived free radicals are required to initiate protection via SK_{Ca} channels, and, importantly, if SK_{Ca} channels are present in cardiac cell inner mitochondrial membrane (IMM). NADH and FAD, superoxide ($O_2^{\bullet-}$), and m[Ca^{2+}] were measured in guinea pig isolated hearts by fluorescence spectrophotometry. SK_{Ca} and IKCa channel opener DCEBIO (DCEB) was given for 10 min ending 20 min before IR. Either TBAP, a dismutator of $O_2^{\bullet-}$, NS8593, an antagonist of SK_{Ca} isoforms, or other K_{Ca} and K_{ATP} channel antagonists, was given before DCEB and before ischemia. DCEB treatment resulted in a 2-fold increase in LV pressure on reperfusion and a 2.5 fold decrease in infarct size *vs*. non-treated hearts associated with reduced $O_2^{\bullet-}$ and m[Ca^{2+}], and more normalized NADH and FAD during IR. Only NS8593 and TBAP antagonized protection by DCEB. Localization of SK_{Ca} channels to mitochondria and IMM was evidenced by a) identification of purified m SK_{Ca} protein by Western blotting, immuno-histochemical staining, confocal microscopy, and immuno-gold electron microscopy, b) 2-D gel electrophoresis and mass spectroscopy of IMM protein, c) [Ca^{2+}]–dependence of mSK_{Ca} channels in planar lipid bilayers, and d) matrix K^+ influx induced by DCEB and blocked by SK_{Ca} antagonist UCL1684. This study shows that 1) SK_{Ca} channels are located and functional in IMM, 2) mSK_{Ca} channel opening by DCEB leads to protection that is $O_2^{\bullet-}$ dependent, and 3) protection by DCEB is evident beginning during ischemia.

1. Introduction

Depressed mitochondrial (m) bioenergetics, excess reactive oxygen species (ROS) generation, and mCa^{2+} loading are major factors underlying ischemia and reperfusion (IR) injury[283]. Prophylactic measures targeted in part to mitochondria that reduce cardiac IR injury[26,339] include ischemic pre-conditioning (IPC, i.e., brief pulses of ischemia and reperfusion before longer ischemia) and pharmacologic pre-conditioning (PPC), i.e., cardiac protection elicited sometime after the drug is washed out. PPC is theoretically a better approach because it does not require the heart to first undergo brief ischemia. We reported previously that activation of a large (big) conductance Ca^{2+} – sensitive K^+ channel (mBK_{Ca}), which may be located in the cardiac myocyte inner mitochondrial membrane (IMM), can induce PPC[32]. The BK_{Ca} channel has not been found in the cardiac myocyte plasma membrane, but we have shown that a BKCa channel opener, NS1619, has biphasic effects on mitochondrial respiration, membrane potential (ψ_m), and superoxide radical ($O_2^{\bullet-}$) production in isolated mitochondria[224,239]. This suggested that opening of other mitochondrial K^+ channels could also elicit PPC.

There are other K_{Ca} channels of intermediate or small conductances identified in non-cardiac cells[340–342] that are membrane bound, calmodulin (CaM) –dependent and gated by Ca^{2+} and other factors. These channels have smaller unit conductances of 3-30 (small, SK_{Ca}) and 20-90 (intermediate IK_{Ca}) pS[343]. The opening of SK_{Ca} channels is initiated by Ca^{2+} binding to calmodulin at the C terminus of the channel[228,344] (Schumacher et al. 2001; Bruening-Wright et al. 2002). Of the known isoforms of SK_{Ca} channels that have been identified in endothelial cells, one is $K_{Ca}2.3$, which was found to exert a potent, tonic hyperpolarization that reduced vascular smooth muscle tone[345]. Moreover, there is evidence for the $K_{Ca}2.2$ isoform in rat and human hearts using Western blot analysis and reverse transcription -polymerase chain reaction[346] (Xu et al. 2003). Clones of the channel from atria and ventricles showed much greater expression in atria compared to ventricles, and electrophysiological recordings exhibited much greater atrial than ventricular sensitivity to AP repolarization by apamin, a selective SK_{Ca} antagonist[346,347].

We postulated that activation of SK_{Ca} channels induces a pre-conditioning effect similar to that elicited by a BK_{Ca} ($K_{Ca}1.1$, maxi-K) opener, and that this effect is mediated via channels located

in the IMM, i.e., they promote K^+ entry into the mitochondrial matrix. We tested if the $K_{Ca}3.1$ ($IK_{Ca}1$)[340,341,348] and $K_{Ca}2.2$ and $K_{Ca}2.3$ (SK_{Ca})[349–352] opener DCEBIO (DCEB), given transiently before ischemia, elicits PPC in a manner similar to that of the mBK_{Ca} channel opener NS1619[32]. We specifically examined the role of DCEB in attenuating the deleterious effects of IR injury on mitochondrial bioenergetics by near continuous measurement of $m[Ca^{2+}]$, NADH and FAD, and $O_2^{\bullet-}$ in isolated perfused hearts. We infused NS8593 to antagonize SK_{Ca} channel opening[353,354], and several other K^+ channel blockers to rule out effects of DCEB on other putative mK^+ channels, i.e., IK_{Ca} ($K_{Ca}3.1$) BK_{Ca}, and K_{ATP} channels. Because protective effects of putative K_{ATP}[355] and BK_{Ca}[32] channel openers can be abolished by ROS scavengers, we similarly bracketed DCEB with a matrix targeted dismutator of $O_2^{\bullet-}$ to assess the role of SK_{Ca} channel opening on $O_2^{\bullet-}$ production, presumably by mitochondrial respiratory complexes. We used several approaches to furnish solid evidence for the presence and functionality of SK_{Ca} channel proteins in the IMM of guinea pig isolated cardiac mitochondria, and in isolated IMM.

2. Results

2.1. DCEB protects isolated heart against IR injury

Spontaneous heart rate averaged 242±13 beats/min before ischemia for all groups; this was not statistically different at 120 min reperfusion for all groups (data not displayed). If ventricular fibrillation (VF) occurred, it was only once within the first 5 min of reperfusion in any heart; all were converted to sinus rhythm with intracoronary lidocaine. After 5 min reperfusion all hearts remained in sinus rhythm, some with occasional pre-ventricular excitations. In data not displayed the incidence of VF on reperfusion was CONTROL 100%, DCEB+TBAP 100%, DCEB 76%, DCEB+TRAM 72%, DCEB+PAX 77%, DCEB+GLIB 77% (all nonsignificant vs. control group).

Figs. 1-4 show the marked degree of dysfunction or damage in the untreated control group during and after global ischemia and the beneficial effects of PPC elicited by DCEB treatment before ischemia. Developed LVP (Fig. 1A) and coronary flow (Fig. 1B) were reduced in each group after ischemia compared to before ischemia, but these changes were much larger in the CONTROL and DCEB+TBAP groups than in the other groups. Similarly, cardiac efficiency (Fig. 2A) was lower and infarct size (Fig. 2B) was largest in the CONTROL and DCEB+TBAP groups than in all other groups. The drug treatments before ischemia had no effects by themselves on any of the functional

variables. These figures indicate that these variables were markedly improved on reperfusion after treatment with DCEB and that these improvements were reversed by TBAP, but not by PAX, TRAM, or GLIB.

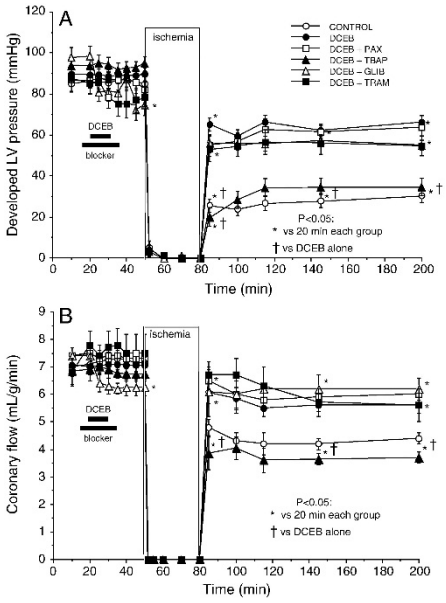

Fig. 1. Improved (**A**) developed (systolic-diastolic) LV pressure and (**B**) coronary flow after preconditioning with 3 μM DCEB. Note that TBAP (synthetic superoxide dismutase mimetic) reversed the protective effects of DCEB whereas antagonists of big (PAX, paxilline) and intermediate (TRAM) conductance K_{Ca} channels did not.

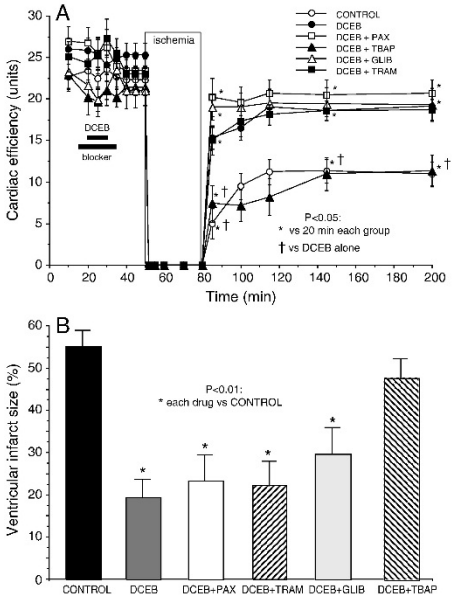

Fig. 2. A: Improved cardiac efficiency (developed LV pressure (mmHg)•heart rate (beats/min))/MVO_2 (μL O_2•g^{-1}•min^{-1}) after pre-conditioning with DCEB. Note that TBAP reversed the protective effects of DCEB whereas antagonists of big (PAX) and intermediate (TRAM) conductance K_{Ca} channels did not. **B**: Marked decrease in infarct size after pre-conditioning with DCEB. Note that TBAP reversed the anti-infarction effect of DCEB whereas

antagonists of big (PAX) and intermediate (TRAM) conductance K_{Ca} channels and K_{ATP} channels (glibenclamide, GLIB) did not.

There was no detectable change in NADH and FAD autofluorescence in any group by drugs given and terminated before ischemia (Fig 3A,B). NADH (Fig. 3A) remained higher at the end of ischemia and fell less during reperfusion after treatment with DCEB; this was reversed by TBAP but not by TRAM. FAD remained lower at the end of ischemia and rose less during reperfusion after treatment with DCEB (Fig 3B); this was reversed by TBAP, but not by TRAM. In other experiments there were no detectable change in NADH or FAD on reperfusion after DCEB+PAX or +GLIB treatment vs. DCEB alone.

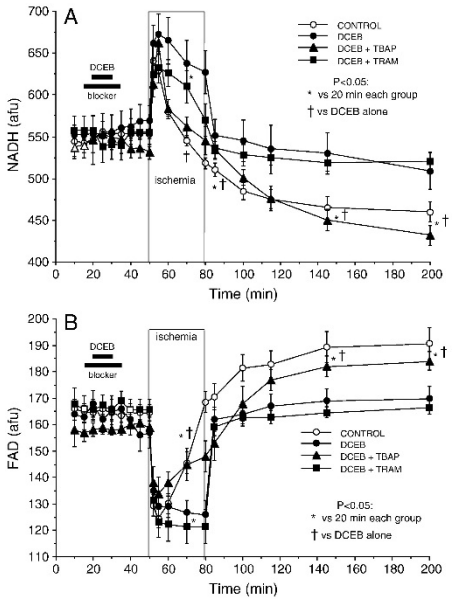

Fig. 3. Improved redox state (**A**: NADH and **B**: FAD autofluorescence) after pre-conditioning with DCEB. Note the inverse changes in NADH and FAD during ischemia and reperfusion and the more normalized responses in the DCEB group. TBAP reversed the protective effects DCEB whereas paxilline (PAX), an antagonist of big conductance BK_{Ca} channels did not.

DHE fluorescence ($O_2^{\bullet-}$ formation) (Fig. 4A) and indo 1 fluorescence (m[Ca^{2+}]) (Fig. 4B) rose markedly in each group during the course of ischemia. TBAP caused a small, but insignificant, decrease in DHE fluorescence before ischemia. TBAP reversed the effect of DCEB to reduce $O_2^{\bullet-}$ and m[Ca^{2+}] on reperfusion. Other experiments (not shown) did not demonstrate detectable changes in ROS formation or m[Ca^{2+}] on reperfusion after DCEB+PAX, +GLIB or +TRAM treatments vs. DCEB alone.

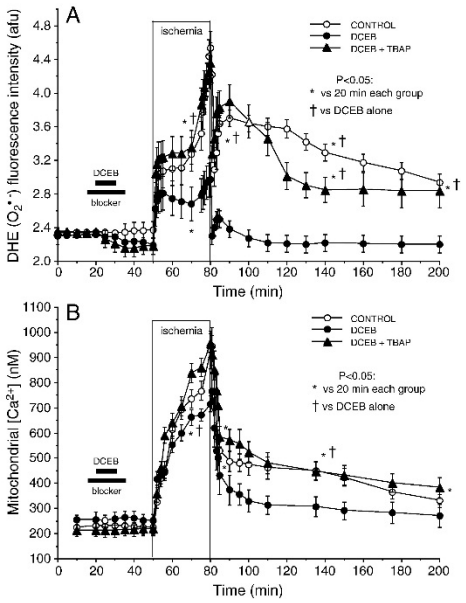

Fig. 4. Reduced (**A**) $O_2^{\bullet-}$ (DHE fluorescence) and (**B**) mitochondrial [Ca^{2+}] (indo 1 fluorescence) after pre-conditioning with DCEB. Note the increases in these signals during ischemia and the slow decline during reperfusion. DCEB attenuated the increase in these signals during ischemia and reperfusion and this was reversed by TBAP.

In companion experiments (Fig. 5A-D) the protective effects of DCEB were abolished or antagonized by the SK_{Ca} channel antagonist NS8593, thus demonstrating that DCEB protected via activation of SK_{Ca} channels. DCEB–induced maintenance of developed LVP was completely blocked, while the maintenance of coronary flow and the reduction of diastolic LVP and FAD oxidation by DCEB were all markedly reversed by NS8593. NS8593 alone significantly depressed developed LVP when given before ischemia and tended (non significantly) to slightly increase coronary flow, possibly indirectly due to reduced ventricular compression; thus the small increase in flow (Fig. 5B) noted in the presence of DCEB is due to NS8593 rather than DCEB. Generally, cardiac depression before ischemia is cardioprotective, but giving NS8593 with DCEB before ischemia, resulted in a worsening of contractile function on reperfusion.

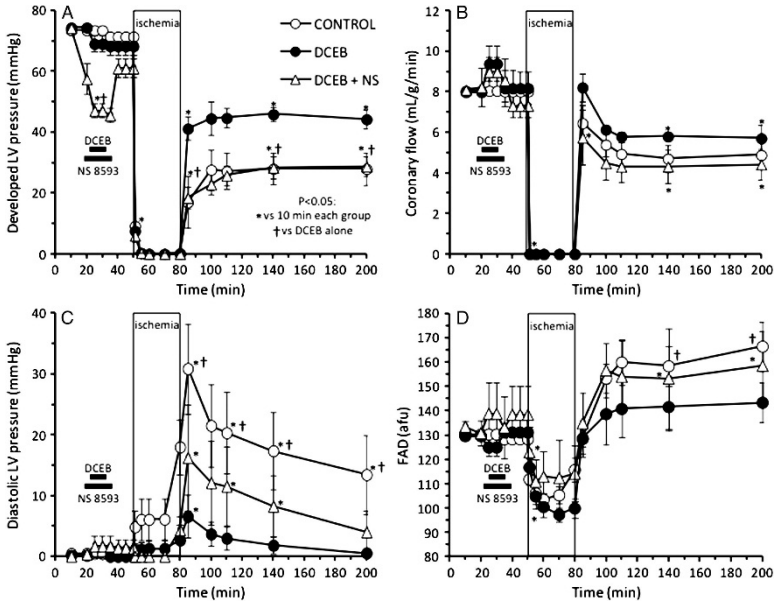

Fig. 5. Improved (**A**) developed LV pressure and coronary flow (**B**), and decreased diastolic LV pressure (**C**) and FAD oxidation (**D**), after pre-conditioning with DCEB. Note that 10 μM NS8593 (a specific SK_{Ca} antagonist) abrogated these protective effects of DCEB.

These studies demonstrated that DCEB had protective effects against cardiac IR injury mediated by the SK_{Ca} channel, and that cardiac mitochondria appeared to be involved in mediating this protection. Studies were then undertaken to isolate and identify the target of DCEB, the SK_{Ca} protein, in cardiac isolated mitochondria and in IMM, and to verify the functionality of the protein in an artificial lipid bilayer.

2.2. Isoelectric focusing and peptide sequences identify SK_{Ca} in isolated IMM

IMM protein, enhanced for calmodulin-binding residues, was separated by 2-D electrophoresis after silver staining. Three peptide spots of approximately 70 kD at pH 5.2 –5.5 were detected as SK_{Ca} using the anti $K_{Ca}2.3$ (anti-hSK3) (Fig. 6, panels a-c). Complementing this finding, a $K_{Ca}2.3$ protein was identified by ESI-mass spectrometry from five matching peptides with an amino acid coverage of 10.73% (Table). There was no evidence for peptides matching Na^+/K^+ ATPase or Ca^{2+} ATPase suggesting the absence of sarcolemmal and t-tubular membranes in the mitochondrial fraction. The mass spectrum of one of these peptide sequences is shown (Fig. 7). These results demonstrated that SK_{Ca} channels were present in the IMM.

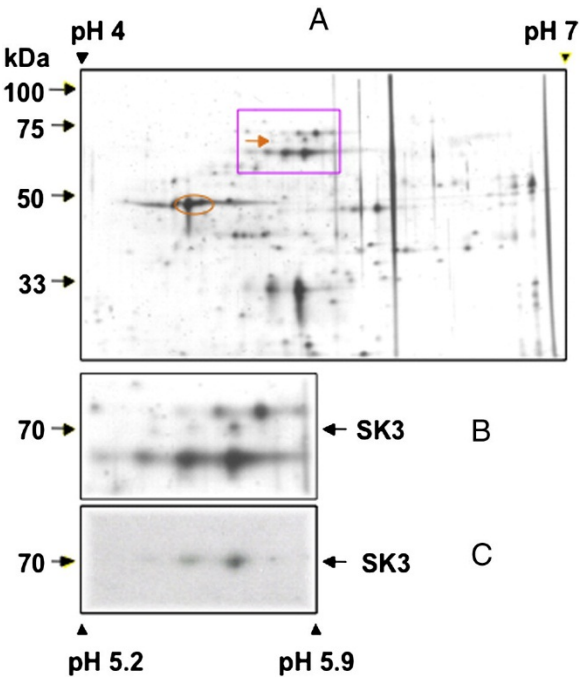

Fig. 6. Identity of small-conductance K_{Ca} channels in IMM from guinea pig heart. Top panel: Silver staining of calmodulin affinity column-purified protein fractions after 2-D gel fractionation. The square indicates the area of interest, which was magnified and is shown in the middle panel. The arrows indicate position of $_{KCa2}$.3 proteins. Bottom panel: Western blot with an antibody targeting SK_{Ca} (anti-hSK3) channel detection at 3 spots at 70 kDa (arrow) between pH 5.2 and 5.5. Negative control was done by pre-incubatingK_{Ca}.3 antibodies with blocking peptide (not shown).

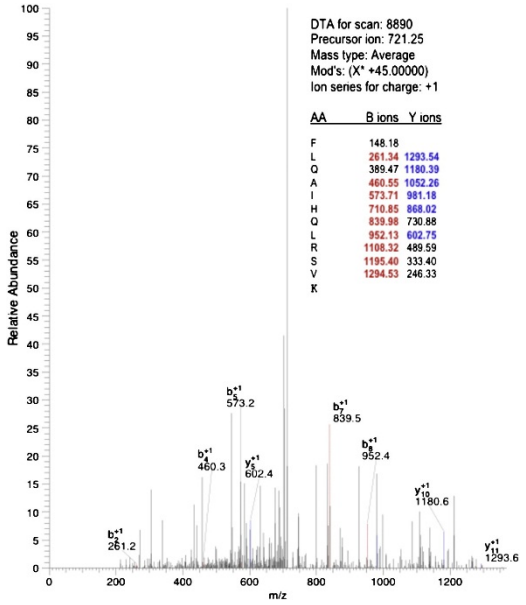

Fig. 7. Identification of one peptide, **FLQAIHQLRSVK** (in CaMBD), from data obtained using nano-LC/MS. The b-ions and y-ions are fragment masses of the above peptide upon its collision fragmentation. Peptides were identified

by searching the rodent subset of Uniprot databases. This protein was identified based on the 5 matching peptide sequences shown in the Table.

Table

Protein coverage matched to an SK_{Ca} subunit 6 isoform by NP LC/SI mass spectromet

Reference gi|21361129|ref|NP_002240small conductance calcium-activated potassium protein 6. Database C:\Xcalibur\database\human_ref.fasta Number of Amino Acids: 736 Average MW: 82026.4 pI:10.07a SKCa3, KCNN3

Note the matching of peptide sequences covering subunit 6 and calmodulin binding domain.

MDTSGHFHDS	GVGDLDEDPK	CPCPSSGDEQ	QQQQQQQQQQQPPPPAPPAA	
PQQPLGPSLQ	PQPPQLQQQQ	QQQQQQQQQQ	QQQQQPPHPL	SQLAQLQSQP
VHPGLLHSSP	TAFRAPPSSN	STAILHPSSR	QGSQLNLNDH	LLGHSPSSTA
TSGPGGGSRH	RQASPLVHRR	DSNPFTEIAM	SSCKYSGGVM	KPLSRLSASR
RNLIEAETEG	QPLQLFSPSN	PPEIVISSRE	DNHAHQTLLH	HPNATHNHQI
AGTTASSTTF	PKANKRKNQN	IGYKLGHR**RA**	**LFEKR**KRLSD	YALIFGMFGI
VVMVIETELS	WGLYSKDSMF	SLALKCLISL	STIILLGLII	AYHTREVQLF
VIDNGADDWR	IAMTYERILY	ISLEMLVCAI	HPIPGEYKFF	WTARLAFSYT
PSRAEADVDI	ILSIPMFLRL	YLIARVMLLH	SKLFTDASSR	SIGALNKINF

2.3. Western blots of serially purified mitochondria demonstrate SK_{Ca} channel protein

Mitochondria exhibited increasing band densities for both SK_{Ca} and ANT protein (Fig. 8) when enriched by Percoll gradient serial purification. This furnished compelling Western blot evidence that SK_{Ca} channel protein increases in abundance with ANT, which is present only in the IMM.

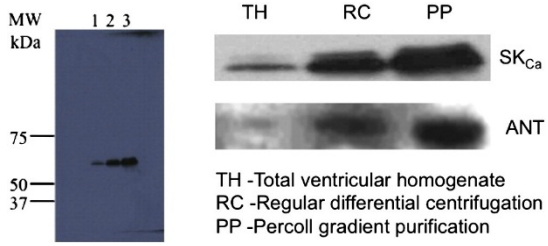

Fig. 8. Western blots of serially purified mitochondria showed increasing amounts of SK_{Ca} protein. Equal amounts of protein were loaded in the gel. Total homogenate (lane 1, TH) showed least band intensity, followed by mitochondria isolated by differential centrifugation (lane 2 RC); mitochondrial purified further by Percoll gradient purification (lane 3, PP) had the highest band intensity. Protein bands of SK_{Ca} are approximately 68 KDa. Purity of mitochondria was followed by assaying the increased amount of ANT, along with SK_{Ca} protein in their respective purification fractions.

2.4. Immunochemistry and confocal microscopy identify SK_{Ca} channel protein in mitochondria

Confocal microscopy was used to localize SK_{Ca} protein to intact mitochondria. Cardiac mitochondria were visualized as stained by an antibody against ANT (green), and SK_{Ca} channel protein was visualized using the anti-K_{Ca}2.2 (anti-SK2) antibody (red) (Fig. 9). Overlay of the two images (yellow) shows co-localization of SK_{Ca} and ANT proteins in cardiac mitochondria. Since ANT localizes only to the IMM, this suggested that SK_{Ca} channel protein also localizes to the IMM.

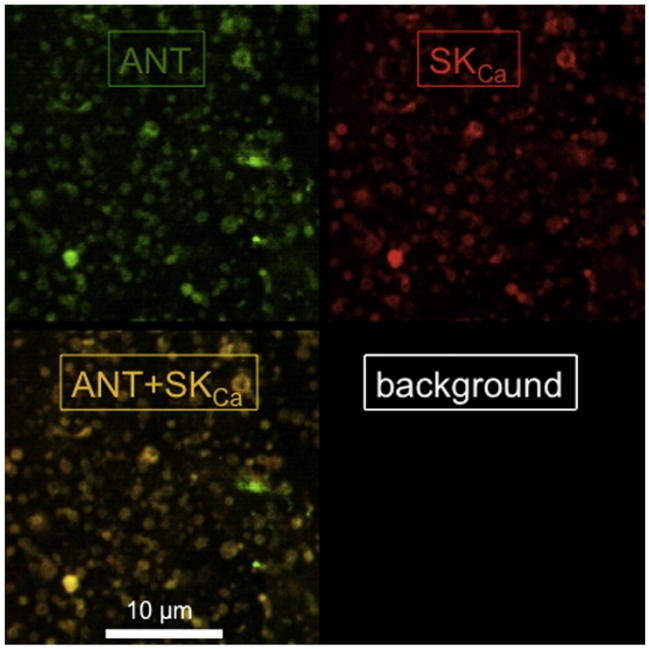

Fig. 9. SK_{Ca} protein identified in isolated mitochondria and visualized by confocal microscopy. Overlay of the two images (anti-ANT, green and anti-SK_{Ca}, red) demonstrates co-localization (yellow) of the SK_{Ca} protein in mitochondria.

2.5. Immuno-gold labeling and EM show localization of SK_{Ca} channels in mitochondrial matrix

To further confirm the presence and localization of the SK_{Ca} channels on the IMM, mitochondria were visualized at high resolution using IEM. A large field EM view shows largely normal appearing cardiac mitochondria with intact outer membranes and cristae (Fig. 10). Enhanced resolution of immuno-gold labeled mitochondria show gold particles attributed to SK_{Ca} channels (Fig. 11A, B) or cytochrome *c* oxidase (COX) (Fig. 11C) within the matrix; in detailed examination of electron micrographs approximately 50% contained at least 2 gold particles. Negative controls (Fig. 11D) (non-immune rabbit polyclonal serum showed no gold particles in any field. Figs. 8, 9,

and 11 confirm that SK_{Ca} channels are located in mitochondria and most likely in the IMM.

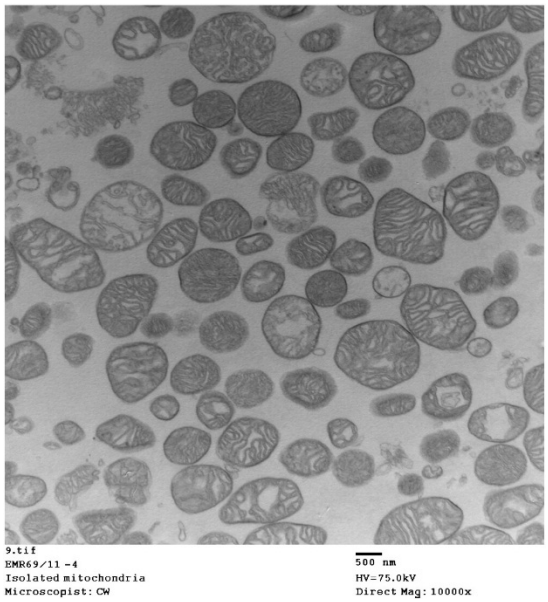

Fig. 10. Electron micrograph of isolated mitochondria. Larger field view of untreated mitochondria shows largely intact structural characteristics after isolation from guinea pig hearts.

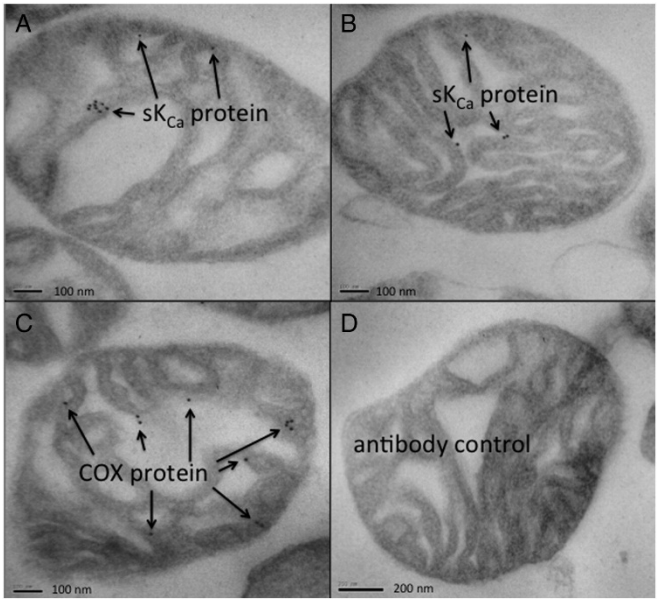

Fig. 11. Immuno-electron microscopy of isolated cardiac mitochondria. **A, B**: SK_{Ca} protein as visualized in two mitochondria; 50% of all viewed mitochondria exhibited gold labeling. Gold labeling was obtained by immuno-gold secondary antibody conjugated to primary rabbit polyclonal anti-K_{Ca2}.2 (anti-SK2). **C**: Positive control was anti-cytochrome *c* oxidase (COX1) conjugated to goat anti-rabbit or mouse conjugated to colloidal gold; each mitochondrion in a large field view exhibited at least two gold particles. **D**: Negative control was only secondary polyclonal rabbit antibody conjugated to gold; there was no gold labeling of any mitochondria in any views.

2.6. Mitochondrial SK_{Ca} protein forms a functional channel

To test if purified mitochondrial SK_{Ca} protein forms a functional channel, SK_{Ca} protein, isolated as noted above (*2.9*), was incorporated into a planar lipid bilayer for electrophysiological measurements. In the lipid bilayer, the SK_{Ca} protein exhibited robust activity in the presence of 100 μM [Ca^{2+}] (Fig. 12A). Two conducting states with chord conductances of 230 and 730 pS were observed when recorded in an ionic condition of equimolar 200 mM KCl. Adding apamin blocked channel activity (Fig. 12B) indicating that the functional channel formed by the mSK_{Ca} protein was inhibited by this SK_{Ca} channel blocker. The mSK_{Ca} channel protein incorporated into the planar lipid bilayer also displayed Ca^{2+}–dependent activity (Fig. 13). The mSK_{Ca} channel exhibited increasing activity as [Ca^{2+}] was serially increased from 1 to 100 μM. As shown, channel open probability (P_o) increased from P_o=0.5 at 1 μM [Ca^{2+}] to P_o=1.0 at 50 and 100 μM Ca^{2+}. A notable observation was also the [Ca^{2+}] dependent increase in the number of conducting states. At 1 μM Ca^{2+} the predominant conductance was 180 pS; however, at 50 and 100 μM Ca^{2+} multiple, larger conductances were revealed. Thus, as [Ca^{2+}] was increased the mSK_{Ca} channel exhibited greater conducting states while at lower [Ca^{2+}], low conductance states dominated. This observation is further supported by the existence of a smaller conductance channel of 70 pS which was detected, albeit infrequently, at 1 μM Ca^{2+} (Fig. 13, inset).

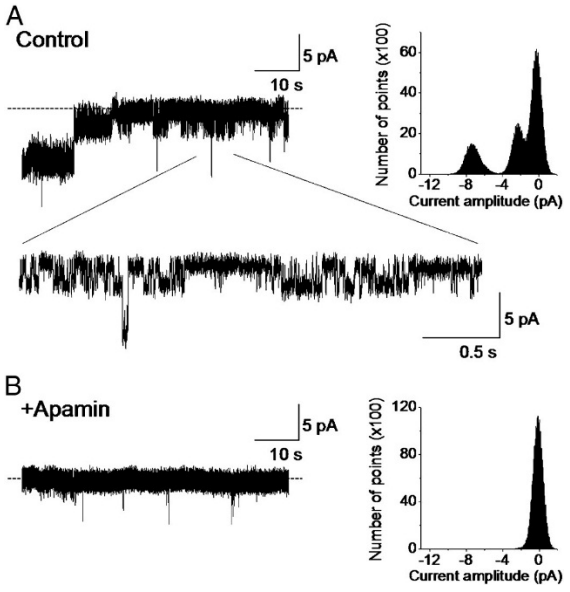

Fig. 12. mSK_{Ca} channel protein activity. Purified mitochondrial SK_{Ca} protein was incorporated into a planar lipid bilayer and channel activity was recorded at a membrane potential of -10 mV in the presence of 100 μM $CaCl_2$. Dotted

lines denote zero current levels and downward deflections denote channel openings. **A**: Two primary conductance states with chord conductances of 230 and 720 pS were observed under control conditions. The current recording is also depicted in an expanded time scale. Corresponding all-points amplitude histogram is also shown. **B**: Channel activity was blocked by adding100 nM apamin.

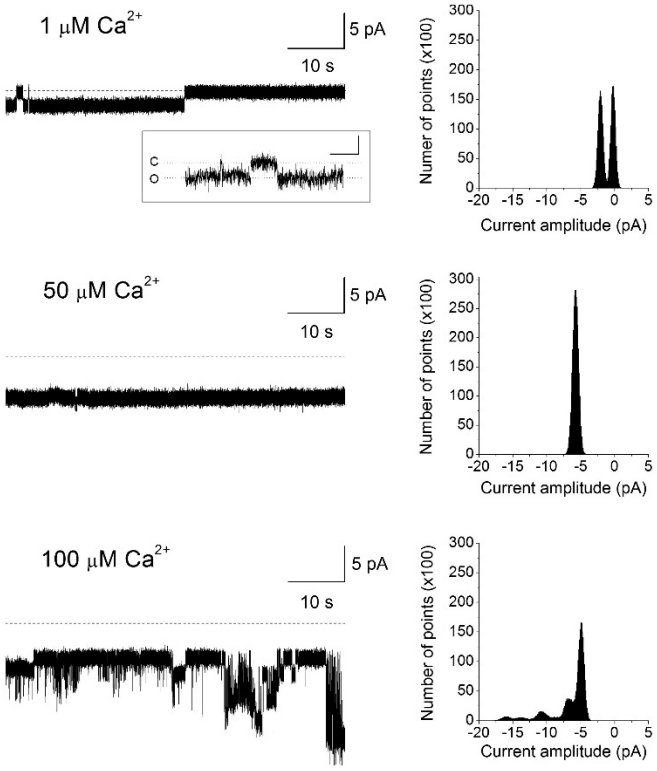

Fig. 13. mSK_{Ca} channel sensitivity to Ca^{2+}. Channel activity of purified mitochondrial SK_{Ca} protein, incorporated into the planar lipid bilayer, was recorded at a membrane potential of -10 mV. $[Ca^{2+}]$ was incrementally increased; dotted lines denote zero current levels and downward deflections denote channel openings. The corresponding all-points amplitude histogram is also shown. The predominant conductance was 180 pS when channel activity was recorded in 1 μM $[Ca^{2+}]^o$ However, we have also observed, infrequently, a smaller conducting state of 70 pS at 1 μM $[Ca^{2+}]$. A sample tracing is depicted in the inset in which the calibration for the x- and y-axis is 200 ms and 1 pA, respectively; C and O denote the closed and open states, respectively.

2.7. DCEB–induced increased matrix $[K^+]$ is blocked by UCL1684

The consequence of opening of SK_{Ca} channels to changes in mitochondrial matrix $[K^+]$ was also determined. In isolated mitochondria the SK_{Ca} channel opener DCEB increased matrix $[K^+]$ in the presence of quinine to inhibit KHE and thus counter K^+ extrusion (Fig. 14A, B). The observed influx of K^+ into the matrix was confirmed by similar K^+ influx induced by the K^+ ionophore valinomycin. The effect of DCEB was blocked by UCL1684 (a SK_{Ca} blocker) but not by iberotoxin (IBX) (a blocker of BK_{Ca} but not SK_{Ca} channels) (Fig. 14B). The increase in matrix K^+ uptake

induced by DCEB and blocked by UCL1684 (Fig. 14), and the Ca^{2+} induced increases in K^+ current and inhibition by apamin in lipid bilayers (Figs. 12, 13) functionally linked DCEB's cardiac effects to SK_{Ca} channels presence and activity in cardiac mitochondria.

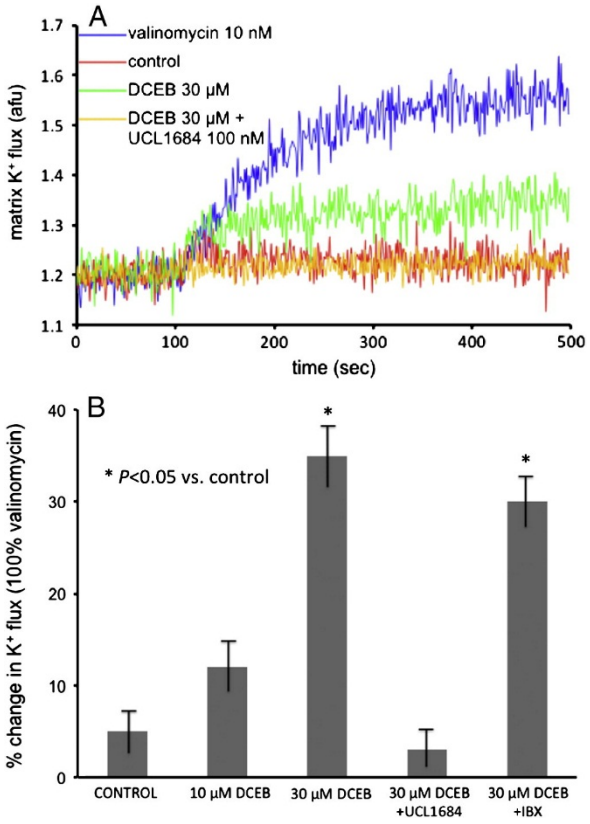

Fig. 14. **A**: Sample time tracing showing effect of 30 µM DCEB in the presence of 500 µM quinine (KHE inhibitor) to increase matrix K^+ (PBFI fluorescence) in mitochondria isolated from a guinea pig heart. No change was observed in the absence of quinine. The DCEB-induced increase in K^+ flux was completely blocked by 100 nM UCL1684. Note larger but similar effect of 1 nM valinomycin, a K^+ ionophore, to DCEB **B**: Summary effects (n = 10 mitochondrial preparations) of DCEB, expressed as a % of valinomycin effect, on increasing matrix K^+ in the presence of quinine. This increase in K^+ was blocked by SK_{Ca} channel blocker UCL1684 but not by 200 nM iberiotoxin (IBX), a blocker of BK_{Ca} channels.

3. Discussion

Our results suggest a novel role for the SK_{Ca} channel in cardiac myocyte pre-conditioning, likely mediated via altered mitochondrial function due to opening of SK_{Ca} channels located in myocyte mitochondrial IMM (mSK_{Ca}). Our comprehensive experimental approach shows that the well-known SK_{Ca} (and IK_{Ca}) channel activator DCEB pre-conditioned hearts and that this was fully

reversible by bracketing DCEB with the intra-matrix $O_2^{\bullet-}$ dismutator TBAP. Cardioprotective effects of DCEB were attributed specifically to activation of SK_{Ca} channels and not to activation of K_{ATP}, IK_{Ca}, or BK_{Ca} channels because NS8593, but not GLIB, TRAM, or PAX blocked its effects. DCEB increased K^+ flux in isolated mitochondria and the purified SK_{Ca} protein formed a functional channel when incorporated into lipid bilayers. Thus mSK_{Ca} channel opening, similar to that of mK_{ATP} and mBK_{Ca} channel opening, appears to induce PPC by an as yet unclear mechanism related to enhanced matrix K^+ entry. Moreover, mitochondrial-derived $O_2^{\bullet-}$ is required to initiate PPC by DCEB, because if $O_2^{\bullet-}$ is rapidly converted to downstream products the protection by DCEB is lost.

Just as we supported our evidence that the SK_{Ca} channel is specifically involved in PPC of isolated hearts, we sought to support specifically that the mSK_{Ca} channel was associated with cardioprotection. To provide evidence that DCEB's has protective effects mediated by mSK_{Ca} channels, it was necessary to rigorously identify mSK_{Ca} protein in purified mitochondria, and specifically in the IMM. To do so we utilized Western analysis and immuno-histochemistry, confocal microscopy, electron microscopy, and mass spectrometry of purified mitochondrial proteins derived from IMM. Organelle location was accompanied by channel functionality in isolated mitochondria and in lipid bilayers, thus supporting that this channel may play a role in cardiac protection via a mitochondrial mechanism. Overall our study indicates that the SK_{Ca} channel, localized in the cardiac cell IMM, mediates the effect of DCEB in pre-conditioning of the heart via a mitochondrial mechanism related to mK^+ flux and $O_2^{\bullet-}$ generation.

The dequalinium analogue, UCL1684, is known to block opening of apamin-sensitive SK_{Ca} channels in mammalian cell lines[356]. We support involvement of the mitochondrion in DCEB's PPC effect because TBAP could block the protective functional effects of DCEB as well as block DCEB's effect to decrease ischemia-induced levels of mCa^{2+} and of $O_2^{\bullet-}$, presumably generated by complexes along the electron transport system[357]. Also, DCEB directly induced an increase in matrix K^+ uptake. Moreover, since DCEB had no significant effects on coronary flow (Fig. 1), automaticity, or contractility, this suggests DCEB had no effect on endothelial/vascular or ventricular cell function. Overall, our results demonstrate the marked cardioprotective effects after pre-conditioning with DCEB and implicate mSK_{Ca} channel opening and generation of $O_2^{\bullet-}$, or its

products, as initiators and inhibitors of mitochondrial as well as cardiac myocyte PPC.

The improvement in cardiac function by DCEB was accompanied by reduced formation of $O_2^{\bullet-}$, reduced m[Ca^{2+}], and improved redox state (more normal NADH and FAD levels) during both ischemia and reperfusion. These cardioprotective effects of DCEB were blocked only by either TBAP or NS8593. We suggest that initial formation of $O_2^{\bullet-}$ is essential for the triggering mechanism of PPC by mSK_{Ca} channel activation. However, a downstream product of $O_2^{\bullet-}$, e.g. H_2O_2, might actually mediate the protective effects of DCEB. A similar dependence for $O_2^{\bullet-}$ has been observed for the mK_{ATP} channel opener diazoxide[355], the BK_{Ca} channel opener NS1619[32] and volatile anesthetics[22,358] Drug lipophilicity with mitochondrial membrane penetration may be an important common denominator for the activity of drugs such as diazoxide, a putative mK_{ATP} channel agonist, and DCEB.

3.1 Distribution and function of Ca^{2+} -sensitive K^+ channels

The cell membranes of vascular smooth muscle, neural, and secretory cells contain large conductance (200-300 pS). i.e. Big Ca^{2+}-sensitive K^+ (BK_{Ca}, aka maxi-K_{Ca}) channels that when opened produce vasodilation, hyperpolarization, and secretion. BK_{Ca} channel opening is activated by increased $[Ca^{2+}]_i$ and by cell membrane depolarization[359]. Activation of BK_{Ca} over a range of [Ca^{2+}] is mediated at several binding sites within the channel[360] so that there is a wide range of [Ca^{2+}] responsiveness (K_d 10-1000 μM)[361]. As K^+ exits the cell with BK_{Ca} channel opening, this elicits cell membrane repolarization or hyperpolarization, which in turn reduces Ca^{2+} entry by closing voltage-dependent Ca^{2+} channels. Altered redox potential in smooth muscle[362] suggested mitochondrial involvement. Xu et al. first furnished evidence that BK_{Ca} channels are located in cardiac mitochondria[223].

The membrane bound, but non-voltage-gated, K_{Ca} channels, i.e., SK_{Ca} and IK_{Ca}[343] are gated by Ca^{2+} and other factors. SK_{Ca} (a.k.a. K_{Ca}2.1-2.3, KCNN1-3 -gene symbol) channels have characteristics that largely differ from the BK_{Ca} channels i.e. small unitary conductance (10-30 pS), voltage independence with activation only by Ca^{2+} at very low K_a (0.3 μM with steep I/V slopes), a sensitivity to apamin, heteromeric assembly of the SK_{Ca} pore forming subunits with

calmodulin (CaM), N rather than C terminal EF hand domain for Ca^{2+} binding, and Ca^{2+} gating near the K^+ selectivity filter [363]. SK_{Ca}'s are unique in that calmodulin forms an integral part of the channel, forming its Ca^{2+}-sensitive subunits[227]. In the presence of Ca^{2+}, two calmodulin binding domains form a dimer, which allows the channel to open[228].

Antibodies against $K_{Ca}2.2$ and $K_{Ca}2.3$ were both used for immuno-staining and Western blot characterizations in purified mitochondria and in the enriched IMM fraction, respectively. We found that the identified protein was positive to both sets of antibodies. Because the sequence homology of the SK_{Ca} family of channels ($K_{Ca}2.1$, $K_{Ca}2.2$, $K_{Ca}2.3$) is highly conserved[226] the commercial antibodies we used might not have been selective enough to definitely identify the molecular identity of the specific mSK_{Ca} isoform. But we did confirm that the purified mSK_{Ca} protein formed a functional channel by recording channel activity after incorporating the protein into a planar lipid bilayer. The channel was inhibited by apamin, a blocker of plasmalemmal membrane SK_{Ca} channels. However, the recorded conductance states were higher than those reported for cell membrane SK_{Ca} channels, which are in the range of 10-14 pS[343,363]. The underlying cause of this discrepancy is unclear. It is possible that mSK_{Ca} channels have biophysical attributes that are different from their cell membrane counterparts. In particular, the mSK_{Ca} channels exhibited multiple conducting states that appear to be Ca^{2+}–dependent. As the [Ca^{2+}] increased, the channel's conductance also increased. Thus, at very low [Ca^{2+}], lower conductances may be revealed that are closer to those reported for the plasmalemmal SK_{Ca} channel. In support of this, in some recordings we infrequently observed a conductance of 70 pS at 1 μM [Ca^{2+}]. However, the mechanism that underlies this Ca^{2+}–dependent gating of the mSK_{Ca} channel has yet to be delineated. Though it is premature to speculate on the structural homology between the mitochondrial and plasmalemmal SK_{Ca} channels, based on our MS data and the Ca^{2+} sensitivity of the mSK_{Ca} channel, the Ca^{2+}calmodulin–binding domain and the S6 transmembrane region appear to be conserved. Indeed, the block of channel activity by apamin showed that this mSK_{Ca} channel does share a pharmacological property similar to the plasmalemmal SK_{Ca}.

However, the planar lipid bilayer experiments appear to indicate that the apamin binding site and the Ca^{2+} binding site are both localized to the same side of the mSK_{Ca} channel. This was an unexpected finding because apamin has been reported to be an external pore blocker that binds to

the outer pore region of the plasmalemmal SK_{Ca} channel[364] whereas the Ca^{2+} sensing region was believed to be on the intracellular side, conferred by calmodulin that is constitutively bound to the C-terminus of the channel[228]. Consequently, our findings would imply that the position of the C-terminus in the mSK_{Ca} channel differs from that in the plasmalemmal SK_{Ca} channel. Therefore, based on the sidedness of the apamin effect and Ca^{2+} sensitivity, together with our observed biophysical properties, the mSK_{Ca} channel may exhibit some functional and structural differences from the plasmalemmal SK_{Ca} channel. Additional experiments will be needed to confirm this possibility.

Our study represents the first conclusive report that identifies SK_{Ca} channels in cardiac myocyte mitochondria. Their presence in the IMM would indicate that they have an important function in fine-tuning regulation of mitochondrial bioenergetics, perhaps via volume control, which is largely controlled by K^+ flux. In contrast, the voltage and Ca^{2+}-dependent BK_{Ca} channels may open only when $\Delta\psi_m$ is high (state 4 respiration) or in response to a large imbalance in $m[Ca^{2+}]$ or cytosolic $[Ca^{2+}]$, much as BK_{Ca} channels regulate cell membrane potential in excitable cells.

Three genes encode the SK_{Ca} family; all have been cloned, and the amino acid sequences predict subunits similar to those in other K^+ channels. Channel specificity resides in the C terminal domains where each SK_{Ca} subtype interacts with the ubiquitous Ca^{2+} sensor CaM. This constitutive binding domain is called CaMBD[365]. Crystal structures show that SK_{Ca}+CaMBD contains two EF hand motifs within each of the globular N and C terminal regions separated by a flexible linker[365]. The C terminus is required to establish the link of SK_{Ca} and CaM. Substitution of neutral amino acids for aspartate and glutamate only in N terminus EF hand region blocks Ca^{2+} gating. This binding site is positioned just below the K^+ selectivity filter, which suggests that conformational changes near or even in the selectivity filter itself function to gate SK_{Ca} channels. The 18 amino acid bee venom toxin apamin is highly selective for SK2 by docking at the pore entrance and between the S3-S4 loops[366].

SK_{Ca} channels in neurons lie adjacent to Ca^{2+} stores and Ca^{2+} channels. In nerve cells SK_{Ca} channels play a role in setting the intrinsic firing frequency, while BK_{Ca} channels regulate action potential shape and may contribute to the unique climbing fiber response[346]. The K^+ flux mediated by BK_{Ca}

and SK_{Ca} channels in mitochondria may be differentiated by both their sensitivities to Ca^{2+} and dependence on $\Delta\psi_m$ during states 3 and 4 respiration. Because there are many differences between these channels, the functional effects of opening these channel are expected to differ; e.g., unlike BK_{Ca}, SK_{Ca} channel opening may "fine tune" matrix K^+ influx due to changing Ca^{2+} levels independent of changes in $\Delta\psi_m$ during the variable rate of oxidative phosphorylation.

3.2. mSK_{Ca} channel opening triggers pre-conditioning via ROS

The presence of both SK_{Ca} and BK_{Ca} channels in cardiac myocyte IMM indicates a functional importance for these channels during excess mCa^{2+} loading; moreover their endogenous opening during IPC, or as a pharmacological therapy, may be an important trigger for cardioprotection. It is unclear if these drugs actually open these K^+ channels directly to elicit pre-conditioning, or if they themselves alter mitochondrial bioenergetics (as mild uncouplers of oxidative phosphorylation), which mediates the memory of -conditioning by other downstream effectors. Although the mitochondrial pre-conditioning effect of DCEB appears to require both mSK_{Ca} channel opening and generation of $O_2^{\bullet-}$, these factors are not effectors of PPC as the DCEB and TBAP are washed out before ischemia.

There is ample evidence that $O_2^{\bullet-}$ is necessary to trigger PPC by mK^+ channel openers but the mechanism of $O_2^{\bullet-}$, and its products or reactants, in mediating PPC is unknown. An increase in redox state (increased NADH, decreased FAD) at a given $[O_2]$ can result in increased $O_2^{\bullet-}$ generation[367]. O_2 derived free radical "bursts" are known to occur during reperfusion when excess O_2 is available. Our group[22,32,358,368] and others[369,370] have shown, moreover, that ROS are also formed in excess during ischemia before reperfusion when tissue O_2 tension decreases, the redox state increases and then decreases, and cytochrome *c* oxidase (complex IV) activity is low[371]. The putative mK_{ATP} channel opener diazoxide[31] mimicked IPC on reducing infarct size and the ROS scavengers, N-acetylcysteine[372] or N-mercapto-propionyl-glycine[355], blocked the pre-conditioning effect of diazoxide. It has been suggested that mK_{ATP} channel opening can cause a small increase in ROS formation[373], which may trigger cardioprotection through activation of protein kinases. Conversely, ROS have also been proposed to activate the sarcolemmal K_{ATP} channel by modulating its ATP binding sites as this effect is blocked by GLIB or by ROS scavengers[374]. Others have

proffered that ROS produced during IPC may afford cardioprotection on reperfusion directly, or via a feed forward mechanism for K_{ATP} channel-induced ROS production[375,376].

In the present study evidence that the protective effect of DCEB is mediated by ROS is indicated by reversal of the protection in the presence of TBAP. $O_2^{\bullet-}$ or $OH^{\bullet}$, or even non-radical reactants like H_2O_2 or $ONOO^-$ (formed in the absence or presence of $NO^{\bullet}$, respectively) may actually produce the pre-conditioning responses, but $O_2^{\bullet-}$ appears necessary to initiate the response. It is also possible that mSK_{Ca}, mBK_{Ca}, and or mK_{ATP} channel activation is altered by ROS as a feed forward controller of mitochondrial function. Enhanced electron transfer before ischemia may minimize respiratory inefficiency, i.e., reduced matrix contraction and improved respiration on reperfusion. mSK_{Ca} channel opening, like mK_{ATP} channel opening, and indeed opening of any mK^+ channel, could induce PPC by mildly enhancing $O_2^{\bullet-}$ generation, which stimulates enzymatic pathways that help to protect the cell from IR injury. Interestingly, we observed that $O_2^{\bullet-}$ dismutation by TBAP blocked protection by DCEB.

When DCEB was given alone or with any of the inhibitors, it had no direct detectable effect on mechanical function or mitochondrial bioenergetics (redox state, $O_2^{\bullet-}$ levels) in isolated hearts. In our related study[32] neither NS1619 nor its antagonist PAX showed any direct effect on measured variables. In the *ex vivo*, intact heart perfused with adequate substrates and O_2, mitochondria are mostly respiring in the non-resting state 3, so small changes in $O_2^{\bullet-}$ between states 3 (ample ADP) and 4 (consumed ADP) respiration cannot be observed. However, in isolated cardiac mitochondria we reported that low, but not high, concentrations of the BK_{Ca} channel opener NS1619 can increase resting state 4 respiration and ROS generation while maintaining IMM potential ($\Delta\psi_m$)[224].

We propose similarly that DCEB, like NS1619, increases intramatrix K^+, which is replaced immediately with H^+ via KHE. We suggest that at low concentrations of these openers a transient increase in matrix acidity, i.e., via a proton leak, stimulates respiration but maintains $\Delta\psi_m$ so that a greater amount of $O_2^{\bullet-}$ is generated at mitochondrial respiratory complexes due to impaired electron transport. $O_2^{\bullet-}$ itself, or a reactant, may in turn stimulate downstream-induced phosphorylation pathways fostering K^+ channel opening as necessary when ischemia occurs. The net effect could be preservation of mitochondrial bioenergetics during ischemia as evidenced by better maintenance

of the reduced state (high NADH and low FAD) and smaller increases in $O_2^{\bullet-}$ generation and less m[Ca^{2+}] overload. This could lead to better preservation of oxidative phosphorylation and ATP turnover leading to better utilization of ATP on initial reperfusion after ischemia.

3.3. Putative mechanism of mitochondrial K^+ flux on mitochondrial protection during IR injury

BK_{Ca} and SK_{Ca} channel openers appear to have a profound ability to induce PPC but the mechanism is unclear. It is possible that brief ischemia as in IPC causes a slight elevation of mCa^{2+} that induces mSK_{Ca} and mBK_{Ca} channel opening and, like mK_{ATP} channel opening, leads to partial dissipation of $\Delta\psi_m$ and or matrix swelling as a protective mechanism against subsequent IR injury. It is now clear that K^+ is required for optimal functioning of oxidative phosphorylation because matrix K^+ flux largely regulates matrix volume and can modulate $\Delta\psi_m$[377–380]. Trans-matrix K^+ flux can also modulate ROS production[224] mSK_{Ca} channels, like mBK_{Ca} channels[223,380] may act to modulate matrix volume during times of increased matrix Ca^{2+} load, such as occurs during IR injury[323,381]. Xu et al. first suggested that opening mBK_{Ca} channels to enhance matrix K^+ influx[223] is an important factor in mitigating IR injury in a manner similar to mK_{ATP} channels. They proposed that the function of mBK_{Ca} channels was to improve the efficiency of mitochondrial energy production[223].

As with the other two K^+ channels reported in mitochondria, K_{ATP} and BK_{Ca}, once the K^+ channel is opened the increase in K^+ uptake leads to changes in the matrix as described by Garlid et al.[382] and Beavis et al.[383]. Electrogenic H^+ efflux driven by the respiratory chain is balanced by electrophoretic K^+ influx. If this were uncompensated, it would cause a very large increase in matrix pH of about 2 pH units. Partial compensation is provided by electroneutral uptake of substrate anions, such as phosphate. The compensation is partial because the concentration of phosphate in the cytosol is much lower than that of K^+, and this imbalance leads to matrix alkalinization[384,385]. Matrix alkalinization now releases the K^+/H^+ antiporter from inhibition by matrix protons[379] causing K^+ efflux to increase in response to increased K^+ uptake until a new K^+ steady state is achieved. An increase in futile K^+ cycling is believed to produce mild uncoupling[382] and regulates mitochondrial bioenergetics and ROS emission.

Although mK_{Ca} channels likely play a role in regulating mitochondrial bioenergetics, it is unknown how opening of these channels leads to more normalized NADH/FAD levels, reduces excess ROS, and decreases Ca^{2+} loading during IR. Just as the existence and function of the mK_{Ca} channel in IMM on mitochondrial respiration is unclear, so is the mechanism of K^+ influx via mK_{ATP} channels in IMM[377,380,386–389]. For the K_{ATP} channel it was proposed that its opening depolarizes the IMM to cause uncoupling and hasten respiration[380,386,390]. Subsequent ischemia would then reduce the driving force for Ca^{2+} influx through the mCa^{2+} uniporter; this could attenuate mCa^{2+} overload[391,392] so that energized mitochondria on reperfusion would perform more efficiently. Indeed the putative mK_{ATP} channel opener diazoxide is reported to reduce the rate of mCa^{2+} uptake by depolarizing the IMM and decreasing the driving force for mCa^{2+} entry[380,386,390] although this could be due to respiratory inhibition distinct from K_{ATP} channel opening[377,393].

Garlid's group, however, proposed that the physiological role of potential mK^+ channels is control of matrix volume rather than dissipation of $\Delta\psi_m$ and uncoupling[377,393]. They postulated that matrix swelling by K^+ uptake is caused by concomitant uptake of Cl^- and water by osmosis. But subsequent activation of mKHE may only slightly dissipate the proton gradient ($\Delta\mu H$) by increasing matrix acidity (proton leak) without significantly altering $\Delta\psi_m$[378,393]. In turn, mitochondrial swelling might optimize mitochondrial function because partial uncoupling was seen to improve efficiency of oxidative phosphorylation[394]. More specifically, during hypoxia matrix K^+ influx appears to maintain a normal matrix volume, which preserves a narrow intermembrane space and helps to facilitate energy transfer to ATP-utilizing sites, to reduce outer membrane permeability to nucleotides, and to slow ATP hydrolysis[377–379]. The end result of mSK_{Ca} channel opening, like mK_{Ca} channel opening, may be to improve mitochondrial efficiency, reduce $m[Ca^{2+}]$ and ROS production, and thereby to protect overall mitochondrial function during IR.

3.4. Interrelationship and timing of mCa^{2+} loading, $\Delta\psi_m$, redox state, and ROS during cardiac IR injury

Prolonged mitochondrial ischemia is marked by the following: decreasing $\Delta\psi_m$, an oxidized redox state, excess ROS, matrix contraction, and increasing mCa^{2+} loading. Ca^{2+} overload due to leaky IMM could impede normal electron transfer so that greater amounts of ROS are produced during

IR. Alternatively, ROS can damage membranes by lipid peroxidation; this can hamper selective permeability to ions and allow cytosolic and mCa^{2+} uptake as a result of increased reverse mode sarcolemmal Na^+/Ca^{2+} exchange (NCE)[395,396].

Our studies in the intact heart model show an interrelationship between $O_2^{\bullet-}$ produced, redox state, and mCa^{2+} influx during ischemia. Continuously measured NADH and $O_2^{\bullet-}$ changed together during ischemia as well as during reperfusion. Ischemia-induced rises in NADH, ROS, and $m[Ca^{2+}]$[22,32,323,355] returned closer to normal values on reperfusion after PPC. These effects were reversed by ROS scavengers or by blocking sarcolemmal K_{ATP} and/or mK_{ATP} channel opening with GLIB or 5-hydroxydecanoate[323,358]. Pre-conditioning also led to reduced ROS generation and improved ATP synthesis in isolated mitochondria[397]. These studies suggest that temporary exposure to distinct cardioprotective drugs before ischemia causes ROS-dependent changes in mitochondrial bioenergetics that initiates a pre-conditioning effect. mK_{Ca} is likely to be activated endogenously as matrix Ca^{2+} rises in response to an increase in Ca^{2+} load, such as occurs during ischemia; opening these channels pharmacologically before ischemia may lead to added protection.

3.5 Summary and limitations

We have furnished ample evidence for the presence of SK_{Ca} channels in purified mitochondria and in IMM from cardiac cells, for the functional effects of the IK_{Ca} and SK_{Ca} channel opener DCEB on K^+ flux in isolated mitochondria, and for the channel conductance of SK_{Ca} proteins incorporated into planar lipid bilayers. Moreover, we have demonstrated that SK_{Ca} channel opener DCEB initiates cardiac PPC as shown by marked metabolic and functional improvements during reperfusion. These are supported by better preserved reduced redox state (high NADH and low FAD), decreased $O_2^{\bullet-}$ production, reduced mCa^{2+} loading during IR, and reduced infarct size. The protection by DCEB was blocked by dismutation of $O_2^{\bullet-}$ with TBAP and by the SK_{Ca} antagonist NS8593. It is possible that mSK_{Ca} channel opening induces a mild proton leak due to mKHE, which accelerates respiration, but maintains $\Delta\psi_m$, so that small amounts of generated $O_2^{\bullet-}$ triggers a downstream protective pathway.

All of the K^+ channel agonists may converge on a pathway that stimulates a small amount of ROS.

That TBAP blocks protection by this drug and that mitochondria are a major source of ROS, suggest that DCEB exerts its effects primarily in mitochondria. Only relative changes in NADH and FAD levels and ROS formation can be assessed in our model. We did not test if the mSK_{Ca} channel is open during IR injury, although we have preliminary evidence that the BK_{Ca} channel is open during reperfusion[239]. It is plausible that some factors that induce pre-conditioning, like small increases in ROS or $m[Ca^{2+}]$, are the same factors, albeit at much greater levels, that cause IR damage. Thus the individual stages of triggering, activation and end-effect must be well delineated to unravel the complicated mechanism underlying the cardiac protection afforded by pre-conditioning.

4. Materials and methods

4.1. Isolated heart model

The investigation conformed to the *Guide for the Care and Use of Laboratory Animals* (NIH Publication 85-23, revised 1996). Guinea pig hearts were isolated and prepared as described in detail[32,323,358,368,381] with care to minimize IPC. These were pre-oxygenation, maintained respiration after anesthesia with ketamine (50 mg/kg), and immediate aortic perfusion with cold perfusate. Hearts were instrumented with a saline filled balloon and transducer to measure left ventricular pressure (LVP) and an aortic flow probe to measure coronary flow (CF). Heart rate and rhythm were measured via atrial and ventricular electrodes. Hearts were perfused at constant pressure with modified Krebs-Ringer's solution at 37˚C. Heart rate (HR) and rhythm, myocardial function (isovolumetric LVP), coronary flow and venous pO_2 were measured continuously. $\%O_2$ extraction, myocardial O_2 consumption (MVO_2) and cardiac efficiency ($HR \bullet LVP/MVO_2$) were calculated. At 120 min reperfusion, hearts not isolated for mitochondria were stained with 2,3,5-triphenyltetrazolium chloride (TTC) and infarct size was determined as a percentage of ventricular heart weight[32,358,398].

4.2. Cardiac fluorescence measurements

Either $m[Ca^{2+}]$, NADH and FAD, or ROS (principally $O_2^{\bullet -}$) was measured near continuously or intermittently in the heart using one of four excitation (λ_{ex}) and emission (λ_{em}) fluorescence spectra described below. NADH and FAD were measured in the same heart; $m[Ca^{2+}]$ and ROS were

measured in different subsets of hearts. A trifurcated fiberoptic probe (3.8 mm^2 per bundle) was placed against the LV to excite and to record light signals at specific λ's using spectrophotofluorometers (SLM Amico-Bowman and Photon Technology International). The incident polychromic light was filtered at 350 or 490 nm and recorded at 390/450 or 540 nm, respectively, to measure NADH[22,381,399,400] and FAD[398,400] tissue autofluorescence. Alternatively, hearts assigned to measure Ca^{2+}, were loaded with 6 μM indo 1 AM for 30 min followed by washout of residual dye for 20 min. Ca^{2+} transients were recorded at the same wavelengths as for NADH. Then hearts were perfused with $MnCl_2$ to quench cytosolic Ca^{2+} to reveal non-cytosolic [Ca^{2+}], mostly [mCa^{2+}][22,322,381]. In other hearts, as reported earlier[22,32,358,368], dihydroethidium (10 μM, DHE), which is used to measure intracellular superoxide ($O_2^{\bullet-}$) level, was loaded for 30 min and washed out of residual dye for 20 min. The LV wall was excited with light λ_{ex} 540 nm; λ_{em} 590 nm) to measure a fluorescence signal that is primarily a marker of the free radical $O_2^{\bullet-}$ [369,401]. DHE enters cells and is oxidized by $O_2^{\bullet-}$ where it is converted to the labile cation, 2-hydroxyethidium (2-HE^+), which causes a red-shift in the EM light spectrum[402,403].

Myocardial fluorescence intensity was recorded in arbitrary fluorescence units (afu) during 35 discrete sampling periods throughout each experiment at a sampling rate of 100 points/s (100 Hz, pulse width 1 μs) during a 12 s triggered period for $O_2^{\bullet-}$ and for a 2.5 s triggered period for NADH and FAD, and m[Ca^{2+}]. For each fluorescence study, no drug alone had any effect on background autofluorescence. Signals were digitized and recorded at 200 Hz (Power LAB/16sp, Chart and Scope version 3.6.3. AD Instruments) on G5 Macintosh computers for later analysis using specifically designed programs with MATLAB (MathWorks) and Microsoft Excel software. All variables were averaged over the 2.5 or 12 s sampling period.

4.3. Protocol

Hearts were infused with 3 μM DCEBIO (DCEB) for 10 min ending 20 min before the onset of 30 min global ischemia. DCEB is derived from the benzimidazolone class of compounds, which are known to stimulate chloride secretion in epithelial cells[322,340,404]. DCEB non-selectively opens K_{Ca}2.2 and 2.3 channels[340,349–352]. In most hearts DCEB was bracketed either with 40 μM PAX (paxilline), a blocker of BK_{Ca} channels[405] 20 μM TBAP, a chemical dismutator of $O_2^{\bullet-}$ that can enter the matrix, 200 μM GLIB (glibenclamide), a K_{ATP} channel blocker, or 100 nM TRAM

(TRAM-34), an established blocker of IK_{Ca} conductance channels[341]. TRAM was selected because DCEB also opens IK_{Ca} channels[340,341,352,353]. PAX, TBAP, GLIB, or TRAM was given 5 min before, during DCEB perfusion, and for 5 min after stopping DCEB. In a separate study DCEB was bracketed with 10 μM NS8593, a specific antagonist of SK_{Ca} channels[353,354] to compare with a no drug IR control. Drug exposure was discontinued 15 min before the onset of global ischemia and lasted 120 min. NS8593 caused a transient fall in systolic (and developed) LVP and an increase in coronary flow. Additional studies (not displayed) showed that each of these drugs, except for NS8593, given alone (without DCEB) for 20 min before ischemia elicited no appreciable effects and had no different effect on IR injury than the drug-free controls.

4.4. Statistical Analyses

A total of 155 isolated heart experiments were divided into 7 groups, a drug-free control, and DCEB alone or plus NS8593, PAX, TBAP, GLIB or TRAM. Functional data were recorded from 12-15 hearts per group. Infarct size was measured in a blinded manner in 8 hearts per group. NADH and FAD were measured in approximately 6-8 hearts per group, $O_2^{\bullet-}$ in 5-7 hearts per group, and $m[Ca^{2+}]$ in 6-8 hearts per group. Because functional studies showed trends that PAX, GLIB, or TRAM did not block protective effects of DCEB, only four groups were compared in NADH and FAD experiments and three groups were compared in $O_2^{\bullet-}$ and $m[Ca^{2+}]$ experiments. All data were expressed as means ± standard error of means. Appropriate comparisons were made among groups that differed by a variable at a given condition or time, and within a group over time compared to the initial control data. Statistical differences were measured across groups at specific time points (20, 50, 85, 145, and 200 min). Differences among variables were determined by two-way multiple ANOVA for repeated measures (Statview® and CLR anova® software programs for Macintosh®); if F tests were significant, appropriate post-hoc tests (e.g., Student-Newman-Keul's, SNK) were used to compare means. The incidence of ventricular fibrillation (VF) vs. sinus rhythm per group, and the number of VF's per heart per group, were determined by Fisher's Exact Test. In mitochondria K^+ flux experiments drug treatments were compared to control using the same statistical tests. Mean values were considered significant at *P* values (two-tailed) <0.05.

4.5. Isolation of cardiac mitochondria and inner mitochondrial membranes (IMMs)

Mitochondria were freshly isolated from 25 guinea pig hearts by differential centrifugation as

described previously[22,224,406,407]. To test mitochondrial viability and function in each preparation, the respiratory control index (RCI, state 3/state 4) was determined under both pyruvate (P, 10 mM), and succinate (S, 10 mM) + rotenone (R, 4 μM) conditions. State 3 respiration was determined after adding 250 μM ADP. Intact mitochondrial preparations were discarded if the RCI was less than 3 with succinate + R or less than 9 with pyruvate.

To isolate fraction-enriched IMMs, isolated mitochondria were shocked osmotically by incubating in 10 mM phosphate buffer saline (PBS) (pH 7.4) for 20 min, and then in 20% sucrose for another 15 min. The IMMs were sonicated for 30 s, 3 times, and then centrifuged at 8,000 *g* for 10 min. The supernatant containing sub-mitochondrial particles was fractionated using a continuous sucrose gradient (30% to 60%) and centrifuged at 80,000 *g* overnight in a SW28 rotor. The IMMs (enriched in the heavy fractions) were suspended with the isolation medium without EGTA and centrifuged at 184,000 *g* for 30 min. The final pellet enriched IMMs were suspended in isolation medium without EGTA and BSA and stored at -80ºC in small aliquots until use.

4.6. Enhancement of calmodulin-binding proteins from IMM

Calmodulin binds to SK_{Ca} channels so the calmodulin binding proteins obtained from the IMMs were concentrated to enhance the sensitivity of detection of mSK_{Ca} channels by Western blotting and by mass spectrometry. For calmodulin column chromatography (calmodulin-sepharose beads) the IMMs (5 mg protein) were solubilized for 2 h at 4°C in washing buffer, 200 mM KCl, 1 mM $MgCl_2$, 200 μM $CaCl_2$, 20 mM HEPES, pH 7.4, and 0.5% CHAPS with protease inhibitors. After centrifugation at 50,000 *g* for 30 min, the supernatant was applied to a calmodulin-sepharose column (10 by 1.5 cm) pre-equilibrated with the solubilization buffer containing 0.1% CHAPS. The column was washed rapidly with 500 mL of washing buffer as above. The proteins were eluted from the column by 2 mM EGTA in the elution buffer (200 mM KCl, 20 mM HEPES, pH 7.4, 0.1% (w/v) CHAPS) after washing. The fractions collected were concentrated and the proteins were separated by 2-D gel electrophoresis as follows.

4.7. Purification of SK_{Ca} channel proteins from IMM by isoelectric focusing

After isolating the IMM protein fraction (*4.5, 4.6*) the first dimension of isoelectric focusing (IEF) during 2-D gel electrophoresis was done in native gel buffer on an Immobilon Drystrips

(Amersham) with pH 4~7 gradient. The antibody was targeted to $K_{Ca}2.3$ (aka, hSK3, KCN3, Osenses Pty, Ltd.). The second dimension was done in a 10% Criterion® tris-SDS gel (Bio-Rad). Two identical gels were run at the same time, with one used for transfer to nitrocellulose membrane for Western blot analysis, and the other for silver staining for visualization.

4.8. IMM protein identification using electrospray LC/MS

IMM proteins (from *2.5, 2.6*) were digested with trypsin and subjected to pH focusing into 10 fractions over pH 3-10 and each fraction was directly analyzed using a NP LC/ESI mass spectrometer (Finnigan™ LTQ™ Ion Trap MS, Thermo Electron Corporation) to generate specific mass spectra typical for a given protein. The instrument utilizes stepped normalized collision energy (SNCE) to improve fragmentation efficiency over a wide mass range. This increases the capacity of a linear trap and the accuracy and sensitivity of peptide detection in the fmol range. A mass database (NCBI Entrez Pubmed protein) was searched for matching proteins and consequently the SK_{Ca} channel protein of interest was tentatively identified in IMM.

4.9. Purification of intact mitochondria by Percoll gradient fractionation

To further verify localization of SK_{Ca} channel protein in an intact mitochondria preparation, the Percoll gradient technique[408,409] with slight modifications, was used to purify intact mitochondria and immuno-histochemical staining was utilized to identify SK_{Ca} channel protein. In brief, mitochondria isolated as previously described (*4.5*) were layered over 30% Percoll (in buffer A containing 450 mM mannitol, 50 mM HEPES, 2 mM EDTA, pH adjusted to 7.4 followed by addition of 50 mg BSA), and centrifuged at 95,000 *g* for 30 min. The lower dense band observed at the bottom of the tube, enriched in mitochondria, was collected using a long tip glass pipette. Collected mitochondria (~4 ml) were resuspended in the same buffer used to dilute Percoll, and centrifuged again at 6300 *g*. The resulting pellet was suspended in the same buffer without BSA (buffer B) and re-centrifuged at 6300 *g*. The mitochondrial pellet was resuspended in a small volume (~0.3 ml) of buffer B and stored until further use.

4.10. Identification and localization of SK_{Ca} channel protein in purified mitochondria

Immuno-histochemical staining with an anti- SK_{Ca} antibody and confocal microscopy were used, in part, to verify that SK_{Ca} channel protein resides in mitochondria. Briefly, mitochondria, isolated

and purified as described above (*4.5*), were fixed onto poly-lysine coated coverslips. Mitochondrial structures were then fixed using paraformaldehyde and membranes were permeabilized using Triton X-100 and non-specific binding sites blocked by goat serum albumin. Coverslips were then incubated in solution containing anti-$K_{Ca}2.2$ (anti-SK2, ETQMENYDKHVTYNAERS, Alomone Labs (1:1000 in 5% milk)) and anti-ANT (adenine nucleotide translocase, Invitrogen) antibodies for 30 min followed by three washes in 0.1 M PBS. Coverslips were then incubated in appropriate secondary antibodies (Alexa Flour 455 and 546 respectively, Invitrogen (1:3000 in 2% milk)) for another 30 min and were then transferred onto microscope slides and visualized using a Leica confocal microscope (TCS SP5). Alternatively, mitochondria were utilized for immuno-gold labeling to localize SK_{Ca} channel protein in individual mitochondria.

4.11. Localization of SK_{Ca} channel protein by immuno-gold labeling and electron microscopy

Immuno-electron microscopy (IEM) was used to localize SK_{Ca} protein in purified cardiac mitochondria similar to the technique used by Douglas et al.[410] to localize BK_{Ca} channel protein in mitochondria. The final mitochondrial pellet, prepared as described above (*4.5*), was resuspended in 500 µL isolation buffer before centrifugation at 16,000 *g* for 20 min. The supernatant was discarded and an EM fixative containing 0.1% glutaraldehyde + 2% paraformaldehyde in 0.1 M NaH_2PO_4 buffer (pH 7.4) was added. After 1h fixation at room temperature the pellet was gently detached from the tube with a 25G needle and processed following the protocols of Berryman and Rodewald[411]. Pellets were washed 3 *x* 20 min in 0.1M NaH_2PO_4 buffer containing 3.5% sucrose and 0.5 mM $CaCl_2$, then rinsed in 0.1 M glycine in NaH_2PO_4 buffer for 1 h on ice before returning to NaH_2PO_4 buffer. The pellets were cut into 1 mm cubes and then washed 4 *x* 15 min in 0.1M tris maleate buffer + 3.5% sucrose, pH 6.5, at 4^{o}C followed by post fixation in 2% Uranyl acetate (w/v) in tris buffer, pH 6, for 2 h at 4^{o}C; specimens were then given a final rinse 2 *x* 5 min in Tris maleate buffer, pH 6.5. The specimens were then processed by the progressive lowering-of-temperature method into Lowicryl K4M resin and the resin was polymerized by UV irradiation. Ultrathin sections (70 nm) were cut onto Formvar/carbon coated grids. Immuno-labeling was performed by floating grids on droplets of 0.1 M NaH_2PO_4 buffer containing 5% BSA (PB-BSA), then incubating with rabbit polyclonal anti-$K_{Ca}2.2$ (anti-SK2, Alomone Labs) diluted 1:50 for 90 min, or with the positive control mitochondrial marker, cytochrome *c* oxidase (anti-COX1: Complex IV, subunit 1) mouse monoclonal antibody diluted 1:500. Non-immune rabbit polyclonal serum

was used as the negative control. This step was followed by 3 *x* 5 min washes in PB-BSA. The sections were then incubated with goat anti-rabbit IgG, or goat anti-mouse IgG, conjugated to 10 nM colloidal gold[412] for 90 min at room temp, rinsed in distilled water, and then stained with 2% aqueous uranyl acetate. Sections were examined in a JEOL JEM2100 TEM at 80 kV.

4.12. Purification/identification of SK_{Ca} channel protein by isoelectric focusing (IEF) and Western blotting

Total mitochondrial protein, once isolated and purified as above (*4.6*), was partitioned by IEF and the resulting fractions analyzed for mSK_{Ca} protein. Mitochondria (1 mg) were suspended in 3 mL electrophoresis buffer (0.1% w/v CHAPS, 0.1% w/v dodecyl maltoside, 5% (v/v) glycerol, 10 mg dithiothreitol) and IEF was performed using the Micro-Rotofor system (BioRad, CA) for 4 h at 400 mA constant current. The fractions thus obtained were collected and analyzed for SK_{Ca} protein by Western blot using the anti-K_{Ca}2.2 (anti-SK2) antibody. Briefly, equal volumes of the 10 fractions obtained by IEF were suspended in Laemmli buffer and resolved using sodium dodecyl sulfate- polyacrylamide gel electrophoresis (SDS-PAGE)[330], as originally described by Laemmli[333], and transferred onto poly vinilidine difluoride membranes using Transblot System (Bio-Rad) in 50 mM tricine and 7.5 mM imidazole transfer buffer. Membranes were blocked with 10% non fat dry milk in tris buffered saline- TBS_t (25 mM Tris-HCl at pH 7.5, 50 mM NaCl and 0.1% Tween 20) by incubating for 1 h followed by incubation in the anti-K_{Ca}2.2 antibody (anti-SK2) solution overnight at 4°C. After three washes with TBS_t the membrane was incubated with an appropriate secondary antibody conjugated to horseradish peroxidase for 3 h. After five washes with TBS_t the membrane was incubated in enhanced chemiluminescence detection solution (ECL-Plus, GE-Amersham) and exposed to X-ray film for autoradiography. The protein fraction containing the largest amount of SK_{Ca} was used for single channel recordings.

4.13. Enriching and incorporating mSK_{Ca} channel protein into lipid bilayers

Channel activity of the purified and enriched mSK_{Ca} protein was monitored by incorporating it into a planar lipid bilayer, as previously described[280]. Briefly, phospholipids were prepared by mixing phosphatidyl-ethanolamine, phosphatidyl-serine, phosphatidyl-choline, and cardiolipin (Avanti Polar Lipids) in a ratio of 5:4:1:0.3 (v/v). The phospholipids were dried under N_2 and re-suspended in n-decane to a final concentration of 25 mg/mL. The *cis/trans* chambers contained

symmetrical solutions of 10 mM HEPES, 200 mM KCl and 100 μM $CaCl_2$ at pH 7.4. The *cis* chamber was held at virtual ground and the *trans* chamber was held at the command voltages. SK_{Ca} protein was added into the *cis* chamber. The effect of the SK_{Ca} blocker apamin, 100 nM, on channel activity was tested by adding it to the *cis* chamber in the presence of 100 μM $CaCl_2$. To test for Ca^{2+} dependence of the SK_{Ca} channel, $[Ca^{2+}]$ was serially increased (1, 50 and 100 μM) in the *cis* chamber. Currents were sampled at 5 kHz and low pass filtered at 1 kHz using a voltage clamp amplifier (Axopatch 200B, Molecular Devices) connected to a digitizer (DigiData 1440, Molecular Devices), and recorded in 1 min segments. The pClamp software (version 10, Molecular Devices) was used for data acquisition and analysis. Additional analyses were conducted using Origin 7.0 (OriginLab).

4.14. Matrix K^+ measured in isolated mitochondria

Cardiac isolated mitochondria (0.5 mg protein/mL) were suspended in respiration buffer containing 130 mM KCl, 5 mM K_2HPO_4, 20 mM MOPS, 2.5 mM EGTA, 1 μM $Na_4P_2O_7$, 0.1% BSA, pH 7.15 adjusted with KOH. Buffer $[Ca^{2+}]$ was less than 100 nM as assessed by the fluorescence dye indo 1. Matrix K^+ was monitored during state 4 respiration (200 μM ATP) with substrate Na-pyruvate (10 mM) in a cuvette-based spectrophotometer (QM-8, Photon Technology International, PTI) with light (λ_{ex} 340 and 380 nm; λ_{ex} 500 nm) in the presence of the fluorescence dye PBFI (1 μM per mg/mL protein, Invitrogen)[326]. PBFI, in the acetylated methyl-ester (AM) form, was added to the mitochondrial preparation and incubated at 25°C for 20 min. After entering the matrix PBFI is retained in the matrix after it is cleaved from the methyl-ester. During the last pellet wash the extra-matrix residual dye was washed out. Most experiments were conducted in the presence of 500 μM quinine to block the mitochondrial K^+/H^+ exchanger (mKHE) and extrusion of the K^+ [326]. In some experiments 0.25 nM valinomycin, a K^+ ionophore, was given to verify an increase in matrix K^+ influx, and to be used as a reference for the change of K^+ influx by DECB ± its antagonist UCL1684.

Acknowledgements and Disclosures

The authors thank Anita Tredeau, Clive Wells, and Glen R. Slocum for their valuable contributions to this research study, which was supported in part by the National Institutes of Health (R01 HL089514 to DFS and R01 HL095122 to AKSC and RK Dash), the American Heart Association

(0355608Z and 0855940G to DFS), and the Veterans Administration (8204-05P to DFS). The authors have nothing to disclose about any conflict of interest.

Experimental contribution:

David F. Stowe: Designed and guided experiments, validated data, wrote and edited manuscript

Ashish K. Gadicherla: Performed confocal and immune-electron microscopy imaging, analyzed data performed and analyzed proteomics experiments, purified proteins for bilayer studies, reviewed and edited manuscript

Yifan Zhou: Performed and analyzed planar lipid bilayer studies

Mohammed Aldakkak: Performed and analyzed studies on isolated mitochondria

Qunli Cheng: Helped with planar lipid bilayer studies

Wai-Meng Kwok: Guided and validated planar lipid bilayer studies; reviewed and edited manuscript

Ming Tao Jiang: Guided proteomics studies

James S. Heisner: Performed ex-vivo Langendorff studies

MeiYing Yang: Reviewed and edited manuscript

Amadou K.S. Camara: Designed and guided experiments, validated data, reviewed and edited manuscript

Chapter 4

Discussion and Conclusion

General Discussion

The general aim of the thesis was to investigate and connect the multiple mitochondrial players in cardiac ischemia-reperfusion injury, and how knowledge on their modulation can be exploited for their use as therapeutic targets and/or development of novel strategies to arrest their dysfunction in pathological conditions. I focused on a) characterization of mitochondrial connexin 43 as a channel and how its modulation can effect mitochondrial calcium dynamics and how this can have an impact on cell death and cardiac injury; b)mitochondrial respiratory complex I in development of ischemic injury and its amelioration by the use of complex I targeting drug ranolazine and c) characterization of novel small conductance calcium sensitive potassium channels in mitochondria and how its modulation is beneficial in cardioprotection.

One of the most intriguing aspects of mitoCx43 is its location in the mitochondria. Studies have shown it to be present in both the IMM and the OMM. However, a conclusive study showing its orientation in the mitochondria is lacking. It has been shown that mitoCx43 is transported via an HSP90/TOM20 dependent pathway[179] However, given a lack of mitochondrial targeting sequence in Cx43, it is perplexing as to how Cx43 is transported. However, Cx43 is not the only nuclear encoded protein without mitochondrial targeting sequence that is transported into the mitochondria. For example, respiratory complex I, which is a multi-subunit protein, is composed of mitochondrial and nuclear DNA encoded proteins, with nuclear encoded subunits being transported into the mitochondria without any mitochondrial targeting sequence[199]. What is further interesting about translocation of Cx43 into the mitochondria is the rapid time line observed (less than 15 minutes to reduce mitoCx43 content by a third) when rat hearts are treated with HSP90 blocker[179]. The importance of such rapid control of translocation of mitoCx43 is yet to be understood.

Most studies to date have focused on the role of mitoCx43 in IPC[184,275,413]. However very little knowledge is available with regard to its role in acute ischemia. The role of mitoCx43 in IPC is closely linked to the generation of ROS[34,184,275] which is supposed to be cytoprotective. However, nothing is known yet about the connection between ROS and mitoCx43 in acute ischemia. In my studies, I have not only seen that (a) Ca^{2+} entry into the mitochondria (a key precursor event of cell

death in IR), is facilitated by Cx43, but also (b) that using Cx43 HC blocker peptides delays MPTP opening, prevents cell death following hypoxia-reoxygenation in isolated cardiomyocytes and (c) that perfusion of isolated mice hearts with Cx43 HC blocking peptides, especially RRNY, before IR significantly reduces infarct size.

A key factor necessary to understand how use of Cx43 HC blocking peptides affords cytoprotection is the opening and closed states of Cx43 HC and GJs and how these are differentially regulated. The interaction of CT and CL domains of Cx43 keeps the GJs closed, while keeping the HCs in a state that is available to open when an opening stimulus such as intracellular acidification, or elevated $[Ca^{2+}]_i$[124,128]. Under these conditions, the peptides do not change the states of either GJs or HCs. However, when an opening stimulus is applied in the presence of peptides, CT-CL interactions are disturbed thereby essentially "locking" the HCs in a closed state and keeping the GJs open. As mentioned previously, the orientation of Cx43, and thus its open or closed state in mitochondria is unknown. However, given that no matter what the orientation, the low $[Ca^{2+}]_i$ or the high negative potential seen by the CT, channels are expected to be open. Hence, mitoCx43 can be presumed to allow Ca^{2+} entry into the mitochondria, perhaps with other ions and metabolites, as shown previously[30,33,240]. As previously stated, unmitigated Ca^{2+} entry into the mitochondria is a hallmark of IR injury, which ultimately leads to apoptosis. By blocking one of the key Ca^{2+} entry pathways by the use of Cx43 blocking peptides, in my studies, I observed a drastic decrease in mitochondrial Ca^{2+} entry and consequently decreased cell death and lower infarct size. This strongly points to the presence of open Cx43 HCs, which can be prevented from opening by the use of peptides, especially RRNY.

The studies on mitoCx43 and IPC have shown a role for diazoxide induced ROS generation via a Cx43 mediated pathway. IPC is known to be afforded via various K^+ channels of the mitochondria, including but not limited to K_{Ca} channels and the K_{ATP} channels. Recent observations by Boengler et al. showed that mitoCx43 acts as a K^+ channel that can be blocked by Gap19[33]. This is an interesting observation in light of correlation between increased myocardial protection by the use of K^+ channel openers[32,224,279]. Mitochondrial volume modulation achieved via the opening of K^+ channels is thought to induce small amounts of ROS generation[25], which in turn trigger downstream protective pathways. Hence, it is plausible that Cx43 mediated ROS generation is a

consequence of altered mitochondrial volume, given the fact that Cx43 is a non-selective channel, permeable to not just ions and metabolites but also water. It would indeed be helpful to see if mitochondrial volume changes in the presence of Cx43 blocking peptides, and its effect on ROS generation.

Unmitigated generation of ROS by CI is a critical feature of IR injury, and blocking CI, during ischemia and not during reperfusion, is a cardioprotective pathway. Gap19 has been shown to block CI activity[180], however, no association between Cx43 and CI had been shown. In my studies, using native gels, I observe a physical association between Cx43 and CI in the form of a supercomplex. The cardioprotective effect of Gap19 and perhaps RRNY in my studies could, by correlation, be attributed to the blockage of Ca^{2+} into the mitochondria, and also perhaps blockage of CI based excess ROS generation.

In conclusion, my studies on mitoCx43, respiratory complex I and small conductance calcium sensitive potassium channels and the complicated interplay between various mitochondrial parameters show that mitochondria are complex organelles contributing to not just cellular energy needs, but also to cellular ion homeostasis. My studies also show that although dynamic buffers, mitochondria are susceptible to dysregulation of ion homeostasis with deleterious effects on energy generation, which in turn feeds back into the vicious loop of further deterioration. Understanding this complex interplay is critical for not just further insight into how pathological insults can act at different sites within the cell, but also in devising newer, more efficient therapeutic strategies. My studies have also shown that when devising therapeutic strategies, it is imperative to study not only the effects of these strategies on cellular parameters associated with the target, but also additional effects on the target itself to prevent inadvertently leading to deleterious effects. This is all the more crucial when targeting organelles such as the mitochondria- which are not only the deciders of cell death, but also for cell survival.

Limitations of experimental models

Although precautions have been taken to minimize avoidable mis-steps in devising experimental models and the studies on them, it is impossible to eliminate all limitations. In view of this, I briefly

mention the limitations that I feel the experimental models have.

First, the studies on mitochondria- aimed towards a better understanding of IR injury, can themselves be exposed to ischemic conditions during isolation process, which will invariably influence experimental results. Second- given the knowledge that mitochondria exist in two subpopulations- the SSM and IFM, only one manuscript (Chapter 3.1) takes into consideration of this difference. The other two manuscripts treat the entire mitochondrial pool as one population. Perhaps due to this pooling, I could have missed as yet unknown differences between the two populations with regard to either complex I (Chapter 3.2) or SK_{Ca} (Chapter 3.3). Third- the environment of isolated organs and organelles in the studies is highly artificial. This is sure to have implications on results obtained.

Therefore, a broad experimental approach which includes in vivo experiments as well as investigations at organ, cell and sub-cellular level can minimize the risk of drawing incorrect or partial results from experimental studies.

Future perspectives

Not only the understanding of exact mechanisms of IPC and POC and the players involved in these phenomena, but also pathological conditions such as IR injury and pharmaceuticals currently employed to treat these pathological conditions is incomplete. The results obtained in this thesis demonstrate that mitochondria are critically involved in signal transduction pathways of cardiac IR injury and play a major role in IPC and POC. Furthermore, given the fact that oxidative stress is one of the underlying mechanisms of ageing, diabetes etc. it is likely that mitochondria have a major role in those phenomenon as well. Further studies should investigate whether mitochondria are possible targets for pharmacological therapy for intervention in these pathological conditions as well.

References

1. Orn, S. *et al.* Effect of left ventricular scar size, location, and transmurality on left ventricular remodeling with healed myocardial infarction. *Am. J. Cardiol.* **99,** 1109–1114 (2007).
2. Murry, C. E., Jennings, R. B. & Reimer, K. A. Preconditioning with ischemia: a delay of lethal cell injury in ischemic myocardium. *Circulation* **74,** 1124–1136 (1986).
3. Heusch, G. Molecular basis of cardioprotection: signal transduction in ischemic pre-, post-, and remote conditioning. *Circ. Res.* **116,** 674–99 (2015).
4. Kuzuya, T. *et al.* Delayed effects of sublethal ischemia on the acquisition of tolerance to ischemia. *Circ. Res.* **72,** 1293–1299 (1993).
5. Liu, G. S. *et al.* Protection against infarction afforded by preconditioning is mediated by A1 adenosine receptors in rabbit heart. *Circulation* **84,** 350–356 (1991).
6. Solenkova, N. V, Solodushko, V., Cohen, M. V & Downey, J. M. Endogenous adenosine protects preconditioned heart during early minutes of reperfusion by activating Akt. *Am. J. Physiol. Heart Circ. Physiol.* **290,** H441–9 (2006).
7. Javadov, S. A. *et al.* Ischaemic preconditioning inhibits opening of mitochondrial permeability transition pores in the reperfused rat heart. *J. Physiol.* **549,** 513–524 (2003).
8. Zhao, Z.-Q. *et al.* Inhibition of myocardial injury by ischemic postconditioning during reperfusion: comparison with ischemic preconditioning. *Am. J. Physiol. Heart Circ. Physiol.* **285,** H579–88 (2003).
9. Argaud, L. *et al.* Postconditioning inhibits mitochondrial permeability transition. *Circulation* **111,** 194–197 (2005).
10. Penna, C. *et al.* Post-conditioning reduces infarct size in the isolated rat heart: role of coronary flow and pressure and the nitric oxide/cGMP pathway. *Basic Res. Cardiol.* **101,** 168–179 (2006).
11. Andreadou, I. *et al.* The role of gasotransmitters NO, H2S and CO in myocardial ischaemia/reperfusion injury and cardioprotection by preconditioning, postconditioning and remote conditioning. *Br. J. Pharmacol.* **172,** 1587–1606 (2015).
12. Pan, T.-T., Neo, K. L., Hu, L.-F., Yong, Q. C. & Bian, J.-S. H2S preconditioning-induced PKC activation regulates intracellular calcium handling in rat cardiomyocytes. *Am. J. Physiol. Cell Physiol.* **294,** C169–77 (2008).
13. Smith, C. C. T. *et al.* Leptin-induced cardioprotection involves JAK/STAT signaling that may be linked to the mitochondrial permeability transition pore. *Am. J. Physiol. Heart Circ. Physiol.* **299,** H1265–70 (2010).
14. Freedman, B. M., Hamm, D. P., Everson, C. T., Wechsler, A. S. & Christian, C. M. 2nd. Enflurane enhances postischemic functional recovery in the isolated rat heart. *Anesthesiology* **62,** 29–33 (1985).
15. Warltier, D. C., al-Wathiqui, M. H., Kampine, J. P. & Schmeling, W. T. Recovery of contractile function of stunned myocardium in chronically instrumented dogs is enhanced by halothane or isoflurane. *Anesthesiology* **69,** 552–565 (1988).
16. Novalija, E. & Stowe, D. F. Prior preconditioning by ischemia or sevoflurane improves cardiac work per oxygen use in isolated guinea pig hearts after global ischemia. *Adv. Exp. Med. Biol.* **454,** 533–542 (1998).
17. Tanaka, K., Ludwig, L. M., Kersten, J. R., Pagel, P. S. & Warltier, D. C. Mechanisms of cardioprotection by volatile anesthetics. *Anesthesiology* **100,** 707–721 (2004).
18. Tanaka, K. *et al.* Isoflurane produces delayed preconditioning against myocardial ischemia and reperfusion injury: role of cyclooxygenase-2. *Anesthesiology* **100,** 525–531 (2004).
19. Chiari, P. C. *et al.* Role of endothelial nitric oxide synthase as a trigger and mediator of isoflurane-induced delayed preconditioning in rabbit myocardium. *Anesthesiology* **103,** 74–83 (2005).
20. Chiari, P. C. *et al.* Isoflurane protects against myocardial infarction during early reperfusion by activation of phosphatidylinositol-3-kinase signal transduction: evidence for anesthetic-induced postconditioning in rabbits. *Anesthesiology* **102,** 102–109 (2005).
21. Tonkovic-Capin, M. *et al.* Delayed cardioprotection by isoflurane: role of K(ATP) channels. *Am. J. Physiol. Heart Circ. Physiol.* **283,** H61–8 (2002).
22. Riess, M. L., Camara, A. K. S., Kevin, L. G., An, J. & Stowe, D. F. Reduced reactive O2 species formation and preserved mitochondrial NADH and [Ca2+] levels during short-term 17 degrees C ischemia in intact hearts. *Cardiovasc. Res.* **61,** 580–590 (2004).
23. Elias-Miro, M., Jimenez-Castro, M. B., Rodes, J. & Peralta, C. Current knowledge on oxidative stress in hepatic ischemia/reperfusion. *Free Radic. Res.* **47,** 555–568 (2013).
24. Rimessi, A., Giorgi, C., Pinton, P. & Rizzuto, R. The versatility of mitochondrial calcium signals: from

stimulation of cell metabolism to induction of cell death. *Biochim. Biophys. Acta* **1777,** 808–816 (2008).
25. Garlid, K. D. & Paucek, P. Mitochondrial potassium transport: The K+ cycle. *Biochim. Biophys. Acta - Bioenerg.* **1606,** 23–41 (2003).
26. Camara, A. K. S., Lesnefsky, E. J. & Stowe, D. F. Potential therapeutic benefits of strategies directed to mitochondria. *Antioxid. Redox Signal.* **13,** 279–347 (2010).
27. Di Lisa, F. & Bernardi, P. Mitochondria and ischemia-reperfusion injury of the heart: fixing a hole. *Cardiovasc. Res.* **70,** 191–199 (2006).
28. Glancy, B. & Balaban, R. S. Role of mitochondrial Ca2+ in the regulation of cellular energetics. *Biochemistry* **51,** 2959–2973 (2012).
29. Santo-Domingo, J. & Demaurex, N. Calcium uptake mechanisms of mitochondria. *Biochim. Biophys. Acta - Bioenerg.* **1797,** 907–912 (2010).
30. Srisakuldee, W. *et al.* The FGF-2-triggered protection of cardiac subsarcolemmal mitochondria from calcium overload is mitochondrial connexin 43-dependent. *Cardiovasc. Res.* **103,** 72–80 (2014).
31. Garlid, K. D. *et al.* Cardioprotective effect of diazoxide and its interaction with mitochondrial ATP-sensitive K+ channels. Possible mechanism of cardioprotection. *Circ. Res.* **81,** 1072–1082 (1997).
32. Stowe, D. F. *et al.* Cardiac mitochondrial preconditioning by Big Ca2+-sensitive K+ channel opening requires superoxide radical generation. *Am. J. Physiol. Heart Circ. Physiol.* **290,** H434–40 (2006).
33. Boengler, K., Ungefug, E., Heusch, G., Leybaert, L. & Schulz, R. Connexin 43 impacts on mitochondrial potassium uptake. *Front. Pharmacol.* **4,** 73 (2013).
34. Ruiz-Meana, M. *et al.* Ischemic preconditioning protects cardiomyocyte mitochondria through mechanisms independent of cytosol. *J. Mol. Cell. Cardiol.* **68,** 79–88 (2014).
35. Turrens, J. F. & Boveris, a. Generation of superoxide anion by the NADH dehydrogenase of bovine heart mitochondria. *Biochem. J.* **191,** 421–427 (1980).
36. Demin, O. V, Kholodenko, B. N. & Skulachev, V. P. A model of O2.-generation in the complex III of the electron transport chain. *Mol. Cell. Biochem.* **184,** 21–33 (1998).
37. Green, D. R. & Kroemer, G. The pathophysiology of mitochondrial cell death. *Science* **305,** 626–629 (2004).
38. Huang, W.-Y., Jou, M.-J. & Peng, T.-I. Hypoxic preconditioning-induced mitochondrial protection is not disrupted in a cell model of mtDNA T8993G mutation-induced F1F0-ATP synthase defect: the role of mitochondrial permeability transition. *Free Radic. Biol. Med.* **67,** 314–329 (2014).
39. Bers, D. M. Cardiac excitation-contraction coupling. *Nature* **415,** 198–205 (2002).
40. Wagner, S., Maier, L. S. & Bers, D. M. Role of Sodium and Calcium Dysregulation in Tachyarrhythmias in Sudden Cardiac Death. *Circ. Res.* **116,** 1956–1970 (2015).
41. Dedkova, E. N. & Blatter, L. A. Calcium signaling in cardiac mitochondria. *Journal of Molecular and Cellular Cardiology* **58,** 125–133 (2013).
42. Barth, E., Stammler, G., Speiser, B. & Schaper, J. Ultrastructural quantitation of mitochondria and myofilaments in cardiac muscle from 10 different animal species including man. *J. Mol. Cell. Cardiol.* **24,** 669–681 (1992).
43. Ramesh, V., Sharma, V. K., Sheu, S. S. & Franzini-Armstrong, C. Structural proximity of mitochondria to calcium release units in rat ventricular myocardium may suggest a role in Ca2+ sequestration. *Ann. N. Y. Acad. Sci.* **853,** 341–344 (1998).
44. Szalai, G., Csordas, G., Hantash, B. M., Thomas, A. P. & Hajnoczky, G. Calcium signal transmission between ryanodine receptors and mitochondria. *J. Biol. Chem.* **275,** 15305–15313 (2000).
45. Sharma, V. K., Ramesh, V., Franzini-Armstrong, C. & Sheu, S. S. Transport of Ca2+ from sarcoplasmic reticulum to mitochondria in rat ventricular myocytes. *J. Bioenerg. Biomembr.* **32,** 97–104 (2000).
46. Kennedy, E. D. *et al.* , Glucose-stimulated insulin secretion correlates with changes in mitochondrial and cytosolic Ca 2+. *aequorin-expressing INS-1 cells, J. Clin.* **vest98,** 2524–2538 (1996).
47. Rutter, G. a. *et al.* Stimulated Ca2+ influx raises mitochondrial free Ca2+ to supramicromolar levels in a pancreatic ??-cell line: Possible role in glucose and agonist-induced insulin secretion. *J. Biol. Chem.* **268,** 22385–22390 (1993).
48. Peskoff, A. & Langer, G. A. Calcium concentration and movement in the ventricular cardiac cell during an excitation-contraction cycle. *Biophys. J.* **74,** 153–174 (1998).
49. Andrienko, T. N., Picht, E. & Bers, D. M. Mitochondrial free calcium regulation during sarcoplasmic reticulum calcium release in rat cardiac myocytes. *J. Mol. Cell. Cardiol.* **46,** 1027–1036 (2009).
50. Colegrove, S. L., Albrecht, M. a & Friel, D. D. Dissection of mitochondrial Ca2+ uptake and release fluxes in situ after depolarization-evoked [Ca2+](i) elevations in sympathetic neurons. *J. Gen. Physiol.* **115,** 351–

370 (2000).
51. Pivovarova, N. B., Hongpaisan, J., Andrews, S. B. & Friel, D. D. Depolarization-induced mitochondrial Ca accumulation in sympathetic neurons: spatial and temporal characteristics. *J. Neurosci.* **19,** 6372–6384 (1999).
52. Trollinger, D. R., Cascio, W. E. & Lemasters, J. J. Selective loading of Rhod 2 into mitochondria shows mitochondrial Ca2+ transients during the contractile cycle in adult rabbit cardiac myocytes. *Biochem. Biophys. Res. Commun.* **236,** 738–742 (1997).
53. Zhou, Z., Matlib, M. A. & Bers, D. M. Cytosolic and mitochondrial Ca2+ signals in patch clamped mammalian ventricular myocytes. *J. Physiol.* **507 (Pt 2,** 379–403 (1998).
54. Denton, R. M., Randle, P. J. & Martin, B. R. Stimulation by calcium ions of pyruvate dehydrogenase phosphate phosphatase. *Biochem. J.* **128,** 161–163 (1972).
55. Harborne, S. P. D., Ruprecht, J. J. & Kunji, E. R. S. Calcium-induced conformational changes in the regulatory domain of the human mitochondrial ATP-Mg/Pi carrier. *Biochim. Biophys. Acta* **1847,** 1245–1253 (2015).
56. Aldakkak, M., Camara, A. K. S., Heisner, J. S., Yang, M. & Stowe, D. F. Ranolazine reduces Ca 2+ overload and oxidative stress and improves mitochondrial integrity to protect against ischemia reperfusion injury in isolated hearts. *Pharmacol. Res.* **64,** 381–392 (2011).
57. Raffaello, A. *et al.* The mitochondrial calcium uniporter is a multimer that can include a dominant-negative pore-forming subunit. *EMBO J.* **32,** 2362–76 (2013).
58. Mallilankaraman, K. *et al.* MICU1 is an essential gatekeeper for MCU-mediated mitochondrial Ca(2+) uptake that regulates cell survival. *Cell* **151,** 630–644 (2012).
59. Nicchitta, C. V & Williamson, J. R. Spermine. A regulator of mitochondrial calcium cycling. *J. Biol. Chem.* **259,** 12978–83 (1984).
60. Litsky, M. L. & Pfeiffer, D. R. Regulation of the mitochondrial Ca2+ uniporter by external adenine nucleotides: the uniporter behaves like a gated channel which is regulated by nucleotides and divalent cations. *Biochemistry* **36,** 7071–7080 (1997).
61. Sparagna, G. C., Gunter, K. K., Sheu, S. S. & Gunter, T. E. Mitochondrial calcium uptake from physiological-type pulses of calcium. A description of the rapid uptake mode. *J. Biol. Chem.* **270,** 27510–27515 (1995).
62. Buntinas, L., Gunter, K. K., Sparagna, G. C. & Gunter, T. E. The rapid mode of calcium uptake into heart mitochondria (RaM): comparison to RaM in liver mitochondria. *Biochim. Biophys. Acta* **1504,** 248–261 (2001).
63. Gunter, T. E., Buntinas, L., Sparagna, G., Eliseev, R. & Gunter, K. Mitochondrial calcium transport: mechanisms and functions. *Cell Calcium* **28,** 285–296 (2000).
64. Gunter, T. E. & Sheu, S.-S. Characteristics and possible functions of mitochondrial Ca(2+) transport mechanisms. *Biochim. Biophys. Acta* **1787,** 1291–1308 (2009).
65. Wang, L., Yang, X. & Shen, Y. Molecular mechanism of mitochondrial calcium uptake. *Cell. Mol. Life Sci.* **72,** 1489–1498 (2014).
66. Jakob, R. *et al.* Molecular and functional identification of a mitochondrial ryanodine receptor in neurons. *Neurosci. Lett.* **575,** 7–12 (2014).
67. Trenker, M., Malli, R., Fertschai, I., Levak-Frank, S. & Graier, W. F. Uncoupling proteins 2 and 3 are fundamental for mitochondrial Ca2+ uniport. *Nat. Cell Biol.* **9,** 445–52 (2007).
68. Nowikovsky, K. & Bernardi, P. LETM1 in mitochondrial cation transport. *Front. Physiol.* **5,** 83 (2014).
69. Baysal, K., Jung, D. W., Gunter, K. K., Gunter, T. E. & Brierley, G. P. Na(+)-dependent Ca2+ efflux mechanism of heart mitochondria is not a passive Ca2+/2Na+ exchanger. *Am. J. Physiol.* **266,** C800–8 (1994).
70. Gunter, K. K., Zuscik, M. J. & Gunter, T. E. The Na(+)-independent Ca2+ efflux mechanism of liver mitochondria is not a passive Ca2+/2H+ exchanger. *J. Biol. Chem.* **266,** 21640–21648 (1991).
71. Brand, M. D. The stoichiometry of the exchange catalysed by the mitochondrial calcium/sodium antiporter. *Biochem. J.* **229,** 161–166 (1985).
72. Gunter, T. E., Chace, J. H., Puskin, J. S. & Gunter, K. K. Mechanism of sodium independent calcium efflux from rat liver mitochondria. *Biochemistry* **22,** 6341–6351 (1983).
73. Wingrove, D. E. & Gunter, T. E. Kinetics of mitochondrial calcium transport. I. Characteristics of the sodium-independent calcium efflux mechanism of liver mitochondria. *J. Biol. Chem.* **261,** 15159–15165 (1986).
74. Gunter, T. E. & Pfeiffer, D. R. Mechanisms by which mitochondria transport calcium. *Am. J. Physiol.* **258,**

C755–86 (1990).
75. Wingrove, D. E. & Gunter, T. E. Kinetics of mitochondrial calcium transport. II. A kinetic description of the sodium-dependent calcium efflux mechanism of liver mitochondria and inhibition by ruthenium red and by tetraphenylphosphonium. *J. Biol. Chem.* **261,** 15166–15171 (1986).
76. Saez, J. C., Berthoud, V. M., Branes, M. C., Martinez, A. D. & Beyer, E. C. Plasma membrane channels formed by connexins: their regulation and functions. *Physiol. Rev.* **83,** 1359–1400 (2003).
77. Söhl, G. & Willecke, K. Gap junctions and the connexin protein family. *Cardiovasc. Res.* **62,** 228–232 (2004).
78. Laird, D. W., Puranam, K. L. & Revel, J. P. Turnover and phosphorylation dynamics of connexin43 gap junction protein in cultured cardiac myocytes. *Biochem. J.* **273(Pt 1),** 67–72 (1991).
79. Beardslee, M. A., Laing, J. G., Beyer, E. C. & Saffitz, J. E. Rapid turnover of connexin43 in the adult rat heart. *Circ. Res.* **83,** 629–635 (1998).
80. Falk, M. M. & Gilula, N. B. Connexin membrane protein biosynthesis is influenced by polypeptide positioning within the translocon and signal peptidase access. *J. Biol. Chem.* **273,** 7856–7864 (1998).
81. Musil, L. S. & Goodenough, D. A. Multisubunit assembly of an integral plasma membrane channel protein, gap junction connexin43, occurs after exit from the ER. *Cell* **74,** 1065–1077 (1993).
82. John, S. A. & Revel, J. P. Connexon integrity is maintained by non-covalent bonds: intramolecular disulfide bonds link the extracellular domains in rat connexin-43. *Biochem. Biophys. Res. Commun.* **178,** 1312–1318 (1991).
83. Laird, D. W., Castillo, M. & Kasprzak, L. Gap junction turnover, intracellular trafficking, and phosphorylation of connexin43 in brefeldin A-treated rat mammary tumor cells. *J. Cell Biol.* **131,** 1193–1203 (1995).
84. Crow, D. S., Kurata, W. E. & Lau, A. F. Phosphorylation of connexin43 in cells containing mutant src oncogenes. *Oncogene* **7,** 999–1003 (1992).
85. Lampe, P. D. & Lau, A. F. The effects of connexin phosphorylation on gap junctional communication. *Int. J. Biochem. Cell Biol.* **36,** 1171–1186 (2004).
86. Jordan, K. *et al.* Trafficking, assembly, and function of a connexin43-green fluorescent protein chimera in live mammalian cells. *Mol. Biol. Cell* **10,** 2033–2050 (1999).
87. Lauf, U. *et al.* Dynamic trafficking and delivery of connexons to the plasma membrane and accretion to gap junctions in living cells. *Proc. Natl. Acad. Sci. U. S. A.* **99,** 10446–10451 (2002).
88. Thomas, T. *et al.* Mechanisms of Cx43 and Cx26 transport to the plasma membrane and gap junction regeneration. *J. Cell Sci.* **118,** 4451–4462 (2005).
89. Johnson, R. G. *et al.* Gap junctions assemble in the presence of cytoskeletal inhibitors, but enhanced assembly requires microtubules. *Exp. Cell Res.* **275,** 67–80 (2002).
90. Jongen, W. M. *et al.* Regulation of connexin 43-mediated gap junctional intercellular communication by Ca2+ in mouse epidermal cells is controlled by E-cadherin. *J. Cell Biol.* **114,** 545–555 (1991).
91. Wei, C.-J., Francis, R., Xu, X. & Lo, C. W. Connexin43 associated with an N-cadherin-containing multiprotein complex is required for gap junction formation in NIH3T3 cells. *J. Biol. Chem.* **280,** 19925–19936 (2005).
92. Bukauskas, F. F. & Verselis, V. K. Gap junction channel gating. *Biochim. Biophys. Acta* **1662,** 42–60 (2004).
93. Gonzalez, D., Gomez-Hernandez, J. M. & Barrio, L. C. Species specificity of mammalian connexin-26 to form open voltage-gated hemichannels. *FASEB J. Off. Publ. Fed. Am. Soc. Exp. Biol.* **20,** 2329–2338 (2006).
94. Verselis, V. K., Trelles, M. P., Rubinos, C., Bargiello, T. A. & Srinivas, M. Loop gating of connexin hemichannels involves movement of pore-lining residues in the first extracellular loop domain. *J. Biol. Chem.* **284,** 4484–4493 (2009).
95. Gonzalez, D., Gomez-Hernandez, J. M. & Barrio, L. C. Molecular basis of voltage dependence of connexin channels: an integrative appraisal. *Prog. Biophys. Mol. Biol.* **94,** 66–106 (2007).
96. Valiunas, V. Biophysical properties of connexin-45 gap junction hemichannels studied in vertebrate cells. *J. Gen. Physiol.* **119,** 147–164 (2002).
97. Dakin, K. & Li, W.-H. Local Ca2+ rise near store operated Ca2+ channels inhibits cell coupling during capacitative Ca2+ influx. *Cell Commun. Adhes.* **13,** 29–39 (2006).
98. Ripps, H., Qian, H. & Zakevicius, J. Properties of connexin26 hemichannels expressed in Xenopus oocytes. *Cell. Mol. Neurobiol.* **24,** 647–665 (2004).
99. Beahm, D. L. & Hall, J. E. Hemichannel and junctional properties of connexin 50. *Biophys. J.* **82,** 2016–

2031 (2002).
100. Loewenstein, W. R. & Rose, B. Calcium in (junctional) intercellular communication and a thought on its behavior in intracellular communication. *Ann. N. Y. Acad. Sci.* **307,** 285–307 (1978).
101. Firek, L. & Weingart, R. Modification of gap junction conductance by divalent cations and protons in neonatal rat heart cells. *J. Mol. Cell. Cardiol.* **27,** 1633–1643 (1995).
102. Li, H. *et al.* Properties and regulation of gap junctional hemichannels in the plasma membranes of cultured cells. *J. Cell Biol.* **134,** 1019–1030 (1996).
103. Stridh, M. H. *et al.* Enhanced glutathione efflux from astrocytes in culture by low extracellular Ca2+ and curcumin. *Neurochem. Res.* **35,** 1231–1238 (2010).
104. Stridh, M. H., Tranberg, M., Weber, S. G., Blomstrand, F. & Sandberg, M. Stimulated efflux of amino acids and glutathione from cultured hippocampal slices by omission of extracellular calcium: likely involvement of connexin hemichannels. *J. Biol. Chem.* **283,** 10347–10356 (2008).
105. Cotrina, M. L., Lin, J. H. & Nedergaard, M. Cytoskeletal assembly and ATP release regulate astrocytic calcium signaling. *J. Neurosci.* **18,** 8794–8804 (1998).
106. Braet, K. *et al.* Pharmacological sensitivity of ATP release triggered by photoliberation of inositol-1,4,5-trisphosphate and zero extracellular calcium in brain endothelial cells. *J. Cell. Physiol.* **197,** 205–213 (2003).
107. Schalper, K. A. *et al.* Connexin hemichannel composition determines the FGF-1-induced membrane permeability and free [Ca2+]i responses. *Mol. Biol. Cell* **19,** 3501–3513 (2008).
108. De Vuyst, E. *et al.* Intracellular calcium changes trigger connexin 32 hemichannel opening. *EMBO J.* **25,** 34–44 (2006).
109. De Vuyst, E. *et al.* Ca(2+) regulation of connexin 43 hemichannels in C6 glioma and glial cells. *Cell Calcium* **46,** 176–187 (2009).
110. Shintani-Ishida, K., Uemura, K. & Yoshida, K. Hemichannels in cardiomyocytes open transiently during ischemia and contribute to reperfusion injury following brief ischemia. *Am. J. Physiol. Heart Circ. Physiol.* **293,** H1714–20 (2007).
111. Wang, N. *et al.* Connexin mimetic peptides inhibit Cx43 hemichannel opening triggered by voltage and intracellular Ca 2+ elevation. *Basic Research in Cardiology* **107,** 1–17 (2012).
112. Levitan, I. B. Modulation of ion channels by protein phosphorylation. How the brain works. *Adv. Second Messenger Phosphoprotein Res.* **33,** 3–22 (1999).
113. van Veen, T. A., van Rijen, H. V & Jongsma, H. J. Electrical conductance of mouse connexin45 gap junction channels is modulated by phosphorylation. *Cardiovasc. Res.* **46,** 496–510 (2000).
114. Nnamani, C., Godwin, A., Ducsay, C. A., Longo, L. D. & Fletcher, W. H. Regulation of cell-cell communication mediated by connexin 43 in rabbit myometrial cells. *Biol. Reprod.* **50,** 377–389 (1994).
115. Harris, A. L. *Emerging issues of connexin channels: biophysics fills the gap. Quarterly reviews of biophysics* **34,** (2001).
116. Wang, N. *et al.* Connexin targeting peptides as inhibitors of voltage- and intracellular Ca2+-triggered Cx43 hemichannel opening. *Neuropharmacology* **75,** 506–516 (2013).
117. Warner, A., Clements, D. K., Parikh, S., Evans, W. H. & DeHaan, R. L. Specific motifs in the external loops of connexin proteins can determine gap junction formation between chick heart myocytes. *J. Physiol.* **488 (Pt 3,** 721–728 (1995).
118. Braet, K., Vandamme, W., Martin, P. E. M., Evans, W. H. & Leybaert, L. Photoliberating inositol-1,4,5-trisphosphate triggers ATP release that is blocked by the connexin mimetic peptide gap 26. *Cell Calcium* **33,** 37–48 (2003).
119. Decrock, E. *et al.* Connexin 43 hemichannels contribute to the propagation of apoptotic cell death in a rat C6 glioma cell model. *Cell Death Differ.* **16,** 151–163 (2009).
120. Liu, F., Arce, F. T., Ramachandran, S. & Lal, R. Nanomechanics of hemichannel conformations: connexin flexibility underlying channel opening and closing. *J. Biol. Chem.* **281,** 23207–23217 (2006).
121. Hawat, G., Benderdour, M., Rousseau, G. & Baroudi, G. Connexin 43 mimetic peptide Gap26 confers protection to intact heart against myocardial ischemia injury. *Pflugers Arch.* **460,** 583–592 (2010).
122. O'Carroll, S. J., Alkadhi, M., Nicholson, L. F. B. & Green, C. R. Connexin 43 mimetic peptides reduce swelling, astrogliosis, and neuronal cell death after spinal cord injury. *Cell Commun. Adhes.* **15,** 27–42 (2008).
123. Wang, N. *et al.* Selective inhibition of Cx43 hemichannels by Gap19 and its impact on myocardial ischemia/reperfusion injury. *Basic Res. Cardiol.* **108,** (2013).
124. Ponsaerts, R. *et al.* Intramolecular loop/tail interactions are essential for connexin 43-hemichannel activity. *FASEB J.* **24,** 4378–4395 (2010).

125. De Vuyst, E. *et al.* Pharmacological modulation of connexin-formed channels in cardiac pathophysiology. *Br. J. Pharmacol.* **163,** 469–83 (2011).
126. Shibayama, J. Identification of a Novel Peptide That Interferes With the Chemical Regulation of Connexin43. *Circ. Res.* **98,** 1365–1372 (2006).
127. Seki, A. *et al.* Modifications in the biophysical properties of connexin43 channels by a peptide of the cytoplasmic loop region. *Circ. Res.* **95,** e22–8 (2004).
128. Delmar, M., Coombs, W., Sorgen, P., Duffy, H. S. & Taffet, S. M. Structural bases for the chemical regulation of Connexin43 channels. *Cardiovasc. Res.* **62,** 268–275 (2004).
129. Morley, G. E., Ek-Vitorin, J. F., Taffet, S. M. & Delmar, M. Structure of connexin43 and its regulation by pHi. *J. Cardiovasc. Electrophysiol.* **8,** 939–951 (1997).
130. Verma, V. *et al.* Novel pharmacophores of connexin43 based on the 'RXP' series of Cx43-binding peptides. *Circ. Res.* **105,** 176–84 (2009).
131. Verma, V. *et al.* Design and characterization of the first peptidomimetic molecule that prevents acidification-induced closure of cardiac gap junctions. *Heart Rhythm* **7,** 1491–8 (2010).
132. Qin, H. *et al.* Retroviral delivery of connexin genes to human breast tumor cells inhibits in vivo tumor growth by a mechanism that is independent of significant gap junctional intercellular communication. *J. Biol. Chem.* **277,** 29132–29138 (2002).
133. Sun, Y. *et al.* Connexin 43 interacts with Bax to regulate apoptosis of pancreatic cancer through a gap junction-independent pathway. *Int. J. Oncol.* **41,** 941–948 (2012).
134. Rodríguez-Sinovas, A. *et al.* The modulatory effects of connexin 43 on cell death/survival beyond cell coupling. *Prog. Biophys. Mol. Biol.* **94,** 219–32 (2007).
135. Kaplan, S. R. *et al.* Remodeling of myocyte gap junctions in arrhythmogenic right ventricular cardiomyopathy due to a deletion in plakoglobin (Naxos disease). *Hear. Rhythm* **1,** 3–11 (2004).
136. Lo, C. Gap Junction Communication and the Modulation of Cardiac Neural Crest Cells. *Trends Cardiovasc. Med.* **9,** 63–69 (1999).
137. Xu, X., Francis, R., Wei, C. J., Linask, K. L. & Lo, C. W. Connexin 43-mediated modulation of polarized cell movement and the directional migration of cardiac neural crest cells. *Development* **133,** 3629–3639 (2006).
138. Wilson, M. R., Close, T. W. & Trosko, J. E. Cell population dynamics (apoptosis, mitosis, and cell-cell communication) during disruption of homeostasis. *Exp. Cell Res.* **254,** 257–268 (2000).
139. Krysko, D. V, Mussche, S., Leybaert, L. & D'Herde, K. Gap junctional communication and connexin43 expression in relation to apoptotic cell death and survival of granulosa cells. *J. Histochem. Cytochem.* **52,** 1199–1207 (2004).
140. Frank, D. K., Szymkowiak, B., Josifovska-Chopra, O., Nakashima, T. & Kinnally, K. W. Single-cell microinjection of cytochrome c can result in gap junction-mediated apoptotic cell death of bystander cells in head and neck cancer. *Head Neck* **27,** 794–800 (2005).
141. de Pina-Benabou, M. H. *et al.* Blockade of gap junctions in vivo provides neuroprotection after perinatal global ischemia. *Stroke.* **36,** 2232–2237 (2005).
142. Vinken, M. *et al.* Connexins: sensors and regulators of cell cycling. *Biochim. Biophys. Acta* **1815,** 13–25 (2011).
143. Elcock, F. J., Chipman, J. K. & Roberts, R. A. The rodent nongenotoxic hepatocarcinogen and peroxisome proliferator nafenopin inhibits intercellular communication in rat but not guinea-pig hepatocytes, perturbing S-phase but not apoptosis. *Arch. Toxicol.* **72,** 439–444 (1998).
144. Kolaja, K. L., Engelken, D. T. & Klaassen, C. D. Inhibition of gap-junctional-intercellular communication in intact rat liver by nongenotoxic hepatocarcinogens. *Toxicology* **146,** 15–22 (2000).
145. Cusato, K., Zakevicius, J. & Ripps, H. An experimental approach to the study of gap-junction-mediated cell death. *Biol. Bull.* **205,** 197–199 (2003).
146. Krutovskikh, V. A., Piccoli, C. & Yamasaki, H. Gap junction intercellular communication propagates cell death in cancerous cells. *Oncogene* **21,** 1989–1999 (2002).
147. Evans, W. H., De Vuyst, E. & Leybaert, L. The gap junction cellular internet: connexin hemichannels enter the signalling limelight. *Biochem. J.* **397,** 1–14 (2006).
148. Ebihara, L. Physiology and biophysics of hemi-gap-junctional channels expressed in Xenopus oocytes. *Acta Physiol. Scand.* **179,** 5–8 (2003).
149. Ebihara, L., Liu, X. & Pal, J. D. Effect of external magnesium and calcium on human connexin46 hemichannels. *Biophys. J.* **84,** 277–286 (2003).
150. Contreras, J. E. *et al.* Metabolic inhibition induces opening of unapposed connexin 43 gap junction

hemichannels and reduces gap junctional communication in cortical astrocytes in culture. *Proc. Natl. Acad. Sci. U. S. A.* **99,** 495–500 (2002).
151. Johansen, D., Cruciani, V., Sundset, R., Ytrehus, K. & Mikalsen, S.-O. Ischemia induces closure of gap junctional channels and opening of hemichannels in heart-derived cells and tissue. *Cell. Physiol. Biochem.* **28,** 103–114 (2011).
152. Orellana, J. A. *et al.* Hypoxia in high glucose followed by reoxygenation in normal glucose reduces the viability of cortical astrocytes through increased permeability of connexin 43 hemichannels. *Glia* **58,** 329–343 (2010).
153. Orellana, J. A. *et al.* Cation permeation through connexin 43 hemichannels is cooperative, competitive and saturable with parameters depending on the permeant species. *Biochem. Biophys. Res. Commun.* **409,** 603–609 (2011).
154. Retamal, M. A., Cortes, C. J., Reuss, L., Bennett, M. V. L. & Saez, J. C. S-nitrosylation and permeation through connexin 43 hemichannels in astrocytes: induction by oxidant stress and reversal by reducing agents. *Proc. Natl. Acad. Sci. U. S. A.* **103,** 4475–4480 (2006).
155. Hur, K. C., Shim, J.-E. & Johnson, R. G. A potential role for cx43-hemichannels in staurosporin-induced apoptosis. *Cell Commun. Adhes.* **10,** 271–277 (2003).
156. Kalvelyte, A., Imbrasaite, A., Bukauskiene, A., Verselis, V. K. & Bukauskas, F. F. Connexins and apoptotic transformation. *Biochem. Pharmacol.* **66,** 1661–1672 (2003).
157. Vinken, M. *et al.* Connexin32 hemichannels contribute to the apoptotic-to-necrotic transition during Fas-mediated hepatocyte cell death. *Cell. Mol. Life Sci.* **67,** 907–918 (2010).
158. Rhett, J. M. & Gourdie, R. G. The perinexus: a new feature of Cx43 gap junction organization. *Heart Rhythm* **9,** 619–623 (2012).
159. Rhett, J. M., Jourdan, J. & Gourdie, R. G. Connexin 43 connexon to gap junction transition is regulated by zonula occludens-1. *Mol. Biol. Cell* **22,** 1516–1528 (2011).
160. Camelliti, P., Green, C. R. & Kohl, P. Structural and functional coupling of cardiac myocytes and fibroblasts. *Adv. Cardiol.* **42,** 132–149 (2006).
161. Bukauskas, F. F. *et al.* Properties of mouse connexin 30.2 and human connexin 31.9 hemichannels: implications for atrioventricular conduction in the heart. *Proc. Natl. Acad. Sci. U. S. A.* **103,** 9726–9731 (2006).
162. Brisset, A. C., Isakson, B. E. & Kwak, B. R. Connexins in vascular physiology and pathology. *Antioxid. Redox Signal.* **11,** 267–282 (2009).
163. Harris, B. S. *et al.* Remodeling of the peripheral cardiac conduction system in response to pressure overload. *Am. J. Physiol. Heart Circ. Physiol.* **302,** H1712–25 (2012).
164. McCallister, L. P., Trapukdi, S. & Neely, J. R. Morphometric observations on the effects of ischemia in the isolated perfused rat heart. *J. Mol. Cell. Cardiol.* **11,** 619–630 (1979).
165. De Mello, W. C. & van Loon, P. Further studies on the influence of cyclic nucleotides on junctional permeability in heart. *J. Mol. Cell. Cardiol.* **19,** 763–771 (1987).
166. De Mello, W. C. & van Loon, P. Junctional permeability in heart muscle is independent upon the non-junctional membrane potential. *Cell Biol. Int. Rep.* **11,** 1–11 (1987).
167. Kleber, A. G., Riegger, C. B. & Janse, M. J. Electrical uncoupling and increase of extracellular resistance after induction of ischemia in isolated, arterially perfused rabbit papillary muscle. *Circ. Res.* **61,** 271–279 (1987).
168. Kleber, A. G. & Rudy, Y. Basic mechanisms of cardiac impulse propagation and associated arrhythmias. *Physiol. Rev.* **84,** 431–488 (2004).
169. Lampe, P. D., Cooper, C. D., King, T. J. & Burt, J. M. Analysis of Connexin43 phosphorylated at S325, S328 and S330 in normoxic and ischemic heart. *J. Cell Sci.* **119,** 3435–3442 (2006).
170. Akar, F. G., Spragg, D. D., Tunin, R. S., Kass, D. A. & Tomaselli, G. F. Mechanisms underlying conduction slowing and arrhythmogenesis in nonischemic dilated cardiomyopathy. *Circ. Res.* **95,** 717–725 (2004).
171. Boulaksil, M. *et al.* Heterogeneous Connexin43 distribution in heart failure is associated with dispersed conduction and enhanced susceptibility to ventricular arrhythmias. *Eur. J. Heart Fail.* **12,** 913–921 (2010).
172. Fontes, M. S. C., van Veen, T. A. B., de Bakker, J. M. T. & van Rijen, H. V. M. Functional consequences of abnormal Cx43 expression in the heart. *Biochim. Biophys. Acta* **1818,** 2020–2029 (2012).
173. Severs, N. J., Bruce, A. F., Dupont, E. & Rothery, S. Remodelling of gap junctions and connexin expression in diseased myocardium. *Cardiovasc. Res.* **80,** 9–19 (2008).
174. Li, H. *et al.* Paradoxical overexpression and translocation of connexin43 in homocysteine-treated endothelial cells. *Am. J. Physiol. Heart Circ. Physiol.* **282,** H2124–H2133 (2002).

175. Boengler, K. *et al.* Connexin 43 in cardiomyocyte mitochondria and its increase by ischemic preconditioning. *Cardiovasc. Res.* **67,** 234–244 (2005).
176. Goubaeva, F. *et al.* Cardiac mitochondrial connexin 43 regulates apoptosis. *Biochem. Biophys. Res. Commun.* **352,** 97–103 (2007).
177. Eckardt, D. *et al.* Functional role of connexin43 gap junction channels in adult mouse heart assessed by inducible gene deletion. *J. Mol. Cell. Cardiol.* **36,** 101–110 (2004).
178. Boengler, K. *et al.* Presence of connexin 43 in subsarcolemmal, but not in interfibrillar cardiomyocyte mitochondria. *Basic Res. Cardiol.* **104,** 141–7 (2009).
179. Rodriguez-Sinovas, A. *et al.* Translocation of connexin 43 to the inner mitochondrial membrane of cardiomyocytes through the heat shock protein 90-dependent TOM pathway and its importance for cardioprotection. *Circ. Res.* **99,** 93–101 (2006).
180. Boengler, K. *et al.* Mitochondrial connexin 43 impacts on respiratory complex I activity and mitochondrial oxygen consumption. *J. Cell. Mol. Med.* **16,** 1649–55 (2012).
181. Gadicherla, A. K., Stowe, D. F., Antholine, W. E., Yang, M. & Camara, A. K. S. Damage to mitochondrial complex i during cardiac ischemia reperfusion injury is reduced indirectly by anti-anginal drug ranolazine. *Biochim. Biophys. Acta - Bioenerg.* **1817,** 419–429 (2012).
182. Waza, A. A., Andrabi, K. & Hussain, M. U. Protein kinase C (PKC) mediated interaction between conexin43 (Cx43) and K(+)(ATP) channel subunit (Kir6.1) in cardiomyocyte mitochondria: Implications in cytoprotection against hypoxia induced cell apoptosis. *Cell. Signal.* **26,** 1909–17 (2014).
183. Budas, G. R., Churchill, E. N., Disatnik, M.-H., Sun, L. & Mochly-Rosen, D. Mitochondrial import of PKCepsilon is mediated by HSP90: a role in cardioprotection from ischaemia and reperfusion injury. *Cardiovasc. Res.* **88,** 83–92 (2010).
184. Heinzel, F. R. *et al.* Impairment of diazoxide-induced formation of reactive oxygen species and loss of cardioprotection in connexin 43 deficient mice. *Circ. Res.* **97,** 583–586 (2005).
185. Heusch, G., Büchert, A., Feldhaus, S. & Schulz, R. No loss of cardioprotection by postconditioning in connexin 43-deficient mice. *Basic Res. Cardiol.* **101,** 354–356 (2006).
186. Lu, G., Haider, H. K., Jiang, S. & Ashraf, M. Sca-1+ stem cell survival and engraftment in the infarcted heart: dual role for preconditioning-induced connexin-43. *Circulation* **119,** 2587–96 (2009).
187. Martin, P. E. M., Wall, C. & Griffith, T. M. Effects of connexin-mimetic peptides on gap junction functionality and connexin expression in cultured vascular cells. *Br. J. Pharmacol.* **144,** 617–627 (2005).
188. Evans, W. H. & Boitano, S. Connexin mimetic peptides: specific inhibitors of gap-junctional intercellular communication. *Biochem. Soc. Trans.* **29,** 606–612 (2001).
189. Lu, G., Haider, H. K., Porollo, A. & Ashraf, M. Mitochondria-specific transgenic overexpression of connexin-43 simulates preconditioning-induced cytoprotection of stem cells. *Cardiovasc. Res.* **88,** 277–86 (2010).
190. Lu, G., Jiang, S., Ashraf, M. & Haider, K. H. Subcellular preconditioning of stem cells: mito-Cx43 gene targeting is cytoprotective via shift of mitochondrial Bak and Bcl-xL balance. *Regenerative Medicine* **7,** 323–334 (2012).
191. Trudeau, K., Muto, T. & Roy, S. Downregulation of mitochondrial connexin 43 by high glucose triggers mitochondrial shape change and cytochrome C release in retinal endothelial cells. *Invest. Ophthalmol. Vis. Sci.* **53,** 6675–81 (2012).
192. Decrock, E. *et al.* Connexin-related signaling in cell death: to live or let die? *Cell Death Differ.* **16,** 524–536 (2009).
193. Decrock, E. *et al.* Calcium and connexin-based intercellular communication, a deadly catch? *Cell Calcium* **50,** 310–321 (2011).
194. Decrock, E. *et al.* Transfer of IP3 through gap junctions is critical, but not sufficient, for the spread of apoptosis. *Cell Death Differ.* **19,** 947–957 (2012).
195. Carroll, J. *et al.* Bovine complex I is a complex of 45 different subunits. *J. Biol. Chem.* **281,** 32724–32727 (2006).
196. Baradaran, R., Berrisford, J. M., Minhas, G. S. & Sazanov, L. A. Crystal structure of the entire respiratory complex I. *Nature* **494,** 443–448 (2013).
197. Hunte, C., Zickermann, V. & Brandt, U. Functional modules and structural basis of conformational coupling in mitochondrial complex I. *Science* **329,** 448–451 (2010).
198. Chomyn, A. *et al.* URF6, last unidentified reading frame of human mtDNA, codes for an NADH dehydrogenase subunit. *Science* **234,** 614–618 (1986).
199. Hirst, J., Carroll, J., Fearnley, I. M., Shannon, R. J. & Walker, J. E. The nuclear encoded subunits of

complex I from bovine heart mitochondria. *Biochim. Biophys. Acta* **1604,** 135–150 (2003).
200. Kao, M.-C., Matsuno-Yagi, A. & Yagi, T. Subunit proximity in the H+-translocating NADH-quinone oxidoreductase probed by zero-length cross-linking. *Biochemistry* **43,** 3750–3755 (2004).
201. Hirst, J. Mitochondrial complex I. *Annu. Rev. Biochem.* **82,** 551–575 (2013).
202. Xu, A. *et al.* Transient complex I inhibition at the onset of reperfusion by extracellular acidification decreases cardiac injury. *Am. J. Physiol. Cell Physiol.* **306,** C1142–53 (2014).
203. Takeshige, K. & Minakami, S. NADH- and NADPH-dependent formation of superoxide anions by bovine heart submitochondrial particles and NADH-ubiquinone reductase preparation. *Biochem. J.* **180,** 129–135 (1979).
204. Kang, D., Narabayashi, H., Sata, T. & Takeshige, K. Kinetics of superoxide formation by respiratory chain NADH- dehydrogenase of bovine heart mitochondria. *J. Biochem.* **94,** 1301–1306 (1983).
205. Lesnefsky, E. J. *et al.* Ischemia, rather than reperfusion, inhibits respiration through cytochrome oxidase in the isolated, perfused rabbit heart: role of cardiolipin. *Am. J. Physiol. Heart Circ. Physiol.* **287,** H258–H267 (2004).
206. Chen, Q., Camara, A. K. S., Stowe, D. F., Hoppel, C. L. & Lesnefsky, E. J. Modulation of electron transport protects cardiac mitochondria and decreases myocardial injury during ischemia and reperfusion. *Am. J. Physiol. Cell Physiol.* **292,** C137–C147 (2007).
207. Aldakkak, M., Stowe, D. F., Chen, Q., Lesnefsky, E. J. & Camara, A. K. S. Inhibited mitochondrial respiration by amobarbital during cardiac ischaemia improves redox state and reduces matrix Ca2+ overload and ROS release. *Cardiovasc. Res.* **77,** 406–415 (2008).
208. Tanaka-Esposito, C., Chen, Q. & Lesnefsky, E. J. Blockade of electron transport before ischemia protects mitochondria and decreases myocardial injury during reperfusion in aged rat hearts. *Transl. Res.* **160,** 207–216 (2012).
209. Inoue, I., Nagase, H., Kishi, K. & Higuti, T. ATP-sensitive K+ channel in the mitochondrial inner membrane. *Nature* **352,** 244–247 (1991).
210. Paucek, P. *et al.* Reconstitution and partial purification of the glibenclamide-sensitive, ATP-dependent K+ channel from rat liver and beef heart mitochondria. *J. Biol. Chem.* **267,** 26062–26069 (1992).
211. Zhang, D. X. *et al.* Characteristics and superoxide-induced activation of reconstituted myocardial mitochondrial ATP-sensitive potassium channels. *Circ. Res.* **89,** 1177–1183 (2001).
212. Szabò, I. *et al.* A novel potassium channel in lymphocyte mitochondria. *J. Biol. Chem.* **280,** 12790–12798 (2005).
213. Rusznák, Z. *et al.* Mitochondrial expression of the two-pore domain TASK-3 channels in malignantly transformed and non-malignant human cells. *Virchows Arch.* **452,** 415–426 (2008).
214. Toczylowska-Maminska, R. Potassium Channel in Mitochondria of Human Keratinocytes. *Biophys. J.* **102,** 105a (2012).
215. Miro-Casas, E. *et al.* Connexin43 in cardiomyocyte mitochondria contributes to mitochondrial potassium uptake. *Cardiovasc. Res.* **83,** 747–56 (2009).
216. Sze, H. & Solomon, A. K. Calcium-induced potassium pathway in sided erythrocyte membrane vesicles. *Biochim. Biophys. Acta* **554,** 180–194 (1979).
217. Deitmer, J. W. & Eckert, R. Two components of Ca-dependent potassium current in identified neurons of Aplysia californica. *Pflugers Arch.* **403,** 353–359 (1985).
218. Schwindt, P. C., Spain, W. J. & Crill, W. E. Calcium-dependent potassium currents in neurons from cat sensorimotor cortex. *J. Neurophysiol.* **67,** 216–226 (1992).
219. Nelson, M. T. *et al.* Relaxation of arterial smooth muscle by calcium sparks. *Science* **270,** 633–637 (1995).
220. Deschaux, O. & Bizot, J. C. Effect of apamin, a selective blocker of Ca2+-activated K+-channel, on habituation and passive avoidance responses in rats. *Neurosci. Lett.* **227,** 57–60 (1997).
221. Balderas, E., Zhang, J., Stefani, E. & Toro, L. Mitochondrial BKCa channel. *Front. Physiol.* **6,** 104 (2015).
222. Siemen, D., Loupatatzis, C., Borecky, J., Gulbins, E. & Lang, F. Ca2+-activated K channel of the BK-type in the inner mitochondrial membrane of a human glioma cell line. *Biochem. Biophys. Res. Commun.* **257,** 549–554 (1999).
223. Xu, W. *et al.* Cytoprotective role of Ca2+- activated K+ channels in the cardiac inner mitochondrial membrane. *Science (80-.).* **298,** 1029–1033 (2002).
224. Heinen, A. A. *et al.* Mitochondrial Ca2+-induced K+ influx increases respiration and enhances ROS production while maintaining membrane potential. *Am. J. Physiol. Cell Physiol.* **292,** C148–56 (2007).
225. Guéguinou, M. *et al.* KCa and Ca2+ channels: The complex thought. *Biochim. Biophys. Acta - Mol. Cell Res.* **1843,** 2322–2333 (2014).

226. Kohler, M., Hirschberg, B., Bond, C. & Kinzie, J. Small-conductance, calcium-activated potassium channels from mammalian brain. *Sci. (New York, NY)* (1996). at <http://www.sciencemag.org/cgi/content/abstract/sci;273/5282/1709>
227. Xia, X. M. *et al.* Mechanism of calcium gating in small-conductance calcium-activated potassium channels. *Nature* **395,** 503–507 (1998).
228. Schumacher, M. a *et al.* Structure of the gating domain of a Ca2+-activated K+ channel complexed with Ca2+/calmodulin. *Nature* **410,** 1120–1124 (2001).
229. Auchampach, J. A., Grover, G. J. & Gross, G. J. Blockade of ischaemic preconditioning in dogs by the novel ATP dependent potassium channel antagonist sodium 5-hydroxydecanoate. *Cardiovasc. Res.* **26,** 1054–62 (1992).
230. Yao, Z. & Gross, G. J. Activation of ATP-sensitive potassium channels lowers threshold for ischemic preconditioning in dogs. *Am. J. Physiol.* **267,** H1888–H1894 (1994).
231. Cole, W. C., McPherson, C. D. & Sontag, D. ATP-regulated K+ channels protect the myocardium against ischemia/reperfusion damage. *Circ. Res.* **69,** 571–581 (1991).
232. Kouchi, I., Murakami, T., Nawada, R., Akao, M. & Sasayama, S. KATP channels are common mediators of ischemic and calcium preconditioning in rabbits. *Am. J. Physiol.* **274,** H1106–H1112 (1998).
233. Yang, Q., Huang, J. H., Man, Y. B., Yao, X. Q. & He, G. W. Use of intermediate/small conductance calcium-activated potassium-channel activator for endothelial protection. *J. Thorac. Cardiovasc. Surg.* **141,** 501–510 (2011).
234. Sandow, S. L., Neylon, C. B., Chen, M. X. & Garland, C. J. Spatial separation of endothelial small- and intermediate-conductance calcium-activated potassium channels (K(Ca)) and connexins: possible relationship to vasodilator function? *J. Anat.* **209,** 689–698 (2006).
235. Allen, D. *et al.* SK2 channels are neuroprotective for ischemia-induced neuronal cell death. *J. Cereb. Blood Flow Metab.* **31,** 2302–2312 (2011).
236. Tanabe, M., Mori, M., Gähwiler, B. H. & Gerber, U. Apamin-sensitive conductance mediates the K(+) current response during chemical ischemia in CA3 pyramidal cells. *J. Neurophysiol.* **82,** 2876–2882 (1999).
237. Cipolla, M. J. & Godfrey, J. a. Effect of Hyperglycemia on Brain Penetrating Arterioles and Cerebral Blood Flow Before and After Ischemia/Reperfusion. *Transl. Stroke Res.* **1,** 127–134 (2010).
238. Yang, Q., Underwood, M. J. & He, G.-W. Calcium-activated Potassium Channels in Vasculature in Response to Ischemia-Reperfusion. *J. Cardiovasc. Pharmacol.* **59,** 109–115 (2012).
239. Heinen, A. A. *et al.* Reverse electron flow-induced ROS production is attenuated by activation of mitochondrial Ca2+-sensitive K+ channels. *Am. J. Physiol. Heart Circ. Physiol.* **293,** H1400–H1407 (2007).
240. Azarashvili, T. *et al.* Calcium-induced permeability transition in rat brain mitochondria is promoted by carbenoxolone through targeting connexin43. *Am. J. Physiol. Cell Physiol.* **300,** C707–20 (2011).
241. Azarashvili, T. *et al.* Carbenoxolone induces permeability transition pore opening in rat mitochondria via the translocator protein TSPO and connexin43. *Arch. Biochem. Biophys.* **558,** 87–94 (2014).
242. Evans, W. H. & Leybaert, L. Mimetic peptides as blockers of connexin channel-facilitated intercellular communication. *Cell Commun. Adhes.* **14,** 265–273 (2007).
243. Hale, S. L. & Kloner, R. A. Ranolazine, an inhibitor of the late sodium channel current, reduces postischemic myocardial dysfunction in the rabbit. *J. Cardiovasc. Pharmacol. Ther.* **11,** 249–255 (2006).
244. Stone, P. H. Ranolazine: new paradigm for management of myocardial ischemia, myocardial dysfunction, and arrhythmias. *Cardiol. Clin.* **26,** 603–614 (2008).
245. Stone, P. H. *et al.* The anti-ischemic mechanism of action of ranolazine in stable ischemic heart disease. *J. Am. Coll. Cardiol.* **56,** 934–942 (2010).
246. Boden, W. E. Ranolazine and its anti-ischemic effects: revisiting an old mechanistic paradigm anew? *Journal of the American College of Cardiology* **56,** 943–945 (2010).
247. Antzelevitch, C., Burashnikov, A., Sicouri, S. & Belardinelli, L. Electrophysiologic basis for the antiarrhythmic actions of ranolazine. *Heart Rhythm* **8,** 1281–1290 (2011).
248. Gunter, T. E., Yule, D. I., Gunter, K. K., Eliseev, R. a. & Salter, J. D. Calcium and mitochondria. *FEBS Lett.* **567,** 96–102 (2004).
249. Kristián, T. & Siesjö, B. K. Calcium in ischemic cell death. *Stroke.* **29,** 705–718 (1998).
250. O'Rourke, B. Mitochondrial ion channels. *Annu. Rev. Physiol.* **69,** 19–49 (2007).
251. Schulz, R. *et al.* Connexin 43 is an emerging therapeutic target in ischemia/reperfusion injury, cardioprotection and neuroprotection. *Pharmacol. Ther.* **153,** 90–106 (2015).
252. Srisakuldee, W. *et al.* Phosphorylation of connexin-43 at serine 262 promotes a cardiac injury-resistant state. *Cardiovasc. Res.* **83,** 672–81 (2009).

253. Fiori, M. C., Reuss, L., Cuello, L. G. & Altenberg, G. a. Functional analysis and regulation of purified connexin hemichannels. *Front. Physiol.* **5 FEB,** 1–15 (2014).
254. Schalper, K. A. *et al.* Connexin 43 hemichannels mediate the Ca2+ influx induced by extracellular alkalinization. *Am. J. Physiol. Cell Physiol.* **299,** C1504–15 (2010).
255. De Bock, M. *et al.* Connexin 43 hemichannels contribute to cytoplasmic Ca2+ oscillations by providing a bimodal Ca2+-dependent Ca2+ entry pathway. *J. Biol. Chem.* **287,** 12250–66 (2012).
256. De Bock, M. *et al.* Endothelial calcium dynamics, connexin channels and blood-brain barrier function. *Prog. Neurobiol.* **108,** 1–20 (2013).
257. Lewandowski, R. *et al.* RXP-E: A Connexin43-Binding Peptide That Prevents Action Potential Propagation Block. *Circ. Res.* **103,** 519–526 (2008).
258. Ishikawa, S. *et al.* Role of connexin-43 in protective PI3K-Akt-GSK-3 signaling in cardiomyocytes. *AJP Hear. Circ. Physiol.* **302,** H2536–H2544 (2012).
259. Retamal, M. a, Schalper, K. a, Shoji, K. F., Bennett, M. V. L. & Sáez, J. C. Opening of connexin 43 hemichannels is increased by lowering intracellular redox potential. *Proc. Natl. Acad. Sci. U. S. A.* **104,** 8322–8327 (2007).
260. Kim, D. Y., Kam, Y., Koo, S. K. & Joe, C. O. Gating connexin 43 channels reconstituted in lipid vesicles by mitogen-activated protein kinase phosphorylation. *J. Biol. Chem.* **274,** 5581–7 (1999).
261. De Stefani, D. & Rizzuto, R. Molecular control of mitochondrial calcium uptake. *Biochem. Biophys. Res. Commun.* **449,** 373–376 (2014).
262. Lax, A., Soler, F. & Fernández-Belda, F. Mitochondrial damage as death inducer in heart-derived H9c2 cells: More than one way for an early demise. *J. Bioenerg. Biomembr.* **41,** 369–377 (2009).
263. Pinton, P., Giorgi, C., Siviero, R., Zecchini, E. & Rizzuto, R. Calcium and apoptosis: ER-mitochondria Ca2+ transfer in the control of apoptosis. *Oncogene* **27,** 6407–6418 (2008).
264. Chacon, E. & Acosta, D. Mitochondrial regulation of superoxide by Ca2+: an alternate mechanism for the cardiotoxicity of doxorubicin. *Toxicol. Appl. Pharmacol.* **107,** 117–28 (1991).
265. Kim, S. M. *et al.* Tat-antioxidant 1 protects against stress-induced hippocampal HT-22 cells death and attenuate ischaemic insult in animal model. *J. Cell. Mol. Med.* **19,** 1333–45 (2015).
266. Thimm, J., Mechler, A., Lin, H., Rhee, S. & Lal, R. Calcium-dependent Open/Closed Conformations and Interfacial Energy Maps of Reconstituted Hemichannels. *J. Biol. Chem.* **280,** 10646–10654 (2005).
267. Liang, G. S. L. *et al.* Severe neuropathy with leaky connexin32 hemichannels. *Ann. Neurol.* **57,** 749–54 (2005).
268. Lemasters, J. J., Theruvath, T. P., Zhong, Z. & Nieminen, A.-L. Mitochondrial calcium and the permeability transition in cell death. *Biochim. Biophys. Acta* **1787,** 1395–1401 (2009).
269. Webster, K. a. Mitochondrial membrane permeabilization and cell death during myocardial infarction: roles of calcium and reactive oxygen species. *Future Cardiol.* **8,** 863–84 (2012).
270. Stewart, S., Lesnefsky, E. J. & Chen, Q. Reversible blockade of electron transport with amobarbital at the onset of reperfusion attenuates cardiac injury. *Transl. Res.* **153,** 224–231 (2009).
271. Battaglia, V. *et al.* Glycyrrhetinic acid as inhibitor or amplifier of permeability transition in rat heart mitochondria. *Biochim. Biophys. Acta* **1778,** 313–23 (2008).
272. Fiore, C. *et al.* On the mechanism of mitochondrial permeability transition induction by glycyrrhetinic acid. *Biochim. Biophys. Acta* **1658,** 195–201 (2004).
273. De Bock, M. *et al.* Connexin channels provide a target to manipulate brain endothelial calcium dynamics and blood-brain barrier permeability. *J. Cereb. Blood Flow Metab.* **31,** 1942–57 (2011).
274. Wong, C. W. *et al.* Connexin37 protects against atherosclerosis by regulating monocyte adhesion. *Nat. Med.* **12,** 950–4 (2006).
275. Boengler, K. *et al.* Loss of ischemic preconditioning's cardioprotection in aged mouse hearts is associated with reduced gap junctional and mitochondrial levels of connexin 43. *Am. J. Physiol. Heart Circ. Physiol.* **292,** H1764–9 (2007).
276. Pahujaa, M., Anikin, M. & Goldberg, G. S. Phosphorylation of connexin43 induced by Src: Regulation of gap junctional communication between transformed cells. *Exp. Cell Res.* **313,** 4083–4090 (2007).
277. De Vuyst, E. *et al.* Connexin hemichannels and gap junction channels are differentially influenced by lipopolysaccharide and basic fibroblast growth factor. *Mol. Biol. Cell* **18,** 34–46 (2007).
278. Agullo-Pascual, E. *et al.* Super-resolution imaging reveals that loss of the C-terminus of connexin43 limits microtubule plus-end capture and NaV1.5 localization at the intercalated disc. *Cardiovasc. Res.* **104,** 371–381 (2014).
279. Stowe, D. F. *et al.* Protection against cardiac injury by small Ca2+-sensitive K+ channels identified in

guinea pig cardiac inner mitochondrial membrane. *Biochim. Biophys. Acta - Biomembr.* **1828,** 427–442 (2013).
280. Cheng, Q., Sedlic, F., Pravdic, D., Bosnjak, Z. J. & Kwok, W. M. Biphasic effect of nitric oxide on the cardiac voltage-dependent anion channel. *FEBS Lett.* **585,** 328–334 (2011).
281. Ladilov, Y. V, Siegmund, B. & Piper, H. M. Protection of reoxygenated cardiomyocytes against hypercontracture by inhibition of Na+/H+ exchange. *Am. J. Physiol.* **268,** H1531–9 (1995).
282. Riess, M. L., Rhodes, S. S., Stowe, D. F., Aldakkak, M. & Camara, A. K. S. Comparison of cumulative planimetry versus manual dissection to assess experimental infarct size in isolated hearts. *J. Pharmacol. Toxicol. Methods* **60,** 275–280 (2009).
283. Stowe, D. & Camara, A. Mitochondrial reactive oxygen species production in excitable cells: modulators of mitochondrial and cell function. *Antioxidants Redox Signal.* **11,** (2009).
284. Paradies, G., Petrosillo, G., Paradies, V. & Ruggiero, F. M. Role of cardiolipin peroxidation and Ca2+ in mitochondrial dysfunction and disease. *Cell Calcium* **45,** 643–650 (2009).
285. Acin-Perez, R. *et al.* Respiratory complex III is required to maintain complex I in mammalian mitochondria. *Mol. Cell* **13,** 805–815 (2004).
286. Fry, M. & Green, D. E. Cardiolipin requirement for electron transfer in complex I and III of the mitochondrial respiratory chain. *J. Biol. Chem.* **256,** 1874–1880 (1981).
287. Hinchliffe, P. & Sazanov, L. A. Organization of iron-sulfur clusters in respiratory complex I. *Science* **309,** 771–774 (2005).
288. Euro, L., Bloch, D. A., Wikstrom, M., Verkhovsky, M. I. & Verkhovskaya, M. Electrostatic interactions between FeS clusters in NADH:ubiquinone oxidoreductase (Complex I) from Escherichia coli. *Biochemistry* **47,** 3185–3193 (2008).
289. Lesnefsky, E. J. & Hoppel, C. L. Cardiolipin as an oxidative target in cardiac mitochondria in the aged rat. *Biochim. Biophys. Acta* **1777,** 1020–1027 (2008).
290. Lesnefsky, E. J., Minkler, P. & Hoppel, C. L. Enhanced modification of cardiolipin during ischemia in the aged heart. *J. Mol. Cell. Cardiol.* **46,** 1008–1015 (2009).
291. Paradies, G. *et al.* Lipid peroxidation and alterations to oxidative metabolism in mitochondria isolated from rat heart subjected to ischemia and reperfusion. *Free Radic. Biol. Med.* **27,** 42–50 (1999).
292. Zacharowski, K., Blackburn, B. & Thiemermann, C. Ranolazine, a partial fatty acid oxidation inhibitor, reduces myocardial infarct size and cardiac troponin T release in the rat. *Eur. J. Pharmacol.* **418,** 105–110 (2001).
293. An, J. *et al.* Blocking Na(+)/H(+) exchange reduces [Na(+)](i) and [Ca(2+)](i) load after ischemia and improves function in intact hearts. *Am. J. Physiol. Heart Circ. Physiol.* **281,** H2398–409 (2001).
294. McCormack, J. G., Baracos, V. E., Barr, R. & Lopaschuk, G. D. Effects of ranolazine on oxidative substrate preference in epitrochlearis muscle. *J. Appl. Physiol.* **81,** 905–910 (1996).
295. McCormack, J. G., Barr, R. L., Wolff, A. A. & Lopaschuk, G. D. Ranolazine stimulates glucose oxidation in normoxic, ischemic, and reperfused ischemic rat hearts. *Circulation* **93,** 135–142 (1996).
296. Wyatt, K. M., Skene, C., Veitch, K., Hue, L. & McCormack, J. G. The antianginal agent ranolazine is a weak inhibitor of the respiratory complex I, but with greater potency in broken or uncoupled than in coupled mitochondria. *Biochem. Pharmacol.* **50,** 1599–1606 (1995).
297. Paradies, G. *et al.* Decrease in mitochondrial complex I activity in ischemic/reperfused rat heart: involvement of reactive oxygen species and cardiolipin. *Circ. Res.* **94,** 53–59 (2004).
298. Han, F., Da, T., Riobo, N. A. & Becker, L. B. Early mitochondrial dysfunction in electron transfer activity and reactive oxygen species generation after cardiac arrest. *Crit. Care Med.* **36,** S447–S453 (2008).
299. Rouslin, W. Mitochondrial complexes I, II, III, IV, and V in myocardial ischemia and autolysis. *Am. J. Physiol.* **244,** H743–8 (1983).
300. Camara, A. K. S. *et al.* ROS scavenging before 27 degrees C ischemia protects hearts and reduces mitochondrial ROS, Ca2+ overload, and changes in redox state. *Am. J. Physiol. Cell Physiol.* **292,** C2021–31 (2007).
301. Davies, K. J. & Goldberg, A. L. Proteins damaged by oxygen radicals are rapidly degraded in extracts of red blood cells. *J. Biol. Chem.* **262,** 8227–8234 (1987).
302. Davies, K. J. & Goldberg, A. L. Oxygen radicals stimulate intracellular proteolysis and lipid peroxidation by independent mechanisms in erythrocytes. *J. Biol. Chem.* **262,** 8220–8226 (1987).
303. Malinska, D. *et al.* Complex III-dependent superoxide production of brain mitochondria contributes to seizure-related ROS formation. *Biochim. Biophys. Acta* **1797,** 1163–1170 (2010).
304. Petrosillo, G., Ruggiero, F. M., Di Venosa, N. & Paradies, G. Decreased complex III activity in

mitochondria isolated from rat heart subjected to ischemia and reperfusion: role of reactive oxygen species and cardiolipin. *FASEB J. Off. Publ. Fed. Am. Soc. Exp. Biol.* **17,** 714–716 (2003).
305. Fato, R. *et al.* Differential effects of mitochondrial Complex I inhibitors on production of reactive oxygen species. *Biochim. Biophys. Acta* **1787,** 384–392 (2009).
306. Chen, Q., Moghaddas, S., Hoppel, C. L. & Lesnefsky, E. J. Ischemic defects in the electron transport chain increase the production of reactive oxygen species from isolated rat heart mitochondria. *Am. J. Physiol. Cell Physiol.* **294,** C460–6 (2008).
307. Grivennikova, V. G. & Vinogradov, A. D. Generation of superoxide by the mitochondrial Complex I. *Biochim. Biophys. Acta - Bioenerg.* **1757,** 553–561 (2006).
308. Chen, Q., Hoppel, C. L. & Lesnefsky, E. J. Blockade of electron transport before cardiac ischemia with the reversible inhibitor amobarbital protects rat heart mitochondria. *J. Pharmacol. Exp. Ther.* **316,** 200–207 (2006).
309. Szel, T. *et al.* Class I/B antiarrhythmic property of ranolazine, a novel antianginal agent, in dog and human cardiac preparations. *Eur. J. Pharmacol.* **662,** 31–39 (2011).
310. Song, Y., Shryock, J. C., Wu, L. & Belardinelli, L. Antagonism by ranolazine of the pro-arrhythmic effects of increasing late INa in guinea pig ventricular myocytes. *J. Cardiovasc. Pharmacol.* **44,** 192–199 (2004).
311. Undrovinas, A. I., Fleidervish, I. A. & Makielski, J. C. Inward sodium current at resting potentials in single cardiac myocytes induced by the ischemic metabolite lysophosphatidylcholine. *Circ. Res.* **71,** 1231–1241 (1992).
312. Camara, A. K. S. *et al.* Na+/H+ exchange inhibition with cardioplegia reduces cytosolic [Ca2+] and myocardial damage after cold ischemia. *J. Cardiovasc. Pharmacol.* **41,** 686–698 (2003).
313. Miyamae, M., Camacho, S. A., Weiner, M. W. & Figueredo, V. M. Attenuation of postischemic reperfusion injury is related to prevention of [Ca2+]m overload in rat hearts. *Am. J. Physiol.* **271,** H2145–53 (1996).
314. Song, Y., Shryock, J. C., Wagner, S., Maier, L. S. & Belardinelli, L. Blocking late sodium current reduces hydrogen peroxide-induced arrhythmogenic activity and contractile dysfunction. *J. Pharmacol. Exp. Ther.* **318,** 214–222 (2006).
315. Antzelevitch, C. *et al.* Electrophysiological effects of ranolazine, a novel antianginal agent with antiarrhythmic properties. *Circulation* **110,** 904–910 (2004).
316. Granger, A. *et al.* Histone deacetylase inhibition reduces myocardial ischemia-reperfusion injury in mice. *FASEB J. Off. Publ. Fed. Am. Soc. Exp. Biol.* **22,** 3549–3560 (2008).
317. Zhao, T. C., Cheng, G., Zhang, L. X., Tseng, Y. T. & Padbury, J. F. Inhibition of histone deacetylases triggers pharmacologic preconditioning effects against myocardial ischemic injury. *Cardiovasc. Res.* **76,** 473–481 (2007).
318. Ingledew, W. J. & Ohnishi, T. An analysis of some thermodynamic properties of iron-sulphur centres in site I of mitochondria. *Biochem. J.* **186,** 111–117 (1980).
319. Vogel, R. O., Smeitink, J. A. M. & Nijtmans, L. G. J. Human mitochondrial complex I assembly: a dynamic and versatile process. *Biochim. Biophys. Acta* **1767,** 1215–1227 (2007).
320. Myers, C. R., Antholine, W. E. & Myers, J. M. The pro-oxidant chromium(VI) inhibits mitochondrial complex I, complex II, and aconitase in the bronchial epithelium: EPR markers for Fe-S proteins. *Free Radic. Biol. Med.* **49,** 1903–1915 (2010).
321. Clarke, B., Wyatt, K. M. & McCormack, J. G. Ranolazine increases active pyruvate dehydrogenase in perfused normoxic rat hearts: evidence for an indirect mechanism. *J. Mol. Cell. Cardiol.* **28,** 341–350 (1996).
322. Chen, Q. *et al.* Cardiac preconditioning with 4-h, 17 degrees C ischemia reduces [Ca(2+)](i) load and damage in part via K(ATP) channel opening. *Am. J. Physiol. Heart Circ. Physiol.* **282,** H1961–9 (2002).
323. Riess, M. L. *et al.* Anesthetic preconditioning attenuates mitochondrial Ca2+ overload during ischemia in Guinea pig intact hearts: reversal by 5-hydroxydecanoic acid. *Anesth. Analg.* **95,** 1540–6, table of contents (2002).
324. Ambrosio, G., Zweier, J. L. & Flaherty, J. T. The relationship between oxygen radical generation and impairment of myocardial energy metabolism following post-ischemic reperfusion. *J. Mol. Cell. Cardiol.* **23,** 1359–1374 (1991).
325. Zweier, J. L., Flaherty, J. T. & Weisfeldt, M. L. Direct measurement of free radical generation following reperfusion of ischemic myocardium. *Proc. Natl. Acad. Sci. U. S. A.* **84,** 1404–1407 (1987).
326. Aldakkak, M., Stowe, D. F., Cheng, Q., Kwok, W.-M. & Camara, A. K. S. Mitochondrial matrix K+ flux independent of large-conductance Ca2+-activated K+ channel opening. *Am. J. Physiol. Cell Physiol.* **298,** C530–41 (2010).

327. Birch-Machin, M. A. & Turnbull, D. M. Assaying mitochondrial respiratory complex activity in mitochondria isolated from human cells and tissues. *Methods Cell Biol.* **65,** 97–117 (2001).
328. Schagger, H. Respiratory chain supercomplexes of mitochondria and bacteria. *Biochim. Biophys. Acta* **1555,** 154–159 (2002).
329. Schagger, H. & Pfeiffer, K. The ratio of oxidative phosphorylation complexes I-V in bovine heart mitochondria and the composition of respiratory chain supercomplexes. *J. Biol. Chem.* **276,** 37861–37867 (2001).
330. Schagger, H. & von Jagow, G. Blue native electrophoresis for isolation of membrane protein complexes in enzymatically active form. *Anal. Biochem.* **199,** 223–231 (1991).
331. Fearnley, I. M. & Walker, J. E. Conservation of sequences of subunits of mitochondrial complex I and their relationships with other proteins. *Biochim. Biophys. Acta* **1140,** 105–134 (1992).
332. Carroll, J., Shannon, R. J., Fearnley, I. M., Walker, J. E. & Hirst, J. Definition of the nuclear encoded protein composition of bovine heart mitochondrial complex I. Identification of two new subunits. *J. Biol. Chem.* **277,** 50311–50317 (2002).
333. Laemmli, U. K. Cleavage of structural proteins during the assembly of the head of bacteriophage T4. *Nature* **227,** 680–685 (1970).
334. Alamdari, D. H. *et al.* High sensitivity enzyme-linked immunosorbent assay (ELISA) method for measuring protein carbonyl in samples with low amounts of protein. *Free Radic. Biol. Med.* **39,** 1362–1367 (2005).
335. Chandran, K. *et al.* Doxorubicin inactivates myocardial cytochrome c oxidase in rats: cardioprotection by Mito-Q. *Biophys. J.* **96,** 1388–1398 (2009).
336. Ohnishi, T. & Nakamaru-Ogiso, E. Were there any 'misassignments' among iron-sulfur clusters N4, N5 and N6b in NADH-quinone oxidoreductase (complex I)? *Biochim. Biophys. Acta* **1777,** 703–710 (2008).
337. Hara, A. & Radin, N. S. Lipid extraction of tissues with a low-toxicity solvent. *Anal. Biochem.* **90,** 420–426 (1978).
338. Barcelo-Coblijn, G. & Murphy, E. J. An improved method for separating cardiolipin by HPLC. *Lipids* **43,** 971–976 (2008).
339. Camara, A. K. S., Bienengraeber, M. & Stowe, D. F. Mitochondrial approaches to protect against cardiac ischemia and reperfusion injury. *Front. Physiol.* **2,** 13 (2011).
340. Singh, S., Syme, C. A., Singh, A. K., Devor, D. C. & Bridges, R. J. Benzimidazolone activators of chloride secretion: potential therapeutics for cystic fibrosis and chronic obstructive pulmonary disease. *J. Pharmacol. Exp. Ther.* **296,** 600–611 (2001).
341. Wulff, H. *et al.* Design of a potent and selective inhibitor of the intermediate-conductance Ca2+-activated K+ channel, IKCa1: a potential immunosuppressant. *Proc. Natl. Acad. Sci. U. S. A.* **97,** 8151–8156 (2000).
342. Stocker, M. Ca(2+)-activated K+ channels: molecular determinants and function of the SK family. *Nat. Rev. Neurosci.* **5,** 758–770 (2004).
343. Hille, B. Ionic channels: molecular pores of excitable membranes. *Harvey Lect.* **82,** 47–69
344. Bruening-Wright, A., Schumacher, M. A., Adelman, J. P. & Maylie, J. Localization of the activation gate for small conductance Ca2+-activated K+ channels. *J. Neurosci.* **22,** 6499–6506 (2002).
345. Taylor, M. S. *et al.* Altered expression of small-conductance Ca2+-activated K+ (SK3) channels modulates arterial tone and blood pressure. *Circ. Res.* **93,** 124–131 (2003).
346. Xu, Y. *et al.* Molecular identification and functional roles of a Ca(2+)-activated K+ channel in human and mouse hearts. *J. Biol. Chem.* **278,** 49085–49094 (2003).
347. Weatherall, K. L., Seutin, V., Liegeois, J.-F. & Marrion, N. V. Crucial role of a shared extracellular loop in apamin sensitivity and maintenance of pore shape of small-conductance calcium-activated potassium (SK) channels. *Proc. Natl. Acad. Sci. U. S. A.* **108,** 18494–18499 (2011).
348. Sheng, J., Ella, S., Davis, M. J., Hill, M. A. & Braun, A. P. Openers of SKCa and IKCa channels enhance agonist-evoked endothelial nitric oxide synthesis and arteriolar vasodilation. *FASEB J. Off. Publ. Fed. Am. Soc. Exp. Biol.* **23,** 1138–1145 (2009).
349. Strobaek, D. *et al.* Activation of human IK and SK Ca2+ -activated K+ channels by NS309 (6,7-dichloro-1H-indole-2,3-dione 3-oxime). *Biochim. Biophys. Acta* **1665,** 1–5 (2004).
350. Pedarzani, P. *et al.* Specific enhancement of SK channel activity selectively potentiates the afterhyperpolarizing current I(AHP) and modulates the firing properties of hippocampal pyramidal neurons. *J. Biol. Chem.* **280,** 41404–41411 (2005).
351. Wulff, H., Kolski-Andreaco, A., Sankaranarayanan, A., Sabatier, J.-M. & Shakkottai, V. Modulators of small- and intermediate-conductance calcium-activated potassium channels and their therapeutic indications. *Curr. Med. Chem.* **14,** 1437–1457 (2007).

352. Pedarzani, P. & Stocker, M. Molecular and cellular basis of small--and intermediate-conductance, calcium-activated potassium channel function in the brain. *Cell. Mol. Life Sci.* **65,** 3196–3217 (2008).
353. Jenkins, D. P. *et al.* Negative gating modulation by (R)-N-(benzimidazol-2-yl)-1,2,3,4-tetrahydro-1-naphthylamine (NS8593) depends on residues in the inner pore vestibule: pharmacological evidence of deep-pore gating of K(Ca)2 channels. *Mol. Pharmacol.* **79,** 899–909 (2011).
354. Diness, J. G. *et al.* Inhibition of small-conductance Ca2+-activated K+ channels terminates and protects against atrial fibrillation. *Circ. Arrhythm. Electrophysiol.* **3,** 380–390 (2010).
355. Pain, T. *et al.* Opening of mitochondrial K(ATP) channels triggers the preconditioned state by generating free radicals. *Circ. Res.* **87,** 460–466 (2000).
356. Shah, M. & Haylett, D. G. The pharmacology of hSK1 Ca2+-activated K+ channels expressed in mammalian cell lines. *Br. J. Pharmacol.* **129,** 627–630 (2000).
357. Ide, T. *et al.* Mitochondrial electron transport complex I is a potential source of oxygen free radicals in the failing myocardium. *Circ. Res.* **85,** 357–363 (1999).
358. Kevin, L. G., Camara, A. K. S., Riess, M. L., Novalija, E. & Stowe, D. F. Ischemic preconditioning alters real-time measure of O2 radicals in intact hearts with ischemia and reperfusion. *Am. J. Physiol. Heart Circ. Physiol.* **284,** H566–74 (2003).
359. Barrett, J. N., Magleby, K. L. & Pallotta, B. S. Properties of single calcium-activated potassium channels in cultured rat muscle. *J. Physiol.* **331,** 211–230 (1982).
360. Xia, X.-M., Zeng, X. & Lingle, C. J. Multiple regulatory sites in large-conductance calcium-activated potassium channels. *Nature* **418,** 880–884 (2002).
361. Sheng, J.-Z. *et al.* Homology modeling identifies C-terminal residues that contribute to the Ca2+ sensitivity of a BKCa channel. *Biophys. J.* **89,** 3079–3092 (2005).
362. Wang, Z. W., Nara, M., Wang, Y. X. & Kotlikoff, M. I. Redox regulation of large conductance Ca(2+)-activated K+ channels in smooth muscle cells. *J. Gen. Physiol.* **110,** 35–44 (1997).
363. Maylie, J., Bond, C. T., Herson, P. S., Lee, W.-S. & Adelman, J. P. Small conductance Ca2+-activated K+ channels and calmodulin. *J. Physiol.* **554,** 255–261 (2004).
364. Ishii, T. M. *et al.* A human intermediate conductance calcium-activated potassium channel. *Proc. Natl. Acad. Sci. U. S. A.* **94,** 11651–11656 (1997).
365. Schumacher, M. A., Crum, M. & Miller, M. C. Crystal structures of apocalmodulin and an apocalmodulin/SK potassium channel gating domain complex. *Structure* **12,** 849–860 (2004).
366. Nolting, A., Ferraro, T., D'hoedt, D. & Stocker, M. An amino acid outside the pore region influences apamin sensitivity in small conductance Ca2+-activated K+ channels. *J. Biol. Chem.* **282,** 3478–3486 (2007).
367. Rumsey, W. L., Schlosser, C., Nuutinen, E. M., Robiolio, M. & Wilson, D. F. Cellular energetics and the oxygen dependence of respiration in cardiac myocytes isolated from adult rat. *J. Biol. Chem.* **265,** 15392–15402 (1990).
368. Kevin, L. G. *et al.* Sevoflurane exposure generates superoxide but leads to decreased superoxide during ischemia and reperfusion in isolated hearts. *Anesth. Analg.* **96,** 949–55, table of contents (2003).
369. Vanden Hoek, T. L., Li, C., Shao, Z., Schumacker, P. T. & Becker, L. B. Significant levels of oxidants are generated by isolated cardiomyocytes during ischemia prior to reperfusion. *J. Mol. Cell. Cardiol.* **29,** 2571–2583 (1997).
370. Becker, L. B., vanden Hoek, T. L., Shao, Z. H., Li, C. Q. & Schumacker, P. T. Generation of superoxide in cardiomyocytes during ischemia before reperfusion. *Am. J. Physiol.* **277,** H2240–6 (1999).
371. Duranteau, J., Chandel, N. S., Kulisz, A., Shao, Z. & Schumacker, P. T. Intracellular signaling by reactive oxygen species during hypoxia in cardiomyocytes. *J. Biol. Chem.* **273,** 11619–11624 (1998).
372. Forbes, R. A., Steenbergen, C. & Murphy, E. Diazoxide-induced cardioprotection requires signaling through a redox-sensitive mechanism. *Circ. Res.* **88,** 802–809 (2001).
373. Liu, Y. & O'Rourke, B. Opening of mitochondrial K(ATP) channels triggers cardioprotection. Are reactive oxygen species involved? *Circulation research* **88,** 750–752 (2001).
374. Tokube, K., Kiyosue, T. & Arita, M. Openings of cardiac KATP channel by oxygen free radicals produced by xanthine oxidase reaction. *Am. J. Physiol.* **271,** H478–89 (1996).
375. Lebuffe, G. *et al.* ROS and NO trigger early preconditioning: relationship to mitochondrial KATP channel. *Am. J. Physiol. Heart Circ. Physiol.* **284,** H299–308 (2003).
376. Stowe, D. F. & Riess, M. L. Reactive oxygen species and cardiac preconditioning: many questions remain. *Cardiovascular drugs and therapy / sponsored by the International Society of Cardiovascular Pharmacotherapy* **18,** 87–90 (2004).

377. Kowaltowski, A. J., Seetharaman, S., Paucek, P. & Garlid, K. D. Bioenergetic consequences of opening the ATP-sensitive K(+) channel of heart mitochondria. *Am. J. Physiol. Heart Circ. Physiol.* **280,** H649–57 (2001).
378. Dos Santos, P. *et al.* Mechanisms by which opening the mitochondrial ATP- sensitive K(+) channel protects the ischemic heart. *Am. J. Physiol. Heart Circ. Physiol.* **283,** H284–95 (2002).
379. Korge, P., Honda, H. M. & Weiss, J. N. K+-dependent regulation of matrix volume improves mitochondrial function under conditions mimicking ischemia-reperfusion. *Am. J. Physiol. Heart Circ. Physiol.* **289,** H66–77 (2005).
380. O'Rourke, B. Pathophysiological and protective roles of mitochondrial ion channels. *J. Physiol.* **529 Pt 1,** 23–36 (2000).
381. Varadarajan, S. G., An, J., Novalija, E., Smart, S. C. & Stowe, D. F. Changes in [Na(+)](i), compartmental [Ca(2+)], and NADH with dysfunction after global ischemia in intact hearts. *Am. J. Physiol. Heart Circ. Physiol.* **280,** H280–93 (2001).
382. Garlid, K. D., Costa, A. D. T., Quinlan, C. L., Pierre, S. V & Dos Santos, P. Cardioprotective signaling to mitochondria. *J. Mol. Cell. Cardiol.* **46,** 858–866 (2009).
383. Beavis, A. D. & Garlid, K. D. Evidence for the allosteric regulation of the mitochondrial K+/H+ antiporter by matrix protons. *J. Biol. Chem.* **265,** 2538–2545 (1990).
384. Andrukhiv, A., Costa, A. D., West, I. C. & Garlid, K. D. Opening mitoKATP increases superoxide generation from complex I of the electron transport chain. *Am. J. Physiol. Heart Circ. Physiol.* **291,** H2067–H2074 (2006).
385. Costa, A. D. T. *et al.* The direct physiological effects of mitoK(ATP) opening on heart mitochondria. *Am. J. Physiol. Heart Circ. Physiol.* **290,** H406–15 (2006).
386. Akao, M., O'Rourke, B., Teshima, Y., Seharaseyon, J. & Marban, E. Mechanistically distinct steps in the mitochondrial death pathway triggered by oxidative stress in cardiac myocytes. *Circ. Res.* **92,** 186–194 (2003).
387. Das, M., Parker, J. E. & Halestrap, A. P. Matrix volume measurements challenge the existence of diazoxide/glibencamide-sensitive KATP channels in rat mitochondria. *J. Physiol.* **547,** 893–902 (2003).
388. Murata, M., Akao, M., O'Rourke, B., Marbán, E. & Marban, E. Mitochondrial ATP-sensitive potassium channels attenuate matrix Ca(2+) overload during simulated ischemia and reperfusion: possible mechanism of cardioprotection. *Circ. Res.* **89,** 891–898 (2001).
389. Drose, S., Brandt, U. & Hanley, P. J. K+-independent actions of diazoxide question the role of inner membrane KATP channels in mitochondrial cytoprotective signaling. *J. Biol. Chem.* **281,** 23733–23739 (2006).
390. Holmuhamedov, E. L., Jovanovic, S., Dzeja, P. P., Jovanovic, A. & Terzic, A. Mitochondrial ATP-sensitive K+ channels modulate cardiac mitochondrial function. *Am. J. Physiol.* **275,** H1567–76 (1998).
391. Di Lisa, F. & Bernardi, P. Mitochondrial function as a determinant of recovery or death in cell response to injury. *Mol. Cell. Biochem.* **184,** 379–391 (1998).
392. Ferrari, R. The role of mitochondria in ischemic heart disease. *J. Cardiovasc. Pharmacol.* **28 Suppl 1,** S1–10 (1996).
393. Garlid, K. D. Opening mitochondrial K(ATP) in the heart--what happens, and what does not happen. *Basic Res. Cardiol.* **95,** 275–279 (2000).
394. Halestrap, A. P. Regulation of mitochondrial metabolism through changes in matrix volume. *Biochem. Soc. Trans.* **22,** 522–529 (1994).
395. Bagchi, D. *et al.* Interrelationship between cellular calcium homeostasis and free radical generation in myocardial reperfusion injury. *Chem. Biol. Interact.* **104,** 65–85 (1997).
396. Goldhaber, J. I. & Qayyum, M. S. Oxygen free radicals and excitation-contraction coupling. *Antioxid. Redox Signal.* **2,** 55–64 (2000).
397. Novalija, E., Kevin, L. G., Eells, J. T., Henry, M. M. & Stowe, D. F. Anesthetic preconditioning improves adenosine triphosphate synthesis and reduces reactive oxygen species formation in mitochondria after ischemia by a redox dependent mechanism. *Anesthesiology* **98,** 1155–1163 (2003).
398. An, J., Camara, A. K. S., Rhodes, S. S., Riess, M. L. & Stowe, D. F. Warm ischemic preconditioning improves mitochondrial redox balance during and after mild hypothermic ischemia in guinea pig isolated hearts. *Am. J. Physiol. Heart Circ. Physiol.* **288,** H2620–7 (2005).
399. Riess, M. L. *et al.* Altered NADH and improved function by anesthetic and ischemic preconditioning in guinea pig intact hearts. *Am. J. Physiol. Heart Circ. Physiol.* **283,** H53–60 (2002).
400. An, J. *et al.* Improved mitochondrial bioenergetics by anesthetic preconditioning during and after 2 hours of

27 degrees C ischemia in isolated hearts. *J. Cardiovasc. Pharmacol.* **46,** 280–287 (2005).
401. Camara, A. K. S., Riess, M. L., Kevin, L. G., Novalija, E. & Stowe, D. F. Hypothermia augments reactive oxygen species detected in the guinea pig isolated perfused heart. *Am. J. Physiol. Heart Circ. Physiol.* **286,** H1289–99 (2004).
402. Zhao, H. *et al.* Superoxide reacts with hydroethidine but forms a fluorescent product that is distinctly different from ethidium: potential implications in intracellular fluorescence detection of superoxide. *Free Radic. Biol. Med.* **34,** 1359–1368 (2003).
403. Zielonka, J., Zhao, H., Xu, Y. & Kalyanaraman, B. Mechanistic similarities between oxidation of hydroethidine by Fremy's salt and superoxide: stopped-flow optical and EPR studies. *Free Radic. Biol. Med.* **39,** 853–863 (2005).
404. Gribkoff, V. K. *et al.* The substituted benzimidazolone NS004 is an opener of the cystic fibrosis chloride channel. *J. Biol. Chem.* **269,** 10983–10986 (1994).
405. Sanchez, M. & McManus, O. B. Paxilline inhibition of the alpha-subunit of the high-conductance calcium-activated potassium channel. *Neuropharmacology* **35,** 963–968 (1996).
406. Riess, M. L. *et al.* KATP channel openers have opposite effects on mitochondrial respiration under different energetic conditions. *J. Cardiovasc. Pharmacol.* **51,** 483–491 (2008).
407. Huang, M., Camara, A. K. S., Stowe, D. F., Qi, F. & Beard, D. A. Mitochondrial inner membrane electrophysiology assessed by rhodamine-123 transport and fluorescence. *Ann. Biomed. Eng.* **35,** 1276–1285 (2007).
408. Hovius, R., Lambrechts, H., Nicolay, K. & de Kruijff, B. Improved methods to isolate and subfractionate rat liver mitochondria. Lipid composition of the inner and outer membrane. *Biochim. Biophys. Acta* **1021,** 217–226 (1990).
409. Graham, J. M. Purification of a crude mitochondrial fraction by density-gradient centrifugation. *Curr. Protoc. Cell Biol.* **Chapter 3,** Unit 3.4 (2001).
410. Douglas, R. M. *et al.* The calcium-sensitive large-conductance potassium channel (BK/MAXI K) is present in the inner mitochondrial membrane of rat brain. *Neuroscience* **139,** 1249–1261 (2006).
411. Berryman, M. A. & Rodewald, R. D. An enhanced method for post-embedding immunocytochemical staining which preserves cell membranes. *J. Histochem. Cytochem.* **38,** 159–170 (1990).
412. Roth, J., Bendayan, M. & Orci, L. Ultrastructural localization of intracellular antigens by the use of protein A-gold complex. *J. Histochem. Cytochem.* **26,** 1074–1081 (1978).
413. Garcia-Dorado, D. *et al.* The end-effectors of preconditioning protection against myocardial cell death secondary to ischemia-reperfusion. *Cardiovasc. Res.* **70,** 274–85 (2006).

Appendix

Slow matrix Ca^{2+} uptake by Ca^{2+} uniport or Ca^{2+}/H^{+} exchange in partially uncoupled cardiac cell mitochondria and its prevention by inhibiting complex V

Johan Haumann,[1,7,#] Ashish Gadicherla,[1,8,#] Age Boelens,[1,7] Christoph A. Blomeyer,[1,9] Amadou K.S. Camara,[1,4] Mohammed Aldakkak,[1] Cory J. Hartman,[1,10] Ranjan K. Dash,[2,3] David F. Stowe[1,2,4-6]

[1]Anesthesiology Research Division, Department of Anesthesiology; [2]Department of Physiology; [3]Bioengineering and Biotechnology Center; [4]Cardiovascular Research Center; Medical College of Wisconsin, Milwaukee, WI 53226, USA [5]Department of Biomedical Engineering, Marquette University, Milwaukee, WI 53233, USA, [6]Research Service, Veterans Affairs Medical Center, Milwaukee, WI 53295, USA Present addresses: [7]Department of Anesthesiology, Academic Medical Center, University of Amsterdam, The Netherlands; [8]Department of Basic Medical Sciences, Ghent University, Ghent, Belgium; [9]Department of Anaesthesia and Critical Care, University of Wuerzburg, Wuerzburg, Germany; [10]Department of Neurosurgery, University of Florida, Gainesville, FL, USA

# Equal contribution

Address for correspondence: David F. Stowe, M.D., PhD., Medical College of Wisconsin, M4020, 8701 Watertown Plank Road, Milwaukee, WI 53216. dfstowe@mcw.edu

Short title: mitochondrial Ca^{2+} flux during ATP hydrolysis

Highlights:

- We examined how Ca^{2+} uptake and pH_m are altered by dinitrophenol (DNP) to stepwise uncouple $\Delta\Psi_m$ and by oligomycin (OMN) to prevent H^+ pumping at mitochondrial complex V.
- The falls in $\Delta\Psi_m$ and pH_m after DNP and added $CaCl_2$ were larger when complex V was blocked.
- Early Ca^{2+} uptake fell as a function of declines in $\Delta\Psi_m$ and pH_m when complex V was blocked.
- Late Ca^{2+} uptake and pH_m rose with permissive H^+ pumping by complex V in absence of OMN.
- Fast mCa^{2+} influx is dependent on pH_m and $\Delta Ca^{2+}{}_m$ in addition to $\Delta\Psi_m$, while slow mCa^{2+} uptake by the Ca^{2+} uniporter or Ca^{2+}/H^+ exchange augments the fall in $\Delta\Psi_m$ and prevents a decline in pH_m.
- ATP_m hydrolysis supports the falling pH_m and promotes slow mCa^{2+} uptake that further uncouples $\Delta\Psi_m$.

Abstract

The aim was to assess and quantify the time and rate dependency of mitochondrial (m) Ca^{2+} uptake by $\Delta\Psi_m$ when altered by graded H^+ leak into the matrix and by outward H^+ pumping during ATP consumption. We postulated that pH_m –dependent mCa^{2+} uptake increases, rather than decreases, in partially uncoupled mitochondria when there is H^+ pumping during ATP consumption by complex V (F_OF_1-ATP synthase/ase). To test this we assessed mCa^{2+} ion uptake quantitatively in mitochondria isolated from guinea pig hearts while stepwise decreasing $\Delta\Psi_m$ with dinitrophenol (DNP) to test the effect of complex V activity on pH_m and $[Ca^{2+}]_m$ uptake in the presence and absence of oligomycin (OMN). We measured $[Ca^{2+}]_m$, $\Delta\Psi_m$, pH_m, and NADH over time by fluorescence spectrophotometry and [ATP] by the luciferin-luciferase reaction. After energizing mitochondria with pyruvic acid, DNP was added to stepwise uncouple $\Delta\Psi_m$, after which $CaCl_2$ (equivalent to 114 and 485 nM $[Ca^{2+}]_e$) was added ± OMN to block complex V. Enhanced F_oF_1-ATPase activity was evidenced by increased ATP consumption that was blocked by OMN and by the maintenance of pH_m in the absence of OMN. DNP caused stepwise decreases in $\Delta\Psi_m$ and pH_m that were larger when complex V was blocked. The falls in pH_m and $\Delta\Psi_m$ were greater at increasing $[Ca^{2+}]_m$. Fast Ca^{2+} uptake rate and $[Ca^{2+}]_m$ fell as a function of the falls in $\Delta\Psi_m$ and pH_m in the presence of OMN. Over time $[Ca^{2+}]_m$ and pH_m were higher as a function of a partial fall in $\Delta\Psi_m$ in the absence of OMN, indicating slow mCa^{2+} uptake via the Ca^{2+} uniporter (CaU) and or Ca^{2+}/H^+ exchange (CHE_m) as this was ruthenium red (RR) dependent. NADH decreased with the falls in $\Delta\Psi_m$ and pH_m only in the presence of OMN. This study demonstrates the relative importance not only of H^+ pumping by complex V to support $\Delta\Psi_m$ during uncoupling due to H^+ leak, but also of the effect of maintaining matrix $[H^+]$ to promote slow mCa^{2+} influx, which augmented the fall in $\Delta\Psi_m$. Because inducing ATP_m hydrolysis during partial uncoupling promotes uptake of mCa^{2+} which in turn further reduces $\Delta\Psi_m$, under conditions of cell stress where uncoupled oxidative phosphorylation and excess mCa^{2+} loading are observed, temporarily inhibiting ATP_m hydrolysis may prevent further mCa^{2+} loading and thus attenuate mitochondrial stress even though $\Delta\Psi_m$ and pH_m are not maintained.

Key Words: cardiac, mitochondria, Ca^{2+}uptake, Ca^{2+} uniporter, Ca^{2+}/H^+ exchange, H^+ leak and pumping, complex V.

Introduction

Mitochondrial matrix (m) Ca^{2+} overload is a damaging consequence of cardiac ischemia-reperfusion (IR) injury and so is an important subject for potential therapy (Brookes et al. 2004; O'Rourke, Cortassa & Aon, 2005; Stowe & Camara, 2009; Camara, Lesnefsky & Stowe, 2010). Mitochondria can consume ATP instead of producing it during ischemia, and this could have consequences for augmenting mCa^{2+} loading with its deleterious effects on the metabolic state that can lead to induction of apoptosis and necrosis. $[Ca^{2+}]_m$ is regulated in part by electrochemical dependent cation fluxes via transporters and exchangers within the inner mitochondrial membrane (IMM) (Brookes et al. 2004; Bernardi, 1999; Gunter & Pfeiffer, 1990; Gunter et al. 1994). One route for mCa^{2+} uptake is the ruthenium red (RR) sensitive Ca^{2+} uniporter (CaU), and a primary mCa^{2+} efflux pathway is via a Na^+/Ca^{2+} exchanger (NCE_m). Another more rapid mode of Ca^{2+} uptake may occur via a mitochondrial type ryanodine receptor. There is also homeostatic evidence of mCa^{2+} influx or efflux through a Na^+-independent Ca^{2+} exchanger (NICE), putatively a Ca^{2+}/H^+ exchanger (CHE_m), a.k.a. Ca^{2+}/H^+ antiporter. Ca^{2+} handling across the IMM is affected by other cations, e.g. Mg^{2+}, and most of the Ca^{2+} entering the matrix is dynamically buffered. Transport through the CaU and NCE_m are largely voltage dependent, whereas CHE_m may be pH dependent, but independent of the mitochondrial membrane potential ($\Delta\Psi_m$).

Many studies have shown a direct correlation between $\Delta\Psi_m$ and mCa^{2+} uptake according to the Nernst equation; a higher (more polarized) $\Delta\Psi_m$ results in a higher $[Ca^{2+}]_m$ (Gunter et al. 1994; Wingrove, Amatruda & Gunter, 1984). Although mCa^{2+} uptake via the CaU is highly dependent on $\Delta\Psi_m$, it is also dependent on the $[Ca^{2+}]_m$, and indirectly, on the $[H^+]_m$ chemical gradient and mCa^{2+} buffering capacity. How the magnitude, rate, and source of mCa^{2+} uptake are affected by manipulation of these electrochemical gradients when mitochondria are partially uncoupled, e.g. during ischemia, is not well characterized. Moreover, it is not known if H^+ pumping with ATP hydrolysis at complex V (F_OF_1-ATPsynthase/ase) to support $\Delta\Psi_m$ (Chinopolous & Adam-Vizi, 2010; Chinopolous, 2011) alters mCa^{2+} flux in partially uncoupled mitochondria. A comprehensive and quantitative understanding of mCa^{2+} uptake during these conditions that mimic IR injury is essential for developing therapeutic approaches to prevent or reduce excess mCa^{2+}.

A high $\Delta\Psi_m$ and a high extra-matrix $[Ca^{2+}]$ promote increased voltage and concentration dependent mCa^{2+} uptake via the CaU (Hoppe, 2010). Thus a decrease in mCa^{2+} uptake is expected from drug-induced graded decreases in $\Delta\Psi_m$ by protonophore-induced H^+ entry ("proton leak") (Gunter et al. 1994; Wingrove, Amatruda & Gunter, 1984). However, the added contribution of outward H^+ pumping by complex V to counteract the H^+ leak at less than fully polarized potentials may enhance slow $\Delta\Psi_m$ –independent mCa^{2+} uptake through CaU or CHE_m indirectly or directly due to the increase in $[H^+]_m$ caused by the H^+ leak. Moreover, induced increases in mCa^{2+} can significantly decrease $\Delta\Psi m$ (Delkam et al. 1998; De Lisa & Bernardi, 1998), due to the large influx of positive charges. In prior studies of mitochondrial Ca^{2+} handling, $[Ca^{2+}]_m$ was not measured over time, and regulatory factors such as redox state, $\Delta\Psi_m$, pH_m and ATP levels were not assessed,

particularly under the condition of an induced H^+ leak.

Our aim was to assess and quantify the time and rate dependence of mCa^{2+} uptake by a falling $\Delta\Psi_m$ caused by a graded H^+ leak into the matrix and by outward H^+ pumping during ATP consumption. To carry out this aim we challenged isolated, energized mitochondria with added buffer $CaCl_2$ while stepwise adding DNP in the absence or presence of the complex V inhibitor oligomycin (OMN) to block ATP hydrolysis, as assessed by timed measurements of matrix [ATP]. To determine how DNP, OMN and RR dynamically alter $[Ca^{2+}]_m$ after adding $CaCl_2$, we also dynamically measured matrix $\Delta\Psi_m$, pH_m, and NADH over time. Our overall goal was to gain greater insight in the bioenergetic mechanisms of mCa^{2+} uptake rate and magnitude via the CaU, and/or the pH_m -dependent CHE_m, when ΔpH_m and $\Delta\Psi_m$ tend to fall due to a graded H^+ leak with compensatory H^+ pumping by complex V in the attempt to restore ΔpH_m and $\Delta\Psi_m$.

Materials and Methods

Mitochondrial Isolation – All experiments conformed to the Guide for the Care and Use of Laboratory Animals and were approved by our institutional Biomedical Resource Center animal studies committee. All chemicals were obtained from Sigma-Aldrich (St. Louis, MO) unless noted otherwise. Guinea pig heart mitochondria were isolated as described before (Heinen et al. 2007; Riess et al. 2007; Haumann et al. 2010). Briefly, guinea pigs (250-350 g) were anesthetized by intraperitoneal injection of 30 mg ketamine; 700 units heparin was given for anticoagulation. Hearts (n = 59) were excised and minced to approximately 1 mm^3 pieces in ice-cold isolation buffer containing in mM: mannitol 200, sucrose 50, KH_2PO_4 5, 3-(N-morpholino) propanesulfonic acid (MOPS) 5, EGTA 1, BSA 0.1%, pH 7.15 (adjusted with KOH). The minced heart was suspended in 2.65 ml buffer with 5U/ml protease, and homogenized at low speed for 20 s; next 17 ml isolation buffer was added, and the suspension was again homogenized for 20 s. The suspension was centrifuged at 8000 *g* for 10 min. The supernatant was discarded and the pellet was suspended in 25 ml of isolation buffer, and centrifuged at 900 *g* for 10 min. The supernatant was centrifuged once more at 8000 *g* to yield the final mitochondrial pellet, which was suspended in 0.5 ml isolation buffer and kept on ice. The mitochondrial protein concentration was measured using the Bradford method,30 and diluted to 12.5 mg mitochondrial protein/ml with isolation buffer.

Fluorescence Measurements – Fluorescence techniques were used to measure mitochondrial matrix $[Ca^{2+}]_m$, NADH, pH_m, and $\Delta\Psi_m$ (Qm-8, Photon Technology International, Birmingham, NJ) spectrophotometrically (Heinen et al. 2007; Haumann et al. 2010; Aldakkak et al. 2010; Huang et al. 2007). A subset of isolated mitochondria (5 mg/ml) was incubated for 20 min at room temperature (25°C) with 5 µM indo-1 acetoxymethyl ester (AM) to measure $[Ca^{2+}]_m$ or 5 µM 2'7'-bis-(2-carboxyethyl)-5'(and 6-) carboxyfluroescein AM (BCECF) to measure pH_m (Invitrogen, Carlsbad, CA), followed by suspension in 25 ml isolation buffer and centrifugation at 8000 *g*. The AM form of the dye is taken up into the mitochondrial matrix where it is de-esterified, so that the dye is retained in the matrix. The dye-loaded pellet was resuspended in 0.5 ml isolation buffer, and

the protein concentration was measured again and diluted to 12.5 mg mitochondrial protein/ml. NADH was measured using autofluorescence and $\Delta\Psi_m$ was measured using rhodamine 123 (R123). Mitochondria were kept on ice for the duration of the studies. All studies were conducted at room temperature.

Experimental Protocol – Mitochondria were suspended (0.5 mg/ml) in experimental buffer solution containing in mM: KCl 130, K_2HPO_4 5, MOPS 20, bovine serum albumin 0.016 and EGTA 0.040 at pH 7.15 (adjusted with KOH). In the OMN groups 100 μM OMN was added to the experimental buffer before the start of the experiment. The experimental buffer was Na^+-free to prevent activation of the NCE. The inactivity of the NCE was verified by comparing data from these experiments to data from experiments with added CGP-37157, a specific mitochondrial NCE inhibitor (data not shown).

Experiments were initiated at t = -120 s; at t = -90 s mitochondria were added (Fig. 1). At t = 0 s pyruvic acid (PA, 0.5 mM) was added, followed by 0, 10, 20, 30 or 100 μM 2,4 dinitrophenol (DNP) at t = 120 s, and either of three levels of $CaCl_2$ (0, 10, and 25 μM in de-ionized H_2O). In some experiments (Supplemental Materials Figs. S.1, 2) 25 μM RR was added 60 s after adding $CaCl_2$. In all fluorescence experiments 4 μM carbonyl cyanide m-chloro phenyl hydrazone (CCCP) was added at t = 760 s to fully abolish $\Delta\Psi_m$. DNP, RR, OMN or CCCP were dissolved in DMSO for a final buffer concentration of 0.4 to 1% (wt/vol).

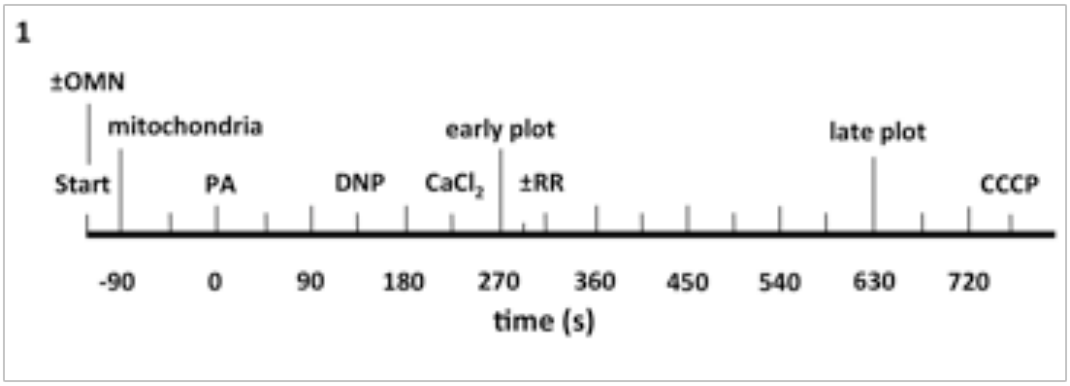

Fig. 1. Time line of experimental protocol: addition of mitochondria, ± oligomycin (OMN), pyruvic acid (PA), dinitrophenol (DNP), $CaCl_2$, and CCCP to respiratory buffer. Early and late plots refer to time points where means of several variables are plotted to summarize their interrelationships.

Measurement of $\Delta\Psi_m$ – $\Delta\Psi_m$ was measured by adding 50 nM rhodamine-123 (R123) (Calbiochem, San Diego, CA) to indo-1 treated mitochondria from 14 hearts to the experimental buffer. At an excitation wavelength (λ_{ex}) of 503 nm the change in fluorescence was measured at the emission wavelength (λ_{em}) of 527 nm. R123 uptake is dependent on $\Delta\Psi_m$. As the dye is taken up, the fluorescence signal decreases as the dye autoquenches; therefore, a decrease in $\Delta\Psi_m$ is represented by an increase in signal. Mitochondria energized with PA were considered fully polarized (0%), whereas the signal after adding CCCP represented complete IMM depolarization (100%).

Measurement of Matrix Ionized [Ca^{2+}] – $[Ca^{2+}]_m$ was measured in indo-1AM loaded mitochondria from 20 hearts. Indo-1 is a fluorescent dye that binds to Ca^{2+} with a K_d tested to be approximately 240 nM. The λ_{em} shifts from 456 nm to 390 nm on binding to Ca^{2+} when a λ_{ex} of 350 nm is applied. The ratio between the two λ_{em}'s corrects for differences in the amount of dye taken up into mitochondria. Since the λ_{ex} and λ_{em} used for Ca^{2+} are the same as for NADH, the two NADH background λ_{em} signals were subtracted from the two λ_{em} indo-1 signals before calculating the ratio (R). The ratios obtained when all indo-1 becomes bound to Ca^{2+} (R_{max}) and when the lowest amount of Ca^{2+} is bound to indo-1 (R_{min}) were measured in energized mitochondria using 500 nM cyclosporine A and 500 µM $CaCl_2$ for R_{max}, and A23187 (Ca^{2+}-ionophore) and 2.5 mM EGTA for R_{min} (Haumann et al. 2010). $[Ca^{2+}]_m$ was calculated using the formula (Grynkiewicz, Poenie & Tsien, 1985):

$$[Ca^{2+}]_m \text{ (nM)} = K_d \bullet (R-R_{min})/(R_{max}-R) \bullet S_{456}$$

The K_d is the binding constant, and S_{456} is the ratio of fluorescence intensities during unsaturated and saturated Ca^{2+} at the 456 nm λ_{em}. Their ratio was measured to be 1.35. The Ca^{2+} signals were normalized to the averaged $[Ca^{2+}]_m$ over all experiments at time point t = 10 s (see *Experimental Protocol*), which was calculated to be approximately 80 nM. A 0.15 decrease in pH increases the K_d negligibly by about 9 nM. ADP and ATP do not differentially alter light transmission at the λ_{ex} and λ_{em} spectra for indo-1 or the alternative Ca^{2+} fluorescent probe Rhod-2.

Measurement of Mitochondrial Redox State – Mitochondria from 9 hearts were used to measure NADH autofluorescence. Unlike NAD, NADH molecules have natural fluorescence properties that can be monitored (Chance et al. 1962). Therefore, an increase in the signal reflects an increase in the ratio of NADH to NAD^+, i.e. a shift to a more reduced state. The emission spectrum of NADH is broad, and peaks at λ_{em} =456 nm and λ_{ex} =350 nm. To correct for differences in total NADH and NAD^+ pool sizes, the ratio of λ_{em} 456/390 nm was measured. In addition to providing data on the mitochondrial redox state, the raw NADH data was used to correct for the background autofluorescence measured by the indo-1 fluorescence probe for $[Ca^{2+}]_m$ (Haumann et al. 2010; Grynkiewicz et al. 1985).

Measurement of Matrix pH – Matrix pH was measured in BCECF-AM treated mitochondria from 9 hearts at λ_{ex} =504 nm and λ_{em} =530 nm. BCECF is a fluorescent probe that becomes less fluorescent in an acidic environment; thus an increase in signal indicates matrix alkalinization and a decrease in signal indicates matrix acidification. The measured signals were normalized for each group to their average photon count at the steady state seen after adding $CaCl_2$ or vehicle to correct for differences in signal strength and dye uptake. The measured signal was converted to pH units by measuring the BCECF signal from tritonized (1% triton X-100) mitochondria incubated in BCECF in buffers with known pH (7.00, 7.15 and 7.25) (Haumann et al. 2010). This gave a linear

relationship, which enabled calculation of pH_m from the signal intensity. Because the wavelengths used for BCECF measurements did not overlap with the NADH autofluorescence signals, the matrix NADH and pH_m measurements were conducted in the same mitochondrial preparation.

Measurement of ATP Concentration – Mitochondrial [ATP] was estimated from ATP consumption in the total mitochondrial buffer: ATP+luciferin → luciferyl adenylate+PP_i; luciferyl adenylate+O_2 → oxyluciferin+AMP+light. In brief, mitochondria from 20 hearts were suspended in experimental buffer and the normal protocol as described above (Fig. 1) was followed, with the exceptions that mitochondria were added at t = -120 s, then PA at t = 0, next DNP (0, 10, 20, 30 or 100 μM), and then $CaCl_2$ (0, 10, or 25 μM) at the same time points. CCCP was not added in these experiments. At specific time points all proteins were precipitated by adding 100 μl of 70% perchloric acid (Sigma-Aldrich) to quench all reactions. The obtained aliquot was centrifuged for 1 min at 50 *g*, 750 μl of the supernatant was collected, and the acidity was reversed by adding 180 μl of 5 M KOH. ATP was measured in buffer containing 200 mM MOPS, 2 mM EGTA, 3 mM $MgCl_2$, 0.3 mM D-luciferin and 1.25 mg/ml luciferase (Invitrogen) at pH 7.20 (adjusted with KOH). Samples of 2.4 μl were added to 97.5 μl buffer, the solution was mixed, and luminescence was measured using a luminometer (Turner Biosystems). Total buffer [ATP] was calculated from the calibration curve generated using 62.5 nM, 125 nM, and 1250 nM [ATP] standards. Mitochondrial [ATP] was estimated from the final mitochondrial protein concentration (8.8 μg/ml) and the ratio of mitochondrial water to protein (Vinnakota & Bassingthwaite, 2004) as follows:

$$\text{Final calculated mitochondrial [ATP]} = \frac{[\text{ATP}](10^{-9}\ \text{M})(10^{-3}\ \text{L/ml})}{(8.8\ \mu\text{g/ml})(66.4/25.0\ \text{nl}/\mu\text{g})(10^{-9}\ \text{L/nl})}$$

where mitochondrial protein mass = 0.25 of the total mitochondrial mass; mitochondrial water mass = 0.664 of the total mitochondrial mass; 66.4 g mito H_2O/g sample = 66.4 nl mito H_2O/μg because 1 μg H_2O = 1 nl H_2O; for example: if buffer [ATP] is 50 nM, then calculated mitochondrial [ATP] = 2.15 mM based on the estimated overall dilution factor of $4.3x10^4$. (See Supplemental Materials for assessment of ATP/ADP ratios by HPLC and luminometry.)

Statistical Analyses – All data are presented and expressed as average ±SEM. Repeated measure ANOVAs followed by a post hoc analyses using Student-Newman-Keuls' test were performed to determine statistically significant differences within each DNP group. Data for analyses were collected at the times noted above, i.e. before and after adding DNP, and early and late after adding $CaCl_2$. Effects of DNP and $CaCl_2$ additions as a function of pH_m were also examined by multiple regression analysis. A P value < 0.05 (two-tailed) was considered significant.

2. Results

Membrane Potential – $\Delta\Psi_m$ decreased (became uncoupled) in a stepwise manner at increasing [DNP] (Fig. 2). $\Delta\Psi_m$ was assessed as % of depolarization (fully coupled to completely uncoupled), where PA = 0 s represents full polarization (0%) and CCCP full depolarization (100%), Adding 20 µl DMSO (DNP vehicle) or 20 µl H_2O alone caused a small decrease of the R123 fluorescence signal (Fig. 2A). Adding 0, 10, 20, 30, or 100 µM DNP reduced $\Delta\Psi_m$ by 9.7±0.3, 16.7±0.7, 18.7±1.1 and 92.4±2.4%, respectively. In the presence of OMN (Fig. 2C), adding 0, 10, 20, 30 or 100 µM DNP reduced $\Delta\Psi_m$ by 3.0±1.0, 6.0±1.0, 14.2±1.6, 31.0±5.0 and 99.0±2.1%, respectively. Overall, with no added $CaCl_2$, the effect of DNP to decrease $\Delta\Psi_m$ was larger in the presence of OMN (Fig. 2C,D vs. 2A,B).

On adding either 10 µM (Fig. 2A,C) or 25 µM (Fig. 2B,D) $CaCl_2$, $\Delta\Psi_m$ was slightly and temporarily increased and this was not [DNP] dependent; this effect was followed by a gradual and graded uncoupling that was dependent on both the [DNP] and the $[Ca^{2+}]_m$. In the absence of added $CaCl_2$ the extent of uncoupling induced by DNP was not altered over time (data not shown). This indicates that adding $CaCl_2$ greatly enhanced $\Delta\Psi_m$ uncoupling only if the $\Delta\Psi_m$ was already partially uncoupled; i.e., adding 25 µM $CaCl_2$ had no effect on changing $\Delta\Psi_m$ if it was not already partially uncoupled. $CaCl_2$-induced uncoupling was faster and greater in the 30 µM DNP group, particularly after adding 25 µM $CaCl_2$ (Fig. 2B). In the presence of OMN (Fig. 2C,D), when $\Delta\Psi_m$ was uncoupled more by DNP, the decrease in $\Delta\Psi_m$ after adding either 10 or 25 µM $CaCl_2$ was even greater than in the absence of OMN.

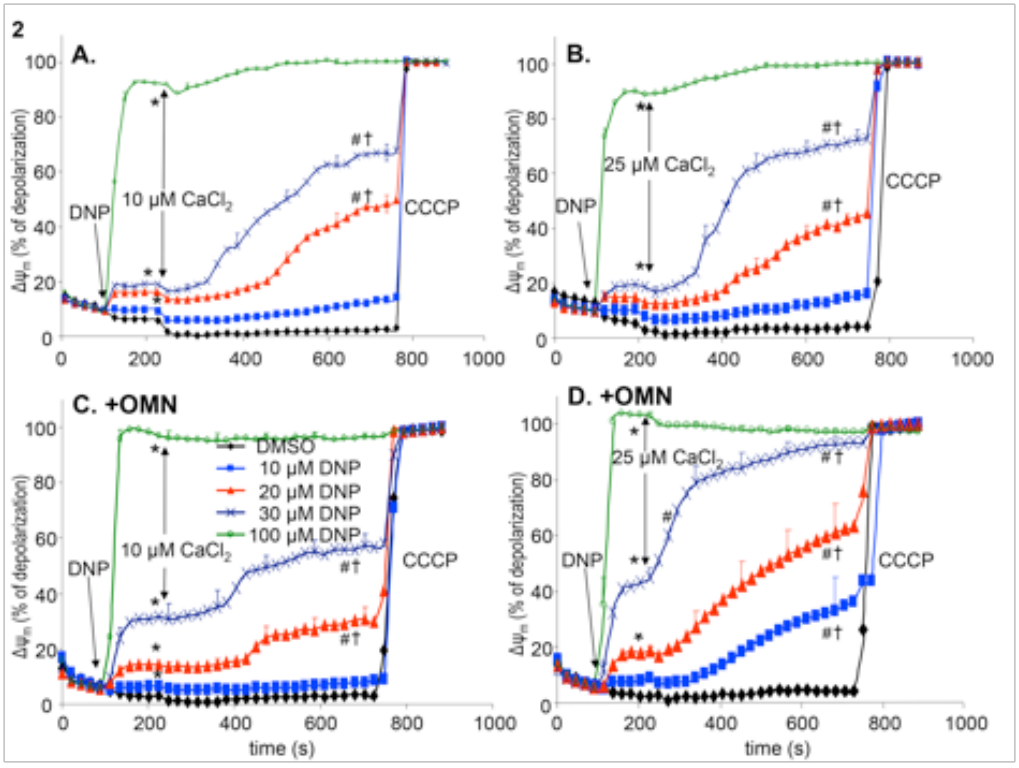

Fig. 2. Change in mitochondrial membrane potential ($\Delta\Psi_m$), measured with rhodamine-123, as a function of time after adding dinitrophenol (DNP) and $CaCl_2$ in the absence (A,B) and presence (C,D) of oligomycin (OMN). Note that adding DNP caused a concentration-dependent decrease in $\Delta\Psi_m$ that was more pronounced in the presence of OMN.

Addition of $CaCl_2$ caused a small polarization, while a continuous uncoupling occurred over time. Addition of 25 µM $CaCl_2$ (B,D) resulted in a more pronounced uncoupling effect compared to 10 µM $CaCl_2$ (A,C). For $P<0.05$: *after vs. before DNP; #after vs. before $CaCl_2$; †late vs. early after $CaCl_2$.

Mitochondrial Free [Ca^{2+}] – Adding 10 or 25 µM $CaCl_2$ without DNP ($\Delta\Psi_m$ fully coupled) increased $[Ca^{2+}]_m$ from 80±9 (no added $CaCl_2$) to 225±20 and 450±43 nM, respectively, at 240 s (Fig. 3A,B); $[Ca^{2+}]_m$ remained unchanged over time after 10 µM $CaCl_2$ but fell gradually over time after 25 µM $CaCl_2$. When $\Delta\Psi_m$ was stepwise uncoupled by 10-30 µM DNP, $[Ca^{2+}]_m$ continued to rise after adding 10 µM $CaCl_2$ (Fig. 3A) and also when stepwise uncoupled by 10 and 20 µM DNP after adding 25 µM $CaCl_2$ (Fig. 3B)); this slow rise in $[Ca^{2+}]_m$ was completely blocked by adding RR 60 s after adding $CaCl_2$ When $\Delta\Psi_m$ was nearly or totally uncoupled by 100 µM DNP in the absence of OMN, the rise in $[Ca^{2+}]_m$ over time in the 10 µM $CaCl_2$ group was negligible but it increased significantly over time in the 25 µM $CaCl_2$ group. In contrast, the presence of OMN to block complex V abolished the gradual rise in $[Ca^{2+}]_m$ over time in the 10 µM $CaCl_2$ group (Fig. 3C) and resulted in reduced $[Ca^{2+}]_m$ over time in the 25 µM $CaCl_2$ group (Fig. 3D).

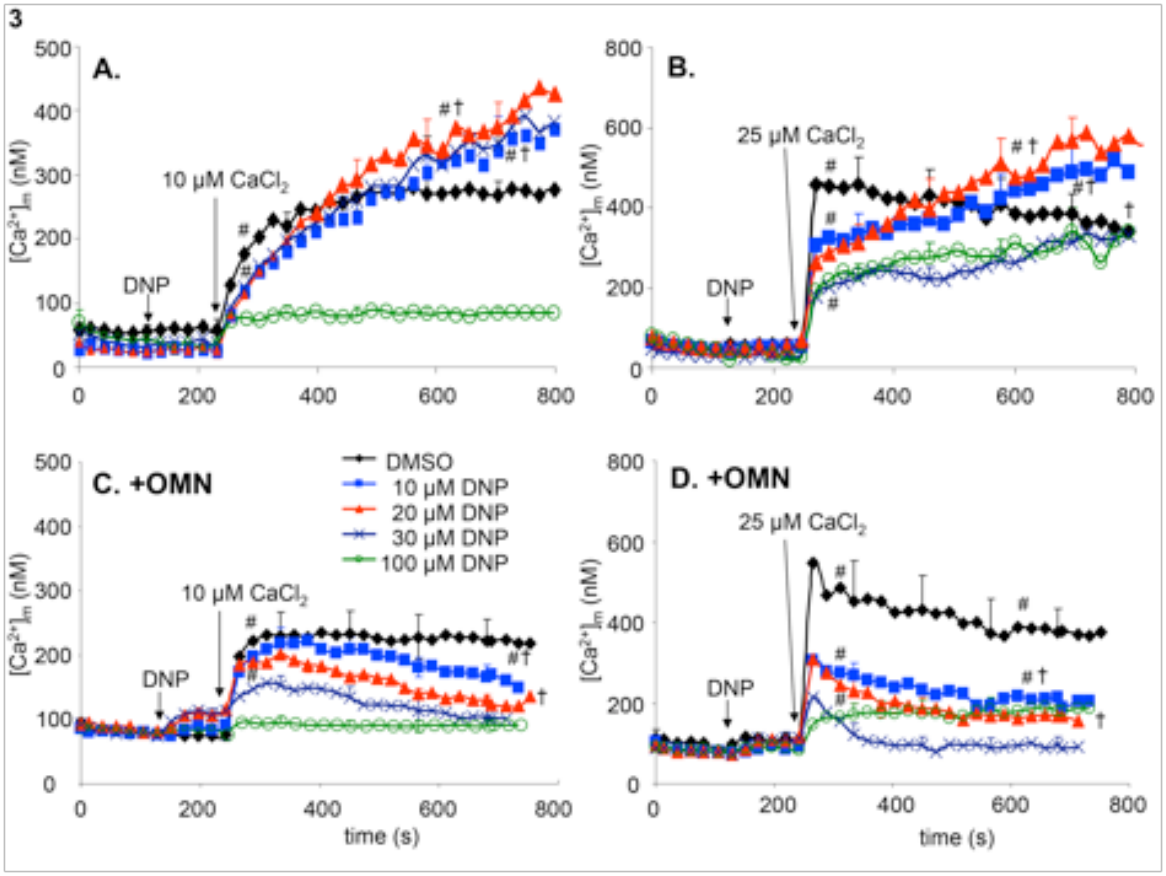

Fig. 3. Change in mitochondrial $[Ca^{2+}]_m$, measured with indo-1, as a function of time after adding DNP and $CaCl_2$ in the absence (A,B) and presence (C,D) of OMN. Note that adding DNP did not alter $[Ca^{2+}]_m$, per se, but did affect $[Ca^{2+}]_m$ depending on the concentration of DNP, the amount of $CaCl_2$ added, and the absence or presence of OMN. Adding 10 µM $CaCl_2$ (A,C) resulted in a lower increase in $[Ca^{2+}]_m$ than 25 µM $CaCl_2$ (B,D). In the presence of OMN

(C,D) DNP caused a concentration-dependent reduction in $[Ca^{2+}]_m$, whereas in the absence of OMN the effect of DNP on $[Ca^{2+}]_m$ was less concentration –dependent and $[Ca^{2+}]_m$ continued to increase over time. See Fig. 2 for statistical notation.

The initial rate of rise in $[Ca^{2+}]_m$ (0-7 s) was faster after adding 25 μM than 10 μM $CaCl_2$ (Fig. 4A,B) and was slowed stepwise at decreasing $\Delta\Psi_m$ with added DNP. The uptake of mCa^{2+} during the first 7 s after adding 10 μM $CaCl_2$ decreased from 8.2 (0 DNP) to 1.9 (100 μM DNP) nM/s, and after adding 25 μM $CaCl_2$, from 87.6 (0 DNP) to 20.2 (100 μM DNP) nM/s. In the presence of OMN, the initial rises in $[Ca^{2+}]_m$ in fully coupled (0 μM DNP) mitochondria were greater than those in the absence of OMN (Fig. 4A,B *vs.* Fig. 4C,D). In the presence of OMN, the initial mCa^{2+} uptake rates decreased from 30.1 (0 DNP) to 4.2 nM/s (100 μM DNP) after adding 10 μM $CaCl_2$ and from 129.9 (0 DNP) to 12.9 nM/s (100 μM DNP) after adding 25 μM $CaCl_2$ (Fig. 4C,D). Thus the mCa^{2+} uptake rates with 10 and 25 μM $CaCl_2$ were faster in the presence of OMN and 10, 20, and 30 μM DNP (Fig. 4C *vs*. A; Fig. 4D *vs*. C).

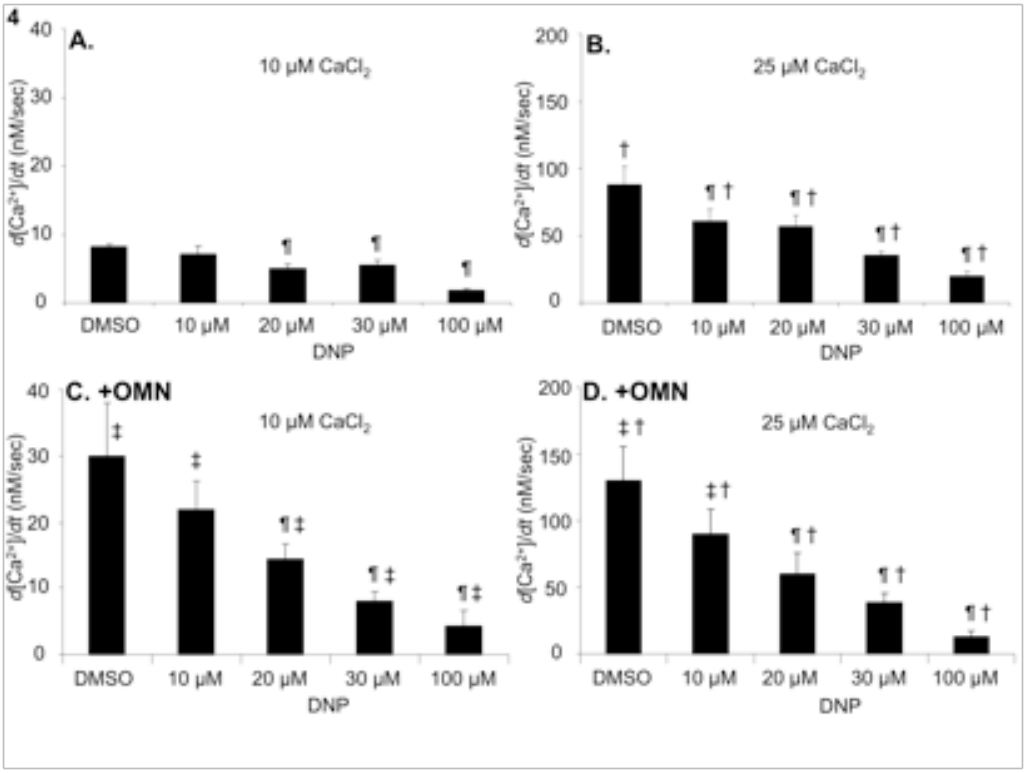

Fig. 4. Summary of data for initial rates of mCa^{2+} uptake (nM/s) as a function of [DNP] after adding $CaCl_2$ in the absence (A,B) or presence (C,D) of OMN. The rate of mCa^{2+} uptake decreased as the degree of $\Delta\Psi_m$ uncoupling increased with increasing [DNP]. Note that mCa^{2+} uptake rate was higher in the presence of OMN (C,D) than in its absence (A,B). For $P<0.05$: ¶DNP vs. DMSO; ‡25 vs. 10 μM $CaCl_2$.

Mitochondrial pH – pH_m, measured with BCECF-AM, increased on addition of PA (data not shown) as more H^+ was pumped out of the matrix via the electron transport chain. In the absence

of OMN, DNP had only a small effect to decrease pH_m at a partially uncoupled $\Delta\Psi_m$ but had a large effect to acidify the matrix when $\Delta\Psi_m$ was fully uncoupled (100 µM DNP) (Fig. 5A,B). Adding $CaCl_2$ had no appreciable effect on pH_m at a partially uncoupled $\Delta\Psi_m$, but enhanced the acidification observed at a fully uncoupled $\Delta\Psi_m$ (Fig. 5A,C). In the presence of OMN there was a strong concentration-dependent acidification of the matrix dependent on the degree of $\Delta\Psi_m$ uncoupling (Fig. 5C,D). This indicated that with complex V blocked, more H^+ ions were able to enter the matrix (or fewer to exit) through the IMM. Conversely, in the absence of OMN when $\Delta\Psi_m$ exhibited partial uncoupling, H^+ ion entry was matched by H^+ ion extrusion as pH_m did not appreciably change. Moreover, the gradual acidification observed after adding $CaCl_2$ was more pronounced in the presence of OMN. Multiple regression analysis showed that pH_m was correlated to both $CaCl_2$ addition and DNP addition. With no OMN, the pH_m was dependent on DNP and $CaCl_2$ addition with a beta of 0.42 ($p<0.001$) and 0.30 ($p<0.05$), respectively, with a correlation coefficient of 0.51. In the presence of OMN the dependences were similar; the beta's were 0.62 ($p<0.001$) and 0.30 ($p<0.05$), respectively, with a correlation coefficient of 0.68.

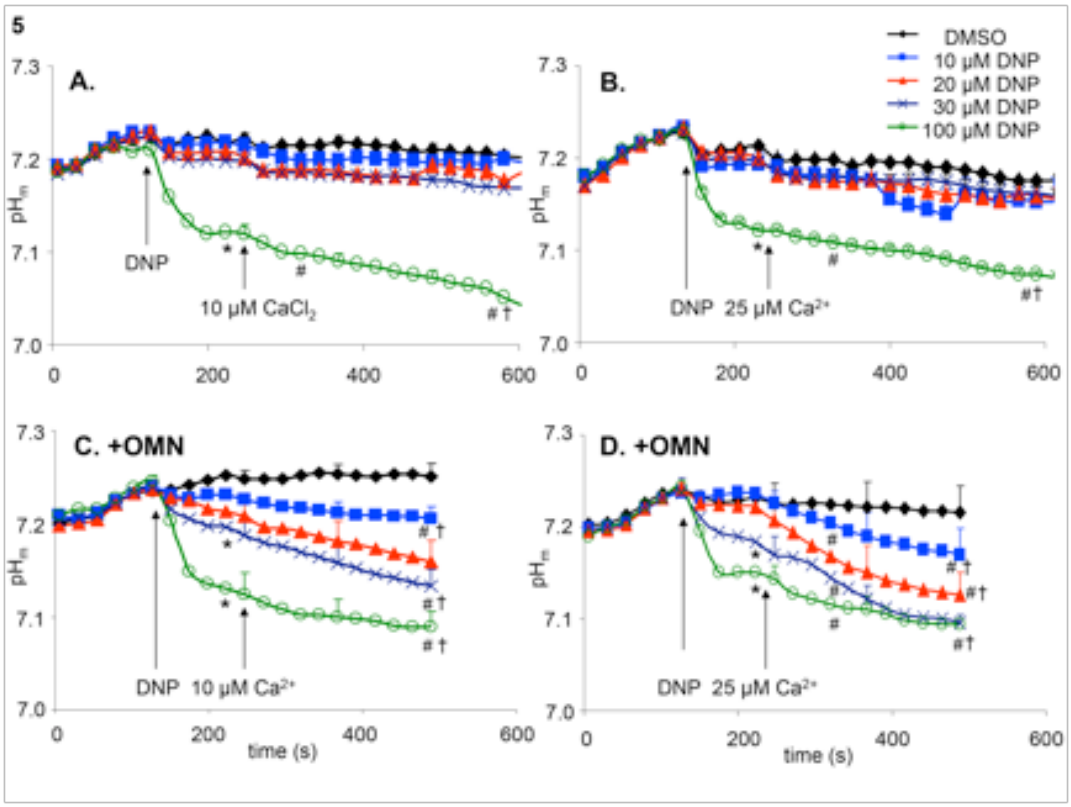

Fig. 5. Change in pH_m, measured with BCECF, as a function of time after adding DNP and $CaCl_2$ in the absence (A,B) or presence (C,D) of OMN. Note that except for 100 µM DNP, neither DNP nor added $CaCl_2$ altered pH_m in the absence of OMN (A,B). However, in the presence of OMN (C,D) graded decreases of $\Delta\Psi_m$ by DNP caused a graded increase in matrix acidity that was further increased in the presence of added $CaCl_2$ (C,D). See Fig. 2 for statistical notation.

Interrelationship of $[H^+]_m$, $[Ca^{2+}]_m$ and $\Delta\Psi_m$ – Changes in $[Ca^{2+}]_m$ as a function of changes in

$\Delta\Psi_m$ or $[H^+]_m$, and of $[H^+]_m$ as a function of $\Delta\Psi_m$, were plotted from the means data of Figs. 2A,B, 3A.B, and 5A,B) taken at two defined time points, early (A) at 270 s, and late (B) at 630 s; (see Fig. 1 time line). These plots display how these interrelationships shifted with time depending on the whether complex V was blocked or not.

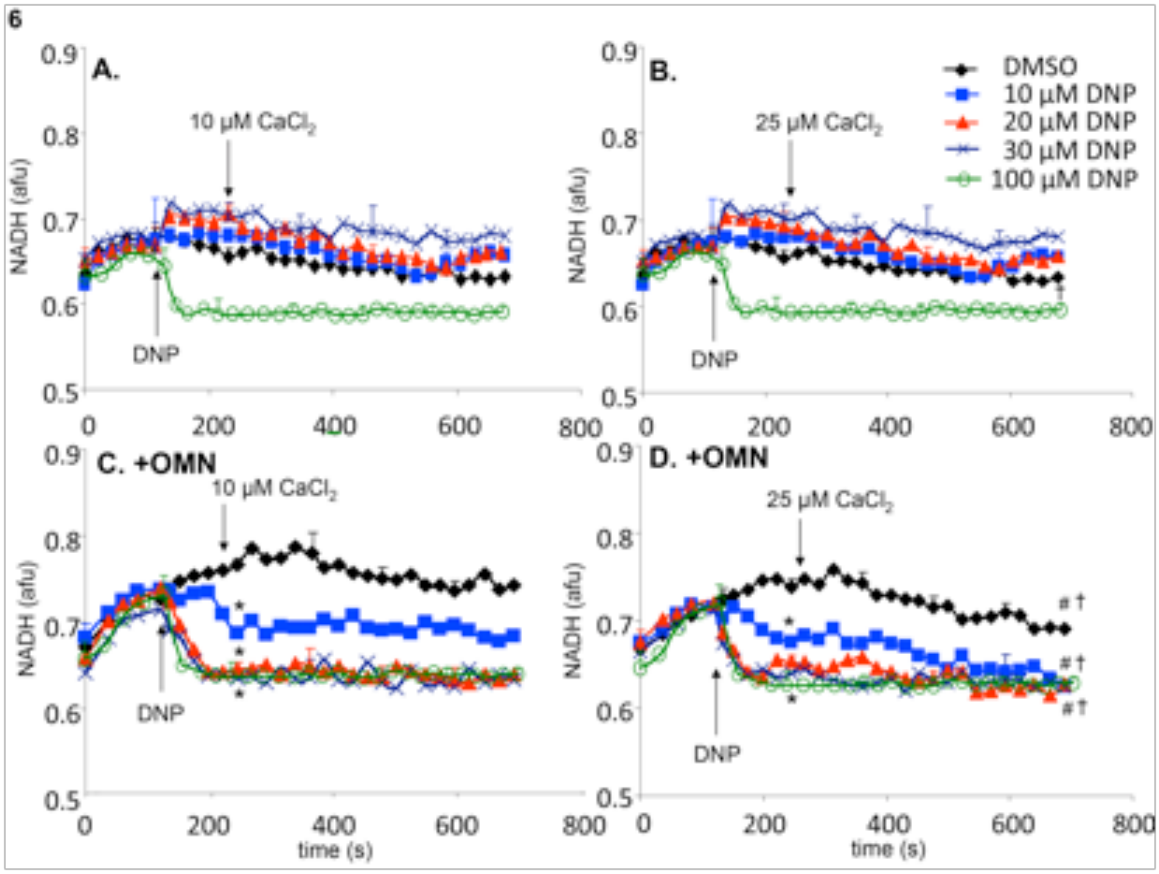

Fig. 6. Change in mitochondrial redox state, measured by NADH autofluorescence, as a function of time after adding DNP and $CaCl_2$ in the absence (A,B) or presence (C,D) of OMN. Note that the redox state was maintained after adding 10-30 µM DNP and $CaCl_2$ in the absence of OMN (A,B) but that in the presence of OMN (C,D) there was a concentration-dependent decrease in NADH autofluorescence. Adding $CaCl_2$ did not alter DNP-induced changes in redox state in the presence of OMN. See Fig. 2 for statistical notation.

Mitochondrial Redox State – Redox state, as assessed by NADH autofluorescence, increased on addition of PA as substrate for the TCA cycle (data not shown). In the absence of OMN, redox state was not altered significantly by 10-30 µM DNP (100 µM DNP completely oxidized NADH, not shown) or by the addition of either 10 or 25 µM $CaCl_2$ (Fig. 6A,B). This indicated that the redox state was maintained despite both substantial uncoupling and increased $[Ca^{2+}]_m$ in the absence of OMN. However, in the presence of OMN to block complex V (Fig. 6C,D) NADH was decreased in a nearly concentration dependent manner by DNP; NADH redox state, however, was not additionally altered by adding $CaCl_2$.

ATP Concentration –Total [ATP] was measured and expressed as mitochondrial [ATP] as explained in **Materials and Methods**. Adding mitochondria to the experimental buffer increased [ATP], as there was sufficient ADP and P_i available for ATP generation (Fig. 7). There was no additional change in [ATP] after adding PA. Adding 10-30 µM DNP alone had little effect on [ATP] until $CaCl_2$ was added which greatly enhanced $\Delta\Psi_m$ uncoupling; then there was a decrease in [ATP] with a fall in $\Delta\Psi_m$ (Fig. 7 A,B). However, a small decrease in $\Delta\Psi_m$ by 10 µM DNP did not significantly change [ATP] before or after adding $CaCl_2$. DNP, 100 µM, alone caused a marked decrease in [ATP] (data not shown). In the presence of the complex V inhibitor OMN (Fig. 7 C,D), adding mitochondria to the experimental buffer alone did not change [ATP], indicating that isolated mitochondria contain limited ATP after isolation. [ATP] remained at a very low level and was unaffected by DNP or $CaCl_2$ in the presence of OMN. ATP/ADP ratios (see Supplemental Materials) also decreased with added DNP and $CaCl_2$, which progressively uncoupled $\Delta\Psi_m$.

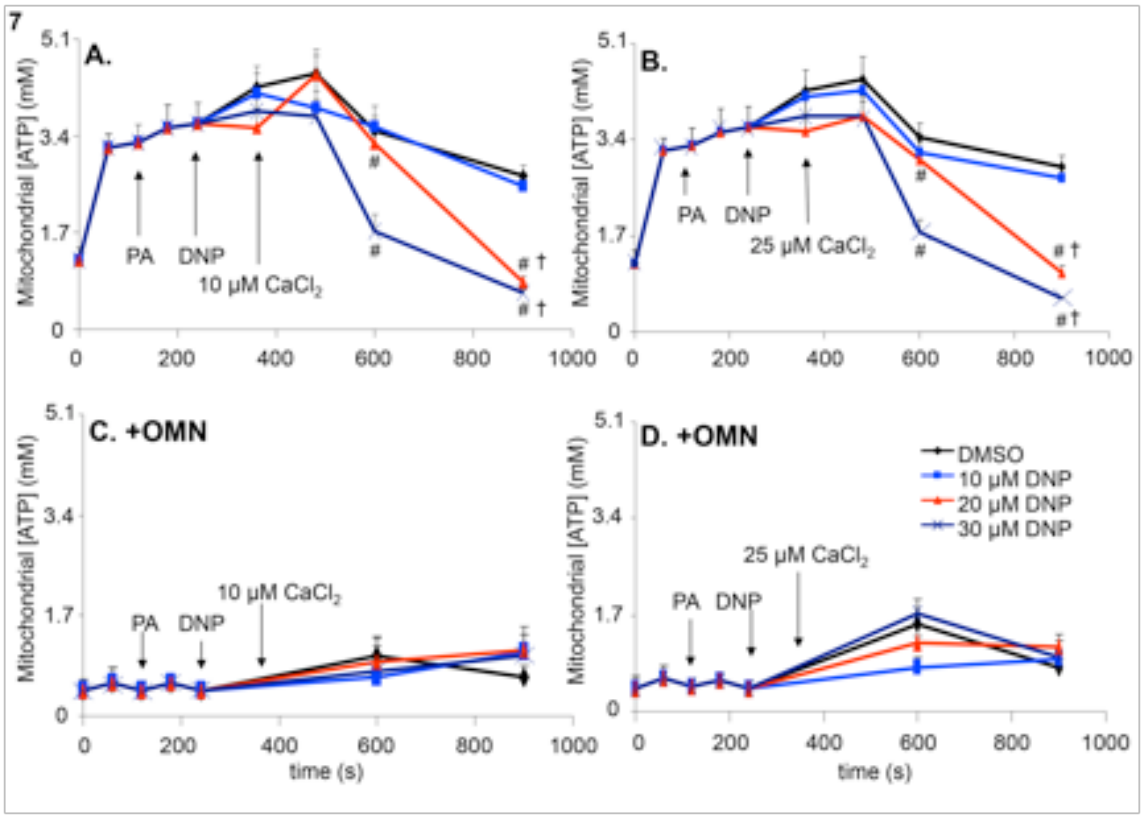

Fig. 7. [ATP], measured in total solution by the luciferin-luciferase reaction, and expressed as the calculated mitochondrial [ATP], was altered as a function of DNP and added $CaCl_2$ in the presence and absence of OMN. Adding mitochondria to the respiration buffer increased [ATP]; adding pyruvic acid (PA) and DNP had no additional effect; but adding $CaCl_2$ after DNP in the absence of OMN resulted in concentration-dependent decreases in [ATP] as graded depolarization of the IMM occurred (A,B). F_OF_1-ATP synthase/ase activity was near zero and remained essentially unchanged after adding PA, DNP, and $CaCl_2$ in the presence of OMN (C,D). See Fig. 2 for statistical notation.

Discussion

The important findings from these results are that:

a) Inducing a limited, but severe, matrix inward H^+ leak by 10-30 μM DNP alone uncouples $\Delta\Psi_m$ stepwise by up to 20% (Fig. 2A,B) without changing the redox state (Fig. 6A,B); these small changes are likely due to reciprocal outward H^+ pumping by complex V as shown by the lack of a decrease in pH_m (Fig. 5A,B) and the lower [ATP] (Fig. 7A,B). In contrast, by inducing a H^+ leak by DNP while inhibiting outward H^+ pumping by complex V by OMN (Fig. 7C,D), this results in increased matrix acidity (Fig. 5C,D), reduced $\Delta\Psi_m$ by up to 40% (Fig. 2C,D), and a lowering of the redox state (Fig. 6C,D).

b) $\Delta\Psi_m$ continued to fall over 6 min after adding $CaCl_2$ (Fig. 2A-D), but only in already partially DNP -uncoupled mitochondria; this effect was compensated by H^+ pumping by complex V (Fig 2. A,B) as the fall in $\Delta\Psi_m$ was augmented. When H^+ pumping was blocked (Fig. 2C,D), $\Delta\Psi_m$ decreased further after adding $CaCl_2$ because the influx of Ca^{2+} brings in positive charges not alleviated by H^+ pumping at complex V. This was manifested by the exaggerated effect of more added $CaCl_2$ on the uncoupling of $\Delta\Psi_m$ over time (Fig. 2C,D), by the slow gradual fall in $[Ca^{2+}]_m$ (Fig. 3C,D), and by the increased matrix acidity (Fig. 5C,D). In contrast, in the presence of compensatory H^+ pumping by complex V, Ca^{2+} continued to enter as shown by the gradual RR-dependent rise in $[Ca^{2+}]_m$, by the lower matrix acidity, and by the lesser fall in $\Delta\Psi_m$ over time (C,D in Figs. 2, 3, 5). Matrix Ca^{2+} influx via CHE_m may occur under these circumstances because pH_m remained more stable (less acidic) when complex V was not blocked Fig. 5A,B *vs*. C,D).

c) In mitochondria fully uncoupled by 100 μM DNP, and accompanied by a fall in pH_m, adding $CaCl_2$ abruptly increased $[Ca^{2+}]_m$ (Fig. 3) but caused a gradual, accentuated fall in pH_m (Fig. 5A-D); this is likely due to a failure of outward H^+ pumping by complex V to counteract H^+ influx by DNP.

d) Only in already partially uncoupled ($\Delta\Psi_m$ lowered by 10-20%) mitochondria did increasing $[Ca^{2+}]_m$ (baseline ≈80 nM), initially to ≈150 nM (10 μM $CaCl_2$) or ≈ 250 nM (25 μM $CaCl_2$), result in additional time and pH_m- dependent increases in $[Ca^{2+}]_m$ over 6 min (270 to 630 s) of up to 400 nM and 550 nM, respectively; this increase in $[Ca^{2+}]_m$ was accompanied by a maintained, less acidic pH_m (Fig. 5A,B) and a maintained redox state (Fig. 6 A,B). We propose this paradoxical doubling of $[Ca^{2+}]_m$ during a concomitant uncoupling of $\Delta\Psi_m$ is linked to outward H^+ pumping by complex V because $[Ca^{2+}]_m$ fell rather than rose (Fig. 5C,D) and $[H^+]_m$ became more acidic (Fig. 5C,D) during an equivalent uncoupling of $\Delta\Psi_m$ after blocking complex V with OMN, as indicted by no change in [ATP] (Fig. 7).

H^+ Pumping by Complex V Results in Slow Matrix Ca^{2+} Loading and Lesser Uncoupling of $\Delta\Psi_m$ – We observed a greater decline in $\Delta\Psi_m$ induced by $CaCl_2$ after OMN despite a lesser rise in mCa^{2+}

influx due to the inability of complex V to pump out H^+ ions. This was accompanied by an increase in matrix acidity and a fall in redox state. In contrast, in the presence of compensatory H^+ pumping by complex V, Ca^{2+} continued to enter the matrix via the CaU or CHE_m as shown a) by the gradual rise in $[Ca^{2+}]_m$ that was RR-dependent (Supplemental Fig. S. 1,2), b) by the absence of enhanced matrix acidity, and c) by the lesser uncoupling of $\Delta\Psi_m$ over time. Overall, these findings suggest that increases in $[Ca^{2+}]_m$ after adding $CaCl_2$ is dependent not only on the existing $\Delta\Psi_m$ and $\Delta[Ca^{2+}]_m$ for mCa^{2+} entry via the CaU, but also on a time-dependent and $\Delta\Psi_m$ -independent slower mCa^{2+} entry via the CaU or CHE_m when the IMM is partially protected against $\Delta\Psi_m$ uncoupling by compensatory H^+ pumping. We propose that slow Ca^{2+} uptake occurs at least in part via CHE_m in the absence of OMN because pH_m becomes more acidic in the presence of OMN. Our proposed mechanism is described schematically in Fig. 8A (– OMN) and 8B (+ OMN).

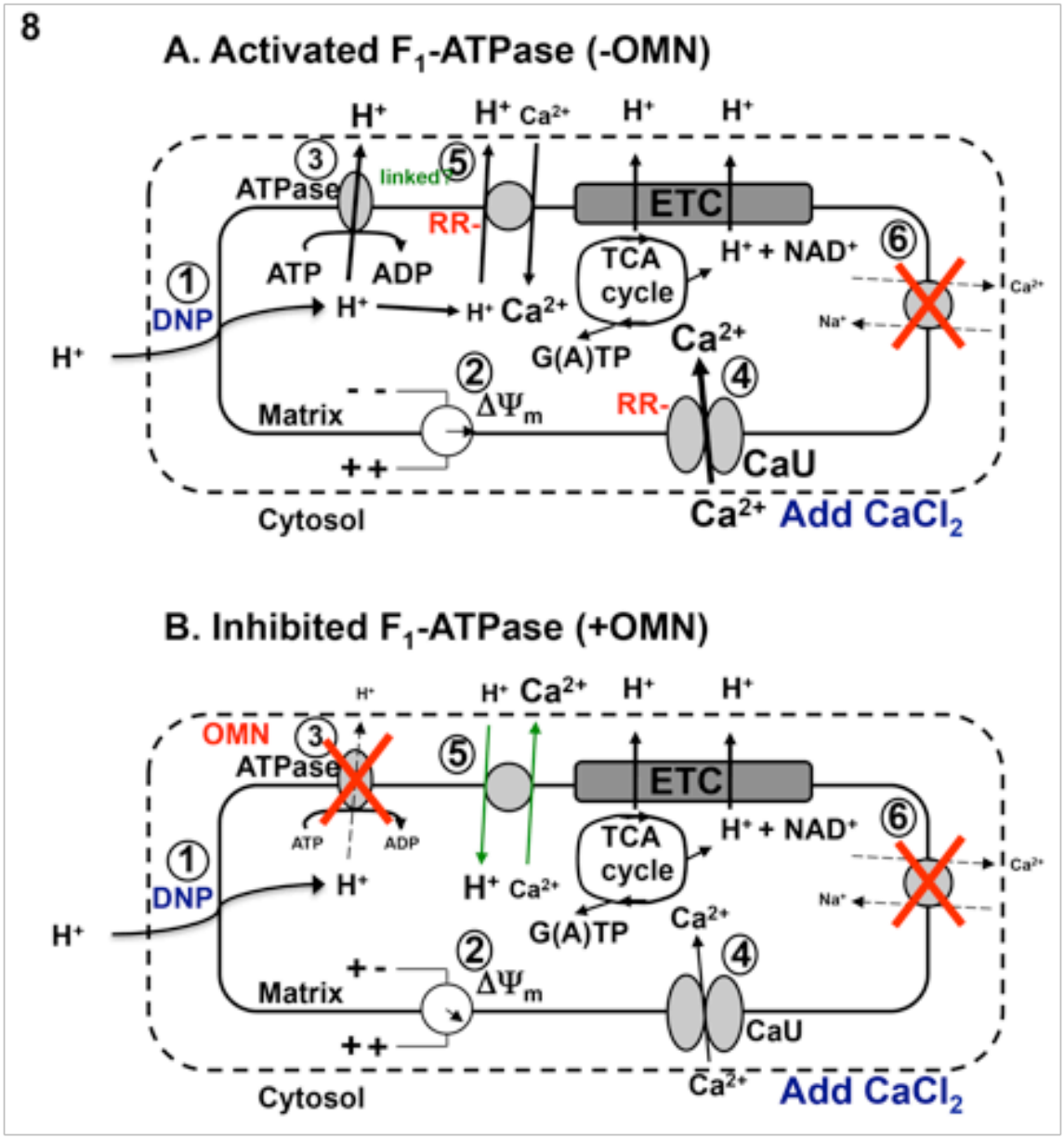

Fig. 8. Schema depicting putative role of CaU/CHE$_m$ during stepwise uncoupling with DNP with un-inhibited (A) *vs*. inhibited (B) F_OF_1-ATPsynthase(ase) (OMN) after increasing buffer [$CaCl_2$]. A. (1) DNP allows H^+ entry that tends to (2) decrease $\Delta\Psi_m$, which enhances H^+ pumping by respiratory complexes, including (3) F_OF_1-ATPase so that pH_m does not decrease and $\Delta\Psi_m$ is supported. Adding $CaCl_2$ further uncouples $\Delta\Psi_m$ by allowing more cations into the matrix via the CaU (4). Over time in the range of 20-60% fall in $\Delta\Psi_m$, pH_m remains unchanged as (5) H^+ exits in exchange for Ca^{2+} entry causing $\Delta\Psi_m$ to fall further when (6) NCE is blocked. B. Alternatively, when (3) F_OF_1-ATPase is inhibited (2) $\Delta\Psi_m$ is less supported and (5) Ca^{2+} exits in exchange for H^+ entry, so that $[Ca^{2+}]_m$ decreases and $[H^+]_m$ increases over time relative to the situation when F_OF_1-ATPase is activated. DNP, dinitrophenol; OMN, oligomycin; ETC, electron transport chain; TCA, tricarboxylic acid.

The dependence of mCa^{2+} uptake on $\Delta\Psi_m$ has been examined extensively (Gunter & Pfeiffer, 1990; Wingrove, Amatruda & Gunter, 10984; Dash, Qi & Beard, 2009), as well as the importance of other factors (Haumann et al. 2010); however, this is the first study to show that when DNP – induced H^+ entry (leak) is supported by H^+ pumping (no change in pH_m), Ca^{2+} slowly continues to enter the matrix either via the CaU despite a progressively lower $\Delta\Psi_m$, or possibly due to Ca^{2+} influx in exchange for $2H^+$ efflux ("reverse mode" CHE_m) secondary to the low $\Delta\Psi_m$. However, when mitochondria are fully coupled and H^+ pumping by complexes I, III, and IV is in a steady state, this slow influx of Ca^{2+} does not occur (Fig. 2A) as we showed previously. Unfortunately, we cannot distinguish if this slow increase in mCa^{2+} influx occurs through the CaU or the CHE_m because there are currently no known specific inhibitors for the putative CHE_m, and unfortunately, RR may also block CHE_m. A recent study identified a leucine zipper EF hand-containing trans-membrane protein (Letm1) as a modulator of CHE_m that is also sensitive to RR. However, prior studies indicate that Letm1 mediates K^+/H^+ exchange so the role of Letm1 in CHE_m requires further study. The possibility that a fall in $\Delta\Psi_m$ leads to a loss of membrane permeability selectiveness and inward Ca^{2+} leak also appears unlikely because the increase in mCa^{2+} uptake did not occur in the presence of RR.

$\Delta\Psi_m < E_{Rev}$ promotes ATP Hydrolysis- F_OF_1-ATPsynthase/ase directionality is governed by $\Delta\Psi_m$ and its "reversal potential "E_{Rev} ", which in turn is dependent on the concentration of the reactants ATP and ADP and ΔpH_m. Related components of E_{Rev} that influence the direction and rate of ATP synthesis/hydrolysis are the free $[P_i]$ and the H^+/ATP coupling ration n. When $\Delta\Psi_m$ becomes less negative than E_{rev}, the electrochemical potential (high $[ATP]_m$ and ΔpH_m, but low $[ADP]_m$ and $\Delta\Psi_m$) is thermodynamically favorable for proton ejection by complex V (Chinopoulous & Adam-Vizi, 2010; Chinopolous, 2011; Chinopolous et al. 2010; Metelkin et al. 2009). ATP hydrolysis and ATP/ADP transport reversal occur at $\Delta\Psi_m$'s of approximately -125 and -110 mV, respectively, at a matrix ADP/ATP ratio of 2. We observed that ATP hydrolysis activity occurred with a relatively small (20-25%) reduction in $\Delta\Psi_m$. For our study (Fig. 2) a 25% reduction in $\Delta\Psi_m$ represents a Ψ_m of approximately -125mV.

Excess Ca^{2+} Plays an Important Role in Mitochondrial Dysfunction - Several mitochondrial TCA cycle enzymes are believed to be modulated by $[Ca^{2+}]_m$, based on increased mitochondrial enzyme activity with increased $[Ca^{2+}]_m$ (Brandes & Bers, 1997; Brandes & Bers, 2002; McCormack, Halestrap & Denton, 1990; Nguyen, Dudycha & Jafri, 2007; Rossi & Lehninger, 1964; Territo et al. 2000). However, using our cardiac, isolated mitochondrial model, we have observed only a small acute increase in resting state respiration with increased $[Ca^{2+}]_m$ (Haumann et al. 2010). In contrast, pathological mCa^{2+} overloading predisposes the mitochondrion to form the mitochondrial permeability transition pore (PTP) (Brookes et al. 2004, O'Rourke, Cortassa & Aon, 2005; Bernardi, 1999; Gunter et al. 1994; Duchen, 2000), which is key to initiating apoptosis. Inhibiting PTP has been shown to reduce IR injury (Argaud et al. 2005; Bopassa et al. 2006; Feng et al. 2005;

Halestrap, Clarke & Javadov, 2004; Hausenloy, Duchen & Yellon, 2003; Nishihara et al. 2007). Interestingly, temporarily blocking F_OF_1-ATPsynthase/ase (Di Lisa et al. 1998; Grover et al. 2004; Rodrigo & Staden, 2005), which was recently proposed as a component of the PTP (Giorgio et al. 2013), is also protective against IR injury. Therefore, the importance of pH_m and mCa^{2+} in both physiological and pathological conditions implies a major role of pH_m as well as $\Delta\Psi_m$ in the regulation of $[Ca^{2+}]_m$. Although we have here given a plausible explanation for the protection induced by complex V blockade (reduced mCa^{2+}), the underlying thermodynamic processes remains incompletely understood.

It is well known that uncoupling caused by a protonophore, such as DNP or CCCP, can induce ATP hydrolysis through reversal of F_OF_1-ATPase. DNP induced uncoupling of $\Delta\Psi_m$ thus reduces the ATP/ADP_m ratio by consuming ATP, if available. The consequent H^+ pumping by complex V will tend to partially restore $\Delta\Psi_m$ to offset the protonophore-induced decreases in pH_m and $\Delta\Psi_m$. The contribution of all these factors indicates that a slight uncoupling of $\Delta\Psi_m$ may not substantially decrease $[ATP]_m$. But stepwise uncoupling initially slows ATP synthesis by F_OF_1-ATPsynthase and then promotes F_OF_1-ATPase to further decrease $[ATP]_m$. Indirectly, the ΔpH_m is correlated to the $\Delta\Psi_m$ and both contribute to the total proton motive force ($\Delta\Psi_m + \Delta pH_m$) because the outward H^+ pumping via respiratory complexes I, III and IV is the major contributor to a high $\Delta\Psi_m$. A new, interesting observation of our study is the important role of complex V in maintaining the proton motive force under increased Ca^{2+} loading conditions. If complex V H^+ pumping is blocked (OMN) to counteract a H^+ leak (DNP), an alkaline matrix pH_m and $\Delta\Psi_m$ cannot be maintained and, if there is concomitant mCa^{2+} loading, the matrix acidity and uncoupling are largely exacerbated (Fig. 8).

ATP Hydrolysis Occurs with Changes in Matrix pH_m and $[Ca^{2+}]_m$ but not NADH – We found that as $\Delta\Psi_m$ was stepwise uncoupled by DNP, $\Delta\Psi_m$ remained at a relatively stable level over time before $CaCl_2$ was added. However, adding $CaCl_2$ resulted in a gradual, more complete uncoupling of $\Delta\Psi_m$ over 6 min. $\Delta\Psi_m$ is normally fully coupled when complex V is blocked by OMN (Valdez, Zaobornyj & Boveris, 2006); however, the effect of DNP to uncouple $\Delta\Psi_m$ was intensified when OMN was present. The increased uncoupling effect of DNP in the presence of OMN indicates that ATP hydrolysis actually supports the $\Delta\Psi_m$ via H^+ pumping even at a relatively small decrease in $\Delta\Psi_m$ with DNP. That ATP hydrolysis occurs is supported by the fall in [ATP] after addition of 20 and 30 μM DNP. The lack of a significant change in ATP production after adding 10 μM DNP suggests that ATP hydrolysis is less evident with mild uncoupling. The reason for this can be found in the two condition-dependent sources of substrate level phosphorylation of ADP in mitochondria that can supply ATP and GTP for hydrolysis by complex V; the TCA cycle enzymes phosphoenolpyruvate carboxykinase and succinate-CoA synthetase (Chinopoulos & Adam-Vizi, 2010; Chinopoulos et al. 2010). Adding PA did not increase [ATP] (Fig. 7) as there was no drive to produce ATP; however, with a continued supply of PA in the buffer the TCA, substrate level phosphorylation presumably supplied the ATP for consumption by complex V.

Supportive evidence for ATP hydrolysis is provided by the changes in pH_m and NADH. Matrix pH did not decrease as expected on addition of DNP as H^+ ions entered the matrix through the IMM. This is most likely due to reciprocal outward H^+ pumping by F_OF_1-ATPase during partial uncoupling because pH_m indeed fell in the presence of OMN when H^+ could not be pumped out. Moreover, the stability of pH_m after DNP was associated with a RR-sensitive increase in $[Ca^{2+}]_m$ related to a lesser uncoupled $\Delta\Psi_m$ during outward H^+ pumping by F_OF_1-ATPase. A previous study showed an increase in $[Ca^{2+}]_m$ upon acidification was independent of Ca^{2+} flux through the CaU (Gambassi et al. 1993). In our previous study (Haumann et al. 2010) we also did not observe a decrease in pH_m that was dependent on mCa^{2+} uptake via the CaU in fully coupled mitochondria.

The finding that NADH did not change significantly when DNP was added in the absence of OMN was interesting as we expected to find that adding the protonophore would lower the redox state, i.e., decrease NADH. Apparently the increasing F_OF_1-ATPase activity, combined with the faster TCA cycle turnover (enhanced reduction of NAD^+ to NADH in respiratory complexes) was able to preserve NADH at normal levels even after DNP was given to uncouple $\Delta\Psi_m$. In the presence of OMN, however, NADH levels were lower indicating the inability to produce sufficient NADH through the TCA cycle to maintain the redox state. It is interesting that adding $CaCl_2$ did not significantly change the NADH levels in this model, as also reported before (Haumann et al. 2010) despite reports that an increase in $m[Ca^{2+}]$ stimulates the NADH producing dehydrogenases (Brandes & Bers, 2002; Gambassi et al. 1993; Wan et al. 1989; McCormack & Denton, 1980; Denton, McCormack & Edgell, 1980).

This discrepancy may be explained in part because our experiments were conducted below the $K_{0.5}$ of 1 μM where these dehydrogenases are reported to be activated (McCormack & Denton, 1980, Denton, McCormack & Edgell, 1980).

ATP Hydrolysis Promotes a Slow Rise in $[Ca^{2+}]_m$ via CaU or CHE_m – We found that the increase in ATP hydrolysis during partial uncoupling was associated with an increase in $[Ca^{2+}]_m$, while the unchanged ATP synthesis/hydrolysis rate after OMN was accompanied by a decrease in $[Ca^{2+}]_m$. It has been postulated that the CaU can also operate in the reverse reaction, i.e. allowing mCa^{2+} efflux and causing $[Ca^{2+}]_m$ to decrease; indeed, this has been reported in completely depolarized mitochondria by measuring an increase in extra-mitochondrial $[Ca^{2+}]$ (Vaur, Sartor & Dufy-Barbe, 2000) In contrast, it is unlikely that there is a large efflux of mCa^{2+} through the CaU, even in partially uncoupled mitochondria, as the electrochemical force is still directed inward. Because of the absence of Na^+ in our buffer, reverse NCE_m activity also cannot occur, so the putative CHE_m, which is dependent on the gradients of both Ca^{2+} and H^+ for charge compensation is a possible cause of the increasing $[Ca^{2+}]_m$ over time. Our study also indicates that complex V hydrolysis did not significantly affect the mCa^{2+} buffering capacity, i.e., a higher rate of ATP hydrolysis did not result in a higher $[Ca^{2+}]_m$ since there was no significant difference between the initial $[Ca^{2+}]_m$ in the presence or absence of OMN. Moreover, the slow rise in mCa^{2+} was not due to spectral

differences between ATP and ADP of indo-1.

The necessity of mCa^{2+} extrusion pathways to oppose mCa^{2+} influx pathways is required to maintain mitochondrial ionic homeostasis. Unlike the transport of Ca^{2+} via the CaU, which is electrochemical, the exchange of Ca^{2+} through the CHE_m is dependent on both $[Ca^{2+}]$ and $[H^+]$ gradients, but may not be directly dependent on $\Delta\Psi_m$ (Rottenberg & Marbach, 1990, Gunter, Zuscik & Gunter, 1991). This implies that the tendency of DNP to decrease the $[H^+]$ gradient, which is countered by H^+ pumping at complex V to restore pH_m and support the $\Delta\Psi_m$, could be linked to a slow increase of mCa^{2+} through the CHE_m, or less likely, via CaU as a plausible cause for the RR-sensitive slow increase in $[Ca^{2+}]_m$ after over time after adding $CaCl_2$ despite the lower $\Delta\Psi_m$. This view is supported largely by the finding that the slow increase in $[Ca^{2+}]_m$ is prevented by OMN, which is associated with increased matrix acidity over time. Matrix acidification may reduce mCa^{2+} uptake in cardiac mitochondria, possibly by the effect of a lower pH_m on reducing $\Delta\Psi_m$ (Gursahani & Schaefer, 2004).

We believe that the CaU and or CHE_m may play a major role in the continued increase in $[Ca^{2+}]_m$ in our model of partially uncoupled mitochondria associated with H^+ pumping by complex V (Fig. 8). However, we also considered that ATP hydrolysis by F_OF_1-ATPase causes a paradoxical increase in $[Ca^{2+}]_m$ by a decrease in mCa^{2+} buffering by ADP *vs*. ATP (Haumann et al. 2010) by reduced precipitation of Ca^{2+} and PO_4^{3-} as $Ca_3(PO_4)_2$ (or other species), or by another mCa^{2+} import mechanism. For example, Ca^{2+} precipitation could be influenced by $[PO_4^{3-}]_m$, which is dependent on the ΔpH_m, as the phosphate carrier co-transports $HPO_4^{2-}/2\ H^+$ (Chalmers & Nicholls, 2003). Alterations in mitochondrial PO_4^{3-} concentration ($[P_i]_m$) can alter $[Ca^{2+}]_m$ as well. A fall in $\Delta\Psi_m$ can result in a decrease in $[P_i]_m$ as the $[P_i]$ entry is dependent on the proton motive force, which is a function of ΔpH_m as well as of $\Delta\Psi_m$. Because the proton motive force is decreased due to depolarization, $[P_i]_m$ should decrease and increase the free (unbound) $[Ca^{2+}]_m$. However, in the present study the changes in ΔpH_m and $\Delta\Psi_m$ were equivalent, or larger, in the presence of OMN *vs*. no OMN when $[Ca^{2+}]_m$ was higher, so reduced $[P_i]_m$ entry is not itself likely to increase $[Ca^{2+}]_m$. On the other hand, hydrolysis of ATP to ADP would tend to increase $[P_i]_m$. Because there was no associated decrease in $[Ca^{2+}]_m$ with ATP hydrolysis, and since the consequent production of P_i is exchanged for H^+ via the P_iH symporter, we assume that changes in $[P_i]_m$ cannot significantly affect $[Ca^{2+}]_m$ in this study. Moreover, in our study we showed that increasing buffer $[PO_4^{3-}]$ from 1 to 10 mM did not significantly alter $[Ca^{2+}]_m$. This gradual increase in $[Ca^{2+}]_m$ is also not likely due to matrix reaction and/or decreased buffering of matrix Ca^{2+} by ADP *vs*. ATP as the decrease in ATP/ADP ratio due to H^+ pumping by complex V was not large. Moreover, when $\Delta\Psi_m$ was completely uncoupled (100 μM DNP), with an even lower expected ATP/ADP ratio, $[Ca^{2+}]_m$ was not higher but lower.

Although we have considered many factors that might indirectly alter $[Ca^{2+}]_m$, our critical finding is that RR completely blocked the observed slow increase in $[Ca^{2+}]_m$ in the OMN free group,

indicating there was active mCa^{2+} influx across the IMM by CaU or CHE_m and not a significant change in matrix mCa^{2+} buffering due to mCa^{2+} precipitation, P_i, or mitochondrial volume. Previous studies have furnished indirect evidence for reversal of F_OF_1-ATPsynthase (reduced mCa^{2+} uptake and fully uncoupled $\Delta\Psi_m$ with CCCP) (Leyssens et al. 1996; Bains et al. 2006), but this is the first study to directly show a graded increase in ATP hydrolysis and maintained pH_m after partial $\Delta\Psi_m$ uncoupling in isolated guinea pig heart mitochondria exposed to mCa^{2+} loading. An intrinsic factor, ATPase inhibitory factor 1 (IF1), is known to inhibit F_OF_1-ATPase (Rouslin & Broge, 1994). This protein is expressed in rabbit heart cells but exact concentrations and interspecies variations remain unclear. The optimal pH for inhibiting F_OF_1-ATPase by IF1 is 6.7, a pH value below that which we measured in the mitochondrial matrix. Therefore, it is unlikely that IF1 is activated fast enough in our mitochondrial preparation to intrinsically block F_OF_1-ATPase.

Conclusions and Limitations –Overall, the results provide new insights into the dynamics of mCa^{2+} flux, which is driven by interrelated chemical and electrical gradients. Our study indicates that compensatory H^+ pumping by complex V during an imposed inward H^+ leak leads to enhanced mCa^{2+} loading through either the CaU or CHE_m even when mitochondria are partially uncoupled, but supported by H^+ pumping, and when NCE is blocked. Compensatory H^+ pumping by complex V to support the ΔpH_m may largely explain the continued mCa^{2+} loading when $CaCl_2$ is added, which in turn uncouples $\Delta\Psi_m$; this is a situation likely to occur during cell ischemia or anoxia. Under these circumstances the pH linked entry of Ca^{2+} by the CaU may lead to stepwise uncoupling of $\Delta\Psi_m$, suggesting that CaU activity is more dependent on a high pH gradient than on $\Delta\Psi_m$. So it is interesting that blocking complex V can prevent this slow mCa^{2+} loading as well as preserve glycolysis and TCA cycle-generated ATP, i.e. substrate level phosphorylation. Although the rapid uptake of mCa^{2+} may be largely $\Delta\Psi_m$ and pH_m dependent, the slow uptake of mCa^{2+} may be more pH_m dependent, but less concentration and $\Delta\Psi_m$ dependent.

An important limitation of our study is the lack of a selective inhibitor to block CHE_m and the poor selectivity of RR, which together greatly hampers elucidation of the mechanisms of trans-matrix Ca^{2+} flux. Another is that the mitochondria were examined outside their normal milieu so that the contributions of ATP synthesis by glycolysis and ATP hydrolysis for cellular metabolic support could not be assessed. We conclude that the differences in the rate and magnitude of mCa^{2+} uptake in partially uncoupled mitochondria in the presence or absence of F_OF_1-ATPase activity can be described in the context of the corresponding changes in pH_m and $\Delta\Psi_m$. However, studies with specific transport inhibitors are needed to assess with certainty the exact mechanism that mediate these changes in $[Ca^{2+}]_m$.

Acknowledgements and Disclosure – The authors wish to thank Drs. Jason Bazil and Kalyan C. Vinnakota for scientific input, and Anita Tredeau for administrative assistance. This work was supported by grants from National Institutes of Health (HL095122, HL089514, HL098490);

American Heart Association (0855940G); and Veterans Administration (Merit Review 8204-05P). The authors have no conflicts to declare.

References

Aldakkak M, Stowe DF, Cheng Q, Kwok WM, Camara AK. Mitochondrial matrix K^+ flux independent of large-conductance Ca^{2+}-activated K^+ channel opening. Am J Physiol Cell Physiol 2010;298:C530-41.

Argaud L, Gateau-Roesch O, Raisky O, Loufouat J, Robert D, Ovize M. Postconditioning inhibits mitochondrial permeability transition. Circulation 2005;111:194-7.

Bains R, Moe MC, Larsen GA, Berg-Johnsen J, Vinje ML. Volatile anaesthetics depolarize neural mitochondria by inhibition of the electron transport chain. Acta Anaesthesiol Scand 2006;50:572-9.

Bazil JN, Blomeyer CA, Pradhan RK, Camara AK, Dash RK. Modeling the calcium sequestration system in isolated guinea pig cardiac mitochondria. J Bioenerg Biomembr 2013;45:177-88.

Bernardi P. Mitochondrial transport of cations: channels, exchangers, and permeability transition. Physiol Rev 1999;79:1127-55.

Blomeyer CA, Bazil JN, Stowe DF, Pradhan RK, Dash RK, Camara AK. Dynamic buffering of mitochondrial Ca^{2+} during Ca^{2+} uptake and Na^+-induced Ca^{2+} release. J Bioenerg Biomembr 2013;45:189-202.

Boelens AD, Pradhan RK, Blomeyer CA, Camara AK, Dash RK, Stowe DF. Extra-matrix Mg^{2+} limits Ca^{2+} uptake and modulates Ca^{2+} uptake-independent respiration and redox state in cardiac isolated mitochondria. J Bioenerg Biomembr 2013;45:203-18.

Bopassa JC, Vandroux D, Ovize M, Ferrera R. Controlled reperfusion after hypothermic heart preservation inhibits mitochondrial permeability transition-pore opening and enhances functional recovery. Am J Physiol Heart Circ Physiol 2006;291:H2265-71.

Bradford MM. A rapid and sensitive method for the quantitation of microgram quantities of protein utilizing the principle of protein-dye binding. Anal Biochem 1976;72:248-54.

Brand MD. Electroneutral efflux of Ca^{2+} from liver mitochondria. Biochem J 1985;225:413-9.

Brandes R, Bers DM. Intracellular Ca^{2+} increases the mitochondrial NADH concentration during elevated work in intact cardiac muscle. Circ Res 1997;80:82-7.

Brandes R, Bers DM. Simultaneous measurements of mitochondrial NADH and Ca^{2+} during increased work in intact rat heart trabeculae. Biophys J 2002;83:587-604.

Camara AK, Lesnefsky EJ, Stowe DF. Potential therapeutic benefits of strategies directed to mitochondria. Antioxid Redox Signal 2010;13:279-347.

Campanella M, Seraphim A, Abeti R, Casswell E, Echave P, Duchen MR. IF1, the endogenous regulator of the F_1F_o-ATPsynthase, defines mitochondrial volume fraction in HeLa cells by regulating autophagy. Biochim Biophys Acta 2009;1787:393-401.

Chalmers S, Nicholls DG. The relationship between free and total calcium concentrations in the matrix of liver and brain mitochondria. J Biol Chem 2003;278:19062-70.

Chance B, Cohen P, Jobsis F, Schoener B. Intracellular oxidation-reduction states in vivo. Science 1962;137:499-508.

Chinopoulos C, Adam-Vizi V. Mitochondria as ATP consumers in cellular pathology. Biochim Biophys Acta 2010;1802:221-7.

Chinopoulos C, Gerencser AA, Mandi M, et al. Forward operation of adenine nucleotide translocase during F_0F_1-ATPase reversal: critical role of matrix substrate-level phosphorylation. FASEB J 2010;24:2405-16.

Chinopoulos C. Mitochondrial consumption of cytosolic ATP: Not so fast. FEBS Lett 2011.

Coty WA, Pedersen PL. Phosphate transport in rat liver mitochondria. Kinetics and energy requirements. J Biol Chem 1974;249:2593-8.

Cross RL, Muller V. The evolution of A-, F-, and V-type ATP synthases and ATPases: reversals in function and changes in the H^+/ATP coupling ratio. FEBS Lett 2004;576:1-4.

Dash RK, Beard DA. Analysis of cardiac mitochondrial Na^+-Ca^{2+} exchanger kinetics with a biophysical model of mitochondrial Ca^{2+} handling suggests a 3:1 stoichiometry. J Physiol 2008;586:3267-85.

Dash RK, Qi F, Beard DA. A biophysically based mathematical model for the kinetics of mitochondrial calcium

uniporter. Biophys J 2009;96:1318-32.

Delcamp TJ, Dales C, Ralenkotter L, Cole PS, Hadley RW. Intramitochondrial [Ca^{2+}] and membrane potential in ventricular myocytes exposed to anoxia-reoxygenation. Am J Physiol 1998;275:H484-94.

Demaurex N, Poburko D, Frieden M. Regulation of plasma membrane calcium fluxes by mitochondria. Biochim Biophys Acta 2009;1787:1383-94.

Denton RM, McCormack JG, Edgell NJ. Role of calcium ions in the regulation of intramitochondrial metabolism. Effects of Na^+, Mg^{2+} and ruthenium red on the Ca^{2+}-stimulated oxidation of oxoglutarate and on pyruvate dehydrogenase activity in intact rat heart mitochondria. Biochem J 1980;190:107-17.

Di Lisa F, Bernardi P. Mitochondrial function as a determinant of recovery or death in cell response to injury. Mol Cell Biochem 1998;184:379-91.

Di Lisa F, Menabo R, Canton M, Petronilli V. The role of mitochondria in the salvage and the injury of the ischemic myocardium. Biochim Biophys Acta 1998;1366:69-78.

Duchen MR. Mitochondria and calcium: from cell signalling to cell death. J Physiol 2000;529 Pt 1:57-68.

Feng J, Lucchinetti E, Ahuja P, Pasch T, Perriard JC, Zaugg M. Isoflurane postconditioning prevents opening of the mitochondrial permeability transition pore through inhibition of glycogen synthase kinase 3beta. Anesthesiology 2005;103:987-95.

Froschauer E, Nowikovsky K, Schweyen RJ. Electroneutral K^+/H^+ exchange in mitochondrial membrane vesicles involves Yol027/Letm1 proteins. Biochim Biophys Acta 2005;1711:41-8.

Gambassi G, Hansford RG, Sollott SJ, Hogue BA, Lakatta EG, Capogrossi MC. Effects of acidosis on resting cytosolic and mitochondrial Ca^{2+} in mammalian myocardium. J Gen Physiol 1993;102:575-97.

Giorgio V, von Stockum S, Antoniel M, et al. Dimers of mitochondrial ATP synthase form the permeability transition pore. Proc Natl Acad Sci U S A 2013;110:5887-92.

Grover GJ, Atwal KS, Sleph PG, et al. Excessive ATP hydrolysis in ischemic myocardium by mitochondrial F_1F_0-ATPase: effect of selective pharmacological inhibition of mitochondrial ATPase hydrolase activity. Am J Physiol Heart Circ Physiol 2004;287:H1747-55.

Grynkiewicz G, Poenie M, Tsien RY. A new generation of Ca^{2+} indicators with greatly improved fluorescence properties. J Biol Chem 1985;260:3440-50.

Gunter KK, Zuscik MJ, Gunter TE. The Na^+-independent Ca^{2+} efflux mechanism of liver mitochondria is not a passive $Ca^{2+}/2H^+$ exchanger. J Biol Chem 1991;266:21640-8.

Gunter TE, Gunter KK, Sheu SS, Gavin CE. Mitochondrial calcium transport: physiological and pathological relevance. Am J Physiol 1994;267:C313-39.

Gunter TE, Pfeiffer DR. Mechanisms by which mitochondria transport calcium. Am J Physiol 1990;258:C755-86.

Gursahani HI, Schaefer S. Acidification reduces mitochondrial calcium uptake in rat cardiac mitochondria. Am J Physiol Heart Circ Physiol 2004;287:H2659-65.

Halestrap AP, Clarke SJ, Javadov SA. Mitochondrial permeability transition pore opening during myocardial reperfusion--a target for cardioprotection. Cardiovasc Res 2004;61:372-85.

Haumann J, Dash RK, Stowe DF, Boelens A, Beard DA, Camara AKS. Mitochondrial free [Ca^{2+}] increases during ATP/ADP antiport and ADP phosphorylation: exploration of mechanisms Biophys J 2010;99:997-1006.

Hausenloy DJ, Duchen MR, Yellon DM. Inhibiting mitochondrial permeability transition pore opening at reperfusion protects against ischaemia-reperfusion injury. Cardiovasc Res 2003;60:617-25.

Heinen A, Camara AK, Aldakkak M, Rhodes SS, Riess ML, Stowe DF. Mitochondrial Ca^{2+}-induced K^+ influx increases respiration and enhances ROS production while maintaining membrane potential. Am J Physiol Cell Physiol 2007;292:C148-56.

Hoppe UC. Mitochondrial calcium channels. FEBS Lett 2010;584:1975-81.

Huang M, Camara AK, Stowe DF, Qi F, Beard DA. Mitochondrial inner membrane electrophysiology assessed by rhodamine-123 transport and fluorescence. Ann Biomed Eng 2007;35:1276-85.

Jiang D, Zhao L, Clapham DE. Genome-wide RNAi screen identifies Letm1 as a mitochondrial Ca^{2+}/H^{+} antiporter. Science 2009;326:144-7.

Leyssens A, Nowicky AV, Patterson L, Crompton M, Duchen MR. The relationship between mitochondrial state, ATP hydrolysis, $[Mg^{2+}]_i$ and $[Ca^{2+}]_i$ studied in isolated rat cardiomyocytes. J Physiol 1996;496:111-28.

Malli R, Graier WF. Mitochondrial Ca^{2+} channels: Great unknowns with important functions. FEBS Lett 2010;584:1942-7.

McCormack JG, Denton RM. Role of calcium ions in the regulation of intramitochondrial metabolism. Properties of the Ca^{2+}-sensitive dehydrogenases within intact uncoupled mitochondria from the white and brown adipose tissue of the rat. Biochem J 1980;190:95-105.

McCormack JG, Halestrap AP, Denton RM. Role of calcium ions in regulation of mammalian intramitochondrial metabolism. Physiol Rev 1990;70:391-425.

Metelkin E, Demin O, Kovacs Z, Chinopoulos C. Modeling of ATP-ADP steady-state exchange rate mediated by the adenine nucleotide translocase in isolated mitochondria. FEBS J 2009;276:6942-55.

Nguyen MH, Dudycha SJ, Jafri MS. Effect of Ca^{2+} on cardiac mitochondrial energy production is modulated by Na^{+} and H^{+} dynamics. Am J Physiol Cell Physiol 2007;292:C2004-20.

Nishihara M, Miura T, Miki T, et al. Modulation of the mitochondrial permeability transition pore complex in GSK-3B-mediated myocardial protection. J Mol Cell Cardiol 2007;43:564-70.

Nowikovsky K, Froschauer EM, Zsurka G, et al. The LETM1/YOL027 gene family encodes a factor of the mitochondrial K^{+} homeostasis with a potential role in the Wolf-Hirschhorn syndrome. J Biol Chem 2004;279:30307-15.

Nowikovsky K, Pozzan T, Rizzuto R, Scorrano L, Bernardi P. Perspectives on: SGP symposium on mitochondrial physiology and medicine: the pathophysiology of LETM1. J Gen Physiol 2012;139:445-54.

O'Rourke B, Cortassa S, Aon MA. Mitochondrial ion channels: gatekeepers of life and death. Physiology (Bethesda) 2005;20:303-15.

O-Uchi J, Jhun BS, Hurst S, et al. Overexpression of ryanodine receptor type 1 enhances mitochondrial fragmentation and Ca^{2+}-induced ATP production in cardiac H9c2 myoblasts. Am J Physiol Heart Circ Physiol 2013;305:H1736-51.

Riess ML, Camara AK, Heinen A, Eells JT, Henry MM, Stowe DF. KATP channel openers have opposite effects on mitochondrial respiration under different energetic conditions. J Cardiovasc Pharmacol 2008;51:483-91.

Riess ML, Kevin LG, McCormick J, Jiang MT, Rhodes SS, Stowe DF. Anesthetic preconditioning: the role of free radicals in sevoflurane-induced attenuation of mitochondrial electron transport in Guinea pig isolated hearts. Anesth Analg 2005;100:46-53.

Rodrigo GC, Standen NB. Role of mitochondrial re-energization and Ca^{2+} influx in reperfusion injury of metabolically inhibited cardiac myocytes. Cardiovasc Res 2005;67:291-300.

Rossi CS, Lehninger AL. Stoichiometry of respiratory stimulation, accumulation of Ca^{2+} and phosphate, and oxidative phosphorylation in rat liver mitochondria. J Biol Chem 1964;239:3971-80.

Rottenberg H, Marbach M. The Na^{+}-independent Ca^{2+} efflux system in mitochondria is a $Ca^{2+}/2H^{+}$ exchange system. FEBS Lett 1990;274:65-8.

Rouslin W, Broge CW. Analysis of factors affecting functional assays for estimating IF1, the mitochondrial ATPase inhibitor. Anal Biochem 1994;222:68-75.

Ryu SY, Beutner G, Kinnally KW, Dirksen RT, Sheu SS. Single channel characterization of the mitochondrial ryanodine receptor in heart mitoplasts. J Biol Chem 2011;286:21324-9.

Santo-Domingo J, Demaurex N. Calcium uptake mechanisms of mitochondria. Biochim Biophys Acta 2010;1797:907-12.

Stowe DF, Camara AK. Mitochondrial reactive oxygen species production in excitable cells: modulators of mitochondrial and cell function. Antioxid Redox Signal 2009;11:1373-414.

Territo PR, Mootha VK, French SA, Balaban RS. Ca^{2+} activation of heart mitochondrial oxidative phosphorylation:

role of the F_0/F_1-ATPase. Am J Physiol Cell Physiol 2000;278:C423-35.

Tewari SG, Camara AK, Stowe DF, Dash RK. Computational analysis of Ca^{2+} dynamics in isolated cardiac mitochondria predicts two distinct modes of Ca^{2+} uptake. J Physiol 2014;592:1917-30.

Valdez LB, Zaobornyj T, Boveris A. Mitochondrial metabolic states and membrane potential modulate mtNOS activity. Biochim Biophys Acta 2006;1757:166-72.

Vaur S, Sartor P, Dufy-Barbe L. Calcium store depletion induced by mitochondrial uncoupling in prostatic cells. Gen Physiol Biophys 2000;19:265-78.

Vinnakota KC, Bassingthwaighte JB. Myocardial density and composition: a basis for calculating intracellular metabolite concentrations. Am J Physiol Heart Circ Physiol 2004;286:H1742-9.

Wan B, LaNoue KF, Cheung JY, Scaduto RC, Jr. Regulation of citric acid cycle by calcium. J Biol Chem 1989;264:13430-9.

Cover page image: Mitochondrial network (in red) in H9C2 cells. Own work.